HOKKAIDO UNIVERSITY

Title	Cretaceous forearc tectonics in central Hokkaido : With special reference to accretion and exhumation processes of greenstones
Author(s)	Ueda, Hayato
Degree Grantor	北海道大学
Degree Name	博士(理学)
Dissertation Number	甲第5387号
Issue Date	2001-03-23
DOI	https://doi.org/10.11501/3182087
Doc URL	https://hdl.handle.net/2115/51496
Type	doctoral thesis
File Information	000000399635.pdf

Hokkaido University Collection of Scholarly and Academic Papers : HUSCAP

Cretaceous forearc tectonics in central Hokkaido: With special reference to accretion and exhumation processes of greenstones

Hayato Ueda

Ph. D. Thesis

Division of Earth and Planetary Sciences, Faculty of Science,
Hokkaido University

January, 2001

Cretaceous forearc tectonics in central Hokkaido: With special reference to accretion and exhumation processes of greenstones

Hayato Ueda

Ph.D. Thesis

Division of Earth and Planetary Sciences, Faculty of Science,
Hokkaido University

January, 2001

Abstract

New geological maps and descriptions on radiolarian ages, metamorphism, and mode of occurrences and geochemistry of greenstones are provided for a very low-grade metamorphosed accretionary complex (Idonnappu Zone: Chapter II) and a high-P/T metamorphosed accretionary complex (Iwashimizu Complex: Chapter III) in southern part of the Sorachi-Yezo Belt. Unconformity and clastic composition in the Yezo Supergroup are also described (Chapter IV). Cretaceous forearc structure and its tectonic evolution are reconstructed based on these informations.

Cretaceous accretionary complexes of the Idonnappu Zone in the Urakawa area consist of five lithological units, which are combined into two geologic complexes: the greenstone-dominant Naizawa Complex and the clastic-dominant Horobetsugawa Complex. Radiolarian ages were determined for each unit. The Naizawa Complex is an alternating stack of slabs of depleted tholeiitic greenstone, and fragments of Triassic seamount volcanics with Triassic - Lower Cretaceous ocean floor to trench-fill deposits. The Horobetsugawa Complex is a pile of Upper Cretaceous ocean floor to trench-fill deposits, which intercalates sheared MORB-type greenstones. Lower Cretaceous to Upper Cretaceous submarine slide and debris flow deposits and latest Cretaceous - Paleocene slope basin deposits (T-Unit) are also intercalated.

The Lower Cretaceous Iwashimizu Complex in the southern Kamuikotan Zone (Mitsuishi-Shizunai area) comprises a pile of four nappe sheets (=units), each of which represents a stacks of greenstone slices with minor chert and clastic rocks. All units suffered a high-P/T metamorphism. An inverted distribution of metamorphic grade is recognized between the lower three units. A gap of metamorphic grade exists at the structural top, where blueschist facies metabasites are overlain by zeolite to lawsonite-albite facies rocks. Most of greenstone slices are of oceanic island type basalts (OIB), except a few slices and blocks of depleted tholeiite.

The Middle Yezo Group in the Mitsuishi area unconformably overlies both the Iwashimizu Complex and the Lower Yezo Group. Sedimentary structures and rootlets show that the Albian basal conglomeratic member (M_0 member) is fluvial deposits. It contains abundant greenstone clasts, part of which are accompanied by high-P/T metamorphic minerals. These stratigraphic and clast composition analysis lead a consequence that the Iwashimizu Complex was rapidly exhumed and subaerially exposed until the Albian time.

Accretion styles of greenstones changed from the Early Cretaceous to the Late Cretaceous, as the subducted oceanic crust got younger, sediment supply into the trench increased, and subduction direction changed from highly oblique to near orthogonal. Seamounts subduction drove an abundant accretion of OIB greenstones in the Early Cretaceous. Whereas thick terrigenous sediments with minor

abyssal basalts accreted in the Late Cretaceous.

Depleted tholeiitic greenstone in the Lower Cretaceous Naizawa and Iwashimizu Complexes are regarded as fragments of the Jurassic Lower Sorachi Group, which represents the basal ophiolite of the Cretaceous forearc basin. Co-occurrence of OIB and depleted tholeiite suggests that a part of the forearc basin was fragmented and mixed with the materials accreted from oceanic plate during the seamount subduction.

The mid-Cretaceous exhumation event of the Iwashimizu Complex is probably caused by the younging of subducted oceanic slab and abundant accretion of seamount volcanics in the late Early Cretaceous.

Contents

CHAPTER I. INTRODUCTION 6

THE AIM OF THIS STUDY 6

CRETACEOUS ARC-TRENCH SYSTEM IN CENTRAL HOKKAIDO 8

CHAPTER II. IDONNAPPU ZONE IN THE URAKAWA AREA: A SHALLOW SECTION OF EARLY CRETACEOUS TO LATE CRETACEOUS ACCRETIONARY COMPLEX 10

INTRODUCTION 10

GEOLOGIC OUTLINE OF THE URAKAWA AREA 10

LITHOLOGICAL DIVISION OF THE IDONNAPPU ZONE IN THE URAKAWA AREA 10

Naizawa Complex (re-defined from Naizawa Formation; Sakai and Kanie, 1986) 12

Horobetsugawa Complex (New Name) 12

FOSSIL AGES OF EACH LITHOLOGICAL UNIT 15

ILLITE CRYSTALLINITY OF MUDSTONES 22

Measurement of illite crystallinity 22

Results 24

MODE OF OCCURRENCE AND PETROLOGY OF GREENSTONES 27

Mode of occurrence 27

Petrographic characteristics 34

Petrochemical characteristics 35

DISCUSSION 45

Reconstruction of the original disposition of lithological units 45

Relative movement of each lithological unit 46

Origin and emplacement of the greenstones in the Idonnappu Zone 49

A model for tectonic evolution of the Idonnappu Zone 53

CONCLUSIONS 54

CHAPTER III. IWASHIMIZU COMPLEX: A DEEP SECTION OF THE LOWER CRETACEOUS ACCRETIONARY COMPLEX 56

INTRODUCTION 56

GEOLOGIC OUTLINE 56

LITHOLOGIC DIVISION 56

Lithological facies 61

Unit definition 63

MAP-SCALE STRUCTURES AND TECTONOSTRATIGRAPHIC FRAMEWORK 68

Structural framework 68
RADIOLARIAN AGES 73
MODE OF OCCURRENCE AND PETROLOGY OF GREENSTONES 82
Mode of occurrence 82
Petrographic characteristics 90
Petrochemical characteristics 93
METAMORPHISM 103
Previous studies 103
Examination on metamorphic grade 108
Description of minerals 108
Mineral assemblages in each unit 117
Metamorphic condition 124
DISCUSSION 128
Origin of constituent lithofacies 128
Inner structure of a seamount collision-type accretionary complex 130
Mode of seamount accretion 131
Correlation with the northern Kamuikotan Zone 134
CONCLUSIONS 136

CHAPTER IV. YEZO SUPERGROUP IN THE MITSUISHI AREA: BLUESCHIST-BEARING FLUVIAL CONGLOMERATE AND UNCONFORMITY IN THE CRETACEOUS FOREARC SEQUENCE 138

INTRODUCTION 138
STRATIGRAPHY OF THE NITARACHI-YEZO SEQUENCE 138
Nitarachi Formation 144
Tsukenai Formation 144
Utafue Formation 144
Age 146
PETROLOGICAL FEATURES OF BASAL CONGLOMERATE 146
Clast composition 146
Radiolarian ages of the siliceous mudstone clasts 155
Detrital metamorphic minerals 155
Detrital igneous clinopyroxene 156
DISCUSSION 156
Sedimentological interpretation for the Utafue Formation 156
Clastic composition of the conglomerate 157
Significance of unconformity 158
Exhumation process of the Iwashimizu Complex 158

CONCLUSIONS 161

CHAPTER V. TECTONIC EVOLUTION OF CRETACEOUS FOREARC IN SOUTH CENTRAL HOKKAIDO 163

COMPARISON OF ACCRETED GREENSTONES IN CENTRAL HOKKAIDO 163

Petrological types of greenstones in central Hokkaido 163

Correlation of geological units in the Sorachi-Yezo Belt 163

RECONSTRUCTION OF CRETACEOUS FOREARC WEDGE 170

TEMPORAL CHANGE IN MODE OF GREENSTONE ACCRETION 176

POSSIBLE CAUSE OF BLUESCHIST EXHUMATION 176

CONCLUSIONS 178

ACKNOWLEDGMENTS 180

REFERENCES 182

Chapter I. Introduction

The aim of this study

Accretion tectonics along oceanic plate subduction zones has been revealed mainly during last two decade, both on present accretionary bodies by seismic and drilling studies, and on ancient accretionary complexes exposed on land by structural and chronological studies. However, as shown by von Huene and Scholl (1993) and Lallemand et al. (1994), typical accretionary bodies are formed in restricted areas no more than 20% of total extent of oceanic plate subduction zone. The rest parts of subduction zone have poorly evolved or no accretionary wedge, and forearc slopes are inferred to be tectonically eroded in some areas. Compared to the well-studied "typical" accretionary bodies, structure and tectonics on immature subduction zones has not been well understood. Perhaps, inner trench slopes composed mainly of volcanic rocks obstruct detailed seismic soundings and deep-level drilling. Furthermore, such types of margins are hardly preserved to be exposed on land because tectonic erosion is dominated, or maybe has not been recognized because of poor knowledge.

Lallemand et al. (1994) tried to solve what factors control the fashion in subduction zone, comparing bathymetric and sounding data from present subduction zones with various factors such as sediment supply into trench, relief of ocean floor, orthogonal convergence rate, etc. However, to solve the problem, there is another way that temporal change in nature of accretionary complex and in sedimentation style of forearc basin deposits are to be described within each ancient subduction zone, and to be compared with reconstructed oceanic plate motion, oceanic plate stratigraphy, and other geohistorical events. This method can provide information's on internal and spatial construction of ancient forearc wedge, and its long-term transition, both of which may never be obtained so much from surface surveys and corings in present subduction zones.

Cretaceous to Paleogene accretionary complexes and forearc basin sequence are widely distributed in the central part of Hokkaido (Fig.1). As shortly described in next section, almost all members of the Cretaceous forearc wedge are exposed: very low-grade accretionary complex, high-P/T metamorphosed accretionary complex, forearc basin sequence and its basal ophiolite, parts of mantle ultramafics, and volcanic arc deposits. These units are rearranged by Tertiary tectonics, especially by folds and thrusts due to the collision of the Kurile Arc (Kimura, 1986; Arita et al., 1998). However, there is no fault with large displacement such as the Median Tectonic Line in southwest Japan, and original stratigraphic and structural relations between the units are preserved. Furthermore, deeper sections of these units are turned up to be exposed owing to the collision: for example, up to 8000m complete sections of the forearc basin sequence (*e.g.* Motoyama et al., 1991; Kawabe et al., 1996), and over 10km thick tectonostratigraphic succession of (oceanic plate? -) accretionary complex and

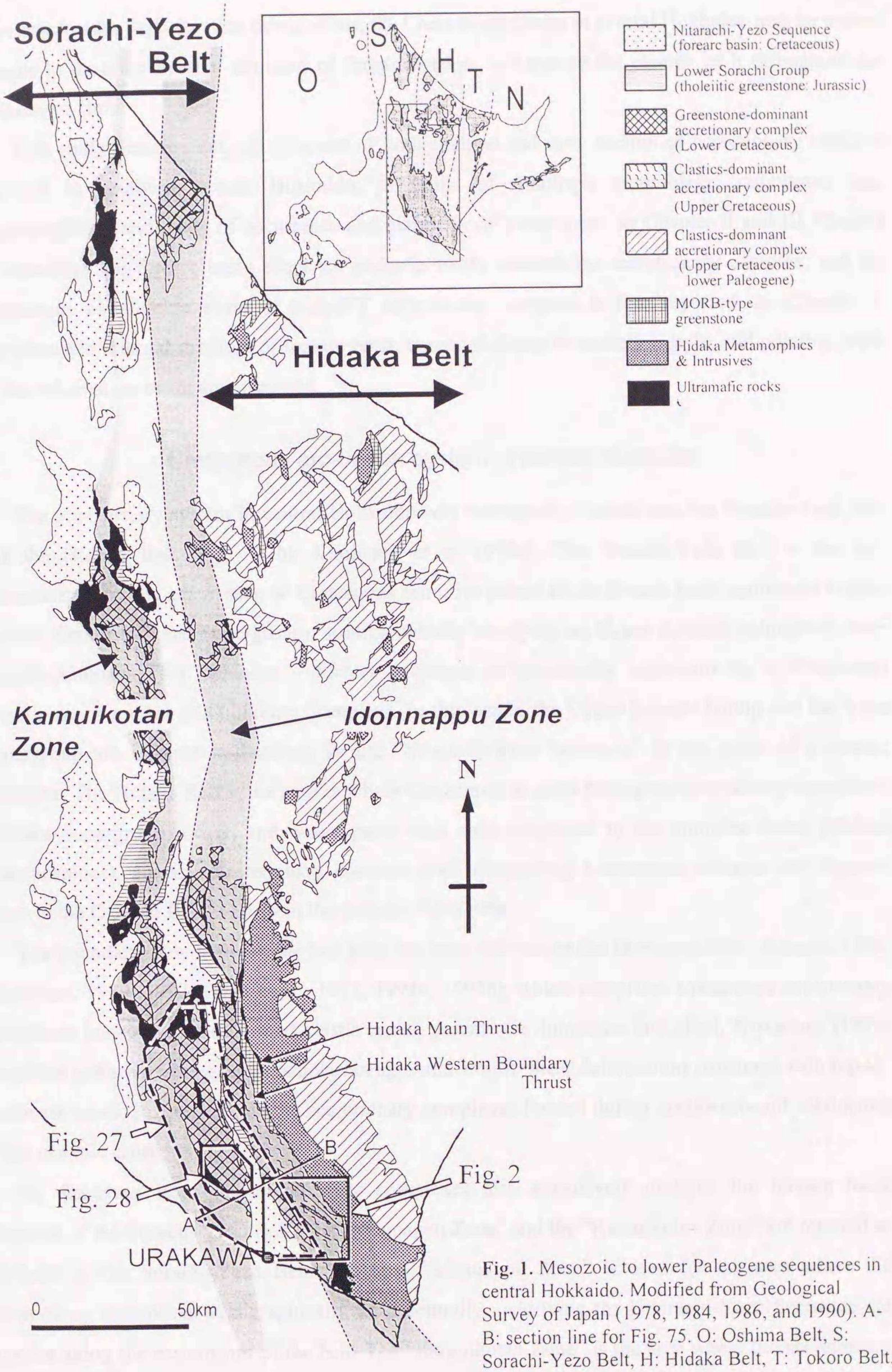


Fig. 1. Mesozoic to lower Paleogene sequences in central Hokkaido. Modified from Geological Survey of Japan (1978, 1984, 1986, and 1990). A-B: section line for Fig. 75. O: Oshima Belt, S: Sorachi-Yezo Belt, H: Hidaka Belt, T: Tokoro Belt, N: Nemuro Belt.

covering forearc deposits (this study). Thus, the Cretaceous system in central Hokkaido may be a good sample to describe internal structure of forearc wedge, and restore the change of it throughout the Cretaceous time.

This study describe internal structure of both shallow and deep section of accretionary complex exposed in southern central Hokkaido, in terms of lithologic assemblage, radiolarian age, metamorphism, and mode of occurrence and petrology of greenstones, in Chapter II and III. Chapter IV describes the forearc basin sequence unconformably overlies the accretionary complex, and the Cretaceous exhumation event of high-P/T accretionary complex is first reported. In Chapter V, reconstructed internal structure of forearc crust, temporal change in accretion style, and possible cause of the exhumation event are discussed.

Cretaceous arc-trench system in central Hokkaido

The pre-Tertiary system in central Hokkaido was tectonically divided into the Sorachi-Yezo Belt and the Hidaka Belt (Fig. 1) by Kiminami et al. (1986). The Sorachi-Yezo Belt is the area characterized by the occurrence of Cretaceous primitive island arc to forearc basin sequences (Upper Sorachi Group to Yezo Supergroup), stratigraphically overlying an Upper Jurassic ophiolite (Lower Sorachi Group). This ophiolite - forearc sequence is structurally underlain by a Cretaceous accretionary complex (Kamuikotan Complex). In this paper, the Upper Sorachi Group and the Yezo Supergroup are referred collectively as the "Nitarachi-Yezo Sequence" in the sense of a forearc sequence. The Hidaka Belt is the area in which Cretaceous to early Paleogene accretionary complexes (Hidaka Supergroup) occur, and where parts were metamorphosed to the granulite facies (Hidaka Metamorphics). Jurassic accretionary complex and overprinting Cretaceous volcanic arc deposits occur in the Oshima Belt, west from the Sorachi-Yezo Belt .

The boundary zone between the two belts has been referred as the Idonnappu Belt (Kimura, 1986; Kiyokawa, 1989, 1992; Ueda et al., 1993, 1994a, 1994b), which comprises Cretaceous accretionary complexes consisting of deformed clastic rocks, greenstone, limestone and chert. Kiyokawa (1992) identified eastward younging of radiolarian ages and simple-shear deformation structures with top-to-southeast sense, suggesting that the accretionary complexes formed during northwestward subduction of the oceanic crust.

As discussed later, the accretionary complexes also extensively underlie the forearc basin sequence of the Sorachi-Yezo Belt. The "Idonnappu Zone" and the "Kamuikotan Zone" are referred as sub-belts in the Sorachi-Yezo Belt. The term "Idonnappu Zone" is used for the area where the accretionary complexes stratigraphically or structurally underlying the Nitarachi-Yezo Sequence are exposed along the eastern rim of the belt. The "Kamuikotan Zone" is the area where the accretionary

complexes are exposed in the core of an anticlinorium (Fig. 1).

Chapter II. Idonnappu Zone in the Urakawa area: a shallow section of Early Cretaceous to Late Cretaceous accretionary complex

Introduction

This Chapter presents new data for the Idonnappu Zone in the Urakawa area, a typical shallow-part section of the Cretaceous accretionary complex, mainly of radiolarian ages, thermal structure from illite crystallinity of mudstones, and mode of occurrence and bulk rock chemistry of greenstones. Internal structure and evolutionary process of the complexes is discussed in the light of this information.

Geologic outline of the Urakawa area

The Urakawa area is located in southern central Hokkaido (Fig.1). Geological map of this area is given in Fig. 2. The Idonnappu Zone is bounded on the east by the east-dipping Hidaka Main Thrust from the Hidaka Metamorphics (Komatsu et al., 1986), and by the east-dipping Nitarachi - Oshorobetsu Fault from the Nitarachi Formation and the Yezo Supergroup on the west (Fig. 2). The Nitarachi Formation consists of Hauterivian siliceous mudstone (Kanie et al., 1981; Taketani and Kanie, 1992) of acidic tuff-origin. The Yezo Supergroup consists of turbidite to shallow marine sequences of Barremian to Maastrichtian (Sakai and Kanie, 1986; Mitsugi and Hirano, 1997), and conformably overlies the Nitarachi Formation. Foliations of the Hidaka Metamorphics dip east, and metamorphic grade decreases eastward. Bedding planes of the Idonnappu Zone and the Nitarachi-Yezo Sequence face west with 90-60°E dips and NNW strikes.

Middle Miocene shallow marine sediments (Kamikineusu Formation: Suzuki et al., 1983) occur sporadically along faults in the Idonnappu Zone and the Yezo Supergroup.

Lithological division of the Idonnappu Zone in the Urakawa area

The pre-Neogene system in the Idonnappu Zone are newly divided into two geologic complexes, the greenstone-dominant Naizawa Complex and the clastic-dominant Horobetsugawa Complex, which consist of two and three lithological units respectively. Each lithological unit is defined based on its lithological assemblage and fabric. The two complexes are separated by the eastward-dipping Redatoi-Okada Thrust (Sakai and Kanie, 1986) and intercalated serpentinite (the Westernmost Hidaka Serpentinite Belt: Niida and Katoh, 1978).

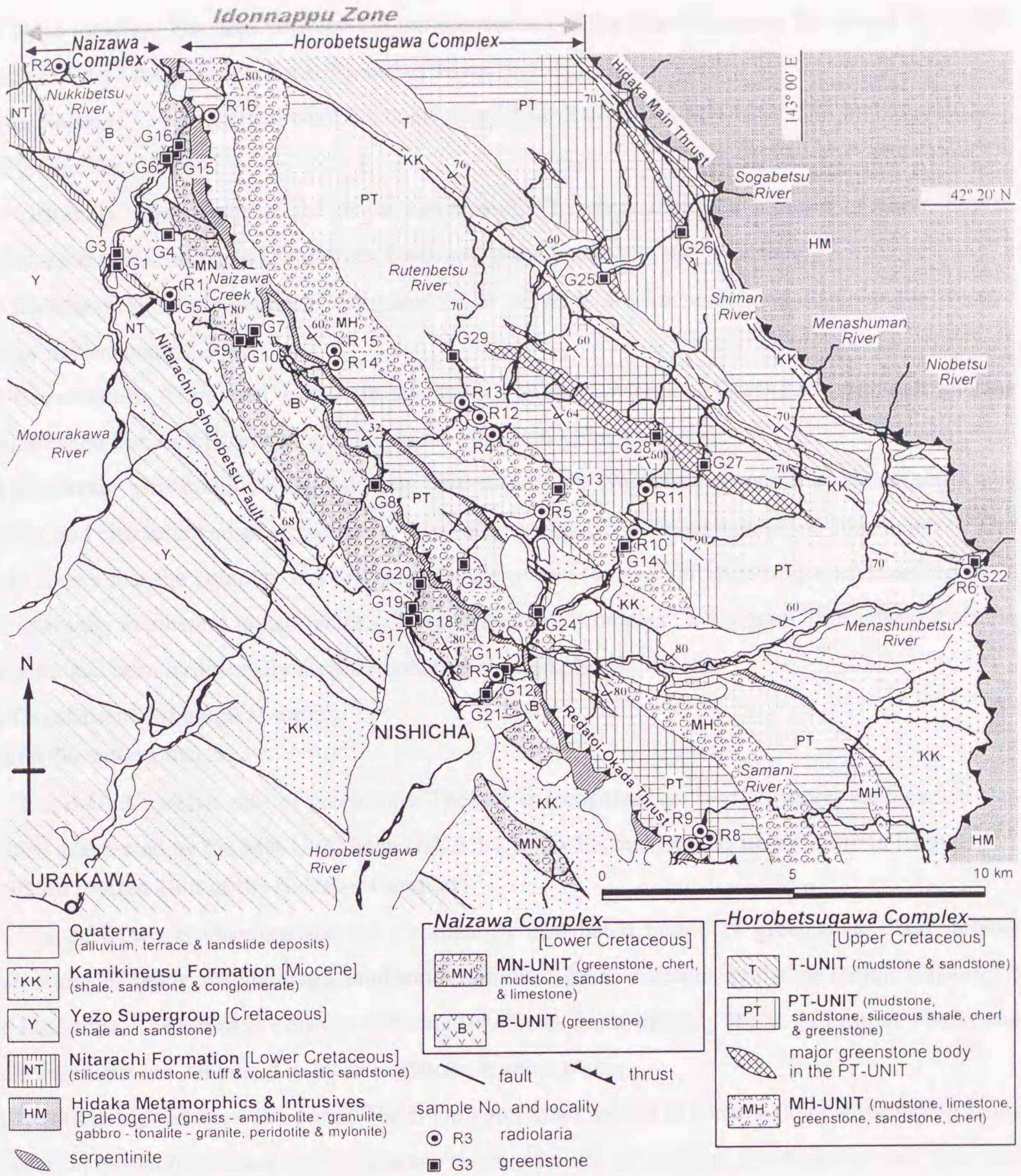


Fig. 2. Geological map of the Idonnappu Zone in the Urakawa area.

Naizawa Complex (re-defined from Naizawa Formation; Sakai and Kanie, 1986)

(1) Type locality: The area between the middle reaches of the Horobetsugawa River and the middle reaches of the Motourakawa River, Urakawa Town (Fig. 2).

(2) Definition: A geological complex consisting of the B-Unit and MN-Unit. The lithology of each unit is described below.

(3) Lithology: Greenstone is the major component. The remainder is a mixture of chert, broken alternations of mudstone and sandstone, black and green mudstone, and limestone.

(4) Distribution: The complex is elongated NNW-SSW, is 3-5 km wide, and occupies the western part of the Idonnappu Zone.

(5) Correlation: Correlated with both the Hidaka Western Marginal Greenstone Sub-belt and the Okuniikappu Sub-belt (Kiyokawa, 1992) in the Niikappu - Shizunai area.

(6) Remarks: This complex was formerly described as the Naizawa Formation by Sakai and Kanie (1986), and characterized as a greenstone-dominant sequence containing submarine slide deposits. Our study shows that the complex is a tectonic mixture of two units of different origin as described later. For internally incoherent mixed facies, we prefer the term "complex" to the term "formation", because the latter has been traditionally used for coherent stratigraphic sequences.

(7) Constituent lithological units:

B-Unit (Basaltic Unit)

The B-Unit consists only of greenstone. The unit is recognized as three (or more) independent slab bodies, intersected by the MN-Unit. Each slab is 1-2 km wide, and extends up to 15 km in length.

MN-Unit (Mixed Unit of the Naizawa Complex)

The MN-Unit is characterized by a complexly distributed bodies of greenstone, chert, broken alternations of sandstone and black mudstone (turbidite), green siliceous mudstone (acidic tuff-origin) and limestone. The contacts between differing lithofacies are commonly faults. Limestone blocks and chert fragments are contained in black mudstone in some places.

(8) Relationship between the units: The B-Unit and MN-Unit are in contact along east-dipping faults exposed in the Motourakawa and Nukkibetsu rivers. Absence of common lithofacies in both units and the tectonically dissected internal structure of the MN-Unit suggest that they are in fault contact throughout the study area. Both units are laterally elongated, and lie slightly obliquely to the general elongation of the Naizawa Complex. Multiple sheets of both the B-Unit and MN-Unit alternate to form a sandwich-like structure at mappable scale (Fig. 2).

Horobetsugawa Complex (New Name)

(1) Type locality: Middle reaches of Horobetsugawa River to Sogabetsu River, Urakawa Town (Fig. 2).

(2) Definition: A geological complex composed of the PT-Unit, accompanied by the MH-Unit and the T-Unit.

(3) Lithology: Most of the Horobetsugawa Complex is black mudstone and broken alternations of sandstone and black mudstone. Greenstone, limestone and chert bodies are occasionally intercalated.

(4) Distribution: In the central to eastern part of the Idonnappu Zone, in a zone 10 to 12 km wide.

(5) Correlation: Correlated with the Kamui Group (Hasegawa et al., 1961; Sakai and Kanie, 1986) in the Urakawa area, and with the Koiboku Sub-belt (Kiyokawa, 1992) in the Niikappu-Shizunai area.

(6) Constituent lithological units:

PT-Unit (Pelagic to Terrigenous Unit)

The PT-Unit is the main constituent of the Horobetsugawa Complex, and consists of black mudstone, alternations of black mudstone and siliciclastic sandstone (turbidites), and massive siliciclastic sandstone. Intercalations of greenstone, bedded gray chert, and gray siliceous mudstone also occur. Red or green mudstone lacking terrigenous silt / sand grains is rarely observed. Limestone is absent. Most of the turbidites are deformed and broken. Some massive sandstone bodies were described as "sand diapirs" by Kawamura and Ueda (1997). Each lithofacies is laterally traceable for several kilometers, and trend is generally concordant with the regional strike. A lithological succession from greenstone and chert through siliceous mudstone and black mudstone to turbidite is frequently observed. This succession is repeated several times within the unit (Fig. 3).

MH-Unit (Mixed Unit of Horobetsugawa Complex)

The MH-Unit is characterized by numerous blocks of limestone, greenstone, sandstone and chert of various sizes contained in a scaly matrix consisting of black mudstone, broken alternations of black mudstone and sandstone, or pebbly mudstone. Block sizes vary from several centimeters to several tens of meters. In some places, the matrix consists of unsheared pebbly mudstone and muddy conglomerate. This unit characteristically contains abundant and large limestone blocks.

T-Unit (Terrigenous Unit)

The T-Unit is characterized by a lack of oceanic materials such as limestone, greenstone and chert. The major components are black mudstone, alternations of sandstone and mudstone (mostly turbidites), and massive sandstone ("sand diapirs" of Kawamura and Ueda, 1997). Gray, green and red siliceous mudstones of acidic tuff-origin also occur. Mudstones are less consolidated, and turbidite are generally less deformed than those of the PT-Unit. Some mudstones are similar to those of the Yezo Supergroup, especially with respect to slaking on weathered outcrop. This unit is correlated with the Menashuman Formation of Sakai and Kanie (1986) and the K-3 unit of Kiyokawa (1992).

(7) Relationship between the units: The MH-Unit is intercalated in the PT-Unit. Along the middle reaches of the Horobetsugawa River, a continuous succession from laminated black mudstone (PT-Unit) to muddy conglomerate containing limestone blocks (MH-Unit) is observed without apparent

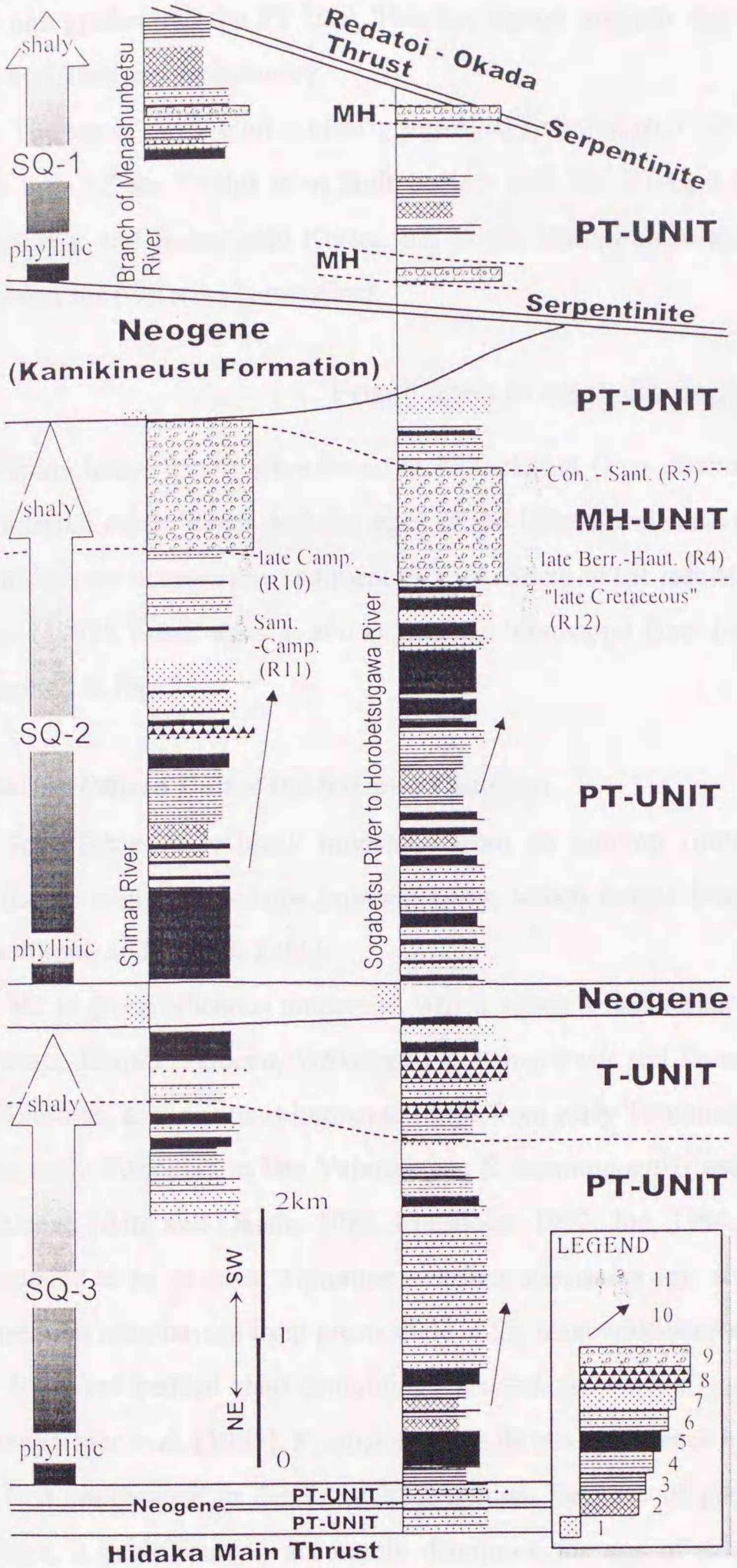


Fig. 3. Typical columnar sections of the Horobetsugawa Complex. Measured routes shown in Fig. 2. 1: Neogene, 2: greenstone, 3: bedded chert, 4: siliceous mudstone, 5: black mudstone, 6: thin-bedded turbidite, 7: thick-bedded turbidite, 8: massive chaotic sandstone (sand diapir), 9: pebbly mudstone with blocks of limestone, greenstone, chert and sandstone (MH-Unit), 10: typical chert-clastics succession in PT-Unit, 11: occurrence of radiolarian fossils (sample no. in parentheses).

tectonic gap. In the top horizon of the MH-Unit, the number of blocks present decreases upward, and the unit grades into the PT-Unit. This succession suggests that the contacts between the PT-Unit and the MH-Unit are sedimentary.

The top of the T-Unit is clearly separated from the phyllitic clastic rocks of the PT-Unit by a fault. The base of the T-Unit is in fault contact with the PT-Unit along a fault in the area between the Sogabetsu and Rutenbetsu Rivers, but in the Menashuman and Motourakawa Rivers, the boundary between the two units is indistinct.

Fossil ages of each lithological unit

Radiolarian fossils were found at 17 localities (Figs. 2 and 4). In Table 1 and Figs. 5 and 6, the radiolarian assemblages and the ages of the lithological units (samples R1-R17) are shown. The B-Unit does not contain any sedimentary rock. Some of the results were already briefly reported by Ueda et al. (1993). Fossil ages in and around the Idonnappu Zone (including data from previous work) are complied in Fig. 7.

MN-Unit (Mixed Unit of the Naizawa Complex)

R1 (Table 1) is black mudstone from an outcrop containing a small limestone block. The mudstone contains *Cecrops septemporatus*, which ranges from late Valanginian to early Barremian (Sanfilippo and Riedel, 1985).

R2 is green siliceous mudstone, which yields a radiolarian assemblage containing *Eucyrtidiellum pyramis*, *Ristola cretacea*, *Sethocapsa kaminogoensis* and *Pseudodictyomitra carpatica*. Among these radiolarians, *E. pyramis* is known to range from early Tithonian to earliest Berriasian, and *R. cretacea* from early Tithonian to late Valanginian, *S. kaminogoensis* and *P. carpatica* first appear in the latest Tithonian (Aita and Okada, 1986; Matsuoka, 1992; Jud, 1994; Baumgartner et al., 1995). The R2 is concluded to be of latest Tithonian - earliest Berriasian age. Kiyokawa (1992) reported Hauterivian - Barremian radiolarians from green shale in the Motourakawa River.

R3 is red bedded chert containing *Pseudodictyomitra* cf. *carpatica* and *P.* cf. *lilyae*. According to Baumgartner et al. (1995), *P. carpatica* has its last occurrence in the early Barremian, and *P. lilyae* has its first appearance in the latest Valanginian. Because of poor preservation and the lack of index species, it is difficult to accurately determine the age of this sample. It is concluded to be Early Cretaceous, and presumably Valanginian - Barremian.

Triassic (late Carnian) conodonts were reported from a chert block from the MN-Unit by Igo et al. (1974). The age of MN-Unit limestone is Middle to Late Triassic (late Ladinian - early Carnian) determined from conodonts (Sakai, 1976) and bryozoans (Sakagami and Sakai, 1979). The MN-Unit is

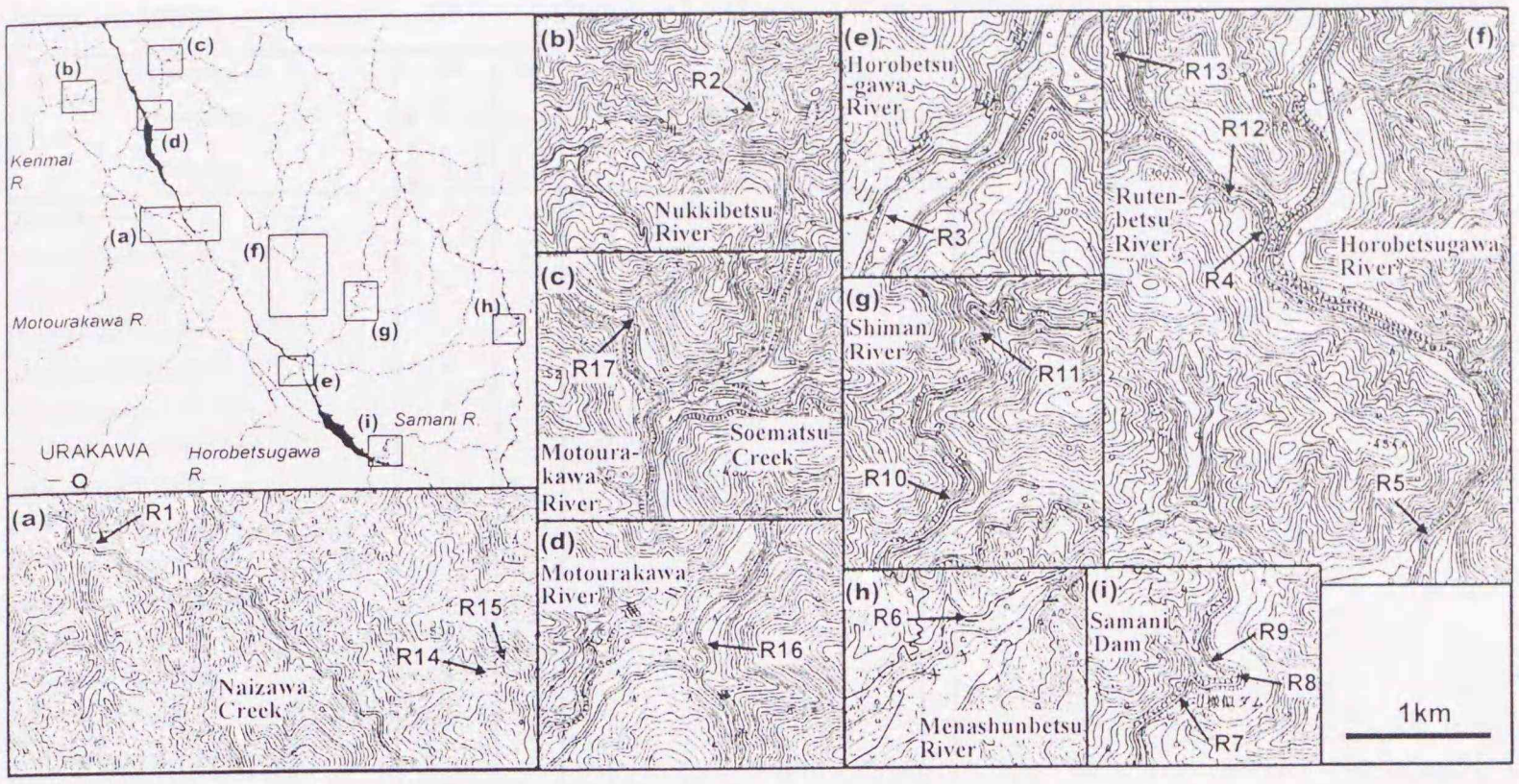


Fig. 4. Sample localities for radiolarian fossils, based on the 1/50,000 scale topographic maps Nishicha, Kamuidake, Rakkodake of the Geographical Survey Institute of Japan. The index map (upper left) covers the same area as Fig. 2.

Table 1. List of radiolarian fossils from the Idonnappu Zone. b-md: black mudstone, b-sil: black siliceous mudstone, g-sil: green siliceous mudstone, r-sil: red siliceous mudstone, r-ch: red chert, a-tf: acidic tuff bed in black mudstone.

Lithological unit: Sample No. / Lithology		MN	MH	PT	T
Bistola cretacea	b-md	R1			
Encyrtidiclium pyramis	g-sil	R2			
Eucyrtidiellum pyramis	r-ch	R3			
Eucyrtidiellum ptyctum	b-md	R4			
Eucyrtidiellum sp.	b-sil	R5			
Eucyrtidiellum sp. A	r-sil	R6			
Eucyrtidiellum sp. B	a-tf	R7			
Eucyrtidiellum sp. C	a-tf	R8			
Eucyrtidiellum sp. D	a-tf	R9			
Eucyrtidiellum sp. E	b-sil	R10			
Eucyrtidiellum sp. F	b-md	R11			
Eucyrtidiellum sp. G	b-md	R12			
Eucyrtidiellum sp. H	b-md	R13			
Eucyrtidiellum sp. I	b-md	R14			
Eucyrtidiellum sp. J	a-tf	R15			
Eucyrtidiellum sp. K	b-md	R16			
Eucyrtidiellum sp. L	b-md	R17			
Eucyrtidiellum unumaense					
Eucyrtidiellum sp. A					
Eucyrtidiellum sp. B					
Eucyrtidiellum sp. C					
Eucyrtidiellum sp. D					
Eucyrtidiellum sp. E					
Eucyrtidiellum sp. F					
Eucyrtidiellum sp. G					
Eucyrtidiellum sp. H					
Eucyrtidiellum sp. I					
Eucyrtidiellum sp. J					
Eucyrtidiellum sp. K					
Eucyrtidiellum sp. L					
Eucyrtidiellum sp. M					
Eucyrtidiellum sp. N					
Eucyrtidiellum sp. O					
Eucyrtidiellum sp. P					
Eucyrtidiellum sp. Q					
Eucyrtidiellum sp. R					
Eucyrtidiellum sp. S					
Eucyrtidiellum sp. T					
Eucyrtidiellum sp. U					
Eucyrtidiellum sp. V					
Eucyrtidiellum sp. W					
Eucyrtidiellum sp. X					
Eucyrtidiellum sp. Y					
Eucyrtidiellum sp. Z					
Eucyrtidiellum sp. AA					
Eucyrtidiellum sp. AB					
Eucyrtidiellum sp. AC					
Eucyrtidiellum sp. AD					
Eucyrtidiellum sp. AE					
Eucyrtidiellum sp. AF					
Eucyrtidiellum sp. AG					
Eucyrtidiellum sp. AH					
Eucyrtidiellum sp. AI					
Eucyrtidiellum sp. AJ					
Eucyrtidiellum sp. AK					
Eucyrtidiellum sp. AL					
Eucyrtidiellum sp. AM					
Eucyrtidiellum sp. AN					
Eucyrtidiellum sp. AO					
Eucyrtidiellum sp. AP					
Eucyrtidiellum sp. AQ					
Eucyrtidiellum sp. AR					
Eucyrtidiellum sp. AS					
Eucyrtidiellum sp. AT					
Eucyrtidiellum sp. AU					
Eucyrtidiellum sp. AV					
Eucyrtidiellum sp. AW					
Eucyrtidiellum sp. AX					
Eucyrtidiellum sp. AY					
Eucyrtidiellum sp. AZ					
Eucyrtidiellum sp. BA					
Eucyrtidiellum sp. BB					
Eucyrtidiellum sp. BC					
Eucyrtidiellum sp. BD					
Eucyrtidiellum sp. BE					
Eucyrtidiellum sp. BF					
Eucyrtidiellum sp. BG					
Eucyrtidiellum sp. BH					
Eucyrtidiellum sp. BI					
Eucyrtidiellum sp. BJ					
Eucyrtidiellum sp. BK					
Eucyrtidiellum sp. BL					
Eucyrtidiellum sp. BM					
Eucyrtidiellum sp. BN					
Eucyrtidiellum sp. BO					
Eucyrtidiellum sp. BP					
Eucyrtidiellum sp. BQ					
Eucyrtidiellum sp. BR					
Eucyrtidiellum sp. BS					
Eucyrtidiellum sp. BT					
Eucyrtidiellum sp. BU					
Eucyrtidiellum sp. BV					
Eucyrtidiellum sp. BW					
Eucyrtidiellum sp. BX					
Eucyrtidiellum sp. BY					
Eucyrtidiellum sp. BZ					
Eucyrtidiellum sp. CA					
Eucyrtidiellum sp. CB					
Eucyrtidiellum sp. CC					
Eucyrtidiellum sp. CD					
Eucyrtidiellum sp. CE					
Eucyrtidiellum sp. CF					
Eucyrtidiellum sp. CG					
Eucyrtidiellum sp. CH					
Eucyrtidiellum sp. CI					
Eucyrtidiellum sp. CJ					
Eucyrtidiellum sp. CK					
Eucyrtidiellum sp. CL					
Eucyrtidiellum sp. CM					
Eucyrtidiellum sp. CN					
Eucyrtidiellum sp. CO					
Eucyrtidiellum sp. CP					
Eucyrtidiellum sp. CQ					
Eucyrtidiellum sp. CR					
Eucyrtidiellum sp. CS					
Eucyrtidiellum sp. CT					
Eucyrtidiellum sp. CU					
Eucyrtidiellum sp. CV					
Eucyrtidiellum sp. CW					
Eucyrtidiellum sp. CX					
Eucyrtidiellum sp. CY					
Eucyrtidiellum sp. CZ					
Eucyrtidiellum sp. DA					
Eucyrtidiellum sp. DB					
Eucyrtidiellum sp. DC					
Eucyrtidiellum sp. DD					
Eucyrtidiellum sp. DE					
Eucyrtidiellum sp. DF					
Eucyrtidiellum sp. DG					
Eucyrtidiellum sp. DH					
Eucyrtidiellum sp. DI					
Eucyrtidiellum sp. DJ					
Eucyrtidiellum sp. DK					
Eucyrtidiellum sp. DL					
Eucyrtidiellum sp. DM					
Eucyrtidiellum sp. DN					
Eucyrtidiellum sp. DO					
Eucyrtidiellum sp. DP					
Eucyrtidiellum sp. DQ					
Eucyrtidiellum sp. DR					
Eucyrtidiellum sp. DS					
Eucyrtidiellum sp. DT					
Eucyrtidiellum sp. DU					
Eucyrtidiellum sp. DV					
Eucyrtidiellum sp. DW					
Eucyrtidiellum sp. DX					
Eucyrtidiellum sp. DY					
Eucyrtidiellum sp. DZ					
Eucyrtidiellum sp. EA					
Eucyrtidiellum sp. EB					
Eucyrtidiellum sp. EC					
Eucyrtidiellum sp. ED					
Eucyrtidiellum sp. EE					
Eucyrtidiellum sp. EF					
Eucyrtidiellum sp. EG					
Eucyrtidiellum sp. EH					
Eucyrtidiellum sp. EI					
Eucyrtidiellum sp. EJ					
Eucyrtidiellum sp. EK					
Eucyrtidiellum sp. EL					
Eucyrtidiellum sp. EM					
Eucyrtidiellum sp. EN					
Eucyrtidiellum sp. EO					
Eucyrtidiellum sp. EP					
Eucyrtidiellum sp. EQ					
Eucyrtidiellum sp. ER					
Eucyrtidiellum sp. ES					
Eucyrtidiellum sp. ET					
Eucyrtidiellum sp. EU					
Eucyrtidiellum sp. EV					
Eucyrtidiellum sp. EW					
Eucyrtidiellum sp. EX					
Eucyrtidiellum sp. EY					
Eucyrtidiellum sp. EZ					
Eucyrtidiellum sp. FA					
Eucyrtidiellum sp. FB					
Eucyrtidiellum sp. FC					
Eucyrtidiellum sp. FD					
Eucyrtidiellum sp. FE					
Eucyrtidiellum sp. FF					
Eucyrtidiellum sp. FG					
Eucyrtidiellum sp. FH					
Eucyrtidiellum sp. FI					
Eucyrtidiellum sp. FJ					
Eucyrtidiellum sp. FK					
Eucyrtidiellum sp. FL					
Eucyrtidiellum sp. FM					
Eucyrtidiellum sp. FN					
Eucyrtidiellum sp. FO					
Eucyrtidiellum sp. FP					
Eucyrtidiellum sp. FQ					
Eucyrtidiellum sp. FR					
Eucyrtidiellum sp. FS					
Eucyrtidiellum sp. FT					
Eucyrtidiellum sp. FU					
Eucyrtidiellum sp. FV					
Eucyrtidiellum sp. FW					
Eucyrtidiellum sp. FX					
Eucyrtidiellum sp. FY					
Eucyrtidiellum sp. FZ					
Eucyrtidiellum sp. GA					
Eucyrtidiellum sp. GB					
Eucyrtidiellum sp. GC					
Eucyrtidiellum sp. GD					
Eucyrtidiellum sp. GE					
Eucyrtidiellum sp. GF					
Eucyrtidiellum sp. GG					
Eucyrtidiellum sp. GH					
Eucyrtidiellum sp. GI					
Eucyrtidiellum sp. GJ					
Eucyrtidiellum sp. GK					
Eucyrtidiellum sp. GL					
Eucyrtidiellum sp. GM					
Eucyrtidiellum sp. GN					
Eucyrtidiellum sp. GO					
Eucyrtidiellum sp. GP					
Eucyrtidiellum sp. GQ					
Eucyrtidiellum sp. GR					
Eucyrtidiellum sp. GS					
Eucyrtidiellum sp. GT					
Eucyrtidiellum sp. GU					
Eucyrtidiellum sp. GV					
Eucyrtidiellum sp. GW					
Eucyrtidiellum sp. GX					
Eucyrtidiellum sp. GY					
Eucyrtidiellum sp. GZ					
Eucyrtidiellum sp. HA					
Eucyrtidiellum sp. HB					
Eucyrtidiellum sp. HC					
Eucyrtidiellum sp. HD					
Eucyrtidiellum sp. HE					
Eucyrtidiellum sp. HF					
Eucyrtidiellum sp. HG					
Eucyrtidiellum sp. HH					
Eucyrtidiellum sp. HI					
Eucyrtidiellum sp. HJ					
Eucyrtidiellum sp. HK					
Eucyrtidiellum sp. HL					
Eucyrtidiellum sp. HM					
Eucyrtidiellum sp. HN					
Eucyrtidiellum sp. HO					
Eucyrtidiellum sp. HP					
Eucyrtidiellum sp. HQ					
Eucyrtidiellum sp. HR					
Eucyrtidiellum sp. HS					
Eucyrtidiellum sp. HT					
Eucyrtidiellum sp. HU					
Eucyrtidiellum sp. HV					
Eucyrtidiellum sp. HW					
Eucyrtidiellum sp. HX					
Eucyrtidiellum sp. HY					
Eucyrtidiellum sp. HZ					
Eucyrtidiellum sp. IA					
Eucyrtidiellum sp. IB					
Eucyrtidiellum sp. IC					
Eucyrtidiellum sp. ID					
Eucyrtidiellum sp. IE					
Eucyrtidiellum sp. IF					
Eucyrtidiellum sp. IG					
Eucyrtidiellum sp. IH					
Eucyrtidiellum sp. II					
Eucyrtidiellum sp. IJ					
Eucyrtidiellum sp. IK					
Eucyrtidiellum sp. IL					
Eucyrtidiellum sp. IM					
Eucyrtidiellum sp. IN					
Eucyrtidiellum sp. IO					
Eucyrtidiellum sp. IP					
Eucyrtidiellum sp. IQ					
Eucyrtidiellum sp. IR					
Eucyrtidiellum sp. IS					
Eucyrtidiellum sp. IT					
Eucyrtidiellum sp. IU					
Eucyrtidiellum sp. IV					
Eucyrtidiellum sp. IW					
Eucyrtidiellum sp. IX					
Eucyrtidiellum sp. IY					
Eucyrtidiellum sp. IZ					
Eucyrtidiellum sp. JA					
Eucyrtidiellum sp. JB					
Eucyrtidiellum sp. JC					
Eucyrtidiellum sp. JD					
Eucyrtidiellum sp. JE					
Eucyrtidiellum sp. JF					
Eucyrtidiellum sp. JG					
Eucyrtidiellum sp. JH					
Eucyrtidiellum sp. JI					
Eucyrtidiellum sp. JJ					
Eucyrtidiellum sp. JK					
Eucyrtidiellum sp. JL					
Eucyrtidiellum sp. JM					
Eucyrtidiellum sp. JN					
Eucyrtidiellum sp. JO					
Eucyrtidiellum sp. JP					
Eucyrtidiellum sp. JQ					
Eucyrtidiellum sp. JR					
Eucyrtidiellum sp. JS					
Eucyrtidiellum sp. JT					
Eucyrtidiellum sp. JU					
Eucyrtidiellum sp. JV					
Eucyrtidiellum sp. JW					
Eucyrtidiellum sp. JX					
Eucyrtidiellum sp. JY					
Eucyrtidiellum sp. JZ					
Eucyrtidiellum sp. KA					
Eucyrtidiellum sp. KB					
Eucyrtidiellum sp. KC					
Eucyrtidiellum sp. KD					
Eucyrtidiellum sp. KE					
Eucyrtidiellum sp. KF					
Eucyrtidiellum sp. KG					
Eucyrtidiellum sp. KH					
Eucyrtidiellum sp. KI					
Eucyrtidiellum sp. KJ					
Eucyrtidiellum sp. KK					
Eucyrtidiellum sp. KL					
Eucyrtidiellum sp. KM					
Eucyrtidiellum sp. KN					
Eucyrtidiellum sp. KO					
Eucyrtidiellum sp. KP					
Eucyrtidiellum sp. KQ					
Eucyrtidiellum sp. KR					
Eucyrtidiellum sp. KS					
Eucyrtidiellum sp. KT					
Eucyrtidiellum sp. KU					
Eucyrtidiellum sp. KV					
Eucyrtidiellum sp. KW					
Eucyrtidiellum sp. KX					
Eucyrtidiellum sp. KY					
Eucyrtidiellum sp. KZ					
Eucyrtidiellum sp. LA					
Eucyrtidiellum sp. LB					
Eucyrtidiellum sp. LC					
Eucyrtidiellum sp. LD					
Eucyrtidiellum sp. LE					
Eucyrtidiellum sp. LF					
Eucyrtidiellum sp. LG					
Eucyrtidiellum sp. LH					
Eucyrtidiellum sp. LI					
Eucyrtidiellum sp. LJ					
Eucyrtidiellum sp. LK					
Eucyrtidiellum sp. LL					
Eucyrtidiellum sp. LM					
Eucyrtidiellum sp. LN					
Eucyrtidiellum sp. LO					
Eucyrtidiellum sp. LP					
Eucyrtidiellum sp. LQ					
Eucyrtidiellum sp. LR					
Eucyrtidiellum sp. LS					
Eucyrtidiellum sp. LT					
Eucyrtidiellum sp. LU					
Eucyrtidiellum sp. LV					
Eucyrtidiellum sp. LW					
Eucyrtidiellum sp. LX					
Eucyrtidiellum sp. LY					
Eucyrtidiellum sp. LZ					
Eucyrtidiellum sp. MA					
Eucyrtidiellum sp. MB					
Eucyrtidiellum sp. MC					
Eucyrtidiellum sp. MD					
Eucyrtidiellum sp. ME					
Eucyrtidiellum sp. MF					
Eucyrtidiellum sp. MG					
Eucyrtidiellum sp. MH					
Eucyrtidiellum sp. MI					
Eucyrtidiellum sp. MJ					
Eucyrtidiellum sp. MK					
Eucyrtidiellum sp. ML					
Eucyrtidiellum sp. MM					
Eucyrtidiellum sp. MN					
Eucyrtidiellum sp. MO					
Eucyrtidiellum sp. MP					
Eucyrtidiellum sp. MQ					
Eucyrtidiellum sp. MR					
Eucyrtidiellum sp. MS					
Eucyrtidiellum sp. MT					
Eucyrtidiellum sp. MU					
Eucyrtidiellum sp. MV					
Eucyrtidiellum sp. MW					
Eucyrtidiellum sp. MX					
Eucyrtidiellum sp. MY					
Eucyrtidiellum sp. MZ					
Eucyrtidiellum sp. NA					
Eucyrtidiellum sp. NB					
Eucyrtidiellum sp. NC					
Eucyrtidiellum sp. ND					
Eucyrtidiellum sp. NE					
Eucyrtidiellum sp. NF					
Eucyrtidiellum sp. NG					
Eucyrtidiellum sp. NH					
Eucyrtidiellum sp. NI					
Eucyrtidiellum sp. NJ					
Eucyrtidiellum sp. NK					
Eucyrtidiellum sp. NL					
Eucyrtidiellum sp. NM					
Eucyrtidiellum sp. NN					
Eucyrtidiellum sp. NO					
Eucyrtidiellum sp. NP					
Eucyrtidiellum sp. NQ					
Eucyrtidiellum sp. NR					
Eucyrtidiellum sp. NS					
Eucyrtidiellum sp. NT					
Eucyrtidiellum sp. NU					
Eucyrtidiellum sp. NV					
Eucyrtidiellum sp. NW					
Eucyrtidiellum sp. NX					
Eucyrtidiellum sp. NY					
Eucyrtidiellum sp. NZ					
Eucyrtidiellum sp. OA					
Eucyrtidiellum sp. OB					
Eucyrtidiellum sp. OC					
Eucyrtidiellum sp. OD					
Eucyrtidiellum sp. OE					
Eucyrtidiellum sp. OF					
Eucyrtidiellum sp. OG					
Eucyrtidiellum sp. OH					
Eucyrtidiellum sp. OI					
Eucyrtidiellum sp. OJ					
Eucyrtidiellum sp. OK					
Eucyrtidiellum sp. OL					
Eucyrtidiellum sp. OM					
Eucyrtidiellum sp. ON					
Eucyrtidiellum sp. OO					
Eucyrtidiellum sp. OP					
Eucyrtidiellum sp. OQ					
Eucyrtidiellum sp. OR					
Eucyrtidiellum sp. OS					
Eucyrtidiellum sp. OT					
Eucyrtidiellum sp. OU					
Eucyrtidiellum sp. OV					
Eucyrtidiellum sp. OW					
Eucyrtidiellum sp. OX					
Eucyrtidiellum sp. OY					
Eucyrtidiellum sp. OZ					
Eucyrtidiellum sp. PA					
Eucyrtidiellum sp. PB					
Eucyrtidiellum sp. PC					
Eucyrtidiellum sp. PD					
Eucyrtidiellum sp. PE					
Eucyrtidiellum sp. PF					
Eucyrtidiellum sp. PG					
Eucyrtidiellum sp. PH					
Eucyrtidiellum sp. PI					
Eucyrtidiellum sp. PJ					
Eucyrtidiellum sp. PK					
Eucyrtidiellum sp. PL					
Eucyrtidiellum sp. PM					
Eucyrtidiellum sp. PN					
Eucyrtidiellum sp. PO					
Eucyrtidiellum sp. PP					
Eucyrtidiellum sp. PQ					
Eucyrtidiellum sp. PR					
Eucyrtidiellum sp. PS					
Eucyrtidiellum sp. PT					
Eucyrtidiellum sp. PU					
Eucyrtidiellum sp. PV					
Eucyrtidiellum sp. PW					
Eucyrtidiellum sp. PX					
Eucyrtidiellum sp. PY					
Eucyrtidiellum sp. PZ					
Eucyrtidiellum sp. QA					
Eucyrtidiellum sp. QB					
Eucyrtidiellum sp. QC					
Eucyrtidiellum sp. QD					
Eucyrtidiellum sp. QE					
Eucyrtidiellum sp. QF					
Eucyrtidiellum sp. QG					
Eucyrtidiellum sp. QH					
Eucyrtidiellum sp. QI					
Eucyrtidiellum sp. QJ					
Eucyrtidiellum sp. QK					
Eucyrtidiellum sp. QL					
Eucyrtidiellum sp. QM					
Eucyrtidiellum sp. QN					
Eucyrtidiellum sp. QO					
Eucyrtidiellum sp. QP					
Eucyrtidiellum sp. QQ					
Eucyrtidiellum sp. QR					
Eucyrtidiellum sp. QS					
Eucyrtidiellum sp. QT					
Eucyrtidiellum sp. QU					
Eucyrtidiellum sp. QV					
Eucyrtidiellum sp. QW					
Eucyrtidiellum sp. QX					
Eucyrtidiellum sp. QY					
Eucyrtidiellum sp. QZ					
Eucyrtidiellum sp. RA					
Eucyrtidiellum sp. RB					
Eucyrtidiellum sp. RC					
Eucyrtidiellum sp. RD					
Eucyrtidiellum sp. RE					
Eucyrtidiellum sp. RF					
Eucyrtidiellum sp. RG					
Eucyrtidiellum sp. RH					
Eucyrtidiellum sp. RI					
Eucyrtidiellum sp. RJ					
Eucyrtidiellum sp. RK					
Eucyrtidiellum sp. RL					
Eucyrtidiellum sp. RM					
Eucyrtidiellum sp. RN					
Eucyrtidiellum sp. RO					
Eucyrtidiellum sp. RP					
Eucyrtidiellum sp. RQ					
Eucyrtidiellum sp. RR					
Eucyrtidiellum sp. RS					
Eucyrtidiellum sp. RT					
Eucyrtidiellum sp. RU					
Eucyrtidiellum sp. RV					
Eucyrtidiellum sp. RW					
Eucyrtidiellum sp. RX					
Eucyrtidiellum sp. RY					
Eucyrtidiellum sp. RZ					
Eucyrtidiellum sp. SA					
Eucyrtidiellum sp. SB					
Eucyrtidiellum sp. SC					
Eucyrtidiellum sp. SD					
Eucyrtidiellum sp. SE					
Eucyrtidiellum sp. SF					
Eucyrtidiellum sp. SG					
Eucyrtidiellum sp. SH					
Eucyrtidiellum sp. SI					
Eucyrtidiellum sp. SJ					
Eucyrtidiellum sp. SK					
Eucyrtidiellum sp. SL					
Eucyrtidiellum sp. SM					
Eucyrtidiellum sp. SN					
Eucyrtidiellum sp. SO					
Eucyrtidiellum sp. SP					
Eucyrtidiellum sp. SQ					
Eucyrtidiellum sp. SR					
Eucyrtidiellum sp. SS					
Eucyrtidiellum sp. ST					
Eucyrtidiellum sp. SU					
Eucyrtidiellum sp. SV					
Eucyrtidiellum sp. SW					
Eucyrtidiellum sp. SX					
Eucyrtidiellum sp. SY					
Eucyrtidiellum sp. SZ					
Eucyrtidiellum sp. TA					
Eucyrtidiellum sp. TB					
Eucyrtidiellum sp. TC					
Eucyrtidiellum sp. TD					
Eucyrtidiellum sp. TE					
Eucyrtidiellum sp. TF					
Eucyrtidiellum sp. TG					
Eucyrtidiellum sp. TH					
Eucyrtidiellum sp. TI					
Eucyrtidiellum sp. TJ					
Eucyrtidiellum sp. TK					
Eucyrtidiellum sp. TL					
Eucyrtidiellum sp. TM					
Eucyrtidiellum sp. TN					
Eucyrtidiellum sp. TO					
Eucyrtidiellum sp. TP					
Eucyrtidiellum sp. TQ					
Eucyrtidiellum sp. TR					
Eucyrtidiellum sp. TS					
Eucyrtidiellum sp. TT					
Eucyrtidiellum sp. TU					
Eucyrtidiellum sp. TV					
Eucyrtidiellum sp. TW					
Eucyrtidiellum sp. TX					
Eucyrtidiellum sp. TY					
Eucyrtidiellum sp. TZ					
Eucyrtidiellum sp. UA					
Eucyrtidiellum sp. UB					
Eucyrtidiellum sp. UC					
Eucyrtidiellum sp. UD					
Eucyrtidiellum sp. UE					
Eucyrtidiellum sp. UF					
Eucyrtidiellum sp. UG					
Eucyrtidiellum sp. UH					
Eucyrtidiellum sp. UI					
Eucyrtidiellum sp. UJ					
Eucyrtidiellum sp. UK					
Eucyrtidiellum sp. UL					
Eucyrtidiellum sp. UM					
Eucyrtidiellum sp. UN					
Eucyrtidiellum sp. UO					
Eucyrtidiellum sp. UP					
Eucyrtidiellum sp. UQ					
Eucyrtidiellum sp. UR					
Eucyrtidiellum sp. US					
Eucyrtidiellum sp. UT					
Eucyrtidiellum sp. UU					
Eucyrtidiellum sp. UV					
Eucyrtidiellum sp. UW					
Eucyrtidiellum sp. UX					
Eucyrtidiellum sp. UY					
Eucyrtidiellum sp. UZ					
Eucyrtidiellum sp. VA					
Eucyrtidiellum sp. VB					
Eucyrtidiellum sp. VC					
Eucyrtidiellum sp. VD					
Eucyrtidiellum sp. VE					
Eucyrtidiellum sp. VF					
Eucyrtidiellum sp. VG					
Eucyrtidiellum sp. VH					
Eucyrtidiellum sp. VI					
Eucyrtidiellum sp. VJ					
Eucyrtidiellum sp. VK					
Eucyrtidiellum sp. VL					
Eucyrtidiellum sp. VM					
Eucyrtidiellum sp. VN					
Eucyrtidiellum sp. VO					
Eucyrtidiellum sp. VP					
Eucyrtidiellum sp. VQ					
Eucyrtidiellum sp. VR					
Eucyrtidiellum sp. VS					
Eucyrtidiellum sp. VT					
Eucyrtidiellum sp. VU					
Eucyrtidiellum sp. VV					
Eucyrtidiellum sp. VW					
Eucyrtidiellum sp. VX					
Eucyrtidiellum sp. VY					
Eucyrtidiellum sp. VZ					
Eucyrtidiellum sp. WA					
Eucyrtidiellum sp. WB					
Eucyrtidiellum sp. WC					
Eucyrtidiellum sp. WD					
Eucyrtidiellum sp. WE					
Eucyrtidiellum sp. WF					
Eucyrtidiellum sp. WG					
Eucyrtidiellum sp. WH					
Eucyrtidiellum sp. WI					
Eucyrtidiellum sp. WJ					
Eucyrtidiellum sp. WK					
Eucyrtidiellum sp. WL					
*Eucyrtidiellum

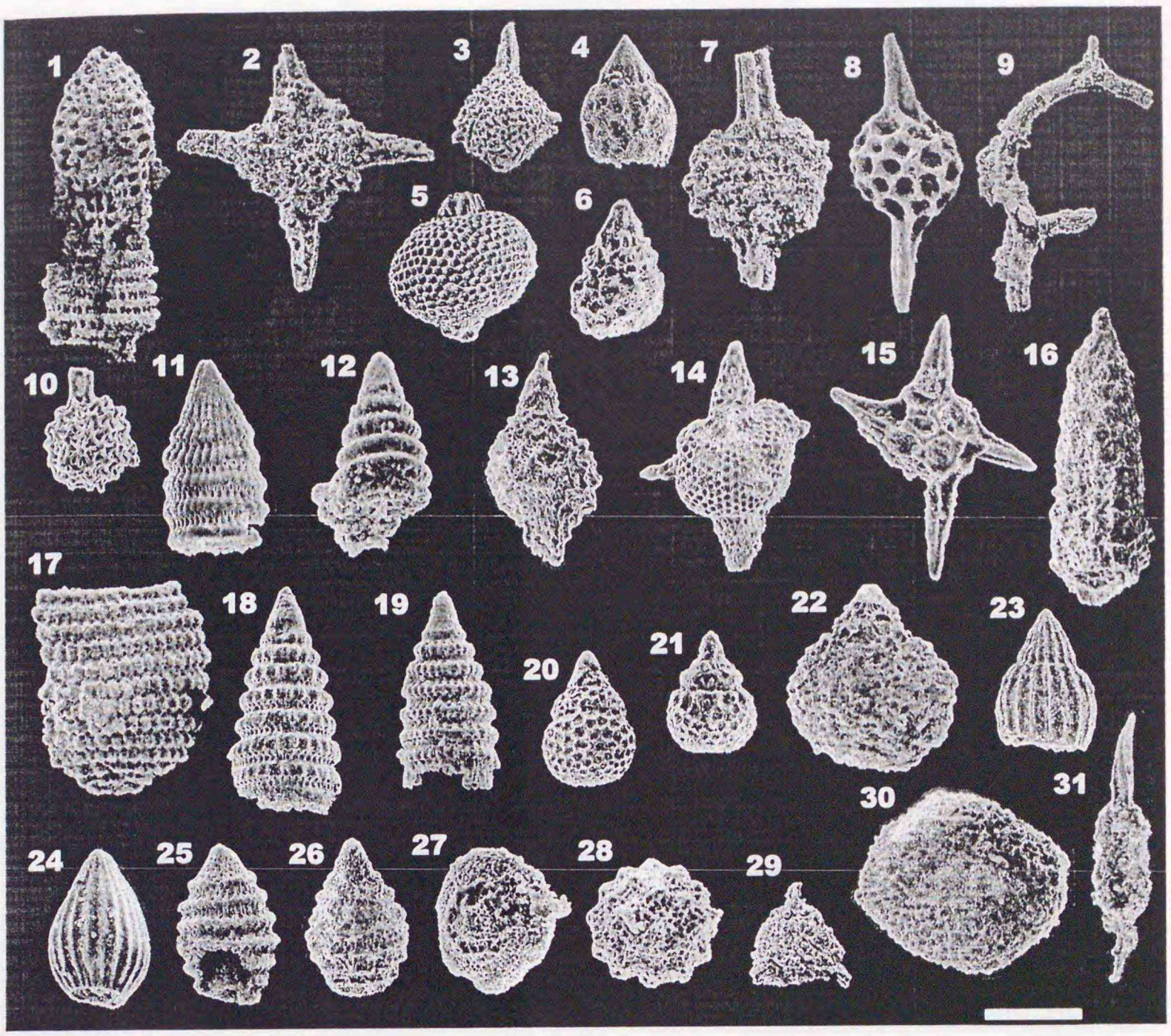


Fig. 5 Radiolarian fossils from the MN-Unit of the Naizawa Complex and the MH-Unit of the Horobetsugawa Complex. SEM photographs. Scale bars: 80m for figs. 3-6 and 29; 100m for 1, 2, 7-13, 18-28, 30, 31; 150m for 14 and 17.

1-16: MN-Unit, Naizawa Complex
1 : *Ristola cretacea* (Baumgartner) sample R2
2 : *Emiluvia* cf. *chica* Foreman sample R2
3 : *Staurocyclia* cf. *martini* Rüst sample R2
4 : *Eucyrtidiellum pyramis* (Aita) sample R2
5 : *Hemicryptocapsa* cf. *capita* Tan sample R2
6 : *Sethocapsa kaminogoensis* Aita sample R2
7 : *Acaeniotyle umbilicata* (Rüst) sample R2
8 : *Pantanellium squinaboli* (Tan) sample R2
9 : *Acanthocircus trizonalis* (Rüst) sample R2
10: *Alievium* cf. *helenae* Schaaf sample R1
11: *Pseudodictyomitra leptoconica* (Foreman) sample R1
12: *Pseudodictyomitra lilyae* (Tan) sample R1
13: *Eucyrtis bulbosus* Renz sample R1
14: *Podobursa* (?) sp. sample R1
15: *Cecrops septemporatus* (Parona) sample R1
16: *Xitus* cf. *alievi* (Foreman) sample R3

17-20: MH-Unit, Horobetsugawa Complex.
17: *Mirifusus* cf. *mediodilatatus* (Rüst) sample R4
18: *Pseudodictyomitra carpatica* (Lozyniak) sample R4
19: *Wrangellium puga* (Schaaf) sample R4
20: *Sethocapsa* (?) *zweilli* Jud sample R4
21: *Sethocapsa uterculus* (Parona) sample R4
22: *Sethocapsa* cf. *trachyostraca* Foreman sample R4
23: *Thanarla pulchra* (Squinabol) sample R4
24: *Thanarla conica* (Aliev) sample R4
25: *Parvicingula boesii* (Parona) sample R4
26: *Parvicingula usotanensis* Tumanda sample R4
27: *Patellula planoconvexa* (Pessagno) sample R5
28: *Praeconocaryomma universa* Pessagno sample R5
29: *Alievium superbum* (Squinabol) sample R5
30: *Orbiculiforma* cf. *quadrata* Pessagno sample R5
31: *Archaeospongoprunum* cf. *triplum* Pessagno sample R5

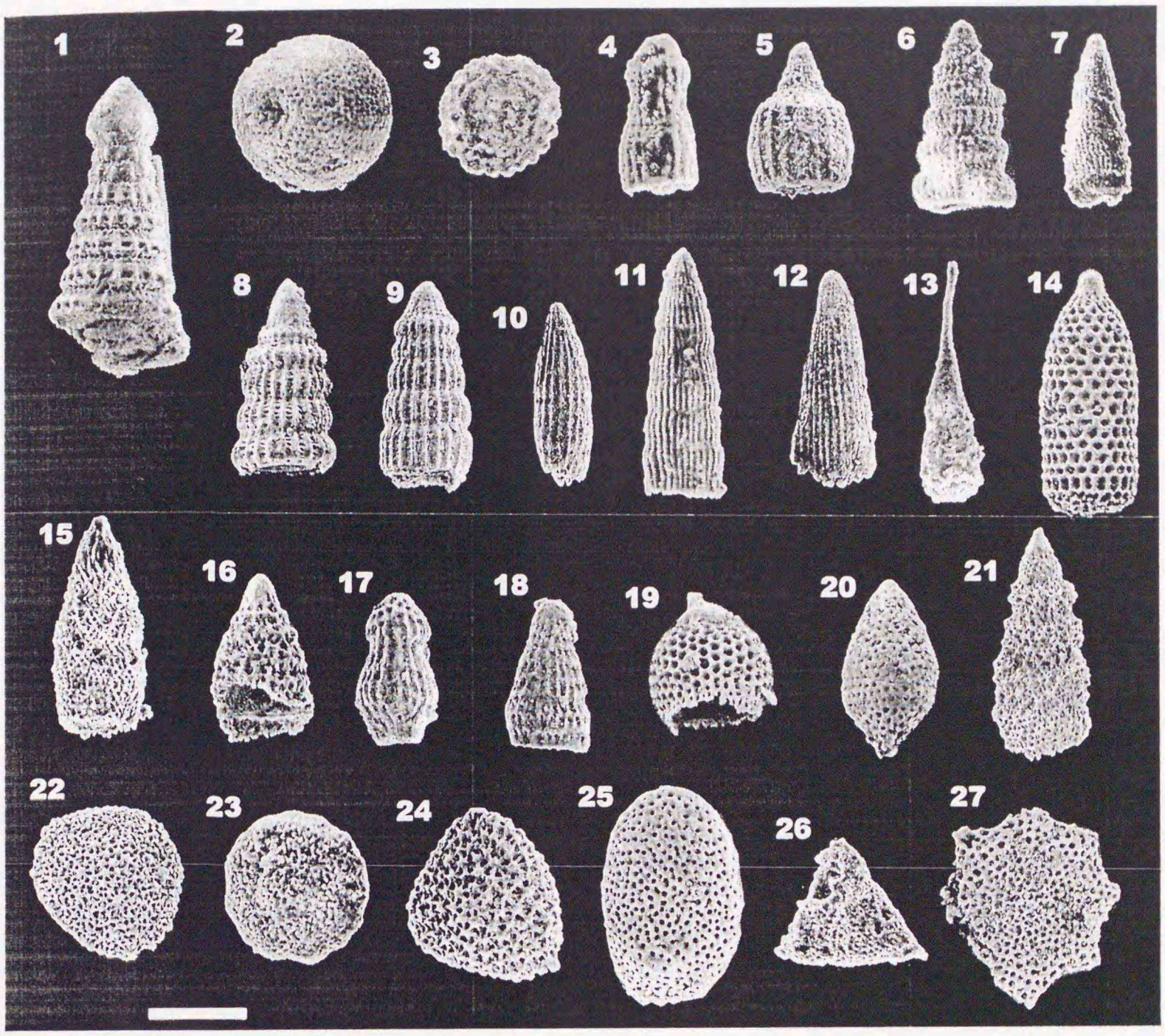


Fig. 6. Radiolarian fossils from the PT-Unit, Horobetsugawa Complex. SEM photographs. Scale bar: 80 m for figs. 3, 4, 6, 10, 13, 17, 18, 20, 26; 100 m for 2, 5, 7-9, 11, 12, 14-16, 19, 21-25, 27; 150 m for 1.

1-6: sample R6, red siliceous mudstone
1 : *Pseudodictyomitra pseudomacrocephala* (Squinabol)
2 : *Holocryptocanium barbui japonicum* (Nakaseko and Nishimura)
3 : *Holocryptocanium geysersensis* Pessagno
4 : *Thanarla veneta* (Squinabol)
5 : *Thanarla elegantissima* (Cita)
6-32: black mudstone and siliceous mudstone
6 : *Dictyomitra multicostata* Zittel sample R15
7 : *Dictyomitra andersoni* (Campbell and Clark) sample R14
8 : *Dictyomitra formosa* Squinabol sample R9
9: *Dictyomitra koslovae* Foreman sample R10
10: *Archaeodictyomitra rhadina* (Foreman) sample R9
11: *Archaeodictyomitra* aff. *lamellicostata* (Foreman) sample R14
12: *Mita regina* (Campbell and Clark) sample R9
13: *Cornutella californica* Campbell and Clark sample R11
14: *Amphipyndax stocki* (Campbell and Clark) sample R10
15: *Amphipyndax tylotus* Foreman sample R10
16: *Amphipyndax* cf. *pseudoconulus* (Pessagno) sample R8
17: *Theocampe lipsa* Foreman sample R9
18: *Theocampe altamontensis* (Campbell and Clark) sample R10
19: *Rhopalosyringium magnificum* Campbell and Clark sample R9
20: *Stichomitra livermorensis* (Campbell and Clark) sample R9
21: *Stichomitra asymbatos* Foreman sample R10
22: *Pseudoaulophacus floresensis* Pessagno sample R8
23: *Pseudoaulophacus parqueraensis* Pessagno sample R16
24: *Alievium gallowayi* (White) sample R9
25: *Phaseliforma concentrica* (Lipman) sample R9
26: *Spongotripus morenoensis* Campbell and Clark sample R15
27: *Orbiculiforma sacramentoensis* Pessagno sample R9

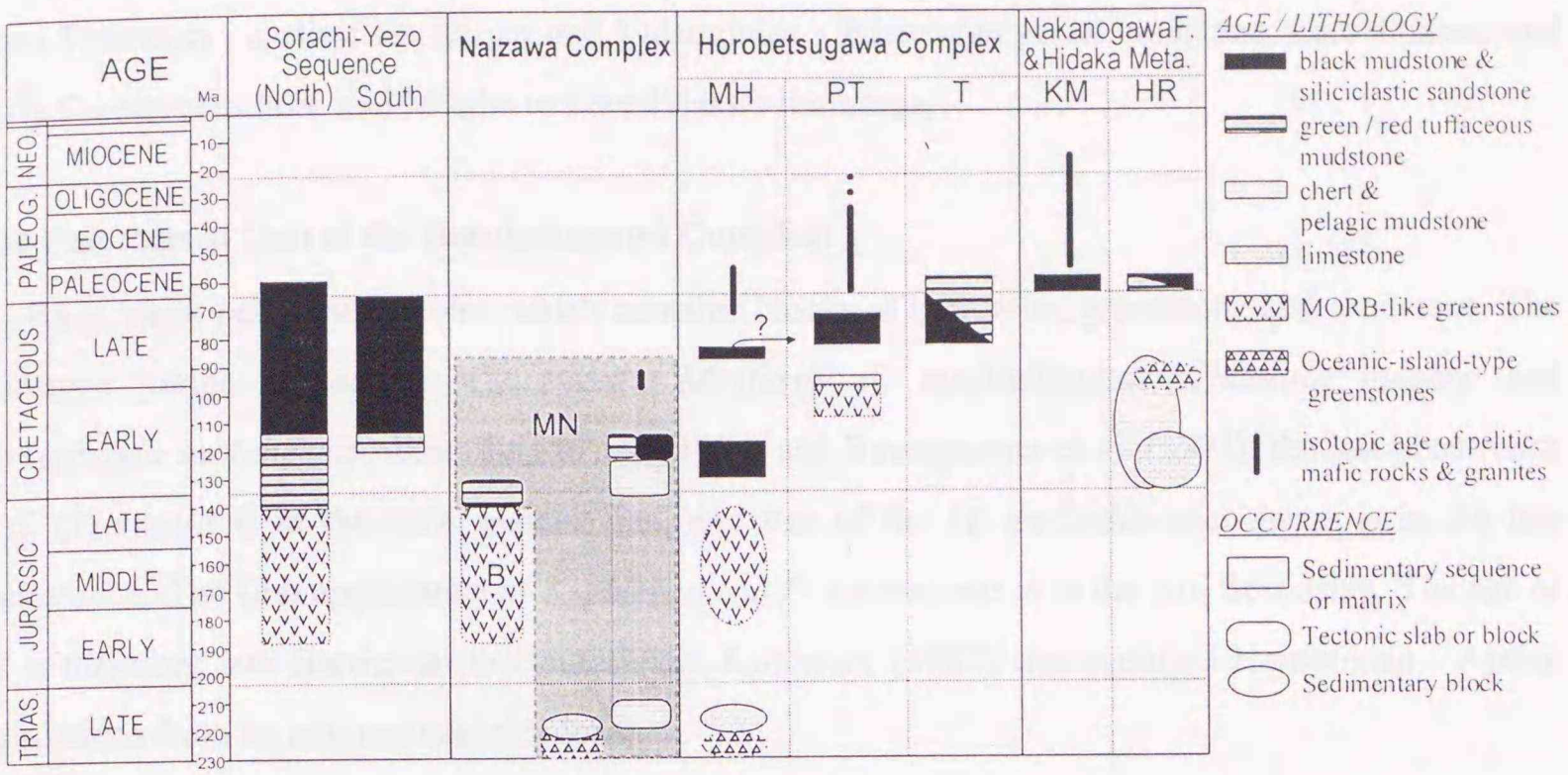


Fig. 7. Compilation of fossil and isotopic ages from the Idonnappu Zone and adjacent units. Columns with dotted lines indicate inferred ages. KM: Kamitoyoni Formation, and HR: Hiroo Complex (Nanayama, 1992). Ages from surrounding areas after Kanie et al. (1981), Taketani (1982), Maeda et al. (1986), Owada et al. (1991, 1992), Kiyokawa (1992), Nanayama (1992), Ota et al. (1993), Hori and Sakakibara (1994), Watanabe et al. (1994), Mitsugi and Hirano (1997), and Nanayama and Ganzawa (1997).

thus a mixture of late Valanginian - early Barremian black mudstone and accompanying turbidite, latest Tithonian - earliest Berriasian and Valanginian - Barremian green mudstone, Late Triassic and Early Cretaceous chert, and Middle to Late Triassic limestone.

MH-Unit (Mixed Unit of the Horobetsugawa Complex)

R4 is black pebbly mudstone, which contains blocks of limestone, greenstone and sandstone. The mudstone yields *Sethocapsa* (?) *zweilli*, *Mirifusus* cf. *mediodilatatus*, *Thanarla pulchra* and *Parvicingula usotanensis*. According to Jud (1994) and Baumgartner et al. (1995), the last occurrence of *S.* (?) *zweilli* is in the early Hauterivian, and that of the *M. mediodilatatus* group is in the late Hauterivian. The first appearance of *T. pulchra* and *P. usotanensis* is in the late Berriasian. The age of R4 is therefore late Berriasian to Hauterivian. Kiminami (1987) also reported Hauterivian - Aptian radiolarians from an outcrop near this locality.

R5 is bedded black siliceous mudstone from the outcrop just below the limestone block contained in the uppermost horizon of the MH-Unit. This locality was previously assigned to the PT-Unit by Ueda et al. (1993). The siliceous mudstone yields *Alievium superbum, Praeconocaryomma universa, Orbiculiforma* cf. *quadrata*, and *Archaeospongoprunum* cf. *triplum*. According to Pessagno (1976) and Taketani (1982), *A. superbum* ranges from middle Turonian to Campanian, *P. universa* from Coniacian to middle Campanian, *O. quadrata* from Coniacian to Santonian, and *A. triplum* in Coniacian. The assemblage in R5 thus indicates a Coniacian to possibly Santonian age Igo et al. (1980) reported Late Triassic (Norian) conodonts from a limestone block in the MH-Unit.

The MH-Unit is thus a mixture of late Berriasian - Aptian and Coniacian - Santonian black mudstone, and Late Triassic limestone. The age of included chert blocks remains unknown.

PT-Unit (Pelagic to Terrigenous Unit)

R6 is red siliceous mudstone interbedded with green and dark gray siliceous mudstone overlying a greenstone body. R6 yields the radiolarians *Thanarla elegantissima*, *T. veneta* and *Pseudodictyomitra pseudomacrocephala*. *Thanarla elegantissima* disappeared in the early Cenomanian, *T. veneta* in the latest Cenomanian, and *P. pseudomacrocephala* in the earliest Turonian (Sanfilippo and Riedel, 1985; Schaaf, 1985; Taketani, 1995). According to Sanfilippo and Riedel (1985) and Schaaf (1985), *P. pseudomacrocephala* and *T. veneta* have their first appearance in the latest Albian. Therefore, the age of R6 is concluded to range from latest Albian to early Cenomanian.

R7 is black mudstone containing an assemblage of latest Jurassic to Early Cretaceous radiolarians (*Pseudodictyomitra carpatica*, *Wrangellium puga*, *Thanarla conica* and others). Short-range species are absent.

Samples R8 to R16 are black mudstone, black siliceous mudstone, and intercalated acidic tuff.

Samples R10 to R13 were taken from horizons below the MH-Unit, and the others from horizons above it. All have Late Cretaceous assemblages. R9 yields the radiolarians *Dictyomitra koslovae*, *D. formosa*, and *Amphipyndax* cf. *pseudoconulus*. According to Taketani (1982, 1995), *D. koslovae* ranges from early Santonian to late Campanian, *D. formosa* from middle Turonian to early Campanian, and *A. pseudoconulus* from early Campanian to middle-late Campanian. Therefore, R9 is of early Campanian age.

R8, R10, R14 and R15 contain *Amphipyndax tylotus*, which ranges from late Campanian to Maastrichtian (Foreman, 1978; Sanfilippo and Riedel, 1985). *Dictyomitra koslovae* also occurs in all samples except R15. Therefore, the ages of R8, R10 and R14 are concluded to be late Campanian, and the age of R15 is late Campanian to possibly early Maastrichtian.

R11 and R16 contain *D. koslovae*, and hence are of Santonian - Campanian age. Kiminami (1987) also reported Campanian - Maastrichtian radiolarians from the Samani River area.

Black mudstones in the PT-Unit are generally considered to be Campanian in age. The pelagic to terrigenous succession in the PT-Unit is thus considered to range from latest Albian to Campanian, though the age of chert is still unknown. The Early Cretaceous black mudstone (R7) is not consistent with the age range above, and the age cannot be easily explained.

T-Unit (Terrigenous Unit)

R17 is black mudstone, which contains poorly preserved Late Cretaceous radiolarians, including *Amphipyndax stocki* and *Dictyomitra multicostata*.

Kiyokawa (1992) reported late Campanian - Maastrichtian radiolarians from green shale in the T-Unit, and Ueda et al. (1993) reported early Paleocene radiolarians from green and red mudstones. Although the age of the black mudstones is not well known, the T-Unit is estimated to be Late Cretaceous - early Paleocene (at least Campanian - Danian).

Illite crystallinity of mudstones

Measurement of illite crystallinity

The appearance of mudstones in the Horobetsugawa Complex changes gradually toward the east (structurally downward), from shale through slate to phyllite. This sequence is repeated at least three times. Each repetition is bounded by fault zones, along which the Neogene Kamikineusu Formation, sporadic limestone blocks and serpentinite occur (Fig. 8). Illite crystallinity of the mudstones is utilized to reveal the significance of this systematic lithological change and structural repetition.

Illite crystallinity has been used to evaluate geothermal records and thermal structures of accretionary complexes (e.g. Underwood et al., 1993; Awan and Kimura, 1996; Tanabe and Kano,

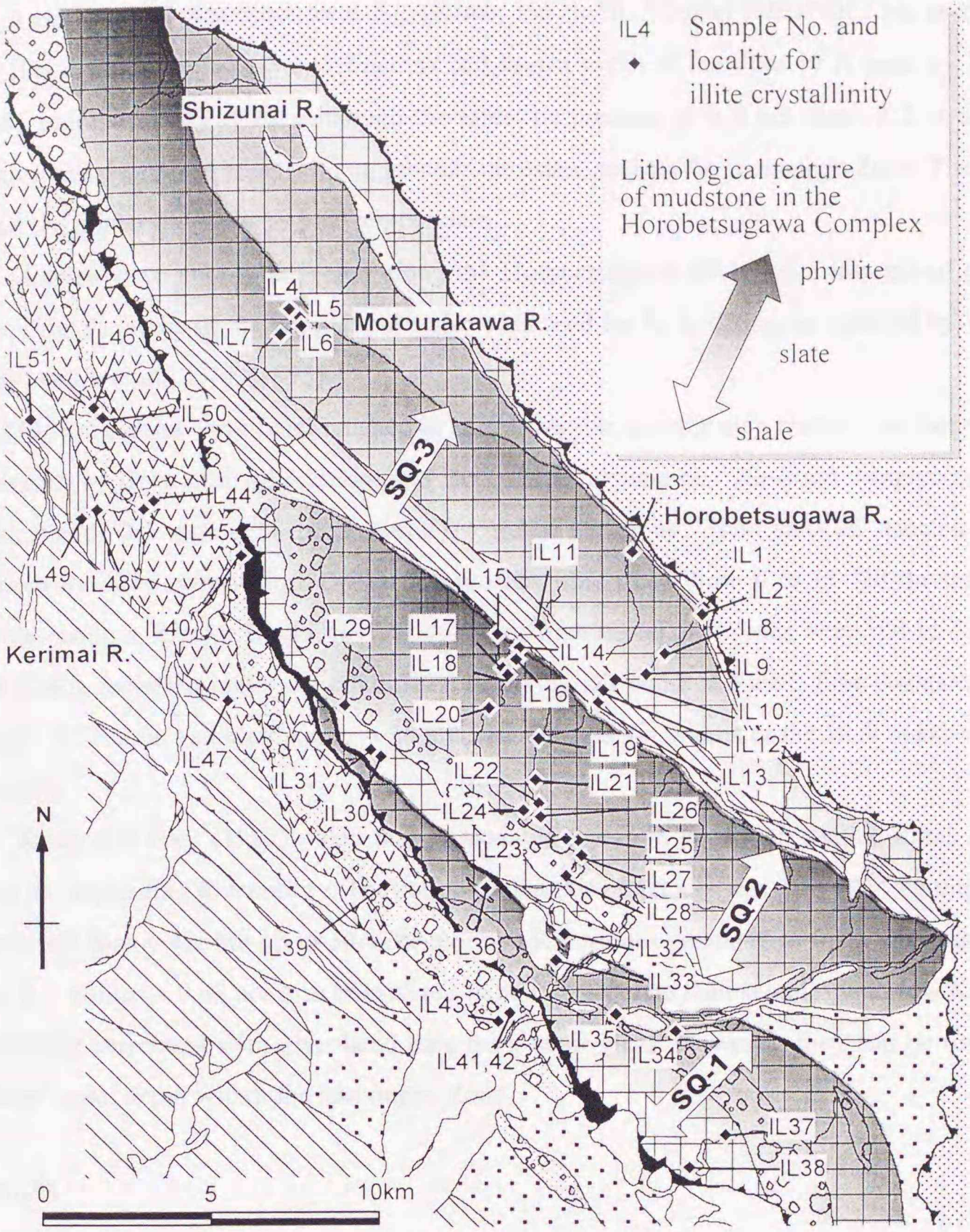


Fig. 8. Lithological distribution (phyllite to shale) in the Horobetsugawa Complex and sample localities for illite crystallinity measurement. Lithology ornaments as in Fig. 2, sample numbers as in Table 2.

1996). The frequency distribution of illite [001] space depends on maximum temperature attained (T_{max}) and the time of succession at T_{max} (Kisch, 1987). The "Kubler Index" (K.I.) is used as a measure of "illite crystallinity". This is defined as half-height width of the illite 10 Å peak by XRD (Kubler, 1968), represented by $\Delta°2\theta$. Although the effect by pressure is still not clear, K.I. is an indicator of relative burial depth in areas without igneous intrusion, such as the Idonnappu Zone. The lower the K.I. value, the higher the metamorphic temperature.

Samples were mainly collected along the Horobetsugawa River, as a transect of the Idonnappu Zone (Fig. 8). Some of the samples have also been used for K-Ar dating, as reported by Watanabe et al. (1994) and Iwasaki et al. (1995).

Mudstone chips were hand-crushed in an iron mortar, and the clay fraction smaller than 2μm then separated by hydraulic elutriation and centrifugal separation. Air-dried (unglycolated) oriented specimens of 2-5 mg/cm^2 were prepared by pipette mounting. Grain sizes of selected samples were checked by SEM observation. Diffraction profiles were made from 6 to 11 °2θ three times for each sample, using a Rigaku Denki 4037A1 X-ray diffractometer. All scans were run at 35 kV / 20 mA with CuKα radiation under the conditions: receiving slit width = 0.09 °, time constant = 5 sec, scan speed = 0.5 °/min, and chart speed = 20 mm/sec. Half-height widths of the 10 Å peaks were measured manually.

Kisch and Frey (1987) noted that expandable layers in poorly crystalline illites affect the K.I. value by responding to humidity. They showed that this effect was less than 10 % on unglycolated K.I. values less than 0.42, but up to 30 % or more on K.I. values greater than 0.42. Our unglycolated data have K.I. values > 0.42 are thus considered to be less accurate than samples with low K.I., and cannot be directly correlated with glycolated data from other areas. However, they can be used to evaluate relative burial depth within the Idonnappu Zone.

Results

Averaged K.I. values are plotted by distance from the boundary faults between successions (termed sequence-boundary faults) in Fig. 9.

In the Horobetsugawa Complex, K.I. gradually decreases structurally downward, and this change is repeated three times at 5-5.5 km intervals due to the sequence-boundary faults (Fig. 9). This trend is compatible with the gradual change in lithological appearance. Each change in K.I. is considered to indicate increase in temperature with structural depth. These thermal structures are herein termed as "thermal sequences", and named as SQ-1, SQ-2 and SQ-3 from south (see Figs. 8, 9). The pattern of K.I. values in SQ-2 appears consistent with that of K-Ar ages (Fig. 9); the lower the K.I., the younger the K-Ar age. Within the PT-Unit, however, the radiolarian ages are ca. 70 - 80 Ma (Campanian)

Table 2. Illite crystallinity of mudstones from the Idonnappu Zone and part of the Nitarachi-Yezo Sequence. PT, T, MH and MN are unit names. Nt: Nitarachi Formation, LY: Lower Yezo Group. Three samples from the Nitarachi Formation (IL47-49) and one from MN-Unit (IL45) are green mudstones, the rest are black mudstones.

No.	SQ	UNIT	distance (km)	K.I. (Δ2θ)				
				1	2	3	average	σ
IL1	4	PT	0.10	0.64	0.62	0.62	0.63	0.01
IL2	4	PT	0.50	0.56	0.56	0.53	0.55	0.01
IL3	3	PT	0.35	0.22	0.22	0.21	0.22	0.00
IL4	3	PT	1.10	0.27	0.25	0.25	0.26	0.01
IL5	3	PT	1.10	0.33	0.33	0.32	0.33	0.00
IL6	3	PT	1.30	0.25	0.25	0.24	0.24	0.00
IL7	3	PT	1.80	0.33	0.33	0.32	0.32	0.00
IL8	3	PT	2.65	0.52	0.50	0.50	0.50	0.01
IL9	3	PT	3.30	0.35	0.34	0.29	0.32	0.03
IL10	3	T	3.93	0.70	0.66	0.65	0.67	0.02
IL11	3	T	4.45	0.94	0.88	0.83	0.88	0.05
IL12	3	T	4.50	0.85	0.77	0.68	0.77	0.07
IL13	3	T	4.60	0.86	0.85	0.81	0.84	0.02
IL14	2	PT	0.15	0.21	0.20	0.20	0.20	0.00
IL15	2	PT	0.45	0.20	0.19	0.19	0.19	0.00
IL16	2	PT	0.70	0.19	0.18	0.18	0.18	0.00
IL17	2	PT	0.85	0.20	0.20	0.20	0.20	0.00
IL18	2	PT	0.90	0.18	0.18	0.17	0.18	0.00
IL19	2	PT	0.90	0.20	0.20	0.19	0.20	0.00
IL20	2	PT	2.10	0.25	0.24	0.24	0.24	0.00
IL21	2	PT	2.50	0.28	0.27	0.25	0.27	0.01
IL22	2	MH	3.30	0.42	0.38	0.38	0.39	0.02
IL23	2	MH	3.35	0.37	0.36	0.35	0.36	0.01
IL24	2	MH	3.45	0.36	0.31	0.28	0.31	0.03
IL25	2	MH	3.45	0.38	0.38	0.36	0.37	0.01
IL26	2	MH	3.50	0.30	0.28	0.24	0.27	0.02
IL27	2	MH	3.65	0.59	0.55	0.55	0.56	0.02
IL28	2	PT	4.60	0.42	0.42	0.41	0.42	0.00
IL29	2	PT	5.40	0.57	0.53	0.53	0.54	0.02
IL30	2	PT	5.49	0.49	0.48	0.47	0.48	0.01
IL31	1	PT	0.10	0.23	0.23	0.23	0.23	0.00
IL32	1	PT	1.00	0.29	0.24	0.23	0.25	0.03
IL33	1	PT	1.25	0.21	0.20	0.20	0.20	0.00
IL34	1	PT	1.45	0.20	0.20	0.20	0.20	0.00
IL35	1	PT	1.85	0.20	0.20	0.19	0.20	0.01
IL36	1	PT	2.10	0.22	0.22	0.21	0.22	0.01
IL37	1	PT	3.20	0.38	0.37	0.35	0.37	0.01
IL38	1	PT	4.40	0.70	0.58	0.56	0.61	0.06
IL39		MN	0.14	0.83	0.78	0.77	0.79	0.03
IL40		MN	0.35	0.62	0.61	0.60	0.61	0.01
IL41		MN	0.75	0.42	0.42	0.41	0.42	0.01
IL42		MN	0.75	0.43	0.41	0.41	0.41	0.01
IL43		MN	1.30	0.55	0.52	0.49	0.52	0.02
IL44		MN	2.30	0.76	0.72	0.63	0.70	0.06
IL45		MN	2.35	0.50	0.48	0.48	0.49	0.01
IL46		MN	2.70	1.02	0.98	0.95	0.99	0.03
IL47		Nt	0.01	0.46	0.45	0.44	0.45	0.01
IL48		Nt	0.03	1.02	0.97	0.97	0.98	0.02
IL49		Nt	0.70	0.63	0.63	0.61	0.62	0.01
IL50		LY	0.10	1.20	1.15	1.15	1.16	0.02
IL51		LY	0.05	0.70	0.60	0.58	0.62	0.06

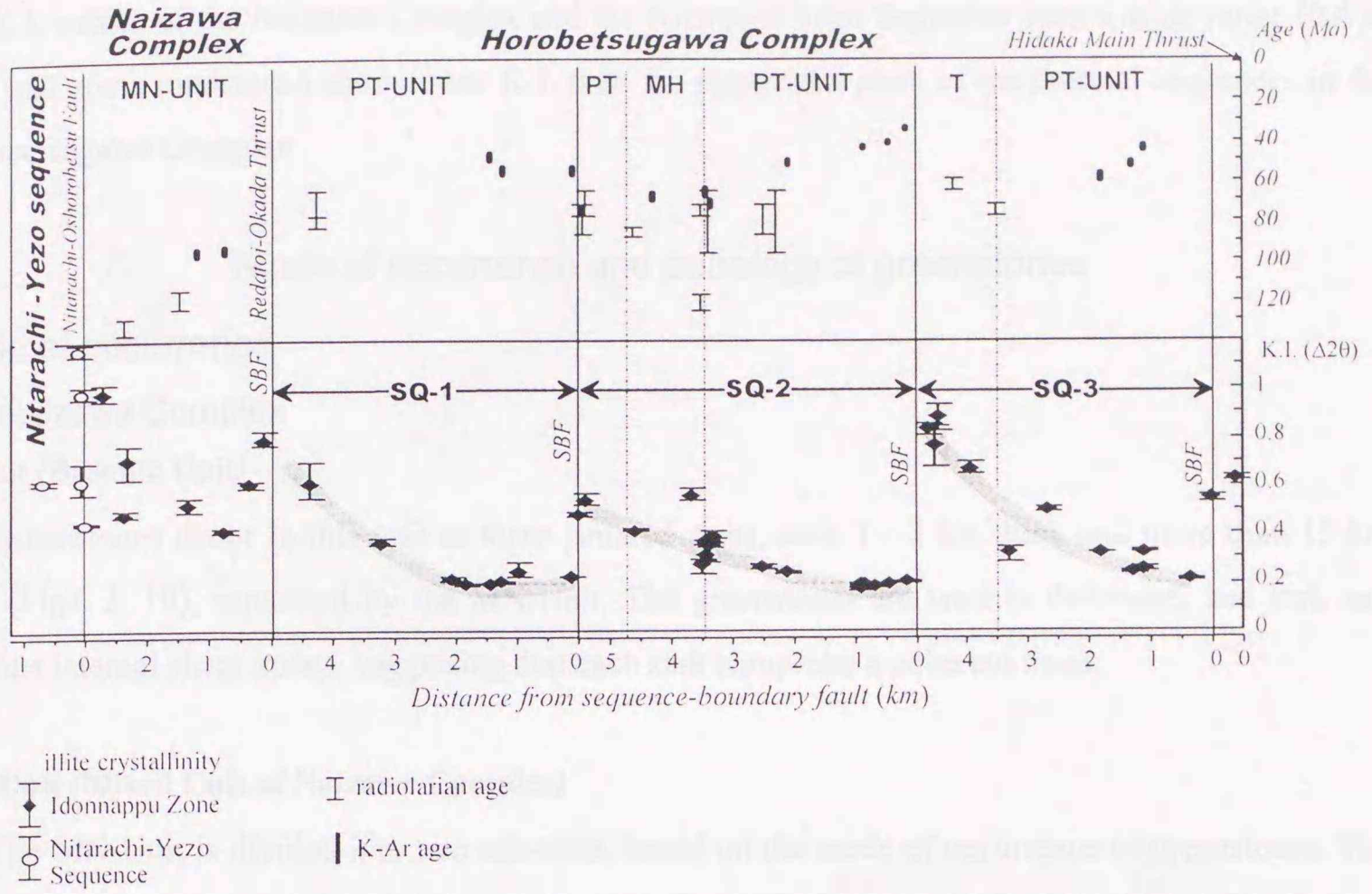


Fig. 9. Distribution of illite crystallinities. K-Ar ages from Watanabe et al. (1994). Radiolarian ages are after Kiyokawa (1992), Ueda et al. (1993) and this work. SBF: boundary fault between thermal sequences.

irrespective of K.I.

K.I. values of the Naizawa Complex and the Nitarachi-Yezo Sequence span a wide range (0.4 to 1.2), and some mudstones show lower K.I. than the uppermost parts of the thermal sequences in the Horobetsugawa Complex.

Mode of occurrence and petrology of greenstones

Mode of occurrence

1. Naizawa Complex

B-Unit *(Basaltic Unit)*

Greenstones occur in this unit as three isolated slabs, each 1 - 2 km thick and more than 15 km long (Figs. 2, 10), separated by the MN-Unit. The greenstones are weakly deformed, and lack any obvious internal shear zones, suggesting that each slab comprises a coherent mass.

MN-Unit *(Mixed Unit of Naizawa Complex)*

The MN-Unit is divided into two sub-units, based on the mode of occurrence of greenstones. The MN_1 sub-unit is dominated by lava bodies, exhibiting elongated slab-like morphology (Fig. 10). The MN_2 sub-unit consists of small blocks (several to several tens meters) of greenstone with chert-clastic sedimentary rocks, and limestone.

The relationship between greenstone and other lithofacies in the MN_2 sub-unit can be observed along the Horobetsu River (Fig. 11). In this outcrop, greenstones occur as blocks, separated from chert-clastic rocks, and reddish micritic limestone by faults. Greenstones are typically fractured along the faults forming cataclastic shear zones. The bedding planes of chert and clastic rocks and lithological boundary faults all tend to strike NNW - SSE. The clastic rocks are only weakly deformed, display recognizable sedimentary structures, and do not contain greenstone, chert, or limestone fragments. The "parquetry" or mosaic structure of this outcrop clearly indicates that the lithological mixture was formed by tectonic slicing, rather than sedimentary processes such as debris flow or submarine slide. Limestone blocks are rarely contained in black mudstone matrix in some other outcrops.

2. Horobetsugawa Complex

MH-Unit *(Mixed Unit of Horobetsugawa Complex)*

Greenstones occur in the MH-Unit as blocks and fragments in a sheared matrix of black pebbly mudstone and broken turbidite. The size of blocks and fragments varies from several centimeters to several tens of meters. The margins of the greenstone blocks are sheared into cataclastic breccia, and are mixed irregularly with clastic matrix. In the basal part (northeastern margin) of the unit along the

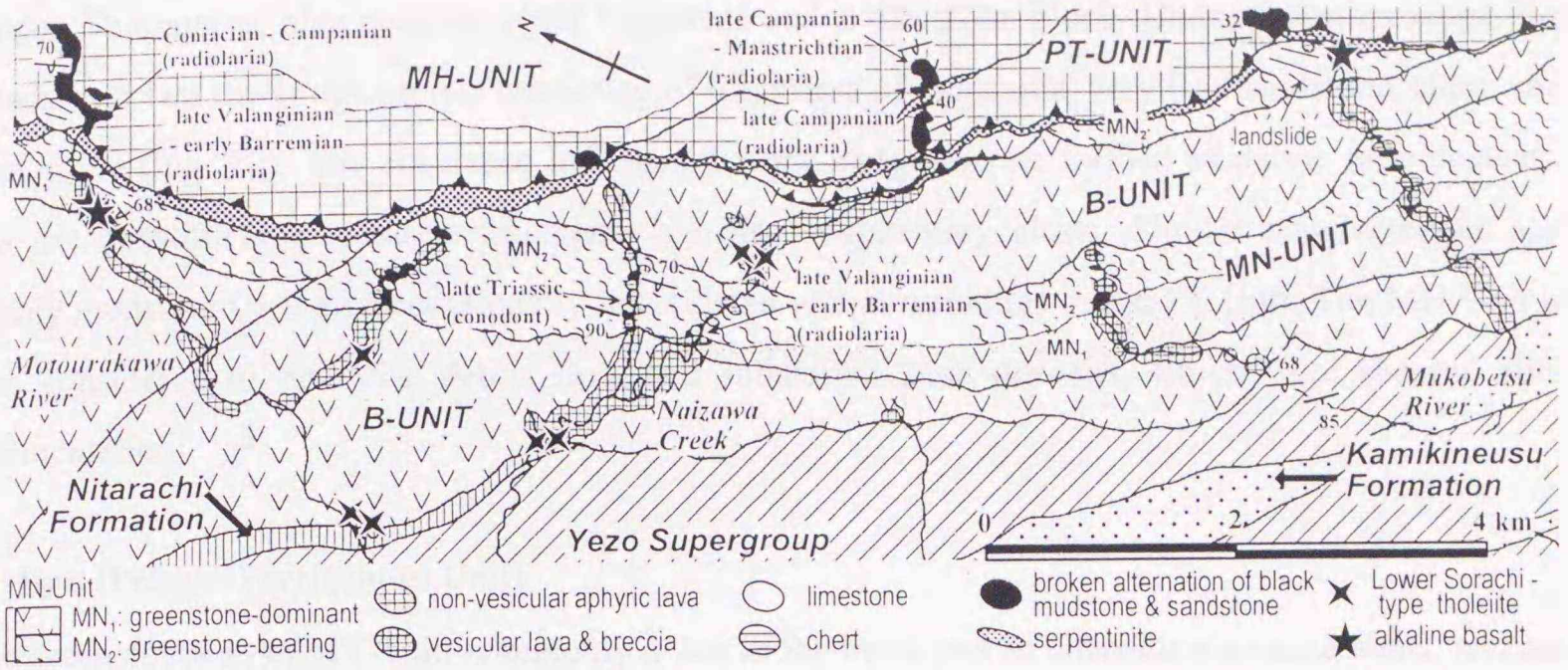


Fig. 10. Detailed geological map of the Naizawa Complex around Naizawa Creek. Fossil ages after Sakagami & Sakai (1979), Kiyokawa (1992), and this study.

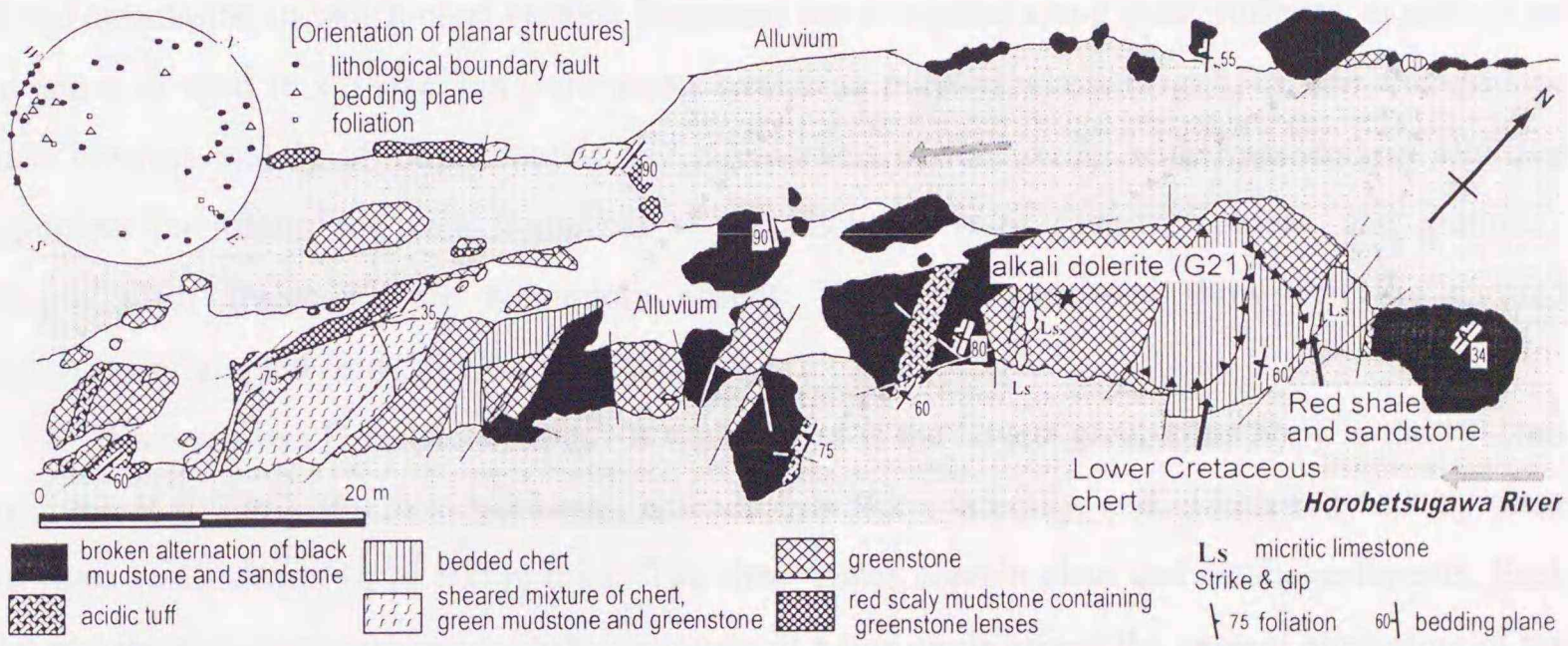


Fig. 11. Outcrop sketch of the MN-Unit (MN2 sub-unit) in the Naizawa Complex in the middle reach of the Horobetsugawa River.

Horobetsu River (Fig. 12), greenstone fragments are contained in a non-sheared "pebbly mudstone" matrix. This matrix also contains chert fragments and a limestone block. Under the microscope, the matrix is in fact the conglomerate consisting of fragments of mudstone, very fine sandstone, chert, and greenstone (Fig. 12). The occurrenc indicates that the conglomerate formed as debris flow deposits, and the constituent greenstone fragments are also sedimentary clasts. Similar conglomerates and pebbly mudstones are also occasionally intercalated within turbidites in the PT-Unit. The MH-Unit is thus considered to comprise debris flow and submarine slide deposits, which were sheared after sedimentation.

PT-Unit (Pelagic-Terrigenous Unit)

The greenstones in the PT-Unit commonly occur in the basal part of chert-clastic successions, and are characteristically sheared. Almost all greenstone bodies are basaltic lava, and only few parts of them are left weakly deformed (Fig. 13a). Dense meshworks of shear planes are dominant in the greenstones, but igneous textures are still preserved (Fig. 13b). Some severely sheared examples are foliated cataclasite, in which most basaltic fragments are elongated along shear surfaces, or pulverized into grains of sand to silt size, but some clasts remain as porphyroclasts (Fig. 13c). The fine-grained matrix consists mainly of clay minerals and micrograins of leucoxene, with fragments of albitized plagioclase microlites and rare fragments of metamorphic veins (quartz, epidote, and prehnite). Volcanic glass fragments are commonly absent. These characteristics show that the sheared greenstones originated from lava, not hyaloclastite.

The "Shimangawa Greenstone Body" is typical, and is the largest greenstone body in the PT-Unit (Fig. 14a). It is 200 - 300 m in thickness, extends over 9 km laterally, and is internally cut by shear zones into small sheets 10 to 100 m thick. The shear zones contain chert and clastic sediments. Each sheet and the dividing shear zones strike obliquely at a low angle across the general elongation of the whole greenstone body, showing imbricate duplex-like structure. In some parts of the shear zone, basaltic cataclasite and mudstone are interlayered to form "striped" or "laminated" texture bounded by slip surfaces (Figs. 13d and 15a), comparable to the "sumi-flow structure" of Kawamura *et al.* (1998). The width of each layer varies from several decimeters to several millimeters.

Fig. 14b illustrates another field occurrence of the sheared greenstone along the Sogabetsu River. The greenstones occur with light-gray chert and reddish / greenish siliceous mudstone. At the base of the greenstone body, thin layers (1 cm to 1.7 m) of fine-grained basaltic cataclasite are intercalated in a broken alternation of black mudstone and sandstone.

In these shear zones, asymmetric deformation structures such as Riedel shear (Fig. 15) and asymmetric fold indicate the simple shear with relative upward displacement of western side (originally top-to-east sense), consistent with Cretaceous westward subduction of the oceanic plate

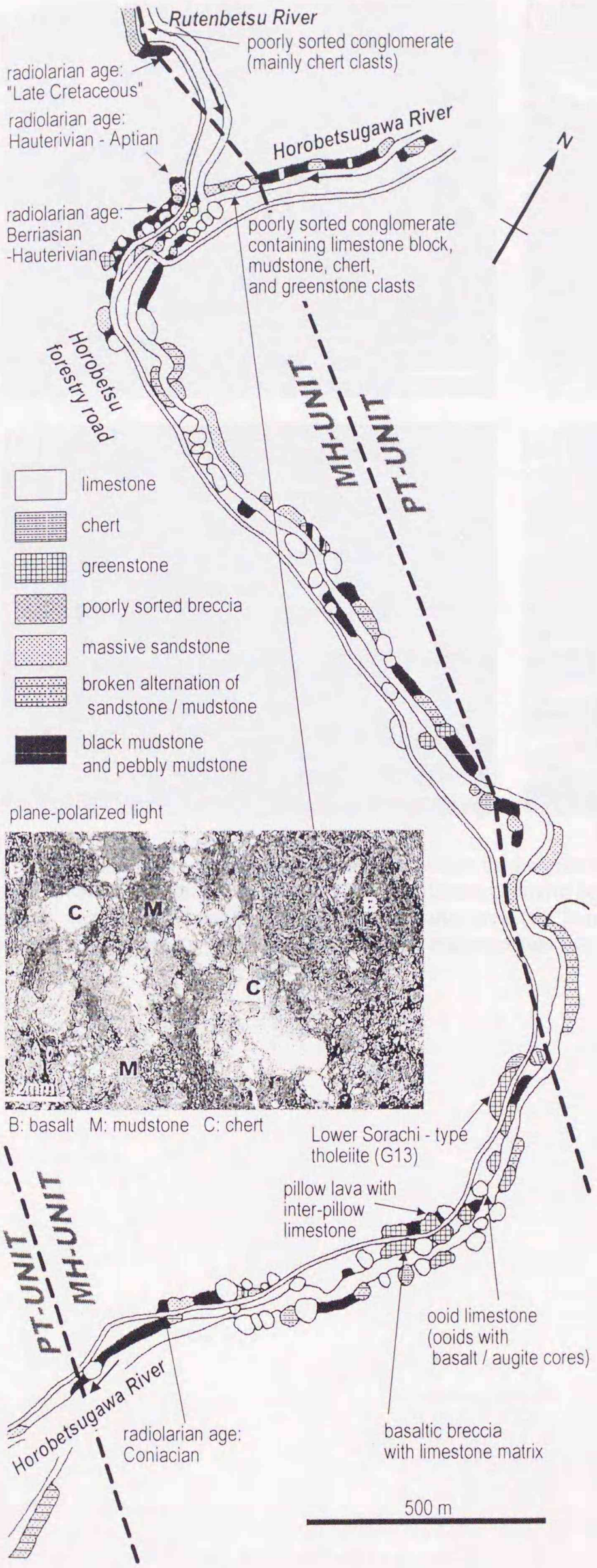


Fig. 12. Route map of the MH-Unit along the Horobetsugawa River. Radiolarian ages after Kiminami (1987) and this study.

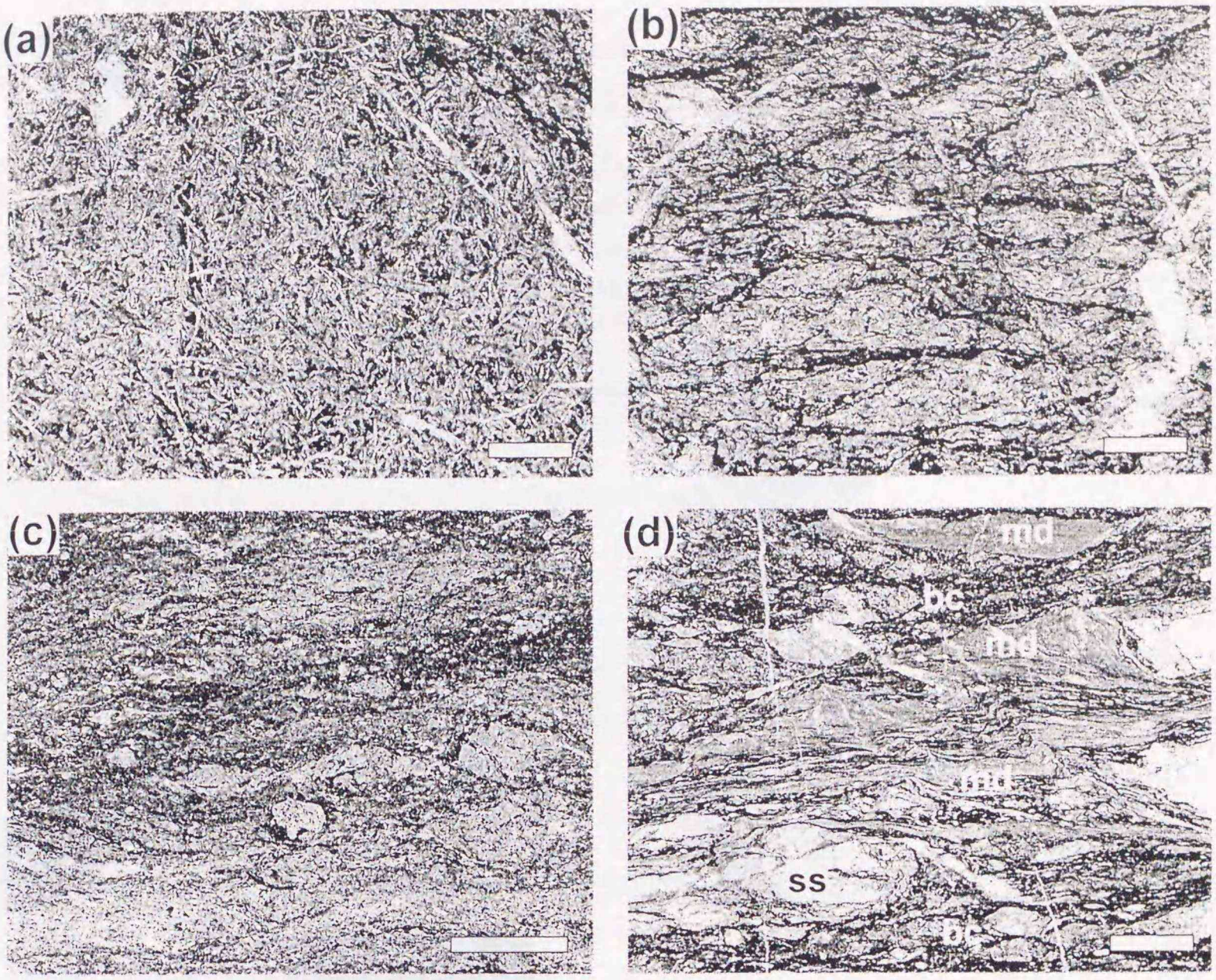


Fig. 13. Photomicrographs of typical deformation in the greenstones of the PT-Unit, under plane-polarized light. Scale bars indicate 1mm. (a) Weakly deformed aphyric lava. (b) Basaltic lava cut by a dense meshwork of slip surfaces. (c) Foliated cataclasite of basaltic lava. (d) "laminated" layered mixture of basaltic cataclasite and clastic sediments. bc: basaltic cataclasite, md: mudstone, ss: sandstone

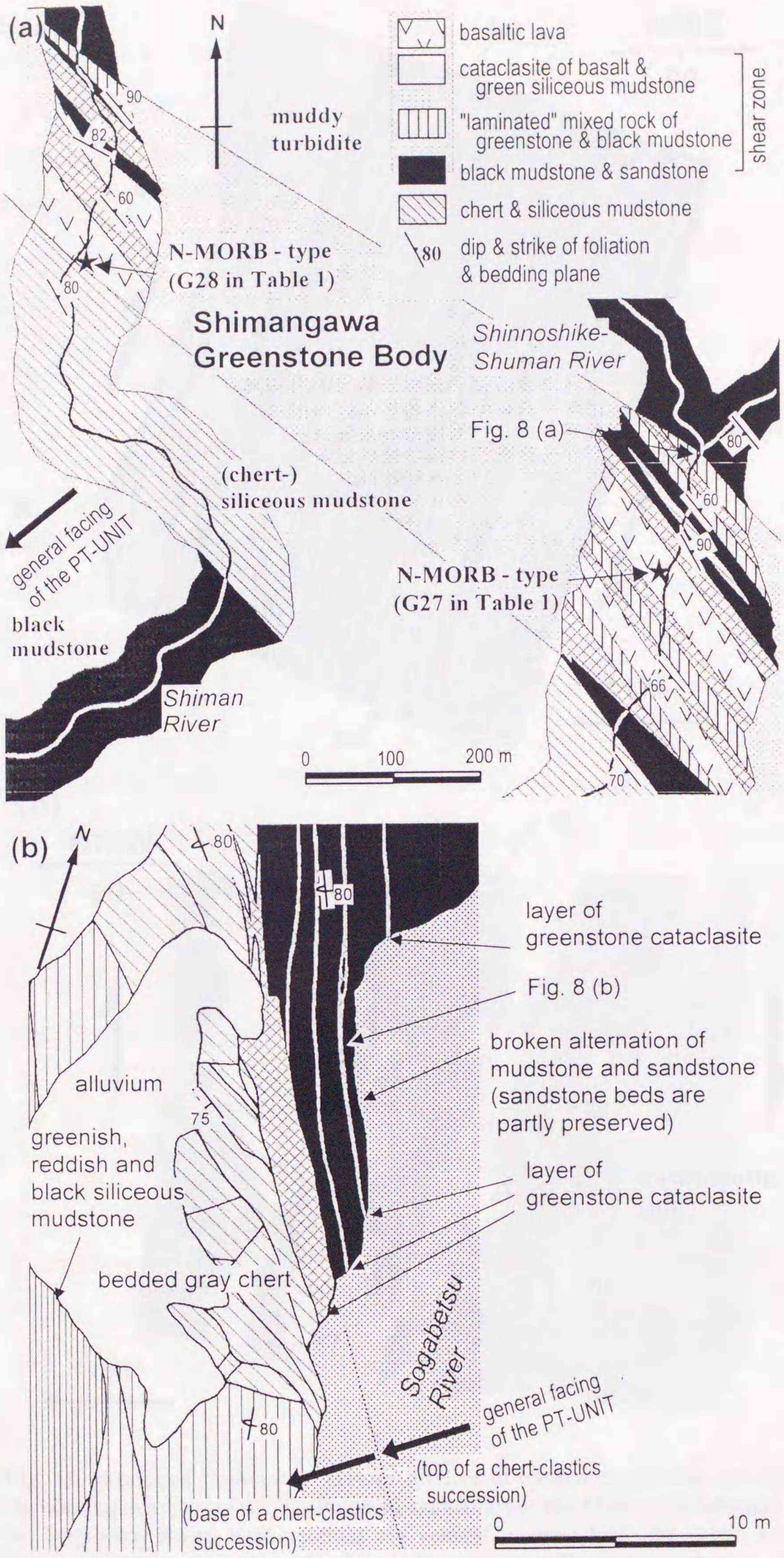


Fig. 14. Occurrences of greenstones in the PT-Unit.
(a) Route map of the Shimangawa Greenstone Body along the Shiman River and Shinnoshikeshuman River.
(b) Outcrop sketch of the basal horizon of the greenstone body in the Sogabetsu River.

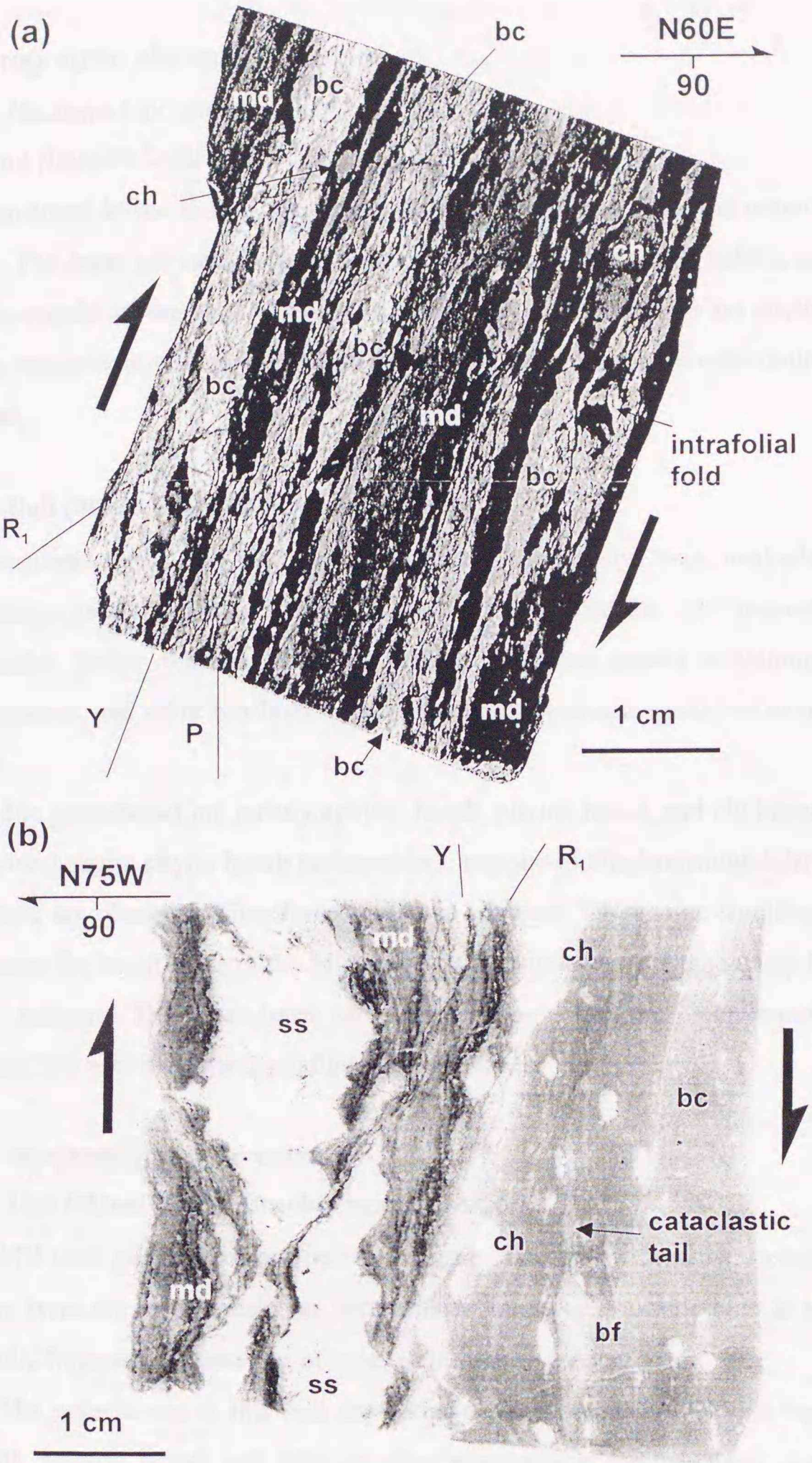


Fig. 15. Fabrics of "laminated" layered mixture of basaltic cataclasite and clastic sediments in the PT-Unit, Horobetsugawa Complex. (a): Polished sample from the Shinnoshikeshuman River, (b): Thin section from the Sogabetsu River. Both sections are vertical, viewed from the south, and are almost perpendicular to compositional layering (Y-surface) and shear banding (R1-surface). Arrows indicate shear sense. md: black mudstone, ss: sandstone boudin, ch: fragment of chert and siliceous mudstone, bf: basalt fragment, bc: fine-grained basalt cataclasite.

(Engebretson *et al.* 1985; Niida & Kito 1986; Kiyokawa 1992).

Petrographic characteristics

1. Naizawa Complex

B-Unit (Basaltic Unit)

Greenstones in the B-Unit are mostly close-packed pillow lava and massive lava; hyaloclastites are rare. The lavas are rarely cut by webbed veinlets of laumontite, calcite, and prehnite. All lavas are non-vesicular or are only poorly vesicular; highly vesicular rocks are absent. Most are aphyric basalt with subordinate olivine basalt and dolerite, metamorphosed into the zeolite or prehnite-pumpellyite facies.

MN-Unit (Mixed Unit of Naizawa Complex)

Greenstones in the MN-Unit commonly consist of massive lava, hyaloclastite, and sorted volcanic sandstone (reworked hyaloclastite). Lavas and hyaloclastites are frequently reddish and are often vesicular. Some volcanic breccias have a limestone matrix containing fragments of crinoids, molluscans, and other bioclasts. Hyaloclastites and volcanic sandstone occur mainly in the MN_2 sub-unit.

The greenstones are mostly aphyric basalt, olivine basalt, and olivine-augite basalt. Occasionally, (olivine-) augite-phyric basalt (ankaramite), aegirine-biotite-kaersutite dolerite, and plagioclase-phyric trachyte are observed. Titaniferous augite is common. There is no significant petrographic difference between the basalt lavas in the MN_1 and MN_2 sub-units, except that glassy basalts occur mostly in the MN_2 sub-unit. The greenstones are metamorphosed into the prehnite-pumpellyite facies, which is compatible with the illite crystallinity of mudstones.

2. Horobetsugawa Complex

MH-Unit (Mixed Unit of Horobetsugawa Complex)

MH-Unit greenstones are mainly massive lava, pillow lava, hyaloclastite, and volcanic breccia. Some lavas are highly vesicular. Inter-pillow limestone, volcanic breccia with limestone matrix, and basaltic fragments at the cores of ooids in limestone are also seen.

The greenstones in this unit are variable petrographically. Olivine basalt, picritic basalt, augite basalt, aphyric basalt and dolerite, plagioclase-phyric trachyte, and rare microgabbro all occur. Titaniferous augite occurs in some samples. All have undergone the prehnite-pumpellyite facies metamorphism, except for a few metabasite blocks which contain epidote + green hornblende + albite ± stilpnomelane.

PT-Unit (Pelagic-Terrigenous Unit)

Because the greenstones in the PT-Unit are intensely sheared, it is difficult to identify original volcanic structure. Hyaloclastite is rare, and lavas are mostly non-vesicular. Massive lava with intergranular to subophitic texture is the dominant type. Quenched textures with dendritic pyroxene and variolite are often seen, mainly in cataclastic fragments in sheared zones.

The greenstones of the PT-Unit are mainly aphyric basalt, rarely with olivine phenocrysts. Plagioclase microphenocrysts are not uncommon. Augite is preserved in weakly deformed examples, but is completely replaced by chlorite in sheared rocks. Metamorphic grade ranges from the prehnite-pumpellyite facies to the greenschist facies, compatible with the illite crystallinity of associated mudstones.

Petrochemical characteristics

Bulk rock chemical compositions were determined for 29 greenstones from the Idonnappu Zone. Six samples (GSJ numbers in Table 3) are registered rock samples of the Geological Survey of Japan.

Samples containing few or no vesicles and veins were collected from the least deformed and altered outcrops (Fig. 2). Any sample chip with visible vesicles or veins was discarded prior to crushing. All analyses were made at Hokkaido University, using a Phillips PW1404 X-ray fluorescence spectrometer. Major element compositions were determined using the method by Tsuchiya *et al.* (1989), and trace elements by those described by Nakagawa *et al.* (1994). Results are listed in Table 3.

In all samples analyzed, olivine and volcanic glass are replaced by chlorite, and most plagioclase is albitized. In such altered or metamorphosed rocks, large-ion-lithophile (LIL) elements tend to be mobile during alteration and metamorphism. However, high-field-strength (HFS) elements are generally immobile in those conditions, and are thus more suitable for determining petrologic characteristics. Consequently, immobile elements such as HFS are mainly used for identification of chemical characteristics. Nb/Y ratio is used for the distinction of alkaline or sub-alkaline series (Winchester & Floyd 1977). N-MORB - normalized trace element patterns (Pearce 1982; Sun & McDonough 1989) and 2Nb-Zr/4-Y systematics (Meschede 1986) are utilized to identify tectonic setting of eruption, and the Ti-V diagram of Shervais (1982) is used to distinguish oceanic basalts from island arc basalts. Nb/Y-Nb/Zr relations (Tatsumi *et al.* 1998) are used to compare with superplume-related oceanic island basalts, and Nb/Y-Zr/Y for comparison with oceanic plateau basalts.

Table 3. Bulk rock chemical compositions of greenstones from the Idonnappu Zone. Major elements in wt% and trace elements in ppm. dol: dolerite, aph: aphyric basalt, P: picritic basalt, A: ankaramite, B: basalt, trach: trachyte, ag: augite (or titanaugite), ol: olivine.

No.	G1	G2	G3	G4	G5	G6	G7	G9	G10	G11	G12	G8	G15	G16	G17
UNIT	B	B	B	B	B	B	B	B	B	B	B	MN	MN	MN	MN
type	dol	aph	dol	aph	dol	dol	ag-B	aph	aph	ag-B	aph	aph	ol-ag-A	ag-A	ol-B
SiO_2	50.30	51.99	51.11	49.62	51.40	48.78	49.49	49.04	49.25	51.13	49.13	49.26	40.38	41.04	46.07
TiO_2	1.12	1.08	1.14	1.07	1.28	1.03	0.91	0.88	1.01	1.10	1.06	1.93	3.82	2.31	2.21
Al_2O_3	14.67	13.15	15.44	13.70	13.32	14.43	14.87	14.77	14.19	13.21	14.23	15.68	11.81	10.18	16.61
$Fe_2O_3^*$	10.36	10.64	9.46	12.53	13.08	12.20	11.24	11.72	12.38	12.32	12.08	11.89	13.16	9.42	10.90
MnO	0.31	0.17	0.32	0.20	0.19	0.20	0.20	0.20	0.20	0.20	0.20	0.15	0.25	0.23	0.18
MgO	7.00	7.22	7.17	7.08	8.62	8.66	8.28	8.34	9.04	7.71	7.30	7.86	12.18	12.84	6.13
CaO	10.73	9.37	9.99	11.87	9.11	11.57	12.30	11.64	10.97	9.98	11.47	9.25	16.38	20.16	12.03
Na_2O	2.87	3.43	2.81	3.31	4.14	2.84	2.82	2.41	3.17	4.28	3.71	3.53	0.73	0.91	4.34
K_2O	2.12	2.30	1.93	0.31	0.16	0.43	0.22	0.78	0.12	0.11	0.07	1.45	0.33	0.17	0.46
P_2O_5	0.09	0.13	0.09	0.09	0.09	0.07	0.07	0.07	0.08	0.08	0.09	0.17	0.41	0.27	0.41
Total	99.57	99.48	99.46	99.78	101.39	100.21	100.40	99.85	100.41	100.12	99.34	101.17	99.45	97.53	99.34
L.O.I.	3.47	1.43	3.45	1.99	2.72	2.53	2.43	1.47	2.80	2.79	3.45	2.67	3.53	5.65	5.29
FeO*/MgO	1.33	1.32	1.19	1.59	1.36	1.27	1.22	1.26	1.23	1.44	1.49	1.36	0.97	0.66	1.60
Ba	–	278	–	33	31	–	–	67	30	30	35	–	68	–	–
Co	–	46	–	45	48	–	–	46	47	47	44	–	62	–	–
Cr	–	376	–	165	298	–	–	251	306	250	236	–	357	–	–
Cu	–	41	–	124	167	–	–	148	150	150	124	–	47	–	–
Nb	–	2.4	–	2.9	2.0	–	–	2.6	2.3	2.4	2.8	–	43.7	–	–
Ni	–	96	–	91	97	–	–	108	111	96	79	–	96	–	–
Pb	–	2	–	2	2	–	–	2	2	1	3	–	3	–	–
Rb	–	47.7	–	6.9	4.1	–	–	15.4	2.1	2.2	2.0	–	5.0	–	–
Sc	–	42	–	43	39	–	–	21	43	36	40	–	55	–	–
Sr	–	229	–	167	183	–	–	198	107	161	151	–	186	–	–
V	–	296	–	349	362	–	–	316	334	292	316	–	416	–	–
Y	–	23	–	26	27	–	–	22	24	24	24	–	24	–	–
Zn	–	74	–	91	96	–	–	81	91	83	85	–	81	–	–
Zr	–	53	–	57	64	–	–	46	52	56	57	–	187	–	–
GSJ No.			R21974		R33412						R22087	R21931			

No.	18	G19	G20	G21	G13	G14	G22	G23	G24	G25	G26	G27	G28	G29
UNIT	MN	MN	MN	MN	MH	MH	MH	MH	P-T	P-T	P-T	P-T	P-T	P-T
type	ol-B	ol-B	trach	dol	ag-B	ol-P	ol-B	aph	ag-B	aph	dol	aph	aph	aph
SiO_2	46.70	46.80	59.36	48.28	50.84	41.03	50.41	53.23	47.02	50.26	51.11	50.70	51.58	51.19
TiO_2	2.25	3.12	0.80	2.32	1.13	0.98	1.61	1.90	1.27	1.75	1.58	1.86	1.99	1.10
Al_2O_3	17.00	17.66	18.54	13.69	13.14	15.36	17.52	15.71	13.50	15.56	13.96	14.95	15.23	12.97
$Fe_2O_3^*$	10.46	10.97	7.62	10.02	12.52	14.16	11.16	12.12	12.60	11.30	11.22	12.29	13.48	11.22
MnO	0.18	0.15	0.23	0.15	0.18	0.25	0.19	0.16	0.23	0.21	0.28	0.20	0.72	0.21
MgO	11.03	7.64	1.63	10.46	8.58	15.26	10.15	5.66	8.53	8.96	8.73	9.30	7.85	7.94
CaO	8.26	7.58	0.90	8.78	9.64	12.52	4.78	7.01	12.59	9.11	9.67	6.34	5.49	11.52
Na_2O	2.84	3.27	6.59	2.50	3.64	0.16	4.83	5.60	2.80	3.36	2.90	3.51	4.55	3.77
K_2O	1.01	1.95	4.36	2.47	0.58	0.02	0.40	0.27	0.17	0.86	0.44	1.71	0.28	0.06
P_2O_5	0.38	0.55	0.34	0.46	0.09	0.10	0.26	0.24	0.09	0.16	0.13	0.15	0.16	0.08
Total	100.11	99.69	100.37	99.13	100.34	99.84	101.31	101.90	98.80	101.53	100.02	101.01	101.33	100.06
L.O.I.	4.89	4.32	2.49	3.82	2.75	5.91	5.36	2.25	2.30	2.93	2.53	3.62	4.26	1.14
FeO*/MgO	0.85	1.29	4.20	0.86	1.31	0.83	0.99	1.93	1.33	1.13	1.16	1.19	1.54	1.27
Ba	757	944	1130	438	129	49	188	72	65	87	104	197	49	–
Co	42	40	7	37	46	76	51	48	53	46	39	47	51	–
Cr	262	206	9	252	241	961	642	293	316	360	162	245	333	–
Cu	38	38	61	30	150	127	64	20	121	45	59	54	57	–
Nb	29.3	45.3	114.5	36.0	2.9	5.9	22.7	7.9	2.6	2.1	1.8	2.5	3.3	–
Ni	185	139	8.2	165	85	362	253	66	97	71	55	76	86	–
Pb	2	2	6	3	2	2	3	3	2	2	2	2	6	–
Rb	10.6	22.4	78.4	49.4	8.3	1.2	6.3	6.3	2.6	18.4	8.4	23.4	7.5	–
Sc	32	35	15	28	40	46	34	34	45	43	36	38	44	–
Sr	796	1091	302	372	244	56	224	308	115	164	204	65	120	–
V	210	226	31	197	339	291	268	269	369	334	345	384	412	–
Y	26	29	42	21	26	28	25	27	28	35	37	38	40	–
Zn	77	80	171	106	87	87	82	110	82	87	88	109	111	–
Zr	156	215	1001	151	61	53	108	117	65	116	94	109	114	–
GSJ No.			R22001					R22098						

Naizawa Complex

B-Unit *(Basaltic Unit)*

The greenstones in this unit are chemically uniform. All samples are sub-alkaline basalt as shown by low Nb/Y ratios (Fig. 16). FeO* wt% tends to increase with increasing FeO*/MgO (Fig. 17a), suggesting a tholeiitic trend. However, TiO_2 wt% does not clearly increase as FeO*/MgO increases (Fig. 17b), suggesting intermediate character between abyssal tholeiite and island-arc tholeiite (IAT). TiO_2 contents range from 0.9 - 1.3 wt%, and P_2O_5 from 0.07 - 0.09 wt%. These characteristics are common with greenstones from the Lower Sorachi Ophiolite in the Sorachi-Yezo Belt (Ishizuka 1981; Kiminami *et al.* 1985; Niida 1992; Nagahashi & Miyashita 1997, See Fig. 17b). Ti-V ratios are ca. 20, also plotting on the boundary between IAT and MORB (Fig. 18). MORB-normalized trace element patterns show that HFS elements are more depleted than MORB, except for Nb where abundances are almost equal to N-MORB (Fig. 19a). These patterns also resemble to those of oceanic plateau basalts (OPB) in the Nauru Basin (Floyd 1986; Saunders 1986). Trace elements ratios (Fig. 20) of the B-Unit greenstones are generally within the MORB range. However, in spite of general HFS element depletion, they show a T-MORB affinity due to the relatively higher abundances of Nb, and shift toward the Nauru Basin OPB, reflecting their Zr depletion (Fig. 20b).

It is difficult to precisely determine the tectonic setting of the B-Unit greenstones by major and trace elements. Our data can only confine their possible origin to MORB or OPB, or also IAT. However, an important point is that the greenstones have the uniform chemical features common with those of the Lower Sorachi Ophiolite ("Lower Sorachi - type" tholeiite).

MN-Unit *(Mixed Unit of Naizawa Complex)*

All samples are classified as alkaline by virtue of their high Nb/Y ratios (Fig. 16). Petrographically, sample G20 is trachyte, and plots in the phonolite field. Samples G15 and G16 are ankaramite, and G15 plots in the basanite field. The remainder are olivine basalts and aphyric dolerites, which plot in the alkaline basalt field. Incompatible elements are clearly enriched relative to N-MORB (Fig. 19a), showing a signature of oceanic island basalt (OIB) (Pearce 1982). Ti-V plots (Fig. 18) and trace element ratios (Fig.20) also indicate an OIB origin. Although some samples show high Nb/Y ratios near to the superplume-type OIB field (Tatsumi *et al.* 1998), all analyzed MN-Unit greenstones are generally within the variation of normal hotspots (Fig. 20a).

2. Horobetsugawa Complex

MH-Unit *(Mixed Unit of Horobetsugawa Complex)*

Four specimens (G13, G14, G22, and G23) were analyzed from this unit, and their chemical characteristics are highly variable. G13 is a non-vesicular augite basalt, which plots in the field of sub-

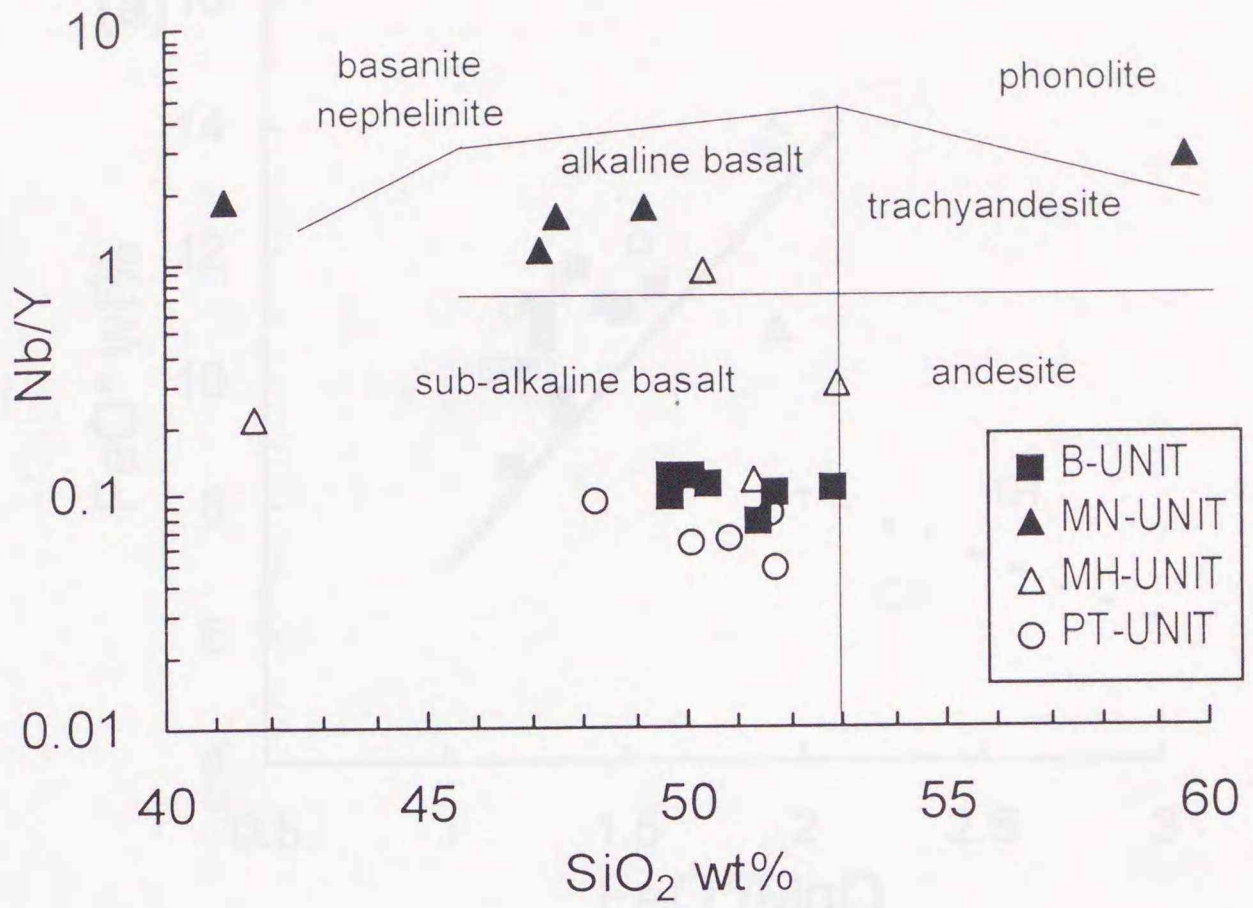


Fig. 16. Nb/Y-SiO2 classification diagram for alkaline / sub-alkaline rocks. Discriminant fields after Winchester & Floyd (1977).

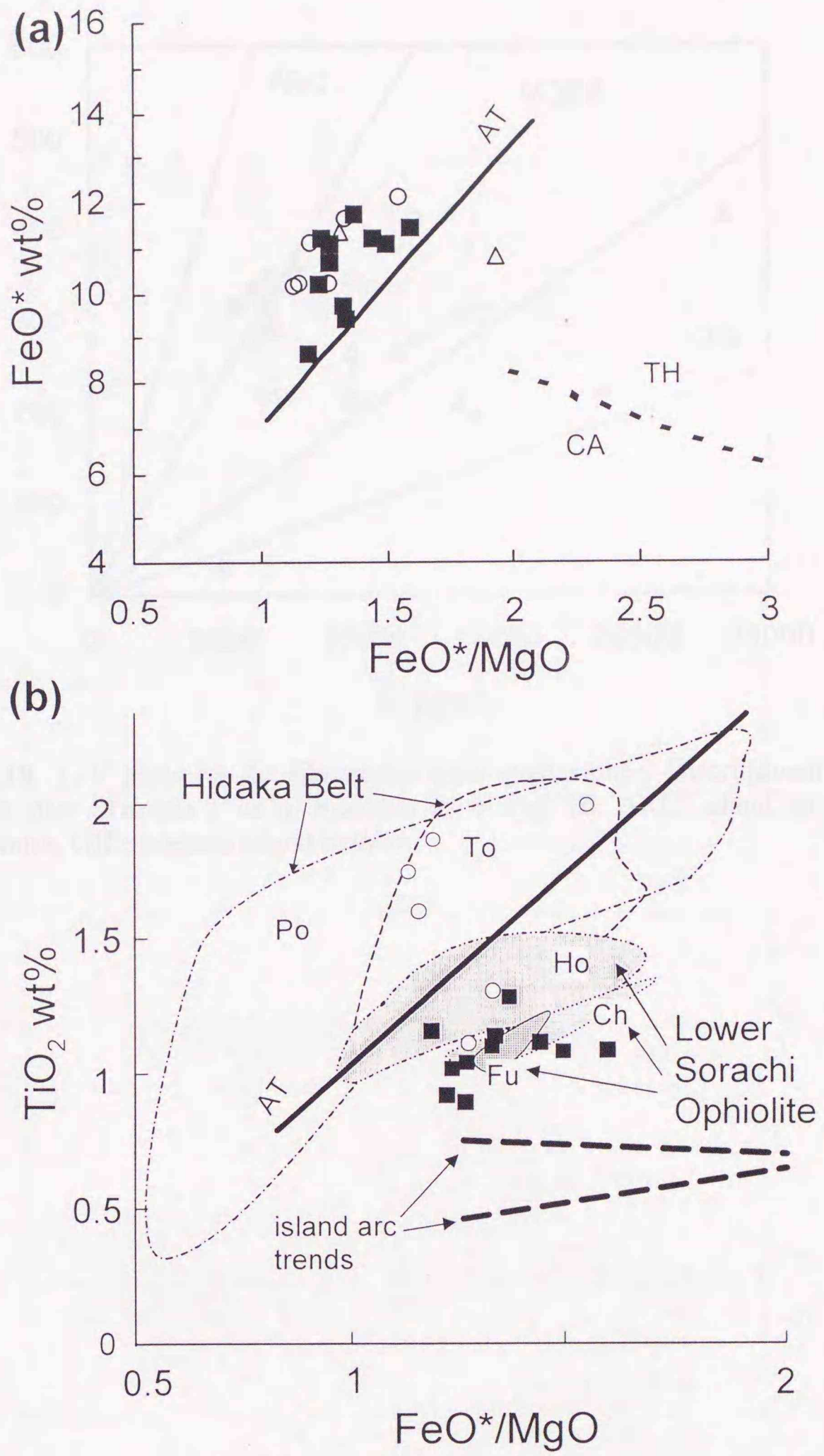


Fig. 17. Major element plots for the non-alkaline rocks. Discriminant fields and trends of abyssal tholeiite and island arc volcanics after Miyashiro (1973). Symbols as in Fig. 16. (a) FeO* vs. FeO*/MgO plot for tholeiitic / calc-alkaline discrimination. TH: tholeiitic, CA: calc-alkaline, AT: abyssal tholeiite. (b) TiO2 vs. FeO*/MgO plot for tholeiitic greenstones of the B-Unit and PT-Unit, compared with the Lower Sorachi Ophiolite and the Hidaka Belt greenstones. Po: Poroshiri Ophiolite (Miyashita 1983), To: Tomuraushi (Miyashita & Katsushima, 1986), Ho: Horokanai Ophiolite (Ishizuka 1981), Ch: Chiroro (Kiminami *et al.*, 1985), and Fu: Furano (Niida, 1992).

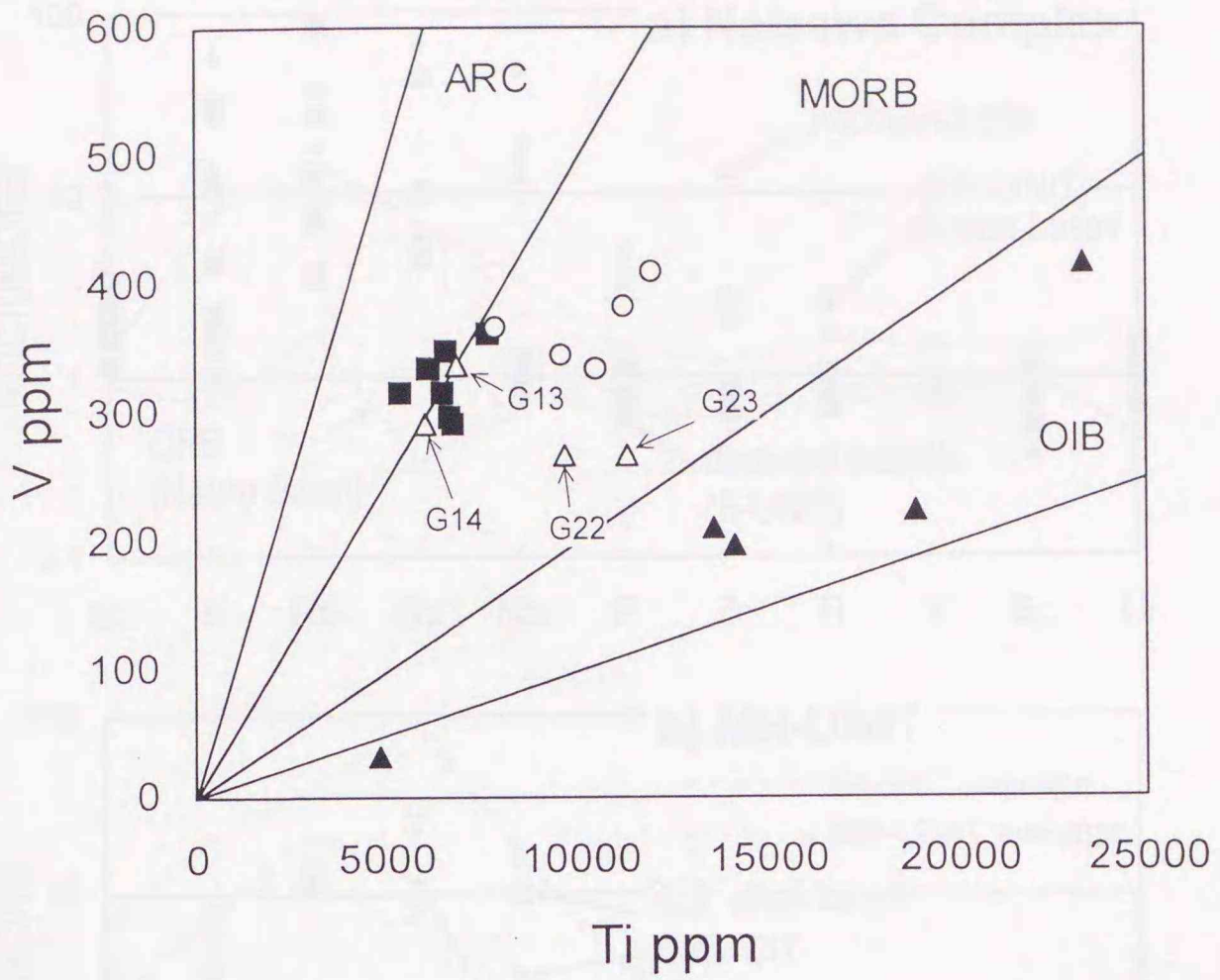


Fig. 18. Ti-V plots for the Idonnappu Zone greenstones. Discriminant fields after Shervais (1982). Symbols as in Fig. 16. ARC: island arc volcanics, OIB: oceanic island basalts.

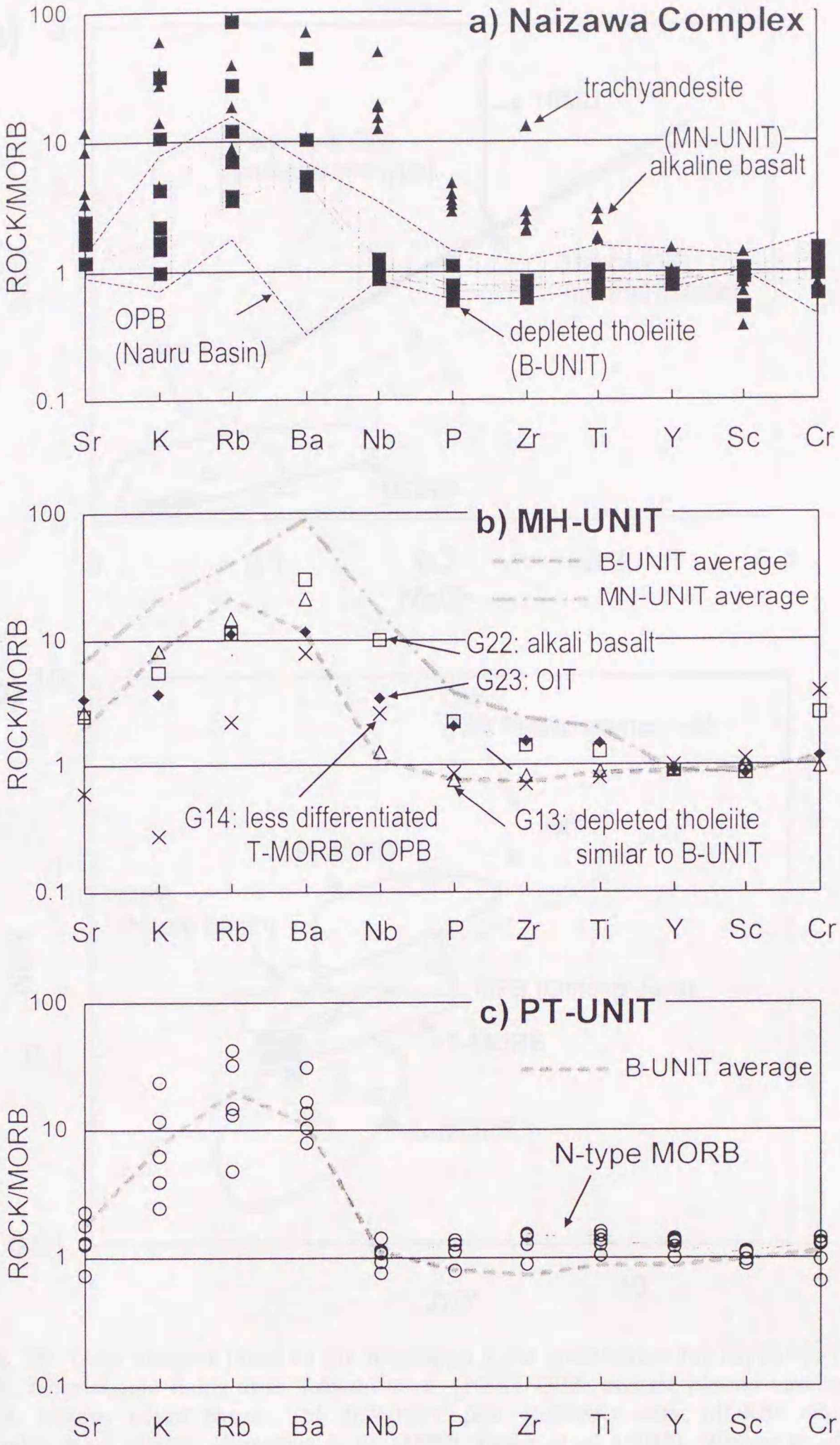


Fig. 19. MORB-normalized trace element patterns for Idonnappu Zone greenstones. N-MORB normalizer from Sun & McDonough (1989), except Cr after Pearce (1982). Symbols as in Fig. 16 except for (b).

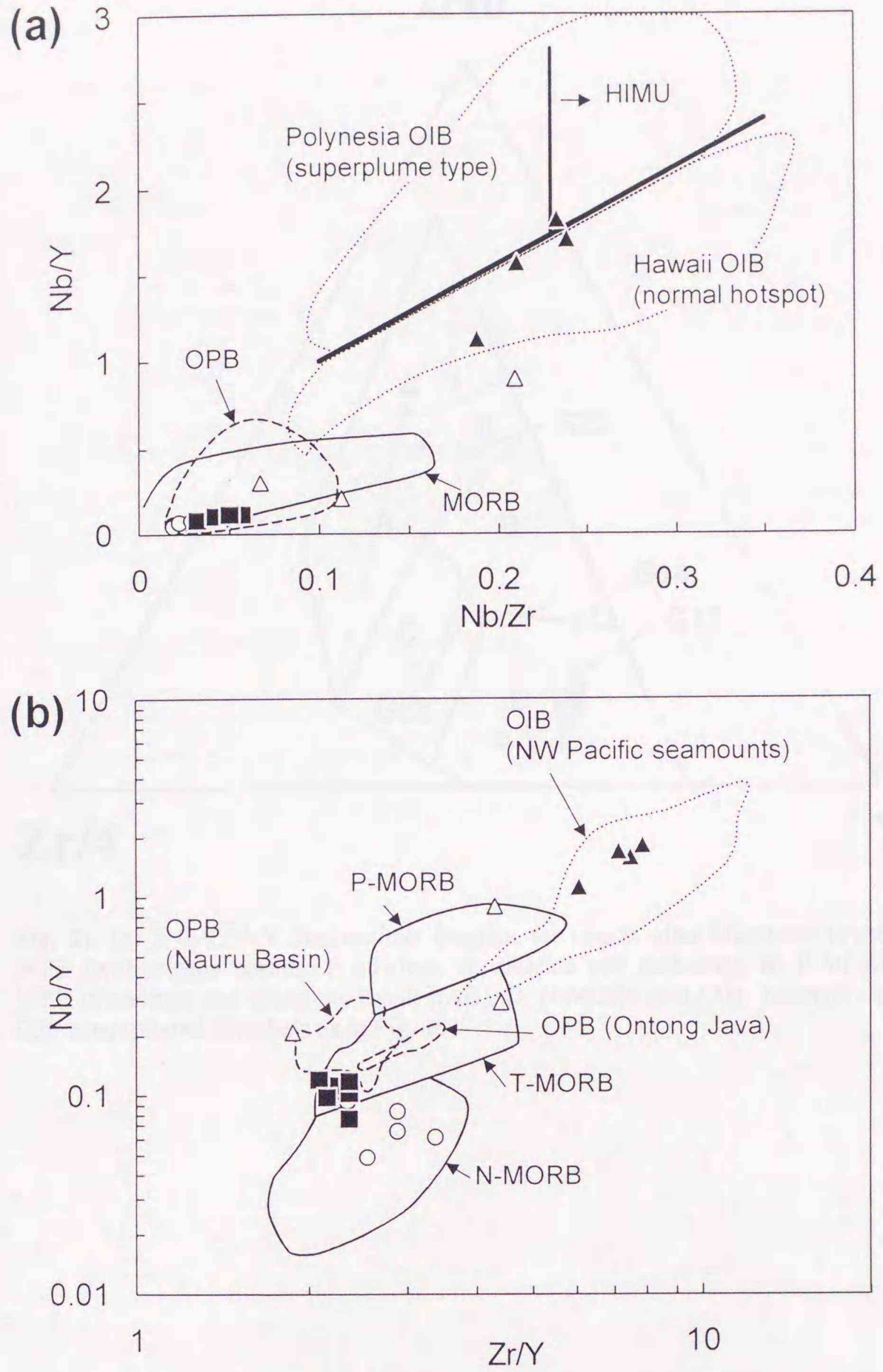


Fig. 20. Trace element ratios of the Idonnappu Zone greenstones. (a) Nb/Zr-Nb/Y plot. Discriminant fields after Tatsumi *et al.* (1998). OPB: oceanic plateau basalts, OIB: oceanic island basalts. (b) Zr/Y-Nb/Y plot. Reference data: MORBs after Rhodes *et al.* (1979), Humphris *et al.* (1980), Drake *et al.* (1985), Weaver *et al.* (1985), Pearce *et al.* (1986), Stakes & Franklin (1994), and Brewer *et al.* (1996); OPB after Floyd (1986), Saunders (1986), and Mahoney *et al.* (1993); NW Pacific OIB after Cambon *et al.* (1980), Baker *et al.* (1995), and Cristie *et al.* (1995). Symbols as in Fig. 16.

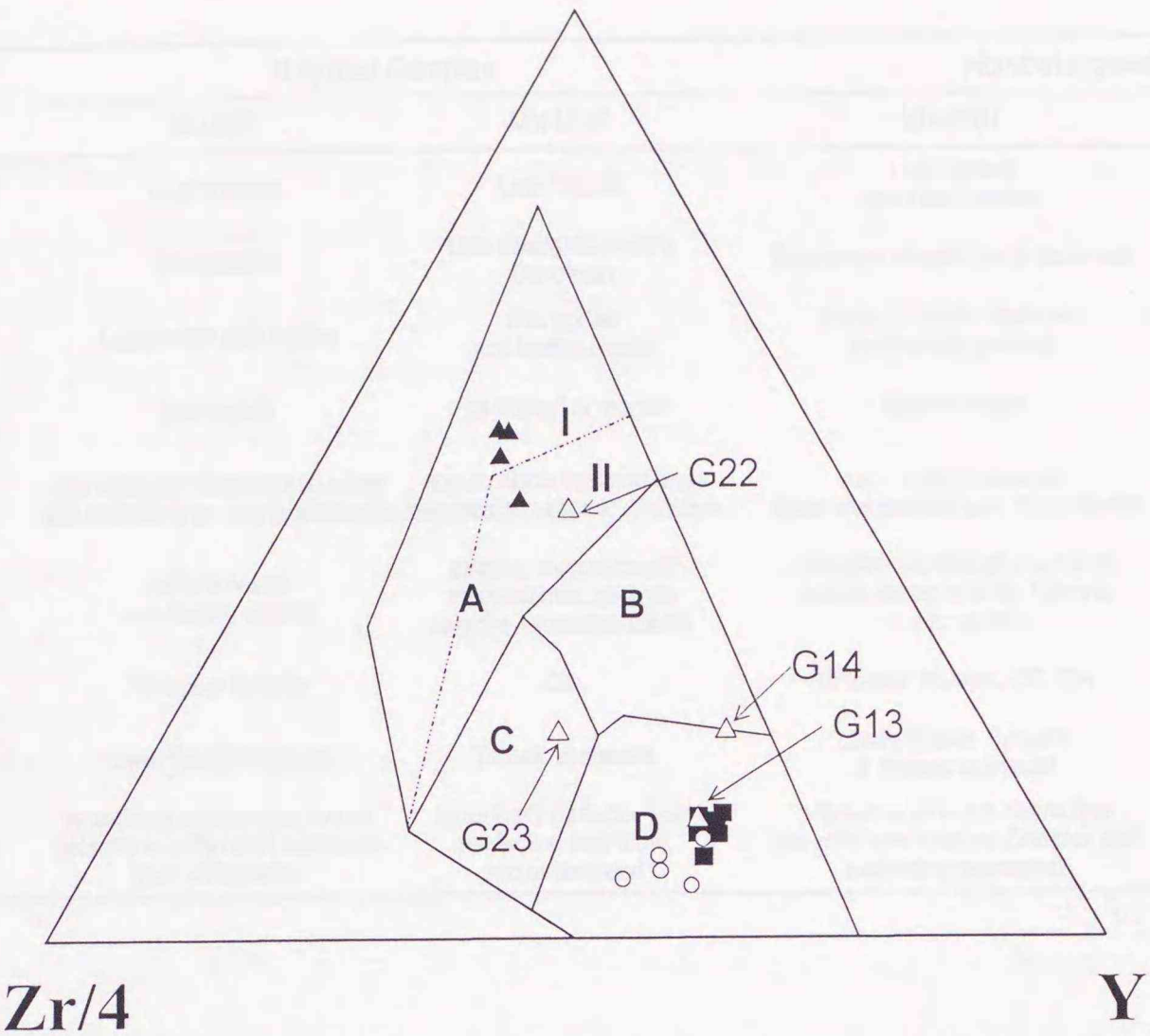


Fig. 21. (a) 2Nb-Zr/4-Y discriminant diagram for basalts after Meschede (1986). A: WPB (within-plate basalts: I: alkaline, II: alkaline and tholeiitic), B: P-MORB, C: WPB (tholeiitic) and island arc basalt (IAB), D: N-MORB and IAB. Trachytic sample G20 is not plotted. Symbols as in Fig. 16.

Table 4. Characterization of the Idonnappu Zone greenstones. OIA: oceanic island - type alkaline rocks, OIT: oceanic island tholeiite.

complex	Naizawa Complex		Horobetsugawa Complex	
unit	B-UNIT	MN-UNIT	MH-UNIT	PT-UNIT
inferred age of greenstones	Late Jurassic	Late Triassic	Late Triassic and Late Jurassic	Albian
age of black mudstone	(no clastics)	Late Valanginian - early Barremian	Berriasian - Hauterivian to Coniacian	Campanian
occurrence	Large scale slab bodies	slab bodies and faulted blocks	blocks in clastic matrix and sedimentary pebbles	imbricate stacks at bases of chert – clastic succession
mixture fabric with sediments	(not mixed)	"parquetry" or mosaic	block-in-matrix	severely sheared layered mixture
lithology	non vesicular close-packed pillow and massive lava, less hyaloclastite	non- to highly vesicular lava, hyaloclastite, volcanic sandstone	non- to highly vesicular pillow and massive lava, hyaloclastite	non-vesicular lava (cataclastic)
petrography	aphyric basalt >>ol-basalt, dolerite	aphyric, ol-(cpx)-basalt >>ankaramite, trachyte, aegirine-kaersutite dolerite	ol-basalt > picrobasalt cpx-basalt, aphyric basalt, dolerite, trachyte >> microgabbro	aphyric basalt (with pl-microphenocryst) >ol-basalt
chemistry	HFS-poor tholeiite	OIA	HFS-poor tholeiite, OIT, OIA	N-MORB
origin	Lower Sorachi Ophiolite	Triassic seamount	Lower Sorachi Ophiolite & Triassic seamount	abyssal basement
emplacement	tectonically eroded from forearc ophiolite at collision of seamount, then underplated	tectonically dissected from subducting seamount, and underplated	submarine slide and debris flow deposits from Naizawa Complex and subducting seamount?	"peeled" off the surface of subducted oceanic crust, accreted with chert-clastics

alkaline basalt (Fig. 16). HFS elements are depleted (Fig. 19b), and show a similar pattern to B-Unit tholeiites. G14 is a picritic basalt with olivine phenocrysts (10 - 15 modal %). It also plots in the sub-alkaline field (Fig. 16), and is poorly differentiated according to low FeO*/MgO, low SiO_2, and high Ni and Cr. Although Ti and Zr contents are low, Nb is slightly enriched relative to N-MORB, showing a OPB (Nauru) - like signature (Figs. 19b and 20b). This sample plots between the N-MORB and P-MORB fields in the Nb-Zr-Y diagram (T-MORB like; Fig. 21). This sample can be identified as poorly differentiated T-MORB or OPB, probably a variation of the Lower Sorachi - type depleted tholeiite. G23 is a subalkaline aphyric basalt (Fig. 16), in which all HFS elements are enriched (Fig. 19b). It plots in the field of within-plate tholeiite of Nb-Zr-Y diagram (Fig. 21), and is thus considered to be an oceanic island - type tholeiite (OIT). G22 is a vesicular olivine basalt pillow lava, which is classified as alkaline basalt (Fig. 16). It shows pronounced enrichment of incompatible elements (Fig. 19b), which is characteristic of alkaline basalts from oceanic islands (Pearce 1982). It is thus similar to the MN-Unit basalts in the Naizawa Complex.

PT-Unit *(Pelagic-Terrigenous Unit)*

All samples analyzed are classified as sub-alkaline basalt, by virtue of low Nb/Y ratios (Fig. 16). As in the B-Unit samples, FeO* increases with increasing FeO*/MgO (Fig. 17a), a feature of the tholeiite series. Although the data are few and there is considerable scatter, two groups can be recognized from HFS contents. The first group consists of G25 - 28, which contain 1.6 - 2.0 wt% TiO_2 (Fig. 17b) and 0.13 - 0.16 wt% P_2O_5. HFS element contents are almost equal to N-MORB (Fig. 19c). Ti-V plots and HFS element ratios also suggest that they have N-MORB characteristics (Figs. 18, 20, and 21). These greenstones are clearly distinguished from those of the B-Unit by their higher TiO_2 abundance, and lie within the compositional range of Hidaka Belt greenstones (Fig. 17b). The second group (G24 and 29) contain 1.1 - 1.3 wt% TiO_2 (Fig. 17b) and 0.08 - 0.09 wt% P_2O_5. HFS abundances are less than N-MORB, and are almost equal to the B-Unit (Fig. 19c). It is not clear whether these two samples are simply variants of the first N-MORB group, or are representatives of the B-Unit type.

The N-MORB -type greenstones of the first group are regarded as typical of the PT-Unit. The greenstone bodies described in Figs. 14a and 14b are of this type.

DISCUSSION

Reconstruction of the original disposition of lithological units

Because terrigenous rocks of the PT-Unit show Campanian radiolarian age in all thermal sequences and overlapping K-Ar ages (Fig. 9), It is concluded that the three thermal sequences were originally a single sequence (Fig. 8). Because the bedding planes and slaty cleavage planes are

vertically dipping to overturned, and exhibit a distinct thermal sequence 5 - 5.5 km thick, the Horobetsugawa Complex is exposed as a nearly vertical section of the Cretaceous accretionary prism. After the metamorphic peak, the sequence was tectonically triplicated, and the apparent thickness doubled. The boundary fault of each thermal sequence strikes obliquely at a low angle to the general tectonic trend of the Idonnappu Zone (see Fig. 8). The boundary faults are thus probably the ramp faults of a map-scale duplex with right lateral strike-slip sense. The Hidaka Main Thrust may be the floor fault of the duplex, and the Redatoi-Okada Thrust the roof fault. The youngest K-Ar age of each thermal sequence is 34 - 48 Ma; therefore, the duplex is considered to have formed after 34 Ma.

Relative movement of each lithological unit

In the Horobetsugawa Complex SQ-2, no obvious gap in K.I. can be recognized between the PT-Unit and the intercalated MH-Unit (Fig. 9). This trend suggests that the present distribution of both units was established soon after the sedimentation of the PT-Unit, and before the time of metamorphism.

SQ-3 in the T-Unit is distinguished from the other units by its high K.I. values. It was located structurally below the MH-Unit based on the reconstructed model (Fig. 22), because SQ-3 lacks the MH-Unit, and rare limestone blocks occur along with the sequence-boundary fault at the top of the T-Unit. The youngest radiolarian age (approx. 65 - 60 Ma) from the T-Unit is younger than the K-Ar age range (65 - 75 Ma: Iwasaki et al., 1995) of the MH-Unit. The T-Unit was thus probably tectonically emplaced below the MH-Unit during the uplift of that unit.

Some mudstones of the Naizawa Complex have lower K.I. than the uppermost horizon of the thermal sequences in the Horobetsugawa Complex (Fig. 9). This suggests that the Naizawa Complex was uplifted relative to the Horobetsugawa Complex after the peak metamorphism. The Horobetsugawa Complex now overlies the Naizawa Complex bounded by the Redatoi-Okada Thrust. However, it is considered that the Naizawa Complex was originally thrust over the Horobetsugawa Complex, and both complexes were subsequently overturned and the thrust inverted.

The assumed relative movement of the units discussed above is summarized in Fig. 23. The Naizawa Complex was buried and thickened until ca. 95Ma after its formation at ca. 120 Ma, attaining low K.I. values, and was subsequently uplifted. The PT-Unit and MH-Unit in the Horobetsugawa Complex were deposited between 90 and 70 Ma, and subsequently attained higher K.I. during the 70 to 40 Ma underthrusting beneath the Naizawa Complex. The T-Unit was emplaced into the actively uplifting Horobetsugawa Complex, and thus acquired low K.I. values.

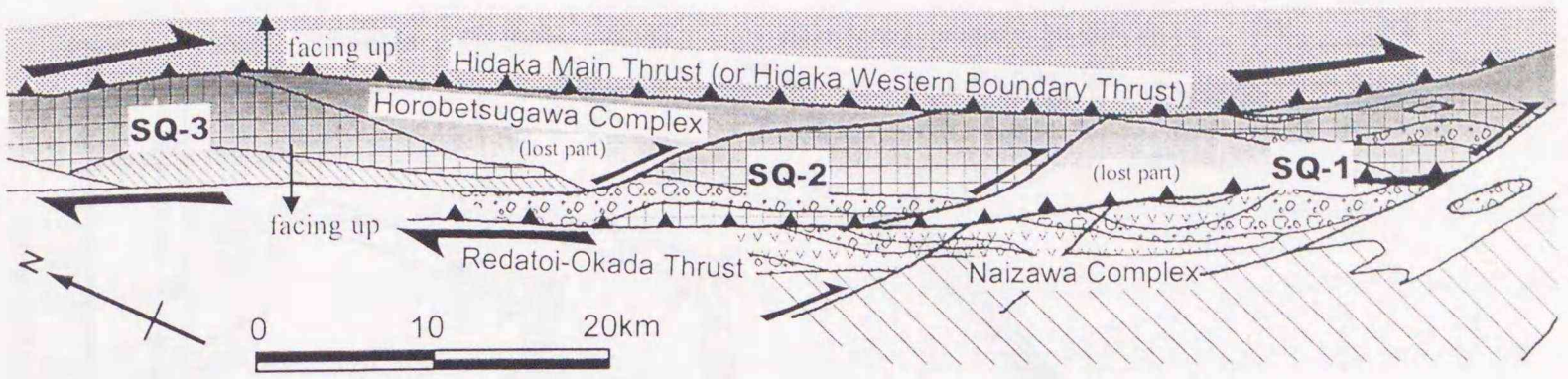


Fig. 22. Simplified reconstruction model for original distribution of the lithological units and the thermal sequences. The model is based on the assumption that duplexing was due only to right-lateral movement. Lithology ornaments as in Fig. 2. Graded tone indicates relative burial depth in the Horobetsugawa Complex (see Fig. 8).

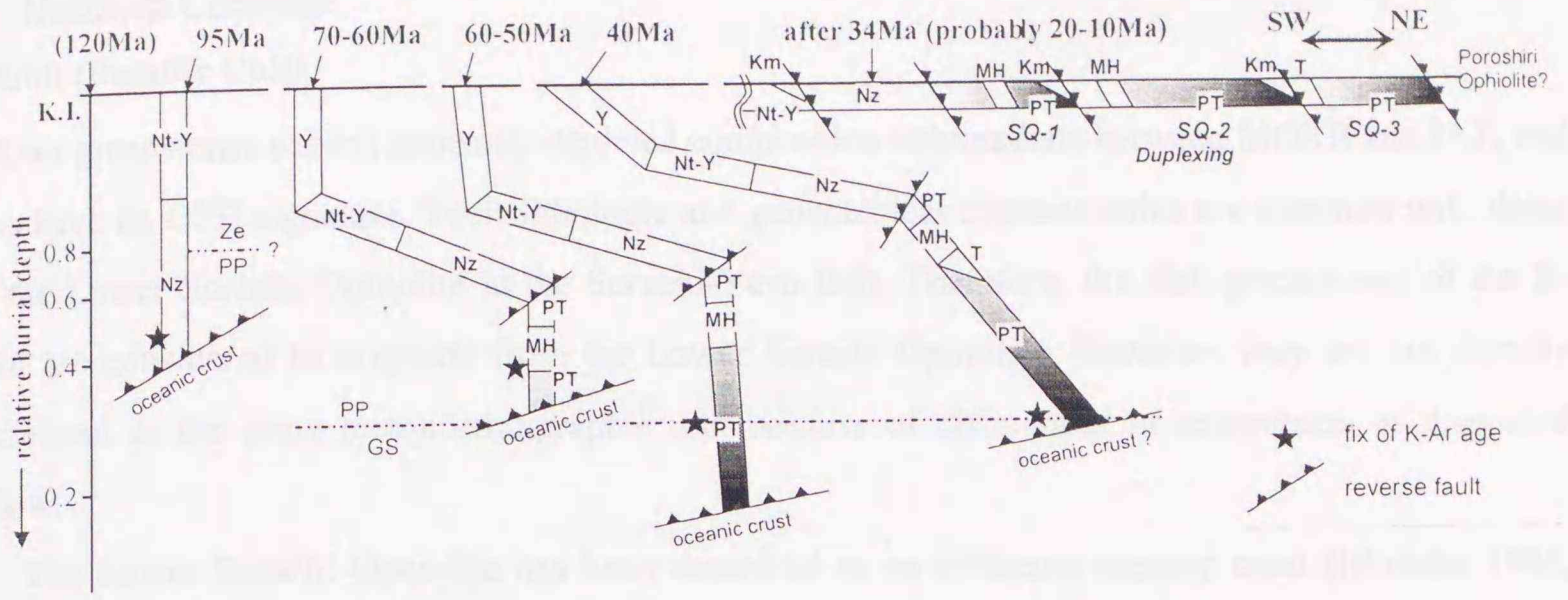


Fig. 23. Inferred burial and uplift history for accretionary and post-accretionary tectonics in the Idonnappu Zone, based on illite crystallinities, K-Ar ages and radiolarian ages. Nt-Y: Nitarachi Formation and part of Yezo Supergroup, Y: part of Yezo Supergroup, Nz: Naizawa Complex, PT: PT-Unit, MH: MH-Unit, T: T-Unit, Km: Neogene Kamikineusu Formation, Ze: zeolite facies, PP: prehnite-pumpellyite facies, GS: greenschist facies. Graded tone indicates relative burial depth in the Horobetsugawa Complex. Inclination of each column shows inferred tectonic tilting schematically.

Origin and emplacement of the greenstones in the Idonnappu Zone

1. Naizawa Complex

B-Unit (Basaltic Unit)

B-Unit greenstones exhibit generally depleted composition intermediate between MORB and IAT, and also have an OPB signature. Their lithologic and geochemical characteristics are common with those of the Lower Sorachi Ophiolite in the Sorachi-Yezo Belt. Therefore, the slab greenstones of the B-Unit are considered to originate from the Lower Sorachi Ophiolite. However, they are not directly correlated as the same tectonostratigraphic unit because of differences in occurrence, as discussed below.

The Lower Sorachi Ophiolite has been described as an obducted oceanic crust (Ishizuka 1980, 1981), a trapped oceanic crust (Niida & Kito 1986), or an accreted oceanic plateau (Kimura *et al.* 1994; Nagahashi & Miyashita 1997). There still seems to be no single model which explains all the features of petrology, stratigraphy, age, and metamorphism, and the origin of the ophiolite is still controversial.

The Upper Jurassic tholeiites of the Lower Sorachi Ophiolite were accreted to the forearc in the Tithonian - Berriasian, based on stratigraphy and clastic composition of the conformably overlying Nitarachi-Yezo Sequence (Kiminami *et al.* 1992; see Fig. 24). The tholeiites do not coexist with oceanic island - type alkaline rocks, nor with Triassic sediments. In spite of the lithologic similarity with the Lower Sorachi Ophiolite, the B-Unit greenstones are separated into several slabs alternating with greenstone-dominant mixed facies of the MN-Unit, and have no stratigraphic continuity with the Nitarachi-Yezo Sequence to the west (Figs. 2, 24). The basal part of the sequence (Tithonian - Berriasian S2 member of Kito 1987) is lacking in the Nitarachi-Yezo Sequence. These differences in occurrence strongly suggest that the slab bodies of the B-Unit do not comprise a coherent forearc sequence as do the Lower Sorachi Ophiolite occurrences, but represent large-scale bodies tectonically sliced from the forearc Lower Sorachi Ophiolite, and were subsequently covered by the Nitarachi-Yezo Sequence.

MN-Unit (Mixed Unit of Naizawa Complex)

According to the evidence for submarine eruption and OIB petrochemical signatures, the MN-Unit greenstones are considered to be fragments of an oceanic island with a limestone cap. Fossil ages of limestone indicate that the oceanic island was older than Late Triassic. The occurrence of the greenstones suggests that the oceanic island was dissected to form slab bodies or faulted blocks, and was tectonically mixed with chert and clastic rocks to form a mosaic fabric.

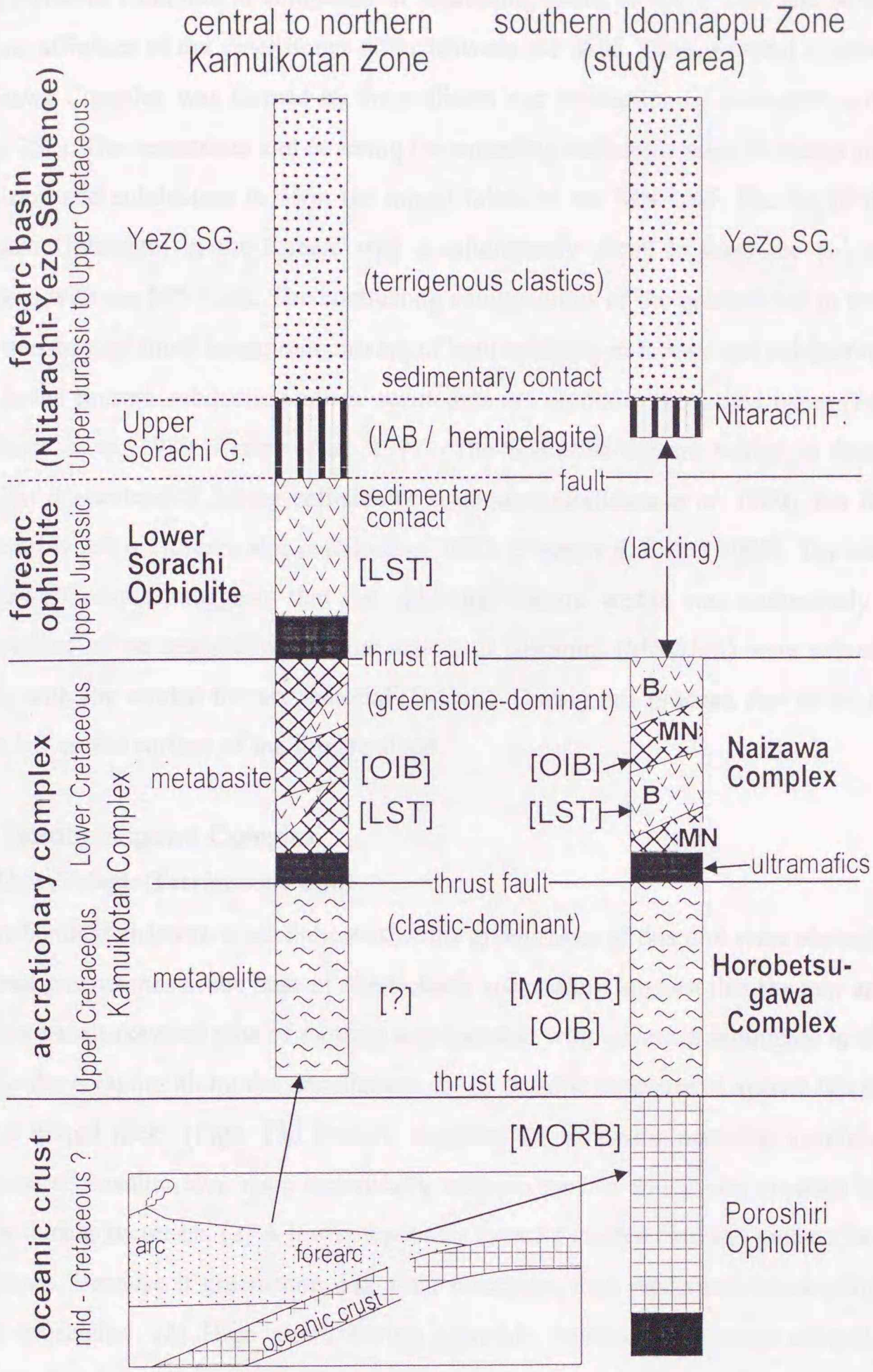


Fig. 24. Tectonostratigraphic comparison between the central to northern Kamuikotan Zone and the southern Idonnappu Zone. LST: Lower Sorachi - type tholeiite, B: B-Unit, MN: MN-Unit.

Mixing of B-Unit and MN-Unit

The Naizawa Complex is composed of alternating slices of the B-Unit and MN-Unit. As discussed above, affinities of the greenstones differ between the units. Thus, a model is newly proposed that the Naizawa Complex was formed by the collision and subduction of seamounts with ophiolitic forearc (Fig. 25a). The seamounts and covering / surrounding sediments were dissected and rearranged during collision and subduction to form the mixed fabric of the MN-Unit. The toe of the ophiolite (Lower Sorachi Ophiolite) in the forearc was simultaneously sliced to form the B-Unit, which was then stacked with the MN-Unit. The contrasting compositions of the greenstones in the Naizawa Complex can thus be explained by tectonic mixing of both ophiolite in forearc and subducting oceanic materials.

In the present subduction zones, seamounts are normally subducted intact (Fryer & Smoot 1985; Ballance *et al.* 1989; Fisher *et al.* 1991). The ophiolitic forearc wedge is destroyed, and tectonic erosion is accelerated during collision of seamounts (Ballance *et al.* 1989), but little or no seamount material is left on forearc slopes (Bloomer 1983; Bloomer & Fisher 1987). The tectonic model for the Naizawa Complex suggests that the ophiolitic forearc wedge was tectonically eroded due to the subduction of the seamounts, and the seamount volcanics (MN-Unit) were subsequently underplated along with the eroded forearc material (B-Unit). During this process, few or no seamount fragments were left on the surface of the forearc slope.

1. Horobetsugawa Complex

PT-Unit *(Pelagic-Terrigenous Unit)*

Petrochemical characteristics indicate that the greenstones of this unit were abyssal tholeiite. Intensely sheared greenstones at the base of chert-clastic successions suggest that the thin uppermost part of the abyssal basalt (several tens of meters) was accreted with covering sediments in the Late Cretaceous, due to the scraping along the decollement in the basaltic basement. Layered fabric in the greenstone-clastic mixed rocks (Figs. 13d and 15) suggests the following accretion conditions. (1) Significant volumes of basaltic lava were tectonically sheared, part of which was crushed into sand - silt sized gouge during accretion. (2) A low competency contrast existed between greenstone-derived gouge and mudstone. Because if greenstone was more competent than mudstone, block-in-matrix fabrics would have dominated. (3) High strain during accretion produced the compositional layering made of mudstone and greenstone-derived gouge.

The duplex-like imbricate structure of small slices of greenstone (Fig. 14a) suggests that the greenstones were accreted as small-scale piles, in contrast to the larger piles of the chert-clastic sequences (Fig. 25b). This occurrence is consistent with the structural model proposed by Kimura & Hori (1993), in which underplated oceanic piles are emplaced into off-scraped clastic piles by out-of-sequence thrusting.

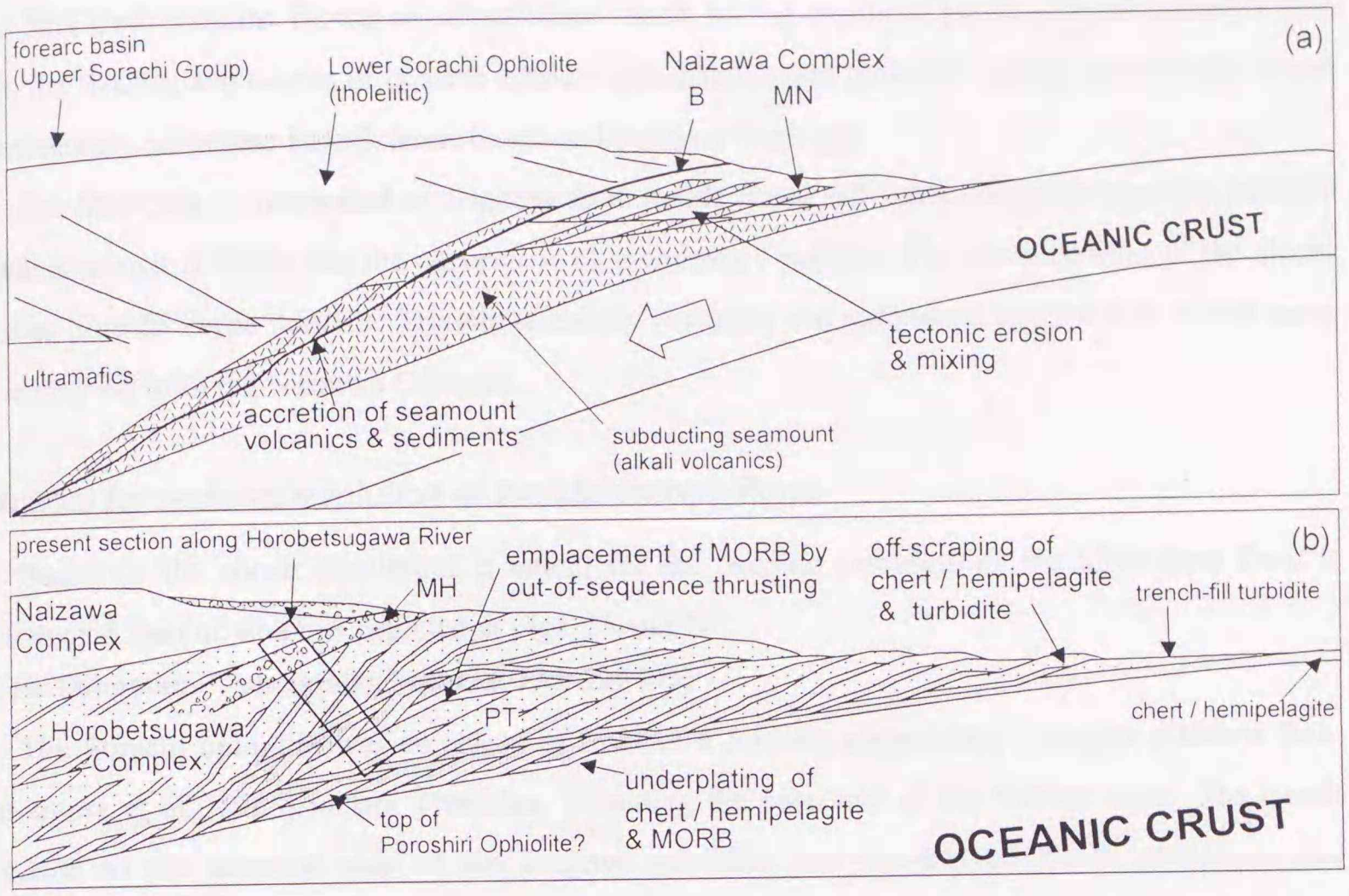


Fig. 25. Models of greenstone emplacement for the Idonnappu Zone. (a) Naizawa Complex in the Early Cretaceous. (b) Horobetsugawa Complex in the Late Cretaceous. B, MN, MH, and PT: Unit names.

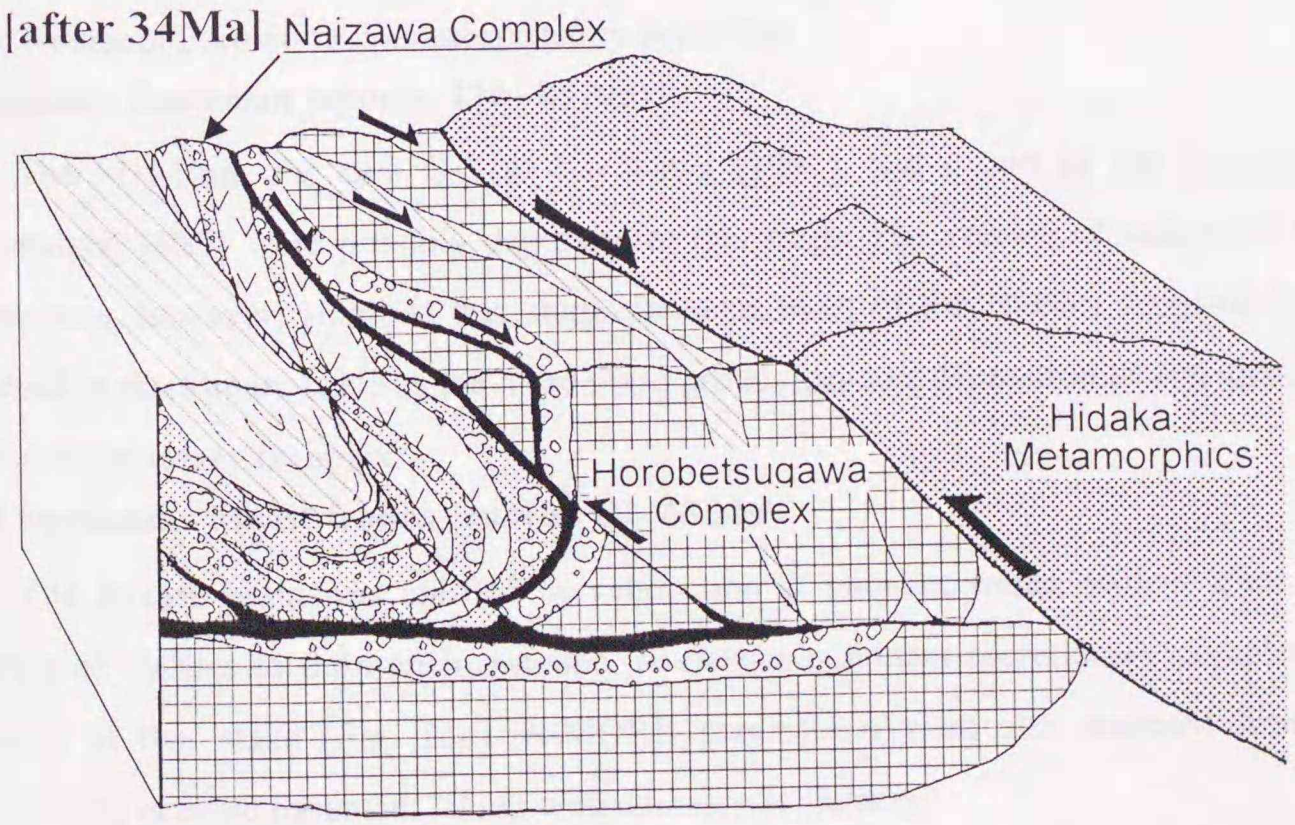


Fig. 26. Model for the post- late Paleogene reorganization of the Idonnappu Zone in Urakawa area.

MH-Unit (Mixed Unit of Horobetsugawa Complex)

The MH-Unit contains blocks of sub-alkaline basalt having common petrochemical characteristics with the B-Unit; and blocks of oceanic island - type alkaline and tholeiitic basalts. The oceanic island volcanics are older than Late Triassic based on limestone fossil age.

The MH-Unit is interpreted to originate from debris flows and submarine slide deposits, because of block-in-matrix fabric and the occurrence of sedimentary pebbles. The characteristics of the blocks (Lower Sorachi - type tholeiite, Triassic seamount volcanics and sediments) suggest that at least some were derived from the Naizawa Complex.

A model for tectonic evolution of the Idonnappu Zone

Based on the above discussion, a model for the tectonic evolution of the Idonnappu Zone is constructed, part of which is depicted in Figs. 25 and 26.

1. late Tithonian - Valanginian (approx. 135 -120 Ma)

The Sorachi ophiolite was emplaced in front of a Jurassic accretionary complex (Oshima Belt: Kawamura et al., 1986) in late Tithonian, becoming the basement of the forearc basin. The trench migrated to the seaward side of the accreted ophiolite, and arc-derived clastic sediments and hemipelagic sediments subsequently deposited on the ophiolite.

2. Hauterivian - Barremian (approx. 120 - 110 Ma)

Siliciclastic turbidites were deposited on the tholeiitic ophiolite and in the trench, due to uplift of the Oshima Belt (Kiminami et al., 1992). Soon after, Triassic seamounts collided to the ophiolite at the trench. The toe of the ophiolite was dissected, and tectonically mixed with sliced seamounts and trench-fill sediments, becoming the Naizawa Complex (Fig. 25a). This process was quite episodic. The Nitarachi Formation was subsequently deposited.

3. Aptian - Santonian (approx. 110 - 85 Ma)

The MH-Unit, the unit O-5 of Kiyokawa (1992), and a part of the Kitami-Esashi Complex (Tumanda, 1989) were possibly deposited at this stage. The volume of sediments in the Idonnappu Zone was, however, small at this stage. Because most of the clastics supplied from the arc were trapped in the forearc basin as the Yezo Supergroup, sporadic olistostromes and turbidites formed only a thin accretionary complex.

4. Campanian - Maastrichtian (approx. 80 - 65 Ma)

The forearc basin was uplifted by subduction of buoyant young oceanic plate, and voluminous supply of clastics to the trench resumed. A clastics-dominant accretionary complex (PT-Unit) grew rapidly in this stage (Fig. 25b). N-MORB greenstones were also accreted from the top of the subducting oceanic basement, along with covering sediments.

5. Paleocene (approx. 65 - 55 Ma)

The trench migrated to the east, and the PT-Unit formed a part of the inner trench-slope through post-accretion thickening. A trench-slope basin formed on the accreted PT-Unit, and clastic and hemipelagic sediments of the T-Unit were deposited within it. N-MORB were erupted around the trench east of the Idonnappu Zone (in the Hidaka Belt), due to ridge subduction (Kiminami, 1989; Miyashita et al., 1997).

6. Oligocene - middle Miocene (approx. 35 - 10 Ma)

The Hidaka Metamorphics began to thrust upon the Idonnappu Zone with right-lateral slip along the thrust fault (Arita et al., 1986). Both the Naizawa Complex and the Horobetsugawa Complex were uplifted and overturned, and the Horobetsugawa Complex was dissected and rearranged by right-lateral duplexing (Fig. 26). In the middle Miocene, both complexes were exposed to subaerial erosion and provided gravelly detritus. The Kamikineusu Formation was thus deposited and was subsequently folded between faults.

Conclusions

(1) The pre-Neogene system of the Idonnappu Zone in the Urakawa area is divided into the greenstone-dominant Naizawa Complex and the clastics-dominant Horobetsugawa Complex, both comprise two and three lithological units, respectively.

(2) Radiolarian assemblages from new 17 localities are reported, and sedimentation ages of each lithologic unit are estimated based on the fossil records. The youngest fossil ages are: Valanginian - Barremian in the MN-Unit of the Naizawa Complex; Coniacian - Santonian in the MH-Unit, Campanian - Maastrichtian in the PT-Unit, and early Paleocene in the T-Unit in the Horobetsugawa Complex.

(3) The Lower Cretaceous Naizawa Complex is regarded as a tectonic mixture of slices of the Lower Sorachi Group (B-Unit) and dissected Triassic seamount with trench-fill deposits (MN-Unit).

(4) The Horobetsugawa Complex is regarded as a pile of Upper Cretaceous clastic sediment and chert (PT-Unit), with intercalated debris flow or submarine slide deposits (MH-Unit), and inner trench-slope basin deposits (T-Unit).

(5) Original disposition of the lithological units has been restored using illite crystallinity patterns. Three gradual thermal trends, bounded by faults, are recognized in the Horobetsugawa Complex. The repetition of the trend suggests a later-stage tectonic triplication of the complex.

(6) Comparing fossil ages, K-Ar ages and lithologic assemblages, the Idonnappu Zone and the Kamuikotan Zone are considered to represent different parts of a continuous accretionary body.

(7) A comprehensive tectonic model was made (Figs. 25 and 26). The greenstone-dominant Naizawa Complex was episodically formed by the collision of Triassic seamount with ophiolitic forearc in the Early Cretaceous. The clastic-dominant Horobetsugawa Complex was formed with voluminous sediment supply to the trench in the Late Cretaceous. The Horobetsugawa Complex was rearranged through thrusting with right-lateral slip of the Hidaka Metamorphics in the Oligocene - Miocene.

Chapter III. Iwashimizu Complex: a deep section of the Lower Cretaceous accretionary complex

Introduction

This chapter presents constituents and inner structure of a high-P/T metamorphosed accretionary complex in the Mitsuishi-Shizunai area of the southern Kamuikotan Zone (Fig. 1), in light of radiolarian ages, metamorphism, and mode of occurrence and geochemistry of greenstones, with a new geologic map. Based on these data, structural framework of the southern Kamuikotan Zone, and modes of greenstone accretion at depth in subduction zone are discussed.

Geologic outline

The Kamuikotan Zone in the Mitsuishi-Shizunai area is occupied by the Iwashimizu Formation and the Idonnappu Formation (Suzuki *et al.*, 1961, Matsushita and Suzuki, 1962). The Iwashimizu Formation consists dominantly of greenstones, with subordinate amount of chert and siliciclastic sedimentary rocks. The Idonnappu Formation consists dominantly of siliciclastic mudstone / sandstone and chert, accompanied by greenstone and limestone. This study attributes both the Iwashimizu and Idonnappu formations together to the single "Iwashimizu Complex", because both lithofacies are complicatedly arranged in a tectonic pile, and cannot be logically divided as described below.

Neogene marine sediments of the Nishikawa Formation unconformably cover the Iwashimizu Complex and the Nitarachi-Yezo Sequence (Wada *et al.*, 1992). The Iwashimizu Complex and the Nishikawa Formation tilted together up to 70-90° dip along the western margin of the complex, and at ca. 20° dip in southwestern part of the study area (Fig. 27).

The Iwashimizu Complex dominantly trusts over the Nitarachi-Yezo sequence along its eastern margin. The complex is also overlain by the Nitarachi-Yezo Sequence in selected routes in the eastern part of the study area, as described in the next chapter.

Lithologic division

Lithology and stratigraphy of the Iwashimizu Complex in study area was formerly described by Nakano (1978, 1981). He concluded that the complex is faulted into blocks, and relations between each blocks has not been understood. ,

The new mapping on 1/10,000 scale (Figs. 28, 29) leads a new conclusion that the constituent lithologic facies are systematically arranged comprising a tectonostratigraphic sequence (Fig. 30). Here the new lithological division is proposed for the Iwashimizu Complex in Mitsuishi-Shizunai area

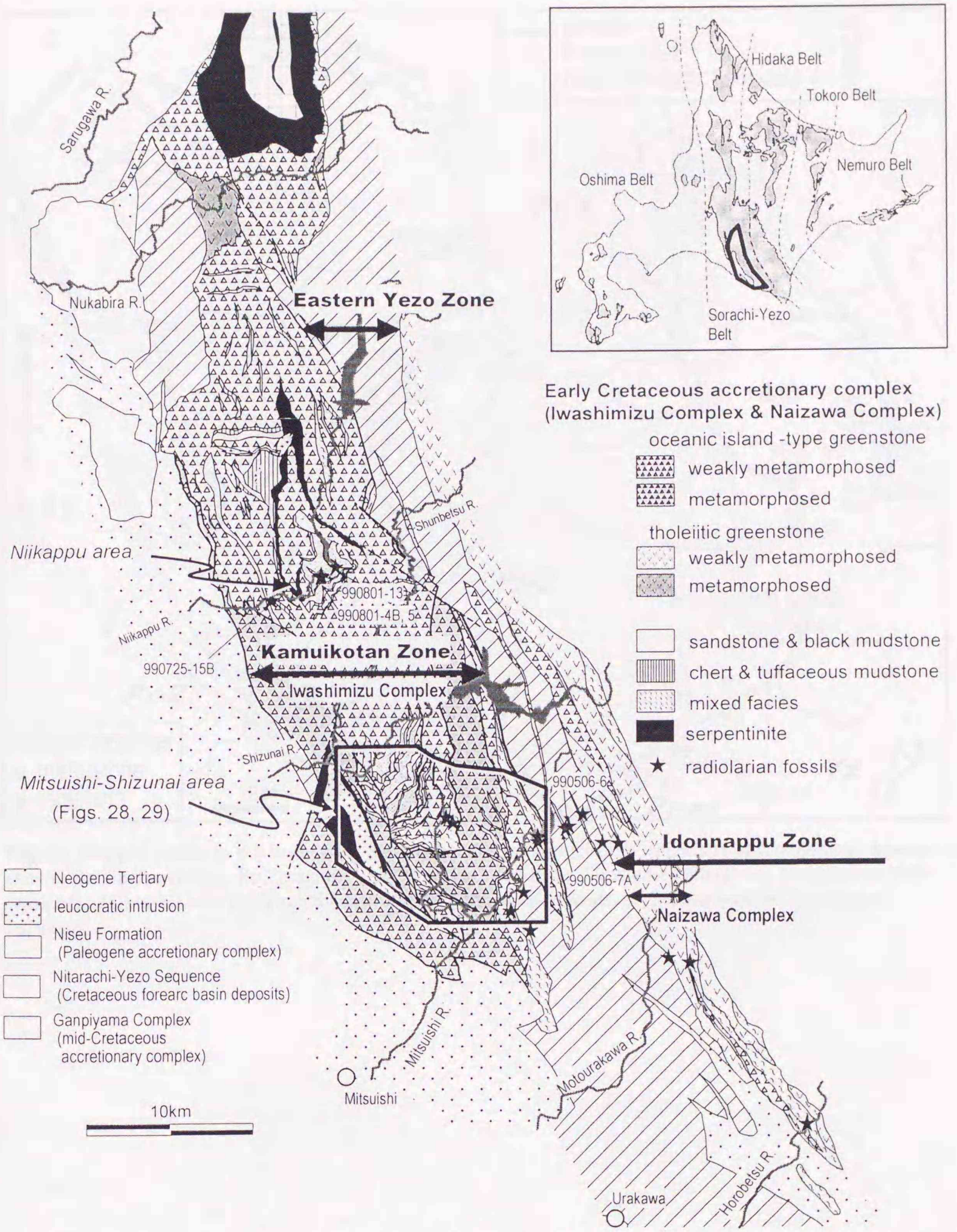


Fig. 27. Geologic map of the southern Kamuikotan Zone. Compiled from Osanai & Matsushita (1959; 1960); Yoshida et al. (1959); Matsushita & Suzuki (1962); Koitabashi et al. (1978); Takahashi & Suzuki (1978); Watanabe & Maekawa (1985); Sakai & Kanie (1986); Watanabe & Niida (1987); Wada et al. (1992); Sakakibara et al. (1999); Kawamura et al. (in press) and this study.

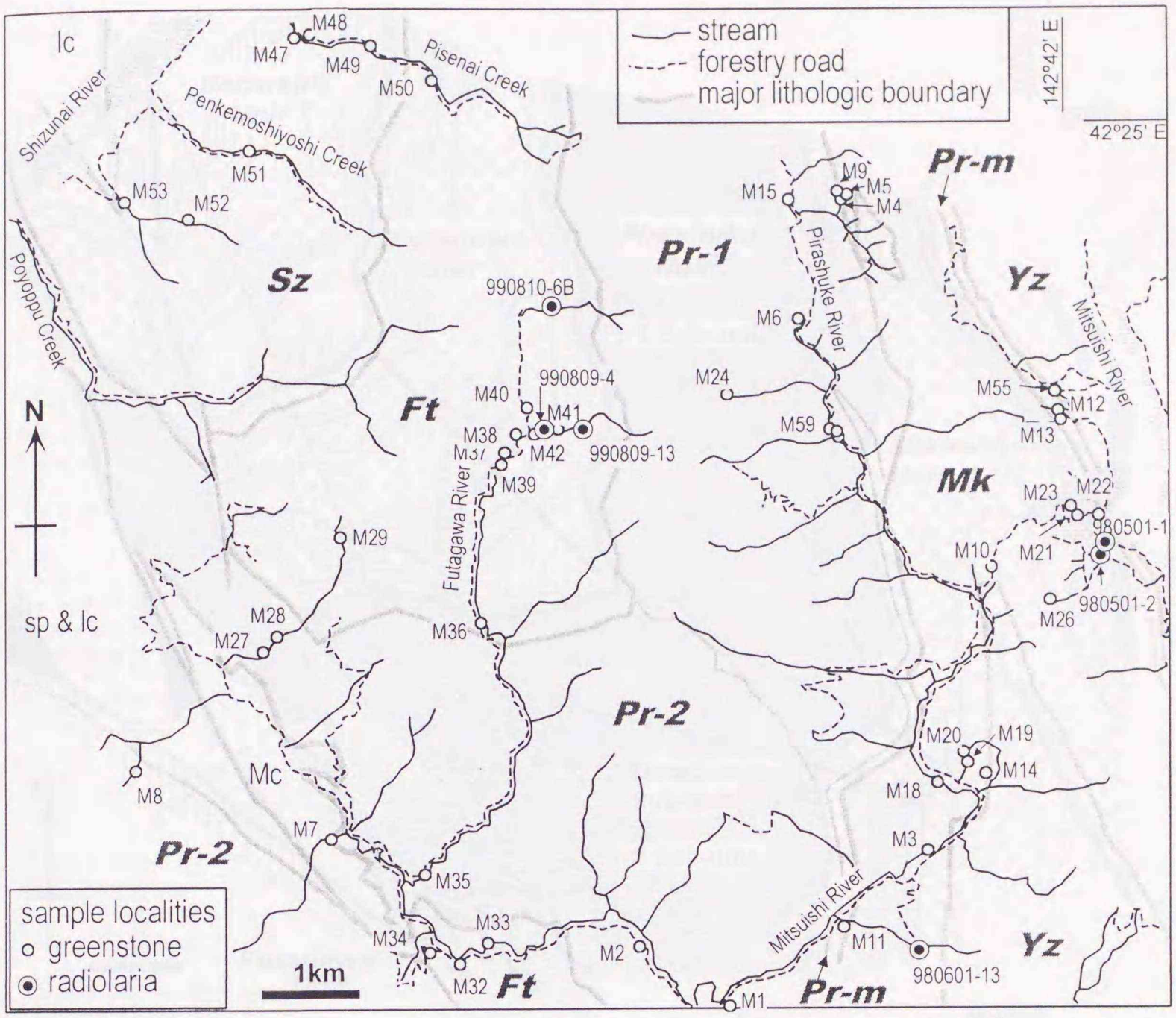


Fig. 28. Mapped routes in the study area. Sample localities for greenstone chemistry and radiolarian ages are shown. Sz: Shizunai Unit, Ft: Futagawa Unit, Pr-1, Pr-2 and Pr-m: Pirashuke Unit (Pr-m: Metadolerite Sub-unit), Mk: Mikawa Unit, Yz: Yezo Supergroup, Mc: Miocene deposits, sp: serpentinite, lc: leucocratic intrusion.

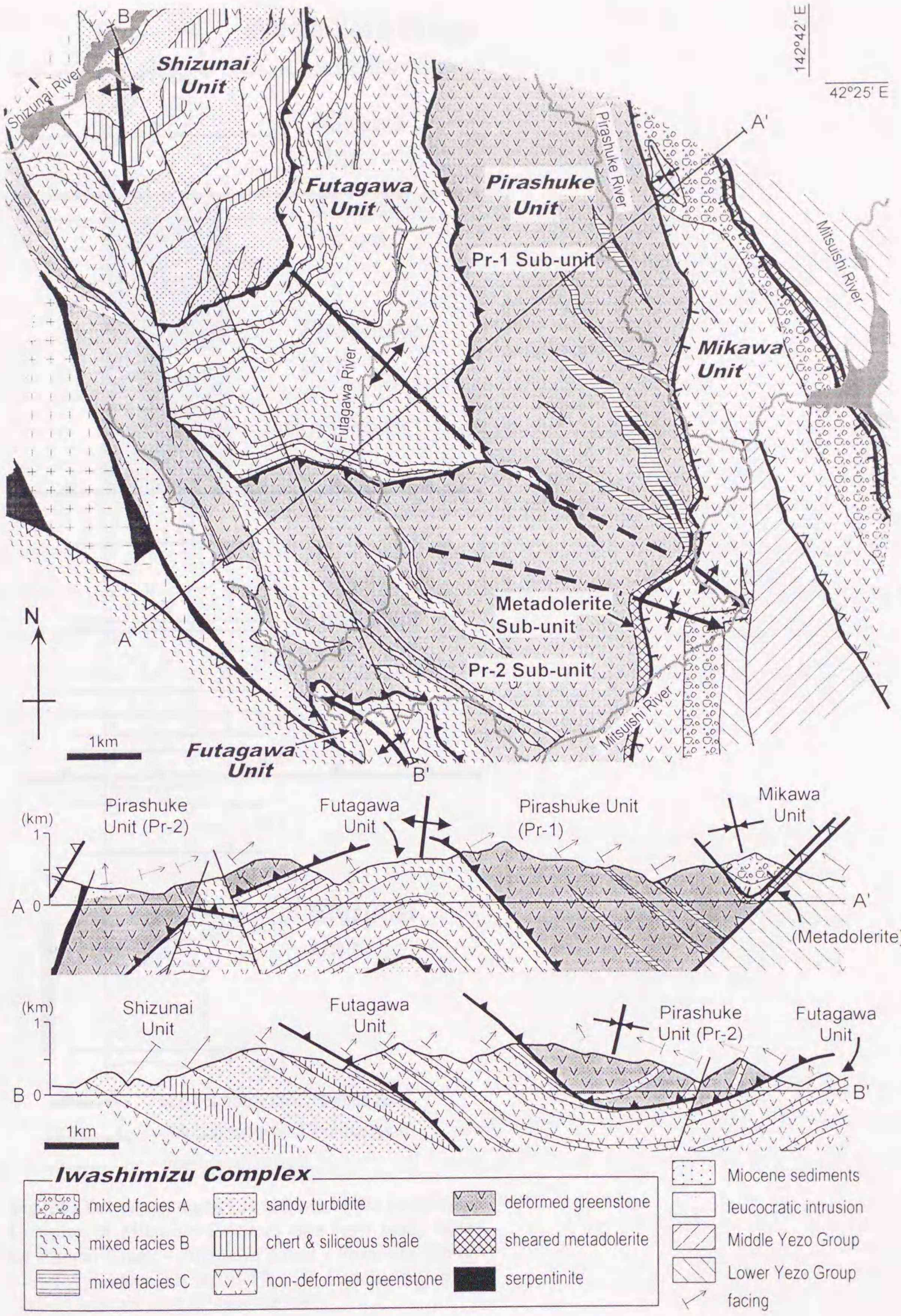


Fig. 29 Geological map and sections of the Iwashimizu Complex in the Mitsuishi - Shizunai area

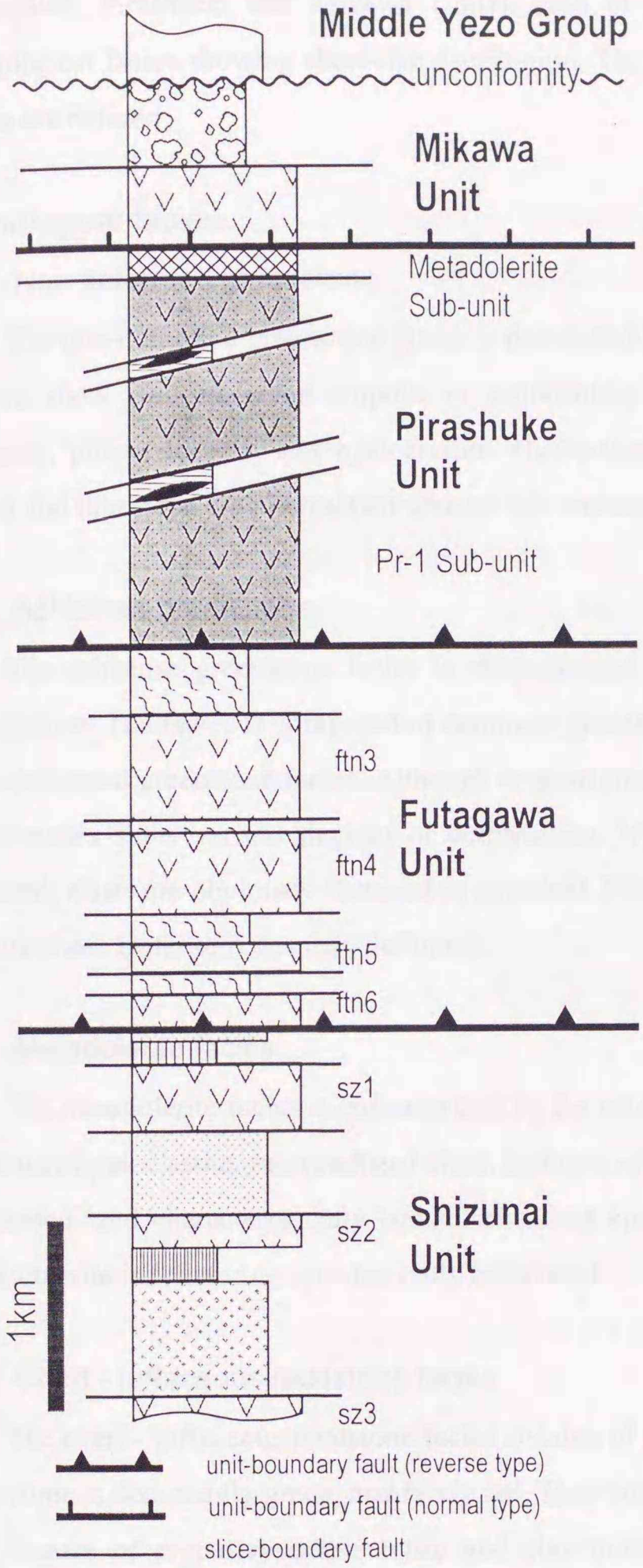


Fig. 30. Tectonostratigraphic column of the Iwashimizu Complex in Mitsuishi-Shizunai area (east wing: based on Pisenai Creek - Futagawa River - Pirashuke River). Lithology ornaments as in Fig. 29. Labels "ftn3-6" & "sz1-3" indicate slab ID (see the text).

based on assemblage of constituent lithofacies. The complex is divided into four units (Shizunai, Futagawa, Pirashuke, and Mikawa Units), each of which is defined by unique assemblage of lithological facies showing sheet-like distribution. The lithological facies are first described, then the units are defined.

Lithological facies

1. Non-deformed greenstone

The non-deformed greenstone facies is dominated by non- or very weakly deformed greenstones, which show well-preserved eruptive or sedimentary structures. The greenstones are pillow lava, dolerite, pillow breccia, and hyaloclastite. Hyaloclastite occasionally shows weak foliation. Minor chert and limestone are intercalated without any obvious shear zone.

2. Schistose greenstone

The schistose greenstone facies is characterized by a occurrence of pale-green and schistose greenstone. The facies is composed of dominant greenstones with minor chert and limestone, as in the non-deformed greenstone facies. Although original structure of greenstones is partly recognizable, the greenstones show various degrees of deformation. Hyaloclastite and pillow breccia are commonly foliated; clasts are obviously flattened or stretched. Pillow lava and its amigdules are weakly flattened or stretched. Dolerite is scarcely deformed.

3. Metadolerite facies

The metadolerite facies is characterized by the occurrence of metamorphosed dolerite, with minor schistose hyaloclastite, recrystallized chert, and rare epidote-amphibolite. Most dolerite bodies are not deformed, and characteristically contain abundant epidote replacing plagioclase. However, is some part, dolerite is foliated or cataclastically brecciated.

4. Chert - tuffaceous mudstone facies

The chert - tuffaceous mudstone facies consists of red chert and tuffaceous mudstone. Tuffaceous mudstone is dominantly green, and rarely red. They consist mainly of feldspar fragments, radiolarians, and matrix of cryptocrystalline felsic and clay minerals which partly shows glass-shard texture. Tuffaceous mudstone conformably overlies chert if not faulted. They are well stratified, and are non-deformed or partly folded.

5. Clastics facies

The clastics facies consists of dominant sandy turbidite, minor muddy turbidite and conglomerate,

and rare pebbly mudstone. Though stratification is broken by deformation in some part, bedding planes commonly keep continuity, and in some part, are mesoscopically non-deformed. Sandstone is dominantly coarse-grained, and contains many quartz and feldspar particles.

6. Mixed facies A

The mixed facies A is characterized by a complicated occurrence of coarse sandstone (and sandy alternation), tuffaceous mudstone, and greenstone bodies. Chert and limestone bodies are rarely contained. Most of the sandstone and tuffaceous mudstone bodies are notably weakly consolidated. Beside their bad exposure, the constituent bodies show distributions laterally traceable. There is no outcrop which show a block-in-matrix fabric except broken turbidite. Therefore, the mixed facies A is a stack of slices of sandstone, tuffaceous mudstone, and greenstone. Each slice is several tens meters thick, and presumably several hundreds meter long. The slices are internally not or very weakly deformed. Greenstone and mudstone is sheared and foliated restrictively along slice boundaries. As described later, the facies characteristically contains greenstone bodies of different metamorphic grade: ones of lawsonite-albite facies with aragonite(high-P/T type); and the others of zeolite facies to prehnite-pumpellyite facies without aragonite (low P/T type).

7. Mixed facies B

The mixed facies B is characterized by a occurrence of strongly sheared and foliated black mudstone, some of which are accompanied by sheared greenstone forming a layered mixture. Recrystallized chert, tuffaceous mudstone, sandstone, and greenstone bodies are also contained. In the layered mixed rock, sheared greenstone and mudstone are several millimeters to several tens centimeter thick, and alternate each other. Such feature is comparable with the "sumi-flow" structure described by Kawamura et al. (1998). Chert and sandstone bodies are not laterally traceable, whereas a tuffaceous mudstone body extends several kilometers laterally.

This facies is interpreted as a broken mixture of greenstone and chert - clastic sequence.

8. Mixed facies C

The mixed facies C is characterized by an lithologic assemblage consisting of metachert, mafic schist, and minor serpentinite. No terrigenous clastic rocks such as black mudstone and siliciclastic sandstone occur. Metachert and mafic schist are deformed, are cut by numerous shear zones, and do not show any stratigraphic succession. Serpentinite is composed by antigorite, brucite, magnetite, and relict chromite. The protolith of serpentinite is assumed as dunite with euhedral chromite and rare bastite.

This facies is interpreted as mixture of greenstone and chert, both of which possibly comprised a

sedimentary sequence. The mixture also contains block or slice of exotic serpentinite.

Unit definition

1. Shizunai Unit

Type locality: On the left bank of Shizunai Dam (Shizunai Town), typically along Pisenai and Penkemoshiyoshi Creeks (Fig. 28).

Definition: A geological complex consisting of the non-deformed greenstone facies, the chert - tuffaceous mudstone facies, and the clastic facies.

Lithology: The unit consists of alternating sheet bodies of greenstone, chert / tuffaceous mudstone, and turbidites (Fig. 29). The greenstone and chert / tuffaceous mudstone slices are almost non-deformed internally, and turbidites are weakly deformed, or occasionally deformed to be broken facies. The slices are cut by faults at both top and bottom, or comprise volcano-sedimentary sequence with other slices. Highly sheared rocks, identical to the mixed facies B, narrowly occur along slice boundaries (not mappable).

Distribution: The Shizunai Unit occupies northwest part of the study area, *i.e.* around the Shizunai Dam Lake. The unit extends northwestward, at least to the Nukabira River. This unit occupies central wide area of the Iwashimizu Complex, at the core of a large-scale culmination (Fig. 27).

Correlation: Correlated with both the Idonnappu Formation and part of the Iwashimizu Formation (Suzuki et al., 1961).

Remarks: I recognized the lithologic assemblage consisting of slices of non-deformed greenstone, chert, and coarse clastic rocks along Niikappu, Biu, Ribira, and Nukabira Rivers (Fig. 27). They are thus correlative with the type Shizunai Unit of the study area. In the Shunbetsu River area, neighboring to the north of the study area, a lithologic assemblage consisting of non-deformed greenstone facies and chert - tuffaceous mudstone facies widely occur. Though it contains only scarce clastic facies, it is temporarily identified as a variation of the Shizunai Unit. The Shizunai Unit assemblage is most dominant in the whole

Iwashimizu Complex, in area and probably also in volume.

2. Futagawa Unit

Type locality: On the upper reaches of Futagawa River (branch of Mitsuishi River), Mitsuishi Town (Figs. 27 and 31).

Definition: A geological complex consisting of the non-deformed greenstone facies and the mixed facies B.

Lithology: The unit consists of alternation of greenstone slices (non-deformed greenstone facies) and "inter-slice" shear zones (mixed facies B) as displayed in Figs. 29 and 31. Original sedimentary, eruptive, and intrusive sequence is preserved in the greenstone slices. Whereas almost no sedimentary sequence is recognizable in the inter-slice shear zones. No mappable chert and turbidite body occur.

Distribution: The Futagawa Unit mainly lies at the central part of the study area (Fig. 29). sedimentary structure indicate that the Futagawa Unit structurally overlies the Shizunai Unit, and is structurally overlain by the Pirashuke Unit (Fig. 30). The Futagawa Unit also occurs in south part of the study area: narrowly on the lower reaches of the Futagawa River, as a fenster among the Pirashuke Unit (Fig. 29).

Correlation: Correlated with a part of the Iwashimizu Formation (Suzuki et al., 1961).

Remarks: Similar lithologic assemblages are observed along the Penkepipi Creek (a branch on the left bank of Shunbetsu River), lower reaches of Niikappu, Biu, and Ribira Rivers. In these areas, there occurs chert bodies larger than ones in the mixed facies B of the study area. It is not sure that the chert bodies are laterally continuous as slices, or discontinuous as bocks / lenses in the mixed facies B. There seems to exist many variations in scale of chert / tuffaceous mudstone and clastic facies in such areas, so that it is possible that the Futagawa and Shizunai Units are not so clearly distinguished from each other as the study area.

3. Pirashuke Unit

Type locality: On the upper reaches of Pirashuke River (branch of Mitsuishi River), Mitsuishi Town (Fig. 28).

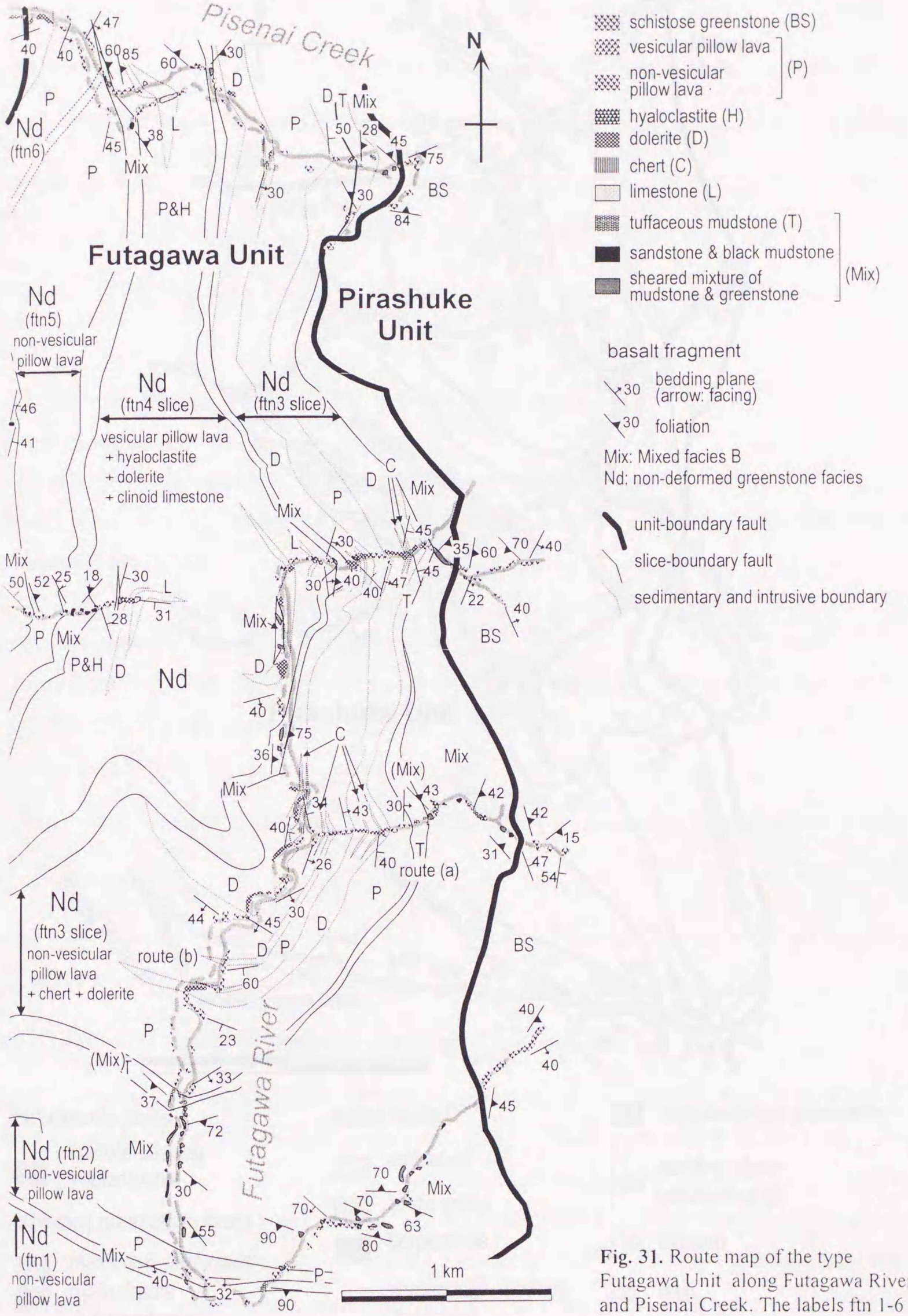
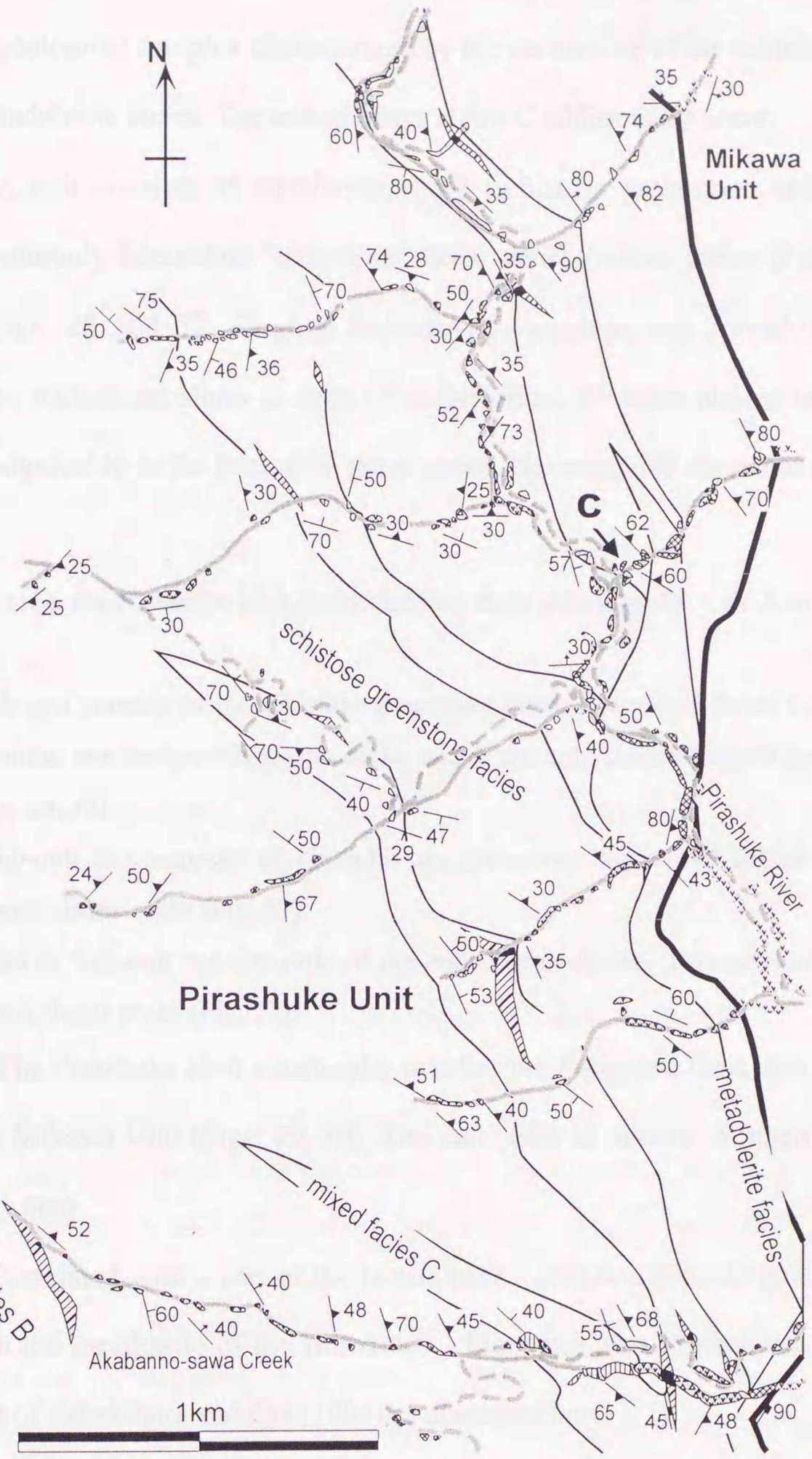


Fig. 31. Route map of the type Futagawa Unit along Futagawa River and Pisenai Creek. The labels ftn 1-6 indicate individual greenstone slices.



metadolerite facies
- epidote-bearing metadolerite

schistose greenstone facies
- massive & pillow lava
- hyaloclastite & pillow breccia

mixed facies C
- metachert
- mafic schist
- serpentinite
- serpentinite - bearing landslide

- non-deformed greenstone
- 30 bedding plane (arrow: facing)
- 30 foliation
- 30 fault

Fig. 32. Route map of the type Pirashuke Unit in the Pirashuke River area.

Definition: A geological complex characterized by the occurrence of the schistose greenstone and / or the metadolerite facies. The mixed facies B and C additionally occur.

Lithology: The unit consists of metabasite slices (schistose greenstone and metadolerite facies), and commonly intercalate "inter-slice" shear zones (mixed facies B and / or C) as displayed in Figs. 29 and 32. Original sedimentary, eruptive, and intrusive sequence is preserved in the metabasite slices in spite of deformation. Whereas almost no sedimentary sequence is recognizable in the inter-slice shear zones. No mappable chert and turbidite body occur.

In the study area, the Pirashuke Unit is divided into three sub-units: Pr-1, Pr-2, and Metadolerite Sub-units.

The Pr-1 Sub-unit consists of the schistose greenstone facies and mixed facies C. This sub-units thus does not contain any terrigenous clastic rocks, and is the only sub-unit which intercalates small serpentinite (Figs. 29, 32).

The Pr-2 Sub-unit is composed of the schistose greenstone facies and mixed facies B, thus contains terrigenous clastic rocks (Fig. 29).

The Metadolerite Sub-unit consists only of the metadolerite facies. This sub-unit does not also contain terrigenous clastic rocks (Fig. 32).

Distribution: The Pirashuke Unit structurally overlies the Futagawa Unit, and is structurally overlain by the Mikawa Unit (Figs. 29, 30). The unit occur at eastern, southern, and western part of the study area.

Correlation: Correlated with a part of the Iwashimizu Formation (Suzuki et al., 1961). Also correlative with the metabasite of the Horokanai - Etanbetsu area (Shibakusa, 1989) *i.e.* the Horokanai Unit of Sakakibara and Ota (1994) as discussed later.

Remarks: The most critical difference between the Pirashuke and Futagawa Units is the nature of greenstone slices. However, there left a problem that the difference between "schistose" and "non-deformed" is ambiguous. In the field, greenstones of the Futagawa and Shizunai Units, except dolerite, are commonly reddish colored, because they contain a low-grade metamorphic mineral assemblage: pumpellyite + hematite ±lawsonite. Meanwhile, greenstones of the Pirashuke Unit are mostly pale-green, because they dominantly contain the hematite-free assemblages such as lawsonite + sodic pyroxene, epidote + pumpellyite etc. (see later description). Hence, describing metamorphic mineral

assemblages is useful to ensure distinguishing these units. Common occurrence of sodic amphiboles is also a characteristic of the Pirashuke Unit.

The schistose greenstone facies occurs at: lower reaches of Shunbetsu River, Kuzuresawa Creek (branch of Shunbetsu River), lower reaches of Niikappu, Biu, and Ribira Rivers. Meta-pillow lava and schistose hyaloclastite with abundant epidote, which are comparable with the metadolerite facies, occur along Nukabira River. All of them occur at the peripheral parts of the Iwashimizu Complex (Fig. 27).

4. Mikawa Unit

Type locality: Around the Mitsuishi Dam Lake (upper reaches of Mitsuishi River), Mitsuishi Town (Fig. 28).

Definition: A geological complex consisting of the mixed facies A and / or the non-deformed greenstone facies.

Lithology: The unit is characterized by the occurrences of mixed facies A. In the type locality (Fig. 33), the mixed facies contains poorly consolidated sandstone and tuffaceous mudstone bodies, as much as metamorphosed greenstone bodies. At the left slope of the Pirashuke River, the mixed facie contains a zeolite- and prehnite- bearing greenstone body of several hundred meters diameter.

Distribution: The Mikawa Unit lies at the eastern margin of the Iwashimizu Complex (Fig. 29). The unit structurally overlies the Pirashuke Unit, and is structurally overlain by the Nitarachi Formation and the Lower Yezo Group, and is unconformably overlain by the Middle Yezo Group (Fig. 30; see Chapter IV).

Correlation: Correlated with a part of the Iwashimizu Formation (Suzuki et al., 1961). The unit in the study area was described as the Iwashimizu Formation by Matsushita and Suzuki (1962), and as both the Hidaka Western Greenstone Belt (non-deformed greenstone facies) and the Yezo Supergroup (mixed facies A) by Nakano (1981).

Remarks: The most notable member of this unit is zeolite- and prehnite-bearing rock. These rocks co-occur with high-P/T rocks in the mixed facies A.

Such low-grade greenstone is recognized along Kuzuresawa Creek (branch of Shunbetsu River) and Nukabira River. In both cases, the low-grade rocks occur at the easternmost (uppermost) part of the Iwashimizu Complex (Fig. 27).

Map-scale structures and tectonostratigraphic framework

Structural framework

Four kinds of geologic structures confine the distribution of the lithologic facies and units in the

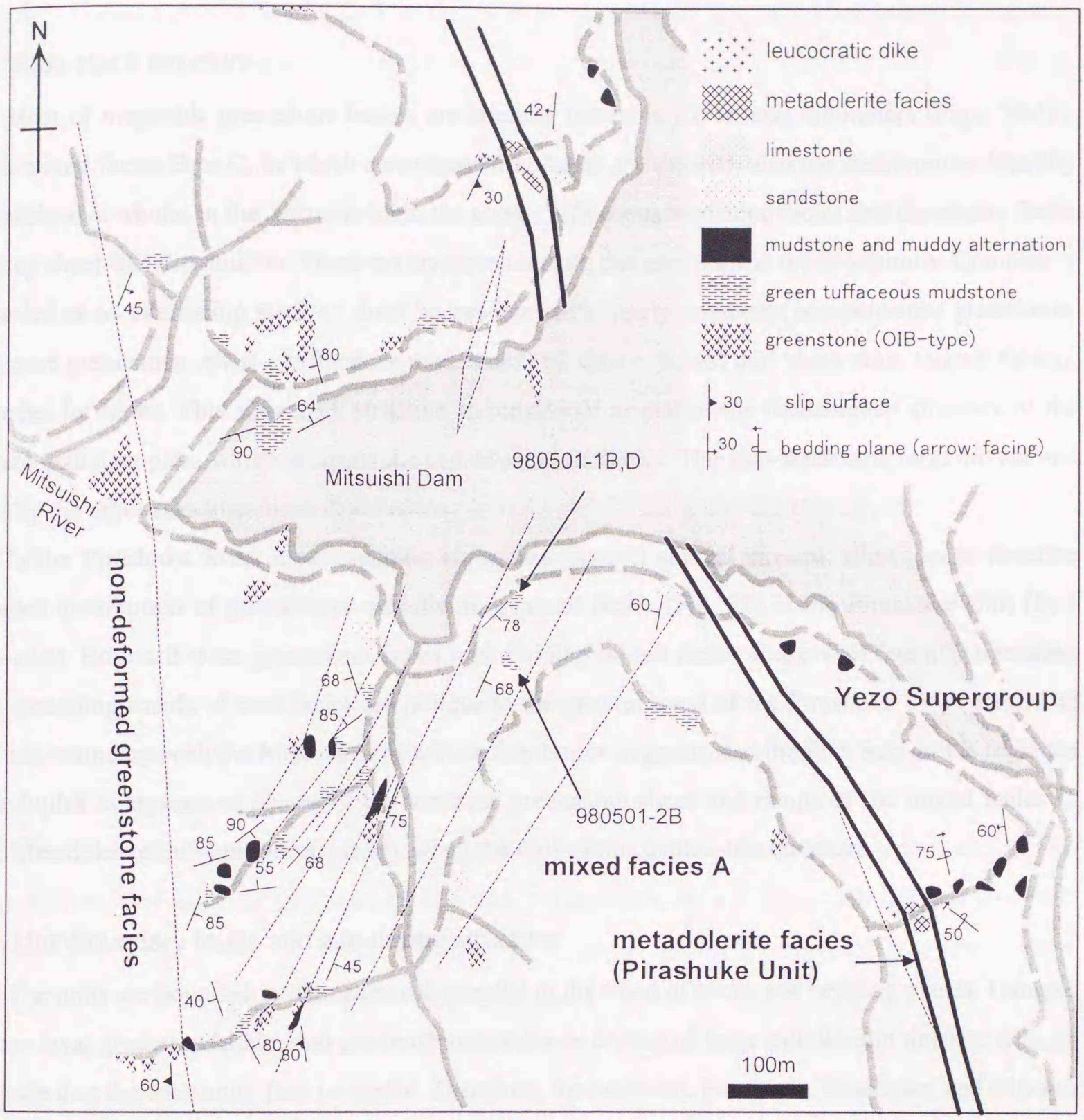


Fig. 33. Route map of the mixed facies A around the Mitsuishi Dam.

study area.

1. Slab-stack structure

Most of mappable greenstone bodies are laterally traceable for several kilometers (Figs. 30-32). Each mixed facies B or C, in which constituent lithofacies are sheared, also has distributions laterally traceable as a whole. In the Shizunai Unit, the chert - tuffaceous mudstone facies and the clastic facies display sheet-like distribution. These occurrences indicate that each unit in the Iwashimizu Complex is regarded as an alternating stack of sheet bodies internally nearly coherent (non-deformed greenstone, schistose greenstone, chert - tuffaceous mudstone, and clastic facies) and shear zone (mixed facies), bounded by faults. This slab-stack structure is considered as one of the fundamental structure of the Iwashimizu Complex, which arranges the constituent lithofacies. The slab-stack structures are cut and bent by the other structures described below.

In the Pirashuke River area, mapping along near-parallel several streams allows us to describe detailed distribution of greenstones and dividing mixed facies (Fig. 32) in the Pirashuke Unit (Pr-1 Sub-unit). Both schistose greenstone facies and dividing mixed facies C are well laterally traceable. The extending trends of both facies are oblique to the general trend of the Pirashuke Unit (parallel to the unit boundary with the Mikawa Unit). This distribution suggests that the Pr-1 Sub-unit is regarded as a duplex composed of horses of the schistose greenstone slices and ramps of the mixed facies C. The Metadolerite Sub-unit occurs nearly along the roof of this duplex-like structure.

2. Unit-boundary faults and pile-nappe structure

The units are bounded by the faults sub-parallel to the trend of slices and bedding planes. Hanging pillow lava, graded turbidite, and clustered amigdules in ceiling of large pillows and dolerite sills, all indicate that the four units face normally. Therefore, the Shizunai, Futagawa, Pirashuke, and Mikawa Units comprise a structural pile in ascending order, bounded by the bedding-subparallel unit-boundary faults.

Along the lower reaches of the Futagawa River in south part of the study area, non-deformed greenstones of the Futagawa Unit occur as a fenster, among the Pirashuke Unit (Pr-2 Sub-unit). Bedding plane and foliation of greenstones and mixed facies in both units gently dip (0-30°). This occurrence suggests that the unit-boundary fault between the Pirashuke and Futagawa Units originally near horizontal, and then tilted to dip 35 to 70° as seen in the middle to northern part of the study area.

The Iwashimizu Complex is, therefore, regarded as a pile of nappe (=units) folded together in later stage.

3. Map-scale folds

The pile-nappe structure is folded by anterooms and syndromes. The most typical fold structure is recognized by the route map along upper reaches of Futagawa River (Fig. 31). In this area, a greenstone slice of the Futagawa Unit (labeled as ftn3 in Fig. 31) is well laterally traceable. Bedding planes of pillow lava and chert, and intrusive boundaries of dolerite sills in the slice strike nearly N-S and dip east with eastward-facing in northern area, whereas it strikes E-W to NW-SE and dip south with southward-facing in southern area. At the junction of both trends on the Futagawa Forestry Road, a gradual change in strike of the intrusive boundary between a dolerite sill and pillow lava / chert is recognized. Accompanying mixed facies sheets and the other greenstone slices also show the same trend. These trends indicate an existence of SE-plunging fold axis, forming an anticline.

An anticline is also recognized along the lower reaches of the Futagawa River. In this area, bedding plane of normally facing pillow lavas (fenster of the Futagawa Unit) gradually changes from NW-dipping in the west to NE-dipping in the east, indicating an existing of probably north-plunging anticline. Pelitic rocks of the mixed facies B overlie these pillow lavas at both sides.

Along Mitsuishi River, a non-deformed greenstone slice, a mixed facies A sheet (both belonging to the Mikawa Unit), and the metadolerite facies (Pirashuke Unit) together show a "Z"-shaped and hook-like fold structure (Fig. 29). Strike of foliation in the mixed facies A changes from NS through NE-SW to NS, from north to south.

Along Pankemoshiyosi Creek, a branch of Shizunai River, a non-deformed greenstone slice of the Shizunai Unit, consisting of dolerite sills and intercalated chert, show a map-scale bending structure: SE-dipping in the east, and SW-dipping in the west. Because this greenstone slice is overturned, the bending structure is therefore a south-plunging antiform.

By the former three fold structures, the unit-boundary fault between the Futagawa and Pirashuke Units are consistently bent. The fold structure along Mitsuishi River area seems to confine the distribution of the Lower Yezo Group, which occur only in the south from the fold. The unconformity at base of the Middle Yezo Group, described in the next chapter, cuts this fold structure. Hence, this fold structure is considered to have formed after the formation of the unit boundary and sedimentation of the Lower Yezo Group, and before the basal unconformity event of the Middle Yezo Group (*i.e.* formed during Barremian-Albian time, see the chapter III).

4. Later faults

Several types of later faults, which intercalate clay and/or gouge, are recognizable, though they are not systematically described.

The major and mappable faults are striking NW-SE to NNW-SSE. Along these faults, the Iwashimizu Complex overlies the Middle Yezo Group and the Miocene Nishikawa Formation. In the

southwest part of the study area, slicken lines (N6E30S) and Riedel's shear (N12W57W) on in fault gouge (Y-surface: N52W68S) between the Iwashimizu Complex and Miocene sediments indicate that the former relatively overrides the latter with dextral slip component. There are many minor faults which show the same trend. The unit-boundary fault between the Pirashuke and Mikawa Units generally strikes N-S to NNW-SSE, and intercalates gouge and clays in several outcrops. Hence, it may have been re-activated since Miocene.

Though only sporadically observed, NE-SW striking dextral faults and NW-SE striking sinistral faults seem to occur, both of which possibly comprise a conjugate set.

5. Tectonostratigraphic framework

Map-scale structures described above lead the original tectonostratigraphic framework of the Iwashimizu Complex. The slab-stack structure and the pile-nappe structure show that the Iwashimizu Complex is regarded as a multiple tectonic pile: the first order stack of greenstone, chert-tuffaceous mudstone, and clastic slices bounded by mixed faces, together forming the lithologic units; and the second order pile of these units bounded by initially near-horizontal unit-boundary faults.

According to facings of both greenstone and clastic rocks, the Shizunai, Futagawa, Pirashuke, and Mikawa Units comprising a tectonostratigraphic succession in ascending order (from structurally bottom to top), which can be typically displayed as an apparent columnar section (Fig. 30) from route maps along Pisenai Creek – branches of Pirashuke River – Mitsuishi River routes (on the east wing of the major antiform).

This tectonostratigraphic succession is folded, generally forming a "half-dome" structure in the study area. The compiled geologic map of the whole Iwashimizu Complex (Fig. 27), partly and preliminarily mapped by this study, implies that constituent lithofacies of Iwashimizu Complex are arranged displaying a culmination (*i.e.* a dome structure) as a whole, though there seem to be many internal folds. The Pirashuke Unit equivalents (mafic schist) generally occur along the margin (structurally upper horizon) of the culmination, and non-deformed greenstones of the Shizunai-Futagawa Units equivalents occur in the central wide part (structurally lower horizon) of the complex. The Mikawa Unit equivalents are currently recognized only along the eastern margin (structurally top) of the complex. Such distributions are likely to be consistent with the tectonostratigraphic framework constructed from the studied Mitsuishi-Shizunai area. Stratigraphic relations with surrounding sedimentary sequences also support this structural framework: the east-facing Middle Yezo Group unconformably overlies the Iwashimizu Complex long the eastern edge of the complex (see Chapter III); and the west-facing Miocene Nishikawa Formation overlies the complex with steeply dipping unconformable boundary along the western wedge. Therefore, the surrounding sequences stratigraphically contact only with the structurally upper horizons of the Iwashimizu Complex.

Radiolarian ages

Radiolarian fossils were extracted from mudstone and chert samples from 11 localities in the Iwashimizu Complex (Figs 27 and 28). Four samples were collected from the Shizunai Unit equivalents exposed along Niikappu River (Fig. 27), the north extent of the study area. The rests are from the study area (Fig. 28), two of which from the Futagawa Unit, and three samples from the Mikawa Unit. Radiolarians were also extracted from greenish mudstones contacting with an isolated greenstone body in the Nitarachi-Yezo Sequence (Fig. 27), which is considered to be the Mikawa Unit equivalents.

Chipped samples were etched in 2-5 % HF solution for 12-24 hours. The residue was collected using #35 and #330 sieves, then was boiled in H_2O_2 and HCl solutions. Handpicked radiolarian tests were observed under SEM. Identified taxa are listed in Table 5, and selected SEM photographs of which are shown in Figs 34 and 35. The obtained fossil ages, with ages previously reported in literatures, are compiled in Fig. 36.

1. Shizunai Unit

The sample 2k0801-5 is from a green tuffaceous mudstone bed (ca. 40cm thick), intercalated in mesoscopically non-deformed mudstone with siliciclastic sandstone laminae (muddy turbidite) of the clastic facies. The siliceous mudstone yields radiolarians: *Cecrops septemporatus* and *Hemicryptocapsa capita*. According to Sanfilippo and Riedel (1985) and Schaaf (1985), *C. septemporatus* ranges from late Valanginian to early Barremian, and *H. capita* from late Valanginian to Hauterivian. The age of this siliceous mudstone is thus concluded to be late Valanginian - early Barremian, and probably constricted to late Valanginian - Hauterivian. This is the first report of well-defined fossil age from terrigenous clastic rock in the Kamuikotan Zone.

The sample 2k0801-4B is green tuffaceous mudstone stratigraphically overlain by terrigenous clastic rocks from which 2k0801-5 was taken. The locality is identical to the loc. no. 2 of Watanabe and Maekawa (1985). It contains poorly preserved radiolarians including *Pseudodictyomitra nuda*, which ranges from Valanginian to Aptian (Jud, 1994). Though this sample does not contain any index species, it is considered as Lower Cretaceous, and considered as Valanginian-Hauterivian to take the stratigraphic relation with 2k0801-5 into account.

The sample 2k0801-13C yields latest Jurassic to Early Cretaceous radiolarians: *Pantanellium squinaboli, Sethocapsa uterculus, Alievium helenae*, but does not contain any short-ranged species.

The sample 2k0725-15B is taken from a bedded chert slice, which structurally overlying pillow lava with minor-fault contact. The chert intercalates reworked hyaloclastite beds within 1.5m above

Table 5. List of radiolarian fossils from the Iwashimizu Complex.

Sample No.	990506-6	990506-7A	980501-1B	980501-1D	980501-2B	980601-11	990809-4	990809-13	990810-6B	2k0801-13C	2k0801-4B	2k0801-5	980725-15B
Lithological unit	Nt	Nt	Mk	Mk	Mk	Mk	Ft	Ft	Ft	Sz	Sz	Sz	Sz
Lithology	grn-silsh	grn-silsh	grn-silsh	grn-silsh	grn-silsh	grn-silsh	brown ch	grn-silsh	brown ch	grn-silsh	grn-silsh	grn-silsh	red ch
Acaeniotyle diaphorogona					+							+	
Acaeniotyle umbilicata		+		+	+			cf		+		+	
Acanthocircus spp.					+					?	?		
Acanthocircus trizonalis						cf						+	
Alievium helenae		+			+	+				cf		+	
Alievium spp.	+		+	+									
Archaeodictyomitra apiarium	+				?	+							
Archaeodictyomitra excellens				+									
Archaeodictyomitra spp.	+	+	+	+	+			+		?	+		
Archaeodictyomitra suzukii	+												
Archaeospongoprunum imlayi	+												
Archaeospongoprunum spp.					+					+	+	+	
Archaeospongoprunum tehamaensis		cf											
Cecrops septemporatus												+	
Cinguloturris carpatica	+												
Crucella spp.				+	+					+			
Cryptamphorella spp.			+		+	+					+	+	
Cyrtocapsa spp.					+								
Dictyomitra spp.				+	+								
Emiluvia nana	cf												
Emiluvia spp.					+								
Eucyrtidium manokawaensis						+							
Foremanella spp.					+			?					
Gongylothorax spp.												+	
hagiastrids gen. et sp. Indet.	+				+								
Hemicryptocapsa capita			cf	+	+	+						+	
Holocryptocanium barbui						+							
Holocryptocanium japonicum			+		+	+		?		+	+	+	
Holocryptocanium tuberculatum				+									
Mirifusus mediodilatatus		+			+								
multicyrtid sp. A	+												
Obesacapsula cetia					aff	aff							
Obesacapsula magniglobosa	aff												
Orbiculiforma spp.				+		+							
Pantanellium squinaboli			+		+	+				+	+	+	
Parahsuum spp.	+												+
Paronaella pygmaea	+												
Paronaella spp.				+	+	?						+	
Parvicingula boesii	+			+		+						+	
Parvicingula dhimenaensis	+												
Parvicingula spinata					cf								
Parvicingula usotanensis				+	+	+						+	
Patellula sp.					+							?	
Podobursa triacantha					+								
Podobursa tricola				+									
Praeconocaryomma spp.	+				+	?					?		
Pseudodictyomitra carpatica		+	+									cf	
Pseudodictyomitra lanceloti						+							
Pseudodictyomitra leptoconica		cf				+						aff	
Pseudodictyomitra lilyae												cf	
Pseudodictyomitra nuda					+						+	+	
Pseudodictyomitra spp.			+	+	+			?		?			

Table 5. Continued.

Sample No.	990506-6	990506-7A	980501-1B	980501-1D	980501-2B	980601-11	990809-4	990809-13	990810-6B	2k0801-13C	2k0801-4B	2k0801-5	980725-15E
Lithological unit	Nt	Nt	Mk	Mk	Mk	Mk	Ft	Ft	Ft	Sz	Sz	Sz	Sz
Lithology	grn-silsh	grn-silsh	grn-silsh	grn-silsh	grn-silsh	grn-silsh	brown ch	grn-silsh	brown ch	grn-silsh	grn-silsh	grn-silsh	red ch
Sethocapsa kaminogoensis		cf	cf	+		+		?				cf	
Sethocapsa orca		cf				aff						aff	
Sethocapsa spp.	?	+	+	+	+						?		
Sethocapsa simplex		cf		+								cf	
Sethocapsa trachyostraca				+						?			
Sethocapsa uterculus		+		+	+	+		?		+		+	
Spongocapsula perampla	+												
Spongocapsula? sp.	+												
Spongotripus sp.	+												
Spumellaria gen. et sp. Indet.							+		+				
Staurocyclia martini	+												
Stichocapsa altiformina				cf									
Stichocapsa pulchella					+								
Stichocapsa spp.						+		?					
Stichocapsa? sp.		+											
Suna echiodes												+	
Syringocapsa spp.				?				+					
Thanarla conica		+	+	?	+	+							
Thanarla elegantissima					+								
Transhsuum brevicostatum	+												
Transhsuum sp.													+
Triactoma sp.	?												
Tritrabs ewingi					+							+	
Tritrabs spp.	+				+	+							
Williriedelum crystallinum	+												
Williriedelum gilkeyi				cf								?	
Wrangellium depressum		+											
Wrangellium puga		+			+	cf						+	
Xitus gifuensis		+			aff	+							
Xitus plenus					+								
Xitus pulcher	aff				aff								
Xitus spicularius					+								
Xitus spp.		+		+	+							+	
Zhamoidellum ovum	+												
ESTIMATED AGE	Oxfordian	Berriasian - Hauterivian	late Valanginian - Hauterivian	late Valanginian - Hauterivian	late Valanginian - Hauterivian	late Valanginian - Hauterivian	?	latest Jurassic - Early Cretaceous	?	latest Jurassic - Early Cretaceous	Early Cretaceous	late Valanginian - Hauterivian	"Jurassic"

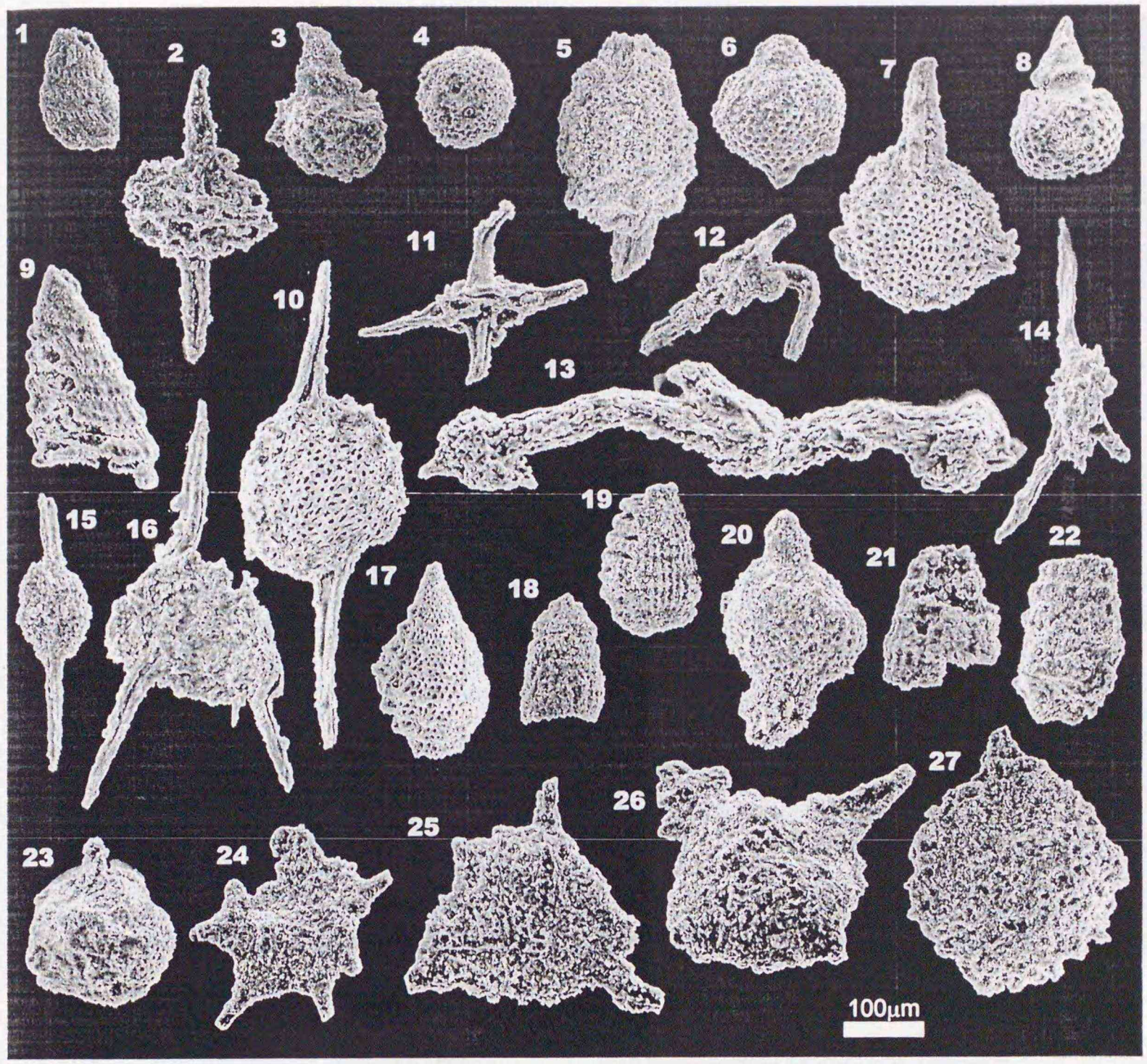


Fig. 34. Radiolarian fossils from the Shizunai Unit (Niikappu are) and the Futagawa Unit (Mitsuishi-Shizunai area).

1 & 2: From sample 2k0801-4B, Shizunai Unit
1 *Pseudodictyomitra nuda* Schaaf
2 *Pantanellium squinaboli* (Parona)
3-5: From sample 2k0801-13C, Shizunai Unit
3 *Sethocapsa uterculus* (Parona)
4 *Holocryptocanium barbui japonicum* (Nakaseko & Nishimura)
5 *Acaeniotyle* cf. *umbilicata* (Rüst)
6-17: From sample 2k0801-5, Shizunai Unit
6 *Hemicryptocapsa capita* (Tan)
7 *Suna echiodes* (Foreman)
8 *Sethocapsa uterculus* (Parona)
9 *Pseudodictyomitra carpatica* (Lozyniak)
10 *Acaeniotyle umbilicata* (Rüst)
11 *Cecrops septemporatus* (Parona)
12 *Acanthocircus trizonalis* (Rüst)
13 *Tritrabs ewingi* (Pessagno)
14 *Alievium helenae* Schaaf
15 *Archaeospongoprunum tehamaensis* Pessagno
16 *Acaeniotyle diaphorogona* Foreman
17 *Parvicingula usotanensis* Tumanda
18 & 19: From sample 2k0725-15B, Shizunai Unit
18: *Parahsuum*? sp.
19 *Transhsuum*? sp.
20-23: From sample 990809-13, Futagawa Unit
20 *Syringocapsa* sp.
21 *Archaeodictyomitra* sp.
22 *Pseudodictyomitra*? sp.
23 *Acaeniotyle* cf. *umbilicata* (Rüst)
24 -27: Spumellaria gen. et sp. indet., from sample 990810-6B, Futagawa Unit

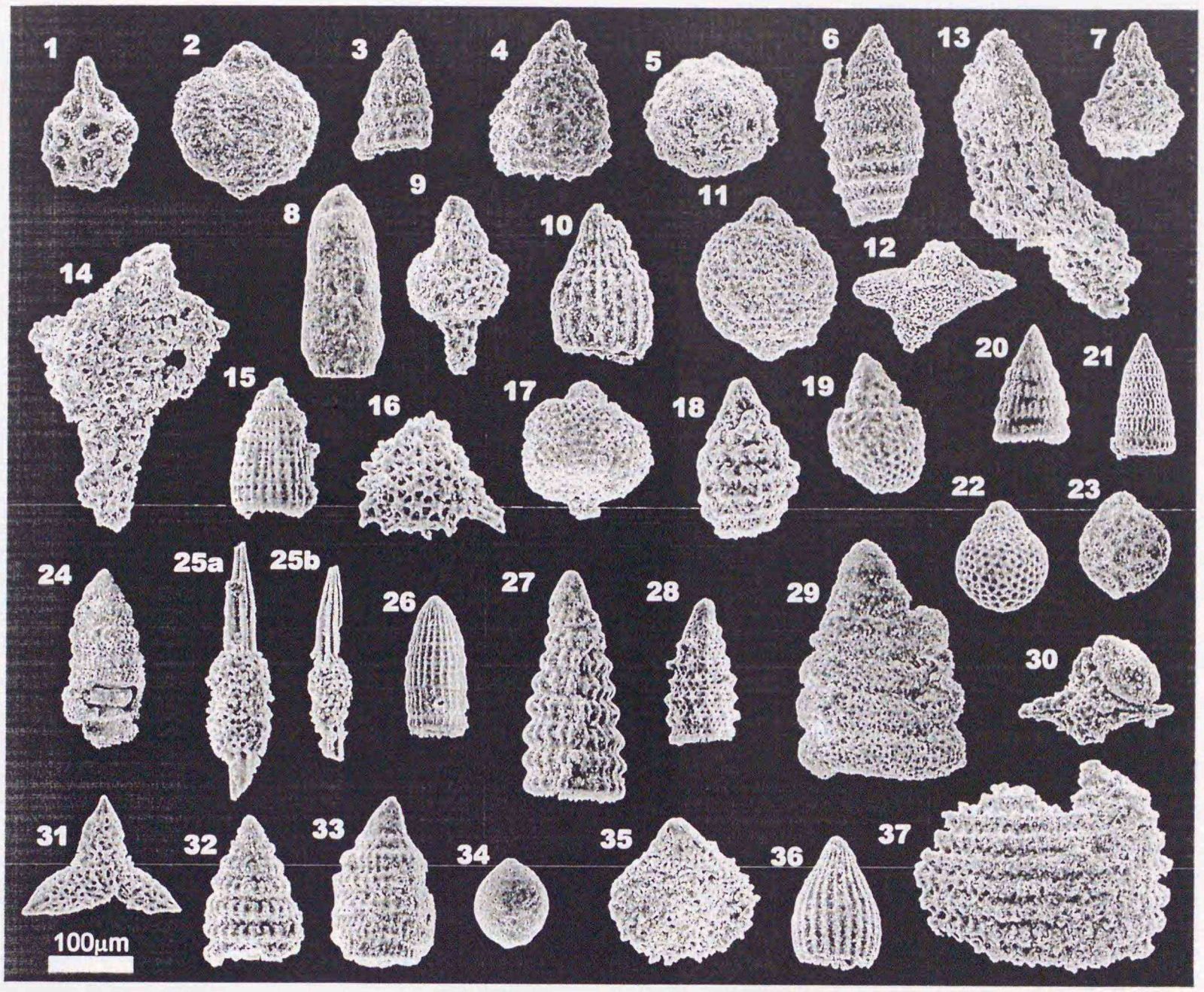


Fig. 35. Radiolarian fossils from the Mikawa Unit and around a greenstone slice in the Eastern Yezo Zone.

1-3: From sample 980501-1B, Mikawa Unit
1 *Pantanellium squinaboli* (Parona)
2 *Hemicryptocapsa* cf. *capita* (Tan)
3 *Pseudodictyomitra carpatica* (Lozyniak)
4-9: From sample 980501-1D, Mikawa Unit
4 *Stichocapsa altiformina* Tumanda
5 *Holocryptocanium tuberculatum* Dumitrica
6 *Parvicingula boesii* (Parona)
7 *Sethocapsa kaminogoensis* (Aita)
8 *Archaeodictyomitra excellens* (Tan)
9 *Podobursa* cf. *tricola* Foreman
10-14: From sample 980501-2B, Mikawa Unit
10 *Thanarla elegantissima* Cita
11 *Hemicryptocapsa capita* (Tan)
12 *Crucella* sp.
13 *Mirifusus mediodilatatus* (Rüst)
14 *Podobursa* cf. *triacantha* Foreman
15-20: From sample 980601-11, Mikawa Unit
15 *Archaeodictyomitra apiarium* (Rüst)
16 *Alievium helenae* Schaaf
17 *Hemicryptocapsa capita* (Tan)
18 *Parvicingula usotanensis* Tumanda
19 *Sethocapsa uterculus* Parona
20 *Pseudodictyomitra leptoconica* Foreman
21-31: Form sample 990506-6, Eastern Yezo Belt
21 multicyrtid gen. et sp. indet.
22 *Zhamoidellum ovum* Dumitrica
23 *Williriedelum crystallinum* Dumitrica
24 *Cinguloturris carpatica* Dumitrica & Mello
25a, b *Archaeospongoprunum imlayi* Pessagno
26 *Archaeodictyomitra suzukii* Aita
27 *Transhsuum brevicostatum* (Ozvoldova)
28 *Parvicingula dhimenaensis* Baumgartner
29 *Spongocapsula perampla* (Rüst)
30 *Emiluvia* cf. *nana* Baumgartner
31 *Paronaella pygmaea* Baumgartner
32-37: From sample 990506-7, Eastern Yezo Belt
32 *Wrangellium puga* (Schaaf)
33 *Wrangellium depressum* Baumgartner
34 *Stichocapsa* ? sp.
35 *Sethocapsa* cf. *trachyostraca* Foreman
36 *Thanarla conica* (Aliev)
37 *Mirifusus mediodilatatus* (Rüst)

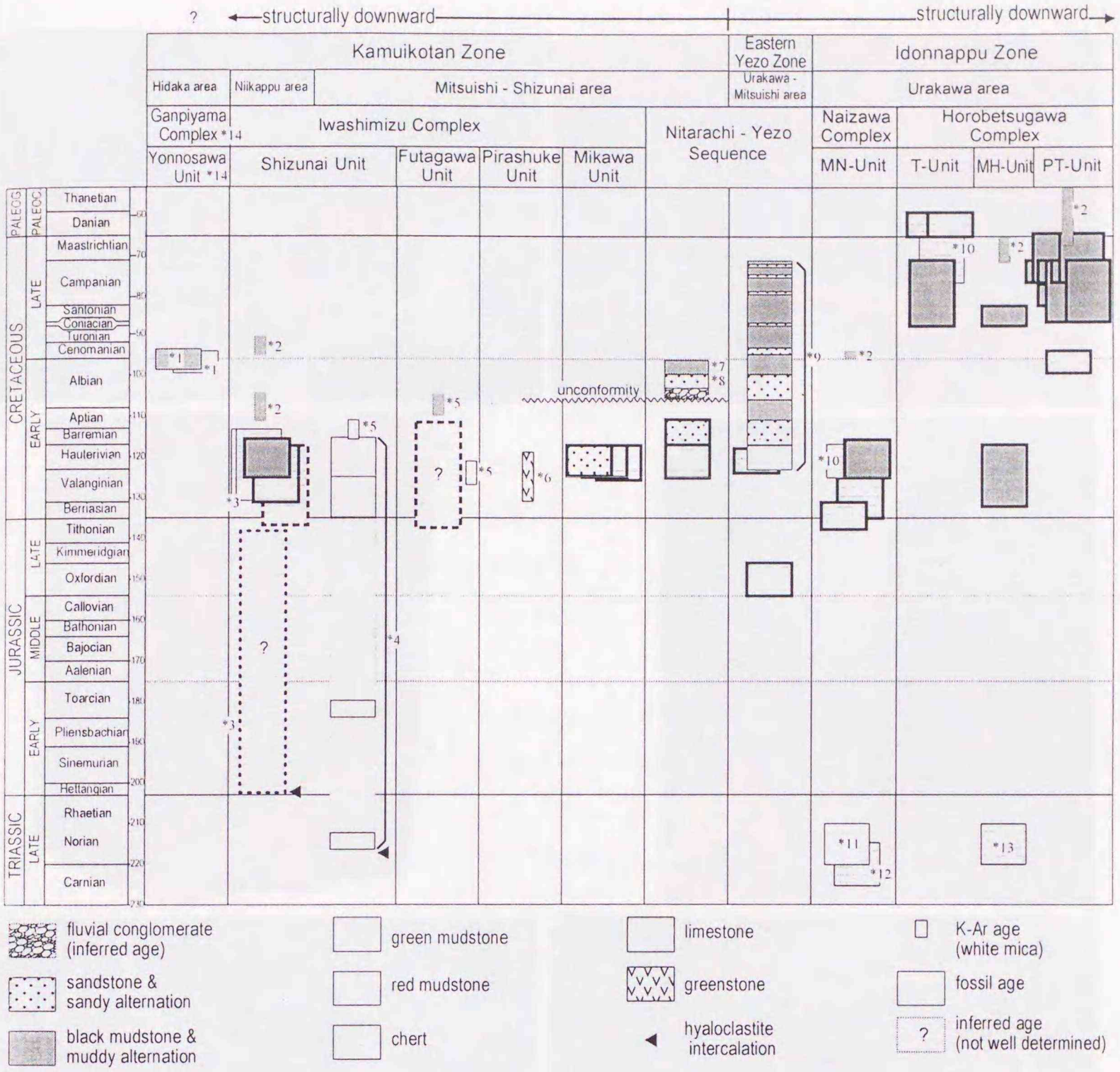
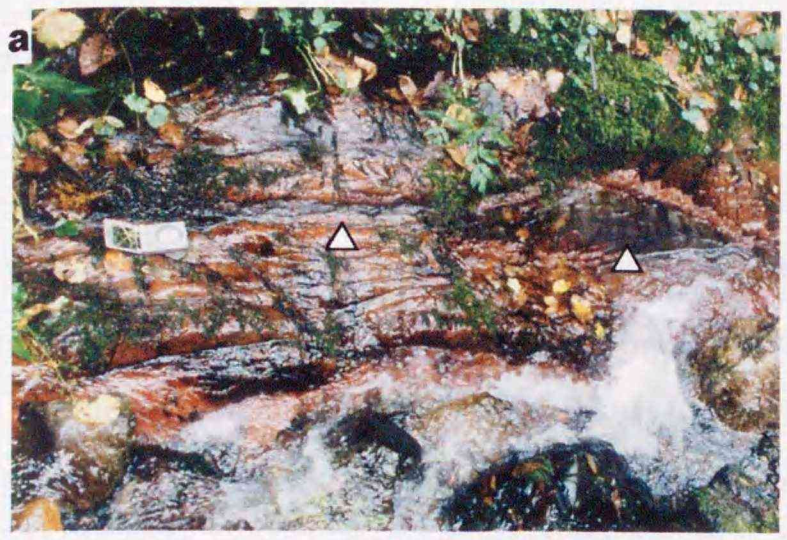
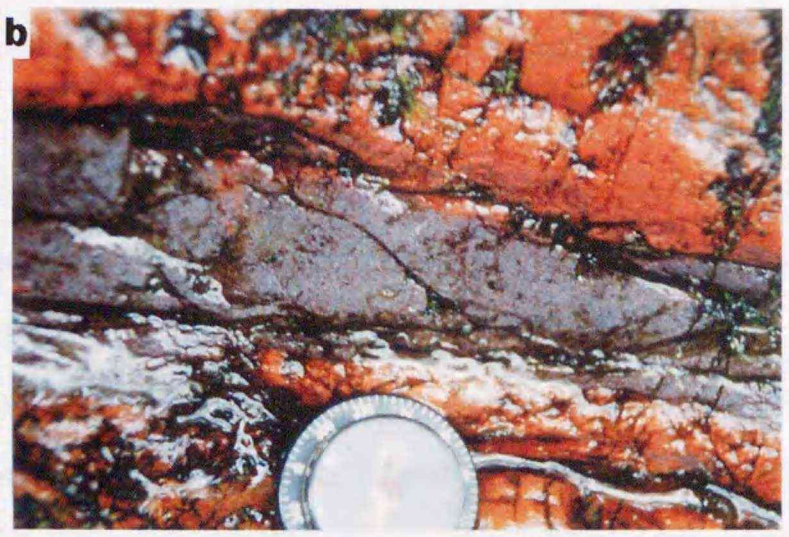
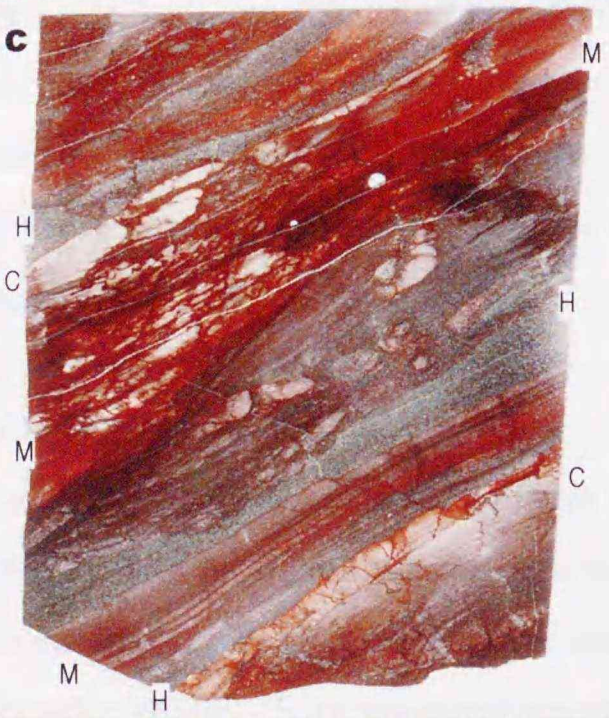
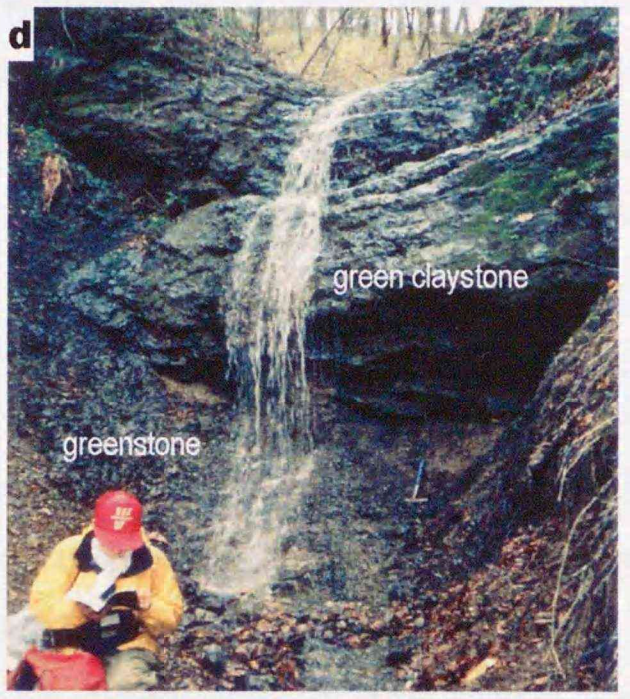


Fig. 36. Summarized geologic ages of the Iwashimizu Complex and the adjacent areas. References cited: *1: Agency of Natural Resources and Energy (1989), *2: Watanabe et al. (1994), *3: Watanabe & Maekawa (1985), *4: Hori & Sakakibara (1994), *5: Ota et al. (1993), *6: Nakagawa & Nakano (1987), *7: Taketani (1982), *8: Matsumoto et al. (1984), *9: Kanie et al. (1981); Sakai & Kanie (1986); Mitsugi & Hirano (1997), *10: Kiyokawa (1992), *11: Igo et al. (1974), *12: Sakai (1976): Sakagami & Sakai (1979), 13:Igo et al. (1980), *14: Kawamura et al. (in press). Bold line: this study.









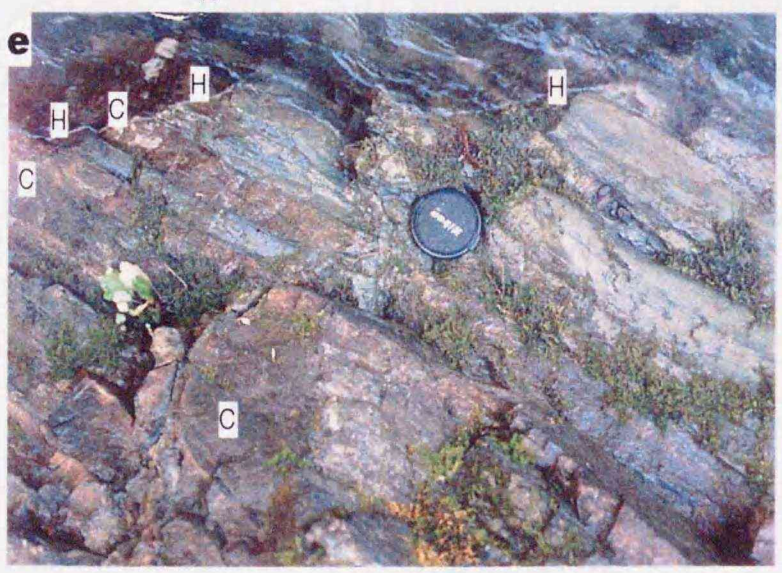




Fig. 37. Occurrences on relation between greenstone and pelagic sedimentary rocks.
(a, b) Reworked hyaloclastite turbidite (white arrow) intercalated in the Upper Triassic chert (Hori & Sakakibara, 1994).
Along Pisenai Creek (Shizunai Unit). b: Close-up view of the hyaloclastite bed. (c) Thin section of alternation of reworked hyaloclastite (H), chert, (C), and red claystone (M). From Penkemoshiyoshi Creek (Shizunai Unit). Late Jurassic green claystone (sample 990506-6) overlying a tholeiitic greenstone slab (LST-type, M25), bounded by a minor fault. Along a branch of Mitsuishi River (Eastern Yezo Zone). (e) Alternation of red chert (C) and fine-grained turbidite of reworked hyaloclastite (H). Along the middle reaches of Futagawa River (Pr-2 Sub-unit). (f) Alternation of reworked hyaloclastite (H) and red limestone (R). Along Pirashuke River (Pr-1 Sub-unit).

the contact. The sample was taken from ca. 5m above the contact. This chert yields poorly preserved radiolarians. Two radiolarian tests show surface structure of *Parahsuum* and *Transhsuum*, both of Jurassic (*e.g.* Baumgartner et al., 1985). Thus the chert, and probably the pillow lava also, is inferred as Jurassic.

Watanabe (1981), and Watanabe and Maekawa (1985) reported Early Cretaceous radiolarians from green siliceous mudstone and red chert, and Jurassic radiolarians from chert in the Niikappu area. Both ages are consistent with the radiolarian ages reported by this study.

In the Mitsuishi-Shizunai area, Hori & Sakakibara (1994) reported a chert-clastic sequence ranging from Late Triassic to Early Cretaceous along Pisenai Creek. I found that two reworked hyaloclastite beds are intercalated in chert (Fig. 37a, b) stratigraphically ca. 10m below the point where Late Triassic radiolarians were reported by Hori & Sakakibara (1994). The hyaloclastite intercalation is laterally traceable, occurring at the same horizon along Penkemoshiyoshi Creek (Fig. 37c). These occurrences indicate that the age of greenstone in the Iwashimizu Complex is, at least partly, as old as Triassic.

2. Futagawa Unit

Samples 990809-4 and 990810-6B are red chert stratigraphically interbedded with pillow lava and intruded by dolerite sills in the non-deformed greenstone slice (ftn3). Both samples yields radiolarian fossils, however, very poor preservation obstructs identification of any taxa.

Sample 990809-13 is green tuffaceous mudstone form the mixed facies B. This sample also contains very poorly preserved radiolarians. However, *Acaeniotyle* cf. *umbilicata, Sethocapsa*? spp. (inferred as *S. uterculus* and *S. kaminogoensis* by outline), *Archaeodictyomitra* sp., *Syringocapsa* sp., and *Pseudodictyomitra?* sp. are identical. These taxa are common in latest Jurassic to Early Cretaceous fauna.

3. Mikawa Unit

Samples 980501-1B, 1D, and 2B are from a green tuffaceous mudstone body in the mixed facies A.

The sample 980501-2B yields radiolarian fossils: *Hemicryptocapsa capita, Mirifusus mediodilatatus, and Thanarla elegantissima*. According to Sanfilippo and Riedel (1985), Schaaf (1985), and Jud (1994), *H. capita* ranges from late Valanginian to Hauterivian, the last occurrence of *M. mediodilatatus* (*M. danie minor*) in the Hauterivian, and the first appearance of *T. elegantissima* in the late Valanginian. Therefore, the sample 980501-2B is concluded to be upper Valanginian to Hauterivian.

The sample 980501-1D yields *H. capita, Podobursa tricola, Stichocapsa* cf. *altiformina,* and

Sethocapsa kaminogoensis. *Podobursa tricola* ranges from late Valanginian to early Aptian (Sanfilippo & Riedel, 1985; Schaaf, 1985), *S. altiformina* ranges from late Valanginian to early Barremian, and the last occurrence of *S. kaminogoensis* is in the early Barremian (Jud, 1994). To consider the occurrence of H. cf. capita, the sample 980501-1D is considered to be upper Valanginian to lower Barremian, and probably constricted to upper Valanginian – Hauterivian. The sample 980501-1B is taken from the same outcrop as 980501-1D. It also contains *H.* cf. *capita* and *S. kaminogoensis*, hence is considered as same age as the sample 980501-1D.

The sample 980601-11 is green tuffaceous mudstone intercalated in weakly deformed sandy alternation of sandstone and mudstone. The sample also yields *H. capita* and *S. kaminogoensis*, and is thus considered to be upper Valanginian to Hauterivian as the other samples described above.

4. Around greenstone body in the Eastern Yezo Zone

The sample 990506-6 is green claystone without any coarse terrigenous particles. It contacts with an isolated greenstone body (less than 10m thick) in the Yezo Supergroup by a minor fault (Fig. 37d). The greenstone is a depleted tholeiite (sample M25: see later section). This claystone yields well-preserved radiolarians including *Archaeodictyomitra apiarium, A. suzukii, Archaeospongoprunum imlayi, Cinguloturris carpatica, Emiluvia* cf. *nana, Parahsuum* sp., *Paronaella pygmaea, Transhsuum brevicostatum, and Zhamoidellum ovum*. According to Baumgartner et al. (1995), *A. apiarium* first appears in middle Callovian - early Oxfordian, *C. carpatica* ranges from late Bathonian to early Tithonian, *E. nana* from middle Bathonian to late Oxfordian, *P. pygmaea* from late Bathonian to late Oxfordian, *T. brevicostatum* from middle Bajocian to early Tithonian, and *Z. ovum* from late Oxfordian to early Tithonian. According to Aita (1987), *A. suzukii* ranges from Callovian to Oxfordian. Thus, the claystone is concluded to be Late Jurassic (Oxfordian).

The sample 990506-7A is green tuffaceous mudstone contacting with the greenstone without any obvious slip surface, at the opposite side of the contact with the green claystone (990506-6). The tuffaceous mudstone thrusts over the overturned turbidite beds of the Lower Yezo Group, together with the greenstone. This mudstone yields *Mirifusus mediodilatatus* and *Sethocapsa* cf. *kaminogoensis*. The last occurrence of *M. mediodilatatus* is in the Hauterivian (Sanfilippo & Riedel, 1985), and the first appearance of *S. kaminogoensis* in the Berriasian (Aita & Okada, 1986; Jud, 1994). Thus, the mudstone is considered to be lower-Lower Cretaceous (Berriasian - Hauterivian).

Mode of occurrence and petrology of greenstones

Mode of occurrence

1. Shizunai Unit

The Shizunai Unit in the study area contains three sheet bodies of the non-deformed greenstone facies (Figs. 29, 30). They are labeled as sz1, sz2, and sz3 in descending order (from top to bottom). Each greenstone sheet is several hundred meters thick and laterally traceable for 3 km (probably more).

The sheet sz3 consists of vesicular pillow lava and hyaloclastite, with dolerite sills several meters thick. Hanging pillow lavas, and clustered amigdules along the ceiling of dolerite sill and large pillow tube also, indicate them facing southeast. This slice is cut by faults on both top and bottom.

The sheet sz2 consists of dolerite sill swarm interbedded with chert (Fig. 38). This greenstone sheet, a chert - tuffaceous mudstone sheet, and a clastic sheet consists of sandy turbidite together, comprise a greenstone - chert - clastic sequence, middle part of which has been reported by Hori & Sakakibara (1994) as the "Pisenai-zawa chert-clastic sequence". The most typical and complete lithologic succession can be observed along Penkemoshiyoshi Creek, a branch of Shizunai River. Along the Penkemoshiyoshi Creek, at least 11 dolerite sills, each of which is 1.5 to 25 m thick, are recognizable. The dolerite sills are non-vesicular, and commonly have chilled margin. The interbedded chert beds are brown, red, white, or light-green colored, occasionally intercalates red to purplish-brown claystone. In the upper horizons of the greenstone sheet, a few beds of reworked hyaloclastite are intercalated in chert and accompanying claystone (Figs. 37a-c). The hyaloclastite beds are sharp-based, normally graded, and with laminae. Two hyaloclastite beds are intercalated in chert, in ca. 5 m upper horizon from which Hori & Sakakibara (1994) reported Late Triassic radiolarian fossils. These occurrences indicate that the dolerites intruded into Triassic chert and hyaloclastite sequence. Graded beds of both sandy turbidite and hyaloclastite indicate that the whole greenstone - chert - clastic sequence is overturned facing to the northwest. The stratigraphic base (structural top) of the sz2 sheet is cut by a fault, contacting with another clastic slice.

The sz3 sheet occurs at the northwestern end of the studied area, and consists of partly vesicular lava. Though this greenstone is temporarily classifies as non-deformed greenstone, cataclastic deformation is internally observed, and limestone blocks are contained.

In the Shizunai Unit, there also occur minor sheared greenstones, tectonically mixed with sheared mudstone, as the mixed facies B. Such sheared greenstones occur along or near slice-boundaries, non of which is mappable.

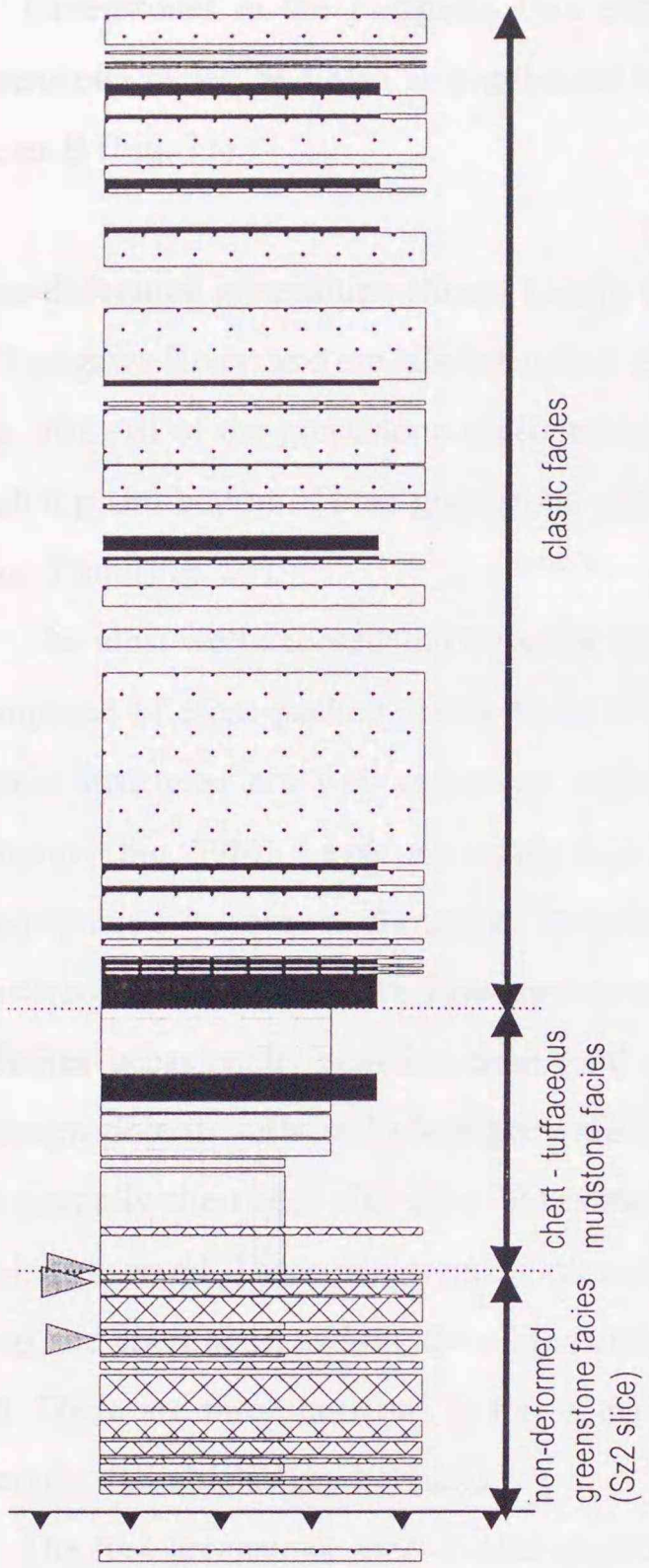


Fig. 38. Columnar section of the full-membered Pisenai-zawa chert-clastic sequence along Penkemoshiyoshi Creek, branch of Shizunai River.

Futagawa Unit

Greenstones in the Futagawa Unit occur as fault-bounded sheets (slices) of the non-deformed greenstone facies, and also as small-scale blocks, lenses, fragments, and sheared layers in the mixed facies B (Fig. 31).

Non-deformed greenstone slices: Totally six greenstone slices are recognizable in the upper reaches of Futagawa River, and are labeled as ftn1 to ftn6 in descending order (from structurally top to bottom: Fig. 30). All of the greenstone sheets normally face east or south, and are bounded by faults both at each top and bottom. These greenstone slices are 150 to over 370 m thick, and laterally traceable for max. 7 km (Fig. 29).

The most well exposed and traceable slice is the ftn3 slice (Fig. 31). This slice is characteristically composed of close-packed pillow lavas (Figs. 39a, b), dolerite sills, and chert beds (Figs. 39 c, d). Pillow structures are well preserved, and even corrugation on the tube surface is observed in an outcrop (Fig. 39b)). Lavas are mostly non- or weakly vesicular. Chert beds are red to brown colored, accompanied by brown claystone. Dolerite sills are 1 to more than 45 m thick. Amigdules are clustered, occasionally with flow structure, along the ceiling of sills more than 30m thick. These dolerites occasionally contains chert (and rarely micritic limestone) xenoliths. Intrusive boundaries between dolerite sills and chert beds are commonly observed: dolerites have chilled margins, and occasionally chert beds also show baked margins. Intrusive boundary between dolerite and pillow lava is also observed. These occurrence indicate that the dolerite sills intruded into an alternation of pillow lavas and chert beds, and the three lithofacies comprises a single stratigraphic-intrusive sequence (Fig. 40). There are three horizons in this sequence where dolerite sills intruded, and these horizons are laterally traceable as key horizons.

The ftn4 greenstone sheet is also characteristic, though it is not well exposed. This sheet consists mainly of well-vesicular pillow lava and hyaloclastite, intruded by a few and thin dolerite sills. About the middle horizon of the sheet, a reworked limestone bed containing clinoid fragments, more than 5 m thick, is intercalated in reworked hyaloclastite.

The ftn1 slice consists of vesicular pillow lavas. The ftn1, ftn2, and ftn5 slices are composed of close-packed pillow lavas similar to the ftn3 sheet. The ftn6 consists of non- to moderately vesicular pillow lava with minor hyaloclastite, and intruded by a dolerite sill in northern area.

Along the lower reaches of Futagawa River, the Futagawa Unit also exposed as a fenster. In this area, there occurs a greenstone body (labeled as fts1) composed of non- and very weakly vesicular pillow lava. Large lobes more than 2 m wide are observable among the pillow lavas.

Mixed facies sheets: There are at least six sheets of the mixed facies B. There is no significant difference in lithology among these sheets. The thickest sheet (ca. 450m thick) occurs structurally

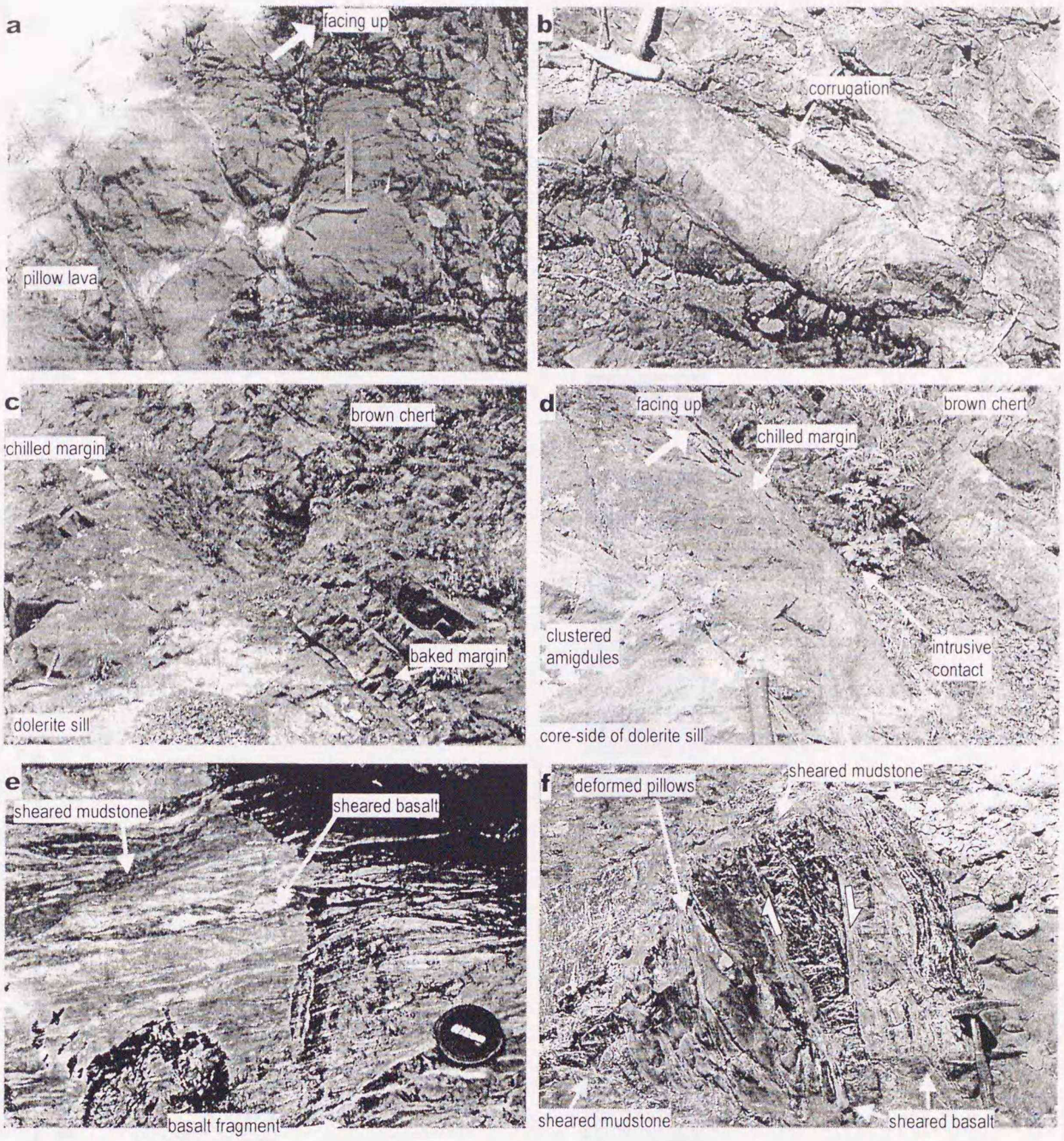


Fig. 39. Field occurrences the non-deformed greenstone facies (a - d) and the mixed facies B (e, f) in the Futagawa Unit.
(a) Hanging pillow lava indicating normal facing. Along a branch of Futagawa River. (b) A pillow tube preserving corrugation on its surface. Along a branch of Futagawa River. (c, d) Intrusive boundary between chert and dolerite sill. Both chilled margin and baked margin are observable. amigdules clusters near the ceiling of the sill. Along the Futagawa Forestry Road. (e) Typical layered mixed fabric of sheared greenstone and mudstone. Along a branch of Futagawa River. (f) A floating block of greenstone - mudstone mixed rock. Pillow structure (with cooling joints) is preserved in deformed greenstone. Sheared mudstone and greenstone show an asymmetric deformation fabric (left-up sense S-C structure). Along the lower reaches of Futagawa River.

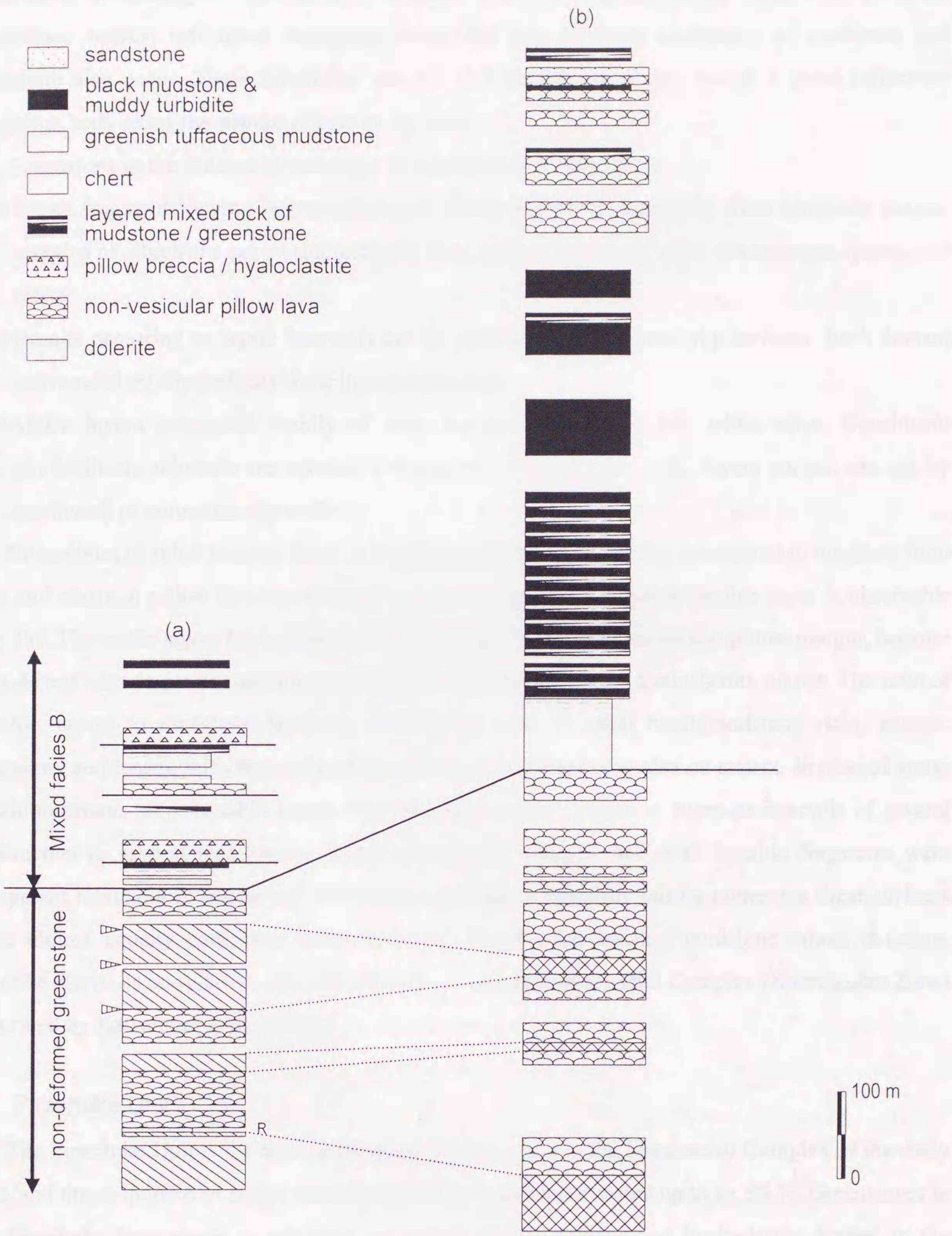


Fig. 40. Columnar sections of the ftn3 greenstone slice and overlying mixed facies B of the Futagawa Unit. Route (a): branch of Futagawa River; and route (b): along Futagawa River and the Futagawa Forestry Road (see Fig. 31).

above the ftn3 greenstone slice, typically exposed along the Futagawa River. The sheet consists dominantly of strongly sheared mixture of black mudstone and greenstone (Fgs. 39e, f). Small greenstone bodies, tuffaceous mudstone, chert, and less-deformed alternation of sandstone and mudstone also occur. These lithofacies are not well traceable laterally, except a green tuffaceous mudstone body along the structural base of the sheet.

Greenstone in the sheared mixed rocks is composed of followings:

a) Basalt fragments having intersertal texture. These fragments commonly show lenticular shapes, margins of which are cut by slip surfaces. They contain numerous veins of carbonate, quartz, and albite.

b) Basalts occurring as layers internally cut by meshwork of numerous slip surfaces. Each domain surrounded by slip surfaces show intersertal texture.

c) Mafic layers composed mainly of very fine-grained chlorite and white mica. Constituent phyllosilicate minerals are oriented forming schistosities. The mafic layers contain are cut by meshwork of numerous slip surfaces.

On account of relict texture, basaltic fragments (a) and layers (b) are considered to originate from lava and clasts in pillow breccia. Transition from pillow lava to sheared basaltic layer is observable Fig. 39f. The mafic layers (c) is considered to originate from hyaloclastite and pillow margin, because they do not contain plagioclase microlites as common non-deformed hyaloclastite do not. The ratio of basaltic layers to mudstone layers is variable. In case of small basalt/mudstone ratio, basaltic fragments and lenses, with sheared mafic mantle, are contained in mudstone matrix. In case of grater basalt/mudstone ratio, basaltic layers alternate with sheared mudstone layers at intervals of several millimeters to several tens meters. These occurrences indicate that small basaltic fragments were competent relatively to mudstone, whereas basaltic layers internally cut by numerous shear surfaces were almost equally competent with mudstone. The layered basalt / mudstone mixed structure, describe above, is correlative with the "sumi-flow" structure of the Biei Complex (Kamuikotan Zone) described by Kawamura et al. (1998).

3. Pirashuke Unit

The Pirashuke Unit is the most greenstone-dominant unit in the Iwashimizu Complex of the study area, and the proportion of mafic rocks in the Pr-1 Sub-unit is estimated up to ca. 95 %. Greenstones in the Pirashuke Unit occur as schistose greenstone slices, dolerite and hyaloclastite bodies in the metadolerite facies, fragments and sheared layers in the mixed facies B, and mafic schist in the mixed facies C.

Schistose greenstone facies: The schistose greenstone facies consists of hyaloclastite and reworked volcanic breccia, pillow lava, and dolerite. Hyaloclastites intercalate, or alternate with chert and red

limestone (Figs. 37e, f). Volcanic breccia contains chert clasts in several outcrops. Pillow lava with recrystallized inter-pillow limestone is not uncommon. These occurrences indicate that the greenstones originally comprised a volcano-sedimentary sequence in each slice, though they are cut by many minor faults and folded internally. It is difficult to estimate precise thickness and lateral extent of the slices because of internal faults and folds, and limited exposure. However, I roughly estimate that these slices are several hundred meters thick and several kilometers in extent.

Pillow lavas are flattened and stretched with indistinct foliation (Fig. 41a). Stretching lineations consisting of deformed amigdules (and rarely of pillow itself) are recognizable in many outcrops. Hyaloclastites and volcanic breccias are commonly flattened with distinct foliation (Fig. 41b). Constituent volcanic fragments and amigdules are elongated to be ellipsoids, uniformly oriented forming a stretching lineation in each outcrop (Fig. 41c). Dolerites are dominantly non- or very weakly deformed, and foliated dolerites are also observed in some outcrops.

Metadolerite facies: Mafic rocks in the metadolerite facies are dolerite, with trace hyaloclastite, epidote amphibolite, and metabasalt. Dolerite characteristically contains abundant and mesoscopically visible epidote. Degree of deformation is variable: non-deformed; foliated; sheared with meshworks of slip surfaces; and partly cataclasite. In deformed part, green siliceous lenses (recrystallized chert or tuffaceous mudstone) are intercalated. These dolerite bodies are less than 100 m thick, and laterally traceable for at least 7 km.

Hyaloclastite, epidote amphibolite, and metabasalt sporadically occur, and are not laterally traceable. Epidote-amphibolite and metabasalt blocks are only seen in Holocene landslide debris, however, Nakano (1981) reported an outcrop of epidote-amphibolite in Takami area, north extension of the study area.

Mixed facies C: Mafic schists are the dominant constituent of the Mixed facies C. They are commonly sheared with distinct foliation, hence, effusive or sedimentary structures are not preserved, except some outcrops where foliated hyaloclastite with flattened clasts occur. These schists alternate with deformed metachert, bounded by slip surfaces (Fig. 41d). They partly show tight folds (Fig. 41e). Though the slices of the mixed facies C are laterally traceable, internal extent of each metachert and mafic schist bodies are indistinct. Non-deformed dolerite rarely and sporadically occurs in the mixed facies C, contacting metachert and mafic schist bounded by slip surfaces.

Mixed facies B: The mixed facies B in the Pirashuke Unit have the same characteristics as that of the Futagawa Unit. Because of limited exposure and probably later rearrangement, this facies in the Pirashuke Unit is less traceable than that in the Futagawa Unit. Greenstone lenses and layers are sheared, mixing with sheared mudstone.

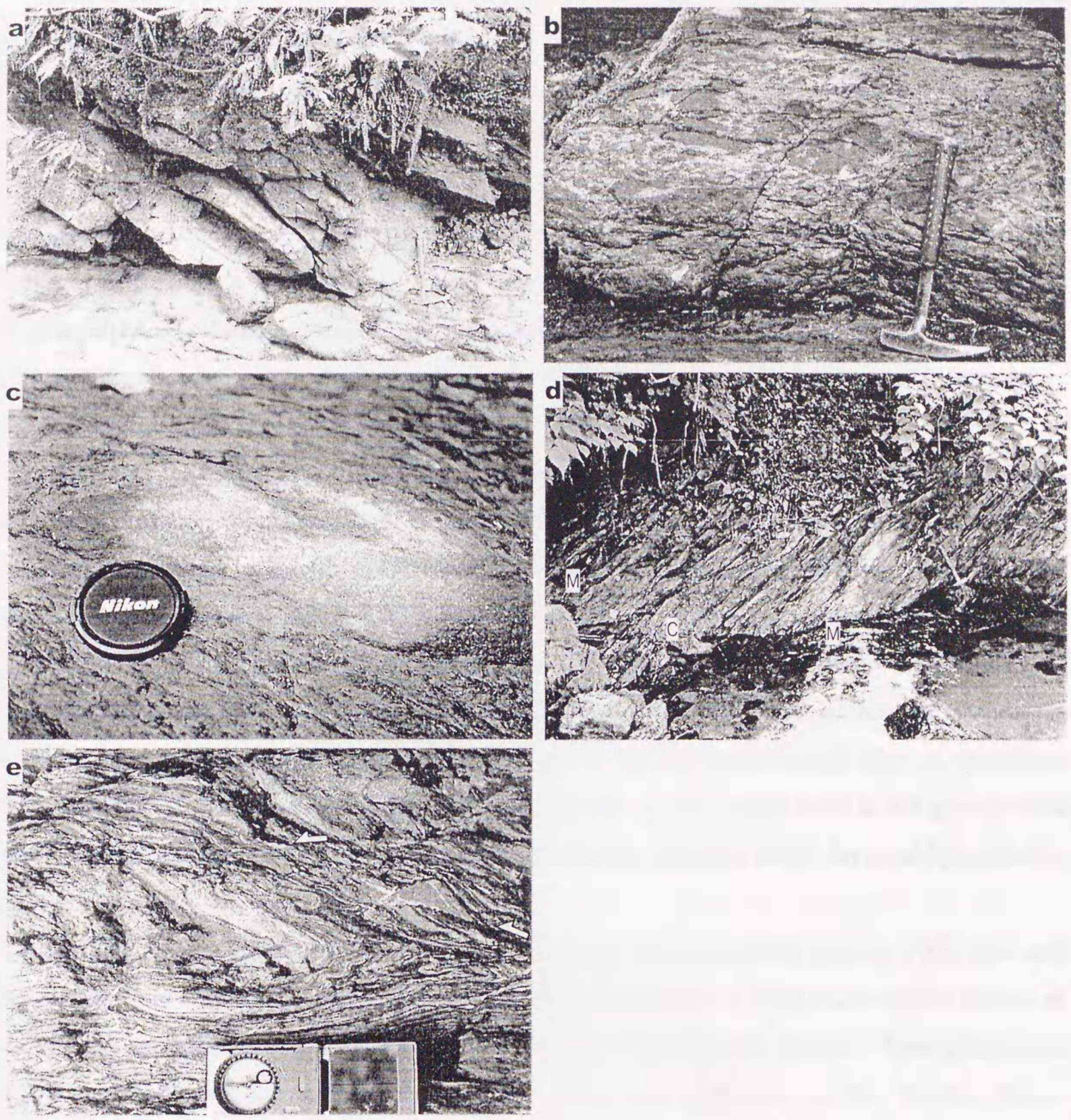


Fig. 41. Occurrences of the schistose greenstone facies (a-c) and the mixed facies C (d, e) in the Pirashuke Unit.
(a) Flattened pillow lava. Along Akabanno-sawa Creek, branch of Mitsuishi River (Pr-1 Sub-unit).
(b) Mafic schist of flattened hyaloclastite. Along a branch of Pirashuke River (Pr-1 Sub-unit).
(c) Stretched clasts and amigdules in hyaloclastite schist. These clasts also show microscopic mineral lineation of acicular magnesio-riebeckite.
(d) Mafic schist (M) intercalating metachert (C). The schist is severely sheared, and any original volcanic structure is not observable. Along a branch of Pirashuke River (Pr-1 Sub-unit).
(e) Folded mafic schist of the mixed facies C. Tight folds are cut by sinistral shear surfaces (white arrows). Along Pirashuke River (Pr-1 Sub-unit).

Mikawa Unit

Greenstones in the Mikawa Unit occur as large non-deformed greenstone slices and smaller greenstone slices and blocks in the mixed facies A.

Non-deformed greenstone slice: Greenstone slices are up to 650m thick and over 8km in extent, and consists mostly of non-deformed greenstone. Greenstones are hyaloclastite, pillow breccia, reworked volcanic breccia, pillow lava, and dolerite, all well preserving original structure. Trace chert and limestone are also contained: Some pillow lavas have inter-pillow limestone; volcanic breccia rarely contains chert fragments. Though there are minor faults internally, these lithofacies are considered to have comprised a volcanic sequence within each slice. Some hyaloclastite show very weak foliation. Margins of the slices are cut by faults, however in several routes, it is difficult to locate clear boundary with smaller greenstone slices of the mixed facies A.

Mixed facies A: Prevented by a bad exposure, detailed mode of occurrence of greenstones is not well determined. However, fragmental occurrences (Fig. 33) suggest that greenstones, sandstone-dominant clastic rocks, and green tuffaceous mudstone occur separately with sheet-like distribution, less than 50 m thick and up to 600m in extent. Along lithological boundaries, sheared mudstone less than 10 m thick occur. Sheared mixture of greenstone and mudstone is also observed along the boundary of greenstone and clastic rocks. There is no outcrop where block-in-matrix fabric is observed. Hence, the mixed facies A is regarded as a tectonic stack of small (mostly thin-skinned) slice of constituent lithofacies. Fig. 33 also suggests that the NE-SW orientation of these slices cross to the general trend (NNW-SSE) of the Mikawa Unit. Greenstones are dominantly vesicular pillow lava and hyaloclastite, with minor dolerite.

In north part of the unit (along branches of Pirashuke River), a greenstone slice ca. 100m thick and 400m (to possibly over 700m) in extent occurs in the mixed facies A. This slice consists mainly of non-vesicular and close-packed pillow lava, with minor hyaloclastite and dolerite. These greenstones contains numerous webbed veins of prehnite, analcime, and carbonate, as the "torifun (birds' droppings)-like" veinlets traditionally described on greenstones of the Sorachi Group. Greenstones having the same characteristics also occur in Kuzuresawa Creek (branch of Shunbetsu River: Fig. 27).

Petrographic characteristics

1. Shizunai Unit

In both basalt and dolerite in the Shizunai Unit, plagioclase was albitized. Part of clinopyroxene was replaced by sodic pyroxene; whole olivine by chlorite and pumpellyite; ilmenite partly by titanite; and glass wholly by chlorite, pumpellyite, hematite, carbonate, and white mica.

The sz1 slice consists of plagioclase-phyric basalt and olivine-plagioclase basalt, commonly with amigdules. Groundmass is composed of plagioclase microlites, acicular ilmenite, rare clinopyroxene,

and glass. Intercalated dolerite consists of titanaugite, plagioclase, and ilmenite, with minor kaersutite and aegirine.

The sz2 slice is dominated by dolerite. The dolerites are petrographically variable from pyroxene-rich (some possibly contained olivine) ones to plagioclase-rich and pyroxene-free ones, probably reflected degree of differentiation. Representative mafic assemblage is: titanaugite + plagioclase ± kaersutite + aegirine + biotite + apatite + ilmenite + interstitial glass. Felsic assemblage is: plagioclase ± biotite + apatite + polygonal opaque (presumably magnetite) + ilmenite + interstitial glass. Hyaloclastite beds, intercalated in chert and dolerite, consist mainly of well vesicular glass fragments with plagioclase microlites and phenocrysts, acicular ilmenite, and rare apatite.

2. Futagawa Unit

Pillow lavas of the ftn1, ftn2, ftn3, and fts1 slices are composed of olivine basalt, aphyric basalt, and olivine-plagioclase basalt, all of which are non- to weakly vesicular. Highly phyric rock is absent. Groundmass is composed of plagioclase ± olivine ± clinopyroxene + acicular ilmenite + glass. Dolerites of the ftn3 slice are non-vesicular and well crystalline, except that quenched parts are variably vesicular and glassier, and partly contain plagioclase and/or olivine phenocrysts as pillow lavas. Crystalline dolerites are composed of: titanaugite (or augite) + plagioclase + ilmenite + interstitial glass ± aegirine ± kaersutite ± biotite ± apatite. Apatite, biotite, aegirine, and kaersutite are less common as titanaugite-bearing dolerites in the Shizunai Unit, but are not rare. Pyroxene-free and plagioclase-rich dolerite is not observed.

Pillow lavas and hyaloclastites of the ftn4 slice consist of olivine basalt, plagioclase basalt and aphyric basalt. Dolerites are composed of titanaugite + plagioclase + ilmenite ± kaersutite ± aegirine ± interstitial glass.

There are only a few thin sections from ftn5 and ftn6 slices. These are olivine (?) basalt, plagioclase basalt, aphyric basalt, and augite-kaersutite dolerite.

Olivine ± plagioclase basalt, plagioclase basalt, aphyric basalt, and (olivine-?) augite basalt are contained in greenstones of the mixed facies B. There is no significant petrographic difference between the mixed facies B and non-deformed greenstone slices, except that plagioclase- highly phyric basalt and augite basalt were observed.

3. Pirashuke Unit

Schistose greenstone facies: Schistose Greenstones are petrographically variable. Aphyric basalt, clinopyroxene (augite and titanaugite) basalt, and plagioclase basalt are the majority. Olivine basalt and clinopyroxene-plagioclase basalt are also common. Clinopyroxene- highly phyric basalts (ankaramite) characteristically occur: containing clinopyroxene, olivine + clinopyroxene, and rarely

clinopyroxene + kaersutite phenocrysts. Picrite and olivine-plagioclase basalt scarcely occur. One sample contains apatite phenocryst. Olivine-bearing assemblage is rarely accompanied by spinel. Typical groundmass assemblage of these basalts is plagioclase+ clinopyroxene+ acicular ilmenite+ glass. Groundmass of basaltic fragments in hyaloclastite consists almost only of glass; small amount of plagioclase microlites is occasionally contained. Some contain polygonal oxide partly replaced by titanite (presumably titanomagnetite) in groundmass. Kaersutite and aegirine are rarely contained in intergranular to subophitic groundmass.

Dolerites in the schistose greenstone facies are composed of clinopyroxene + plagioclase + ilmenite ±kaersutite ± aegirine ± biotite ± apatite. Titanaugite, kaersutite, aegirine, and apatite are common.

Metadolerite facies: Dolerites in the metadolerite facies are petrographically uniform, composed of clinopyroxene (mostly augite) + plagioclase + oxide (ilmenite and presumably titanomagnetite). Small amounts of apatite and interstitial glass are rarely contained.

Epidote amphibolite (floats in Holocene landslide debris) consists of hornblende (originally clinopyroxene and presumably olivine?) + albitized plagioclase partly also replaced by epidote + titanite (ilmenite?) ± apatite. They are mostly coarse-grained: some show banded structure of relatively mafic and felsic layers, implying gabbroic origin; others preserve indistinct ophitic-like texture, implying coarse dolerite origin.

Hyaloclastite are composed of fragments of aphyric basalt, augite basalt, and rarely picritic basalt. They are commonly replaced by abundant mafic minerals (actinolite + chlorite, or metamorphic sodian augite), and very poor in albite.

Mixed facies C: Most basalts are significantly sheared, so that it is difficult to determine igneous petrographical characteristics. Aphyric basalt, clinopyroxene basalt, and dolerite are presumably contained.

Mixed facies B: Five thin sections of greenstones from this facies are aphyric basalt. One sample contains biotite in its groundmass.

4. Mikawa Unit

Non-deformed greenstone facies: The non-deformed greenstone slices consist mainly of olivine basalt, olivine-plagioclase basalt, clinopyroxene basalt, clinopyroxene-plagioclase basalt, and aphyric basalt. Picrite and picritic basalts are not rare. These rocks commonly contain acicular ilmenite in their groundmass. Dolerites contain trace kaersutite, aegirine, biotite, and apatite.

Mixed facies A: The mixed facies A contains dominantly olivine basalt and olivine-plagioclase basalt, as much as aphyric basalt. Some olivine-bearing rocks are picritic. Plagioclase basalt is also seen.

These rocks commonly contain acicular ilmenite in their groundmass, except highly glassy ones. One plagioclase basalt sample also contains apatite phenocrysts. Apatite is also contained in groundmass of some aphyric basalts.

The torifun-type greenstone bodies consist dominantly of aphyric basalt, accompanied by olivine basalt, olivine-clinopyroxene basalt, clinopyroxene-plagioclase basalt, and aphyric dolerite. Polygonal opaque minerals (presumably magnetite) are commonly contained in their groundmass, whereas ilmenite is quite rare. A dolerite sample contains trace apatite. Kaersutite, aegirine, and biotite are never seen.

Petrochemical characteristics

Many major-element bulk-rock compositions, and a few trace-element compositions also, of greenstones in the Iwashimizu Complex has been reported by previous studies (Nakano, 1985; Watanabe & Maekawa, 1985; Watanabe & Niida, 1987; Kimura et al., 1994). They reported both alkaline and tholeiitic greenstones, and the former has been considered as oceanic island alkali basalts (OIA). Whereas, the nature and origin of the tholeiitic basalts have not been well understood. Relation between chemical types and their distribution or unit division is also not yet described.

To elucidate origin of greenstones and relation between rock types and unit division, bulk-rock major and trace element compositions were determined for 53 greenstones from the Iwashimizu Complex (Fig. 28).

Any sample chip with visible vesicles or veins was discarded prior to crushing. All analyses were made at Hokkaido University, using a Phillips PW1404 X-ray fluorescence spectrometer. Major and trace element compositions were determined using the method by Tanaka & Orihashi (1997). Results are listed in Table 6. Sample M54 is from a greenstone body correlative with the Mikawa Unit along Kuzuresawa Creek (Branch of Shunbetsu River). Samples M30 and M31 are from a meta-pillow lava (clinozoisite + tremolitic actinolite) body correlative with the Metadolerite Sub-unit of the Pirashuke Unit, along the Nukabira River Forestry Road. The rests are from the Mitsuishi-Shizunai area.

1. Shizunai Unit

Five dolerite samples form the sz2 sheet and one basalt sample form the sz1 sheet were analyzed. All samples show high TiO_2 (2.8-4.7 wt%) and P_2O_5 (0.8-1.7 wt%) contents (Fig. 42). Nb/Y ratio ranges 2.1-4.0 (Fig. 43), hence, all plot in the alkaline fields (nephelinite, alkali basalt, and trachyandesite) of Winchester & Floyd (1977). MORB-normalized trace-element patterns (Fig. 44) show a pronounced enrichment in high-field-strength (HFS) elements, which is a characteristic of within-plate alkali basalt (Pearce, 1982). All plot in the field of ocean-island alkali basalt on Nb-Zr-Y ternary diagram (Meschede, 1986; see Fig. 45). Hence, basalts and dolerites of the Shizunai Unit are

Table 6. Bulk rock chemical compositions and igneous mineral assemblages of greenstones in the Iwashimizu Complex. Ti: titaniferous, parenthesis: fully altered.

ID	M10	M18	M19	M20	M23	M26	M14	M21	M22	M03	M25	M04	M05	M54	M09	M11	M12	M13
no.	981014-7	981102-1	981102-5	981102-6	981102-13	990508-24	981030-2	981102-10	981102-12	980603-9	990506-5	980612-2	980612-3	2k0602-2	981013-2	981014-11A	981014-1B	981014-2A1
unit	Mikawa Unit (non-deformed greenstone facies)						Mikawa Unit (mixed facies A)									Pirashuke Unit (Metadolerite Sub-unit)		
rock name	ol-pl bas	aph bas	aph bas	dol	dol	pl bas	aph bas	pic	aph bas	ol-pl pic	aph bas	ol bas	dol	pl bas	aph bas	dol	dol	dol
SiO_2	49.71	44.23	47.83	49.20	48.24	47.70	53.46	48.73	49.67	46.89	49.90	49.06	48.39	50.87	48.66	45.55	44.61	46.89
TiO_2	2.46	4.37	2.83	2.72	3.92	4.69	2.85	2.24	3.17	3.24	1.01	1.24	0.91	1.15	1.09	1.81	1.82	1.19
Al_2O_3	15.03	15.65	14.75	14.90	17.03	16.33	17.12	15.84	15.05	16.83	14.93	14.07	14.97	13.62	14.78	14.09	14.99	15.47
Fe_2O_3*	11.57	12.54	11.98	10.85	12.18	16.23	9.54	11.83	14.05	12.20	11.20	13.16	11.47	12.87	11.61	18.17	17.82	13.50
MnO	0.16	0.20	0.17	0.14	0.16	0.28	0.35	0.18	0.22	0.18	0.25	0.21	0.19	0.21	0.23	0.21	0.23	0.20
MgO	7.06	5.07	9.37	7.42	2.83	2.26	4.55	7.72	5.26	8.92	9.63	7.84	9.13	7.03	8.27	7.57	8.22	7.49
CaO	9.67	11.50	10.21	9.57	7.93	3.87	4.40	9.67	6.31	5.29	8.66	10.74	10.40	10.71	10.49	8.15	8.17	12.96
Na_2O	3.97	3.73	3.13	3.57	4.43	4.11	5.82	3.57	4.46	3.71	3.58	3.73	3.34	4.02	3.93	4.22	3.98	3.15
K_2O	0.55	0.77	0.04	1.29	2.03	2.29	0.51	0.22	0.38	1.19	0.34	0.25	0.72	0.06	0.31	0.06	0.06	0.04
P_2O_5	0.27	0.92	0.38	0.39	0.89	1.45	1.01	0.32	1.38	0.79	0.07	0.09	0.06	0.09	0.08	0.10	0.13	0.06
total	100.43	98.98	100.67	100.05	99.63	99.21	99.60	100.31	99.95	99.25	99.56	100.38	99.56	100.62	99.44	99.95	100.01	100.95
LOI	3.05	3.64	4.44	4.91	4.06	4.06	3.81	6.61	5.11	7.07	4.46	2.83	4.31	3.16	4.05	2.82	2.85	2.75
FeO*/MgO	1.47	2.23	1.15	1.32	3.88	6.47	1.89	1.38	2.41	1.23	1.05	1.51	1.13	1.65	1.26	2.16	1.95	1.62
Ba	63	17	---	134	47	164	180	0.8	12	84	1008	355	894	64	354	1.4	---	29
Ce	22	78	38	40	56	81	130	29	108	62	2.1	14	2.3	14	9.2	13	12	12
Cr	297	0.3	370	114	27	31	11	688	3.0	172	374	291	620	134	395	174	364	150
Nb	20	67	24	22	34	42	133	15	60	47	1.8	2.3	1.7	2.7	2.7	1.3	1.5	2.2
Nd	12	31	18	19	24	35	47	14	41	26	6.1	9.3	5.9	10	8.2	9.9	10	8.8
Ni	97	22	155	75	38	58	26	215	13	84	124	91	132	83	125	114	143	83
Rb	12.8	14.4	2.5	16	103	77	17	5.8	18	19	10	8.1	25	7.1	14	6.3	7.0	4.0
Sc	35	37	37	40	49	86	41	33	54	54	36	37	39	37	36	54	51	26
Sr	220	227	235	775	70	76	175	84	67	92	219	283	2502	235	1710	364	466	133
V	273	305	294	297	197	267	123	233	199	282	301	357	292	381	319	358	372	431
Y	23	32	26	26	34	65	35	25	46	30	23	26	19	27	23	26	28	25
Zr	151	426	254	235	442	519	770	175	528	327	50	61	---	56	23	91	99	55
phenocryst ol	*							(*)		(*)		*						
phenocryst cpx																		
phenocryst kaer																		
phenocryst pl	(*)					(*)				(*)				(*)				
phenocryst ap																		
phenocryst sp																		
groundmass ol								(*)		(?)			(*)		(*)			
groundmass cpx	*	Ti	Ti	Ti	(*)				(?)		*	*	*	*	*	*	*	*
groundmass kaer			*															
groundmass aeg					*													
groundmass bi					?													
groundmass pl	(*)	(*)	(*)	(*)	(*)	(*)	(*)	(*)	(*)	(*)	(*)	(*)	*	(*)	*	(*)	(*)	(*)
groundmass ap					*		*		*							*	*	
groundmass ilm		*	*	(*)	*	(*)	*		*		(*)		*	?		*	(*)	(*)
groundmass mt												*		*	*			
groundmass glass	(*)	(*)	(*)	(*)	(*)	(*)	(*)	(*)	(*)	(*)	(*)	(*)	(*)	(*)	(*)			

Table 6. Continued.

ID	M30	M31	M55	M56	M01	M15	M16	M17	M24	M59	M06	M02	M27	M28	M35	M07	M08
no.	990702-3	990702-4	ep-amp A	ep-amp C	980509-1	981031-8	981031-11	981031-12	981103-12	mu_ank	980713-12	980510-7	990622-8	990622-14	990802-6	981006-4	981007-22
unit	Pirashuke Unit (Metadolerite Sub-unit)				Pirashuke Unit (Pr-1 Sub-unit)							Pirashuke Unit (Pr-2 Sub-unit)					
rock name	cpx bas	dol	ep-amp	ep-amp	ap bas	ank	aph bas	pl bas	cpx bas	ank	dol	ank	cpx bas	dol	aph bas	pl bas	cpx-ap bas
SiO_2	49.84	49.55	49.62	48.63	46.82	52.24	43.22	43.66	44.80	47.97	48.57	41.84	45.84	51.41	47.86	45.59	42.09
TiO_2	0.86	0.87	1.10	1.37	3.36	2.63	4.83	4.82	3.80	1.60	0.88	6.65	3.88	3.49	2.36	3.50	3.45
Al_2O_3	13.13	15.03	16.88	16.67	14.87	10.31	17.04	16.58	14.54	5.54	15.77	14.57	12.39	13.86	17.69	15.04	15.79
$Fe_2O_3^*$	12.90	11.26	11.73	13.85	13.66	11.15	15.32	15.64	12.90	12.36	11.68	14.33	14.04	12.82	11.95	16.70	14.01
MnO	0.22	0.18	0.18	0.20	0.27	0.15	0.31	0.23	0.18	0.20	0.17	0.15	0.17	0.15	0.14	0.23	0.26
MgO	10.84	8.66	5.88	4.57	4.05	7.88	7.62	7.50	7.87	18.81	9.13	10.94	7.27	4.48	5.19	8.33	8.36
CaO	10.29	13.45	11.90	10.53	8.87	12.42	6.60	8.14	11.72	11.29	11.48	7.07	13.32	7.40	8.42	4.62	9.86
Na_2O	2.40	1.67	3.58	4.65	4.51	4.37	3.44	2.44	1.72	1.34	3.22	1.42	2.75	5.56	5.90	4.81	2.82
K_2O	0.07	0.05	0.07	0.20	2.40	0.11	0.41	0.27	2.33	0.01	0.08	2.28	0.67	0.56	0.06	0.79	2.17
P_2O_5	0.06	0.06	0.09	0.10	1.72	0.31	0.67	0.67	0.60	0.17	0.06	0.63	0.51	0.49	0.18	0.42	1.58
total	100.60	100.77	101.01	100.77	100.51	101.56	99.47	99.93	100.45	99.30	101.05	99.89	100.82	100.22	99.73	100.03	100.39
LOI	2.87	2.76	2.05	1.64	2.83	5.24	4.79	4.53	3.53	6.00	3.91	5.83	2.75	2.31	4.63	4.76	6.07
FeO*/MgO	1.07	1.17	1.80	2.73	3.03	1.27	1.81	1.88	1.48	0.59	1.15	1.18	1.74	2.57	2.07	1.80	1.51
Ba	9.2	11	10	5.7	1069	---	---	---	214	---	64	15	41	225	21	23	327
Ce	0.1	7.2	14	13	191	32	81	81	55	22	2.5	61	57	38	24	43	225
Cr	386	384	114	25	34	1188	35	30	149	1942	306	299	185	3.5	269	46	5.4
Nb	1.3	1.5	2.4	2.3	172	24	64	61	42	18	2.2	64	39	33	19	31	213
Nd	4.8	7.9	9.6	9.7	67	15	33	31	23	11	5.8	25	24	17	13	19	76
Ni	130	106	65	42	32	164	79	73	105	503	169	155	91	30	170	59	30
Rb	2.6	4.1	4.0	7.2	72	4.9	12.8	10.6	36	0.9	4.4	45	13	16	5.0	20	58
Sc	33	20	24	36	43	35	68	61	37	27	24	75	37	50	37	74	40
Sr	19	214	248	773	1196	165	704	685	185	53	109	50	72	104	189	41	296
V	300	289	324	383	136	316	384	359	319	206	294	462	349	303	177	400	439
Y	22	24	26	31	39	22	32	31	28	18	23	28	29	24	26	28	33
Zr	42	37	52	66	727	185	409	399	339	113	38	525	318	182	161	279	424
phenocryst: ol										(*)		(?)					
phenocryst: cpx	*					*			Ti	*		Ti	Ti				Ti
phenocryst: kaer												*					
phenocryst: pl							(*)	(*)								*	
phenocryst: ap					*												*
phenocryst: sp												*					
groundmass: ol																	
groundmass: cpx	*		(?)	(*)	(*)	*			Ti	*	*		Ti	*	(*)	*	*
groundmass: kaer														*			
groundmass: aeg									*		*						
groundmass: bi														*			
groundmass: pl	(*)	(*)	(*)	(*)	(*)	(*)	(*)	(*)	(*)	(*)	(*)	(*)	(*)	(*)	(*)	(*)	(*)
groundmass: ap														*			*
groundmass: ilm	?	*	(*)	(*)	(*)		*	*	(*)		(*)		*	*		(*)	
groundmass: mt																	*
groundmass: glass	(*)				(?)	(*)	(*)	(*)	(*)	(*)		(*)	(*)	(*)	(*)		(*)

Table 6. Continued.

ID	M29	M32	M33	M34	M36	M37	M38	M39	M40	M41	M42	M50	M47	M48	M49	M51	M52	M53
no.	990622-23	990721-3	990721-6	990722-4	990804-12	990806-3	990806-6	990806-2	990806-9E	990809-6	990809-2	990926-8	990922-6C	990922-9	990923-8	990927-23	990929-7	990929-4
unit						Futagawa Unit										Shizunai Unit		
rock name	aph bas	dol	aph bas	pl bas	trach	dol	dol	ol bas	dol	dol	pl bas	aph bas	dol	dol	dol	dol	dol	aph bas
SiO_2	49.32	49.24	47.92	49.40	50.82	46.96	48.75	48.87	47.42	48.74	47.70	55.13	47.75	49.35	44.11	49.82	43.49	53.07
TiO_2	3.28	2.87	3.11	2.50	2.95	2.05	1.55	2.26	2.03	2.43	2.24	2.39	3.84	2.56	4.59	3.12	3.80	2.79
Al_2O_3	17.45	16.81	16.58	22.44	19.10	16.44	16.78	17.50	16.58	17.90	19.43	17.63	16.08	17.09	13.84	18.75	13.79	17.98
Fe_2O_3*	14.82	12.15	13.56	8.92	12.48	11.74	9.72	11.49	12.42	10.70	9.70	7.93	16.40	12.12	13.33	11.22	14.85	9.05
MnO	0.15	0.22	0.26	0.21	0.14	0.17	0.16	0.19	0.39	0.16	0.20	0.15	0.15	0.23	0.20	0.15	0.18	0.20
MgO	0.95	5.04	8.13	2.57	1.61	8.00	7.15	8.71	8.89	7.83	7.00	0.63	4.45	4.49	10.67	1.27	13.70	2.26
CaO	6.02	5.56	7.44	9.08	6.84	9.60	10.77	6.52	6.67	5.75	8.29	5.71	2.78	5.55	8.78	4.14	6.46	4.51
Na_2O	5.51	5.63	2.05	3.53	4.27	3.93	4.00	3.98	2.98	4.40	2.86	7.00	3.95	4.63	3.14	4.39	1.97	6.29
K_2O	0.78	1.80	0.01	0.84	1.03	0.14	0.39	0.02	2.30	1.35	1.93	1.59	3.16	1.96	0.23	4.94	0.28	2.34
P_2O_5	1.05	0.57	0.40	0.38	0.52	0.26	0.25	0.35	0.29	0.52	0.41	1.16	1.03	1.63	0.98	1.71	0.77	1.32
total	99.32	99.88	99.46	99.88	99.75	99.28	99.51	99.89	99.96	99.78	99.75	99.30	99.58	99.61	99.85	99.53	99.29	99.80
LOI	3.31	4.10	5.65	6.07	4.73	4.48	4.28	5.80	4.97	4.68	6.93	1.97	3.67	7.14	4.57	2.73	6.20	2.52
FeO*/MgO	13.99	2.17	1.50	3.12	6.99	1.32	1.22	1.19	1.26	1.23	1.25	11.34	3.32	2.43	1.12	7.93	0.98	3.60
Ba	47	59	28	54	47	8.6	53	21	51	53	65	131	389	415	---	316	188	382
Ce	49	36	32	31	40	19	21	24	23	39	35	118	100	131	95	126	74	124
Cr	196	126	198	75	130	198	586	185	226	171	166	4	134	3.6	297	1.1	250	2.2
Nb	27	20	17	19	20	12	11	18	14	18	21	92	80	94	79	96	58	125
Nd	22	16	16	15	18	12	12	14	11	19	18	43	38	48	35	46	28	45
Ni	72	75	117	35	66	99	66	86	89	91	155	8.1	93	7.4	164	16	244	30
Rb	39	61	6.0	27	40	6.2	9.1	5.3	37	26	49	30	71	42	7.5	82	8.8	46
Sc	60	50	47	30	49	37	26	46	45	44	29	29	76	47	51	50	56	41
Sr	377	102	108	746	449	180	280	118	100	199	358	218	474	241	316	208	275	231
V	291	176	168	160	151	242	195	242	266	155	202	117	234	72	243	182	245	113
Y	39	31	32	23	24	31	25	31	34	31	31	30	25	40	27	33	26	29
Zr	338	317	233	189	253	151	117	191	164	271	195	657	470	471	478	487	391	547
phenocryst ol	(*)							(*)										
phenocryst cpx																		
phenocryst kaer																		
phenocryst pl				(*)	(*)						(*)							
phenocryst ap																		
phenocryst sp																		
groundmass ol	(*)		(*)			(*)	(?)	(?)			(*)						(?)	
groundmass cpx		(*)	(?)			Ti	*		Ti	Ti		(*)			Ti		Ti	
groundmass kaer							(?)								*		*	
groundmass aeg							*			*					*		*	
groundmass bi									(*)	(?)			(*)	*			*	
groundmass pl	(*)	(*)	(*)	(*)	(*)	(*)	(*)	(*)	(*)	(*)	(*)	(*)	(*)	(*)	(*)	(*)	*	(*)
groundmass ap							*			*				*			*	*
groundmass ilm	*	*	*	*	*	*	*	(*)	*	*	*	*	*	?	*	*	*	*
groundmass mt													*	*	*	*		
groundmass glass	(*)	(*)	(*)	(*)	(*)	(*)	(*)	(*)	(*)	(*)	(*)	(*)	(*)	(*)		(*)	(?)	(*)

Table 7. Summary of characteristics of greenstones in the Iwashimizu Complex.

Petrologic type	Oceanic Island -type (OIB-type) basalts		Lower Sorachi -type tholeiite (LST)
	alkali basalt (OIA)	tholeiite (OIT)	
Occurring units (in study area)	• All units	• Dominantly occur in Futagawa Unit • Less commonly occur in Mikawa and Pirashuke Units	• Limitedly occur in Pirashuke Unit (Pr-1 & Metadolerite Sub-units) & Mikawa Unit (mixed facies A).
Field occurrences	• non- to severely vesicular • commonly accompanied by hyaloclastite • accompanied by red chert and limestone • reddish lava & hyaloclastite are common (bluish green in high-grade unit) • Vesicular dolerites are seen	• non- to weakly vesicular • dominated by close-packed pillow lava and dolerite sill (with scarce hyaloclastite) • accompanied by red/brown chert • pillow lavas are dominantly reddish • Vesicular dolerites are seen	• non-vesicular • dominated by close-packed pillow lava and dolerite (with rare hyaloclastite) • with no sediments (rarely with green siliceous shale) • commonly green (whitish at greenschist facies) • occasionally with webbed ("torifun-like") veinlets in low-grade ones
Microscopic characters	• Phyric rocks are common (dominantly ol→cpx→pl) • Titanaugite phenocrysts are not rare. Some contain apatite or kaersutite phenocrysts. • Ilmenite is the dominant opaque phase in groundmass. • Titanaugite, aegirine, kaersutite, biotite, and apatite are common in dolerite. • Plagioclase-rich dolerite is common (Shizunai Unit)	• moderately to poorly phyric (ol→pl) • Ilmenite is the dominant opaque phase in groundmass • Clinopyroxene is rare in effusive rocks • Titanaugite, aegirine, kaersutite, biotite, and apatite are not rare in dolerite.	• Dominantly aphyric. (ol→cpx→pl?) • Magnetite is the dominant opaque phase in groundmass (ilmenite is common in dolerite) • Dolerites never contain aegirine, kaersutite, and biotite. Apatite is rare. Rarely pale-brown hornblende (possibly metamorphic) is seen.
Cumulus phase	ankaramite (cpx ±ol)	picrite (ol ± pl)	
Petrochemical characters	• Alkali series • Abundantly (and variably) enriched in incompatible elements • Variably evolved	• Tholeiite to tholeiite/alkali transitional series • Less abundantly (and more uniformly) enriched in incompatible elements relative to OIA • Less Variably evolved	• Tholeiite (MORB-IAT intermediate type) • Depleted in HFS elements relative to MORB, except Nb • TiO_2 increases less evidently than MORB • Basalts are uniformly evolved (Some dolerites are more evolved)

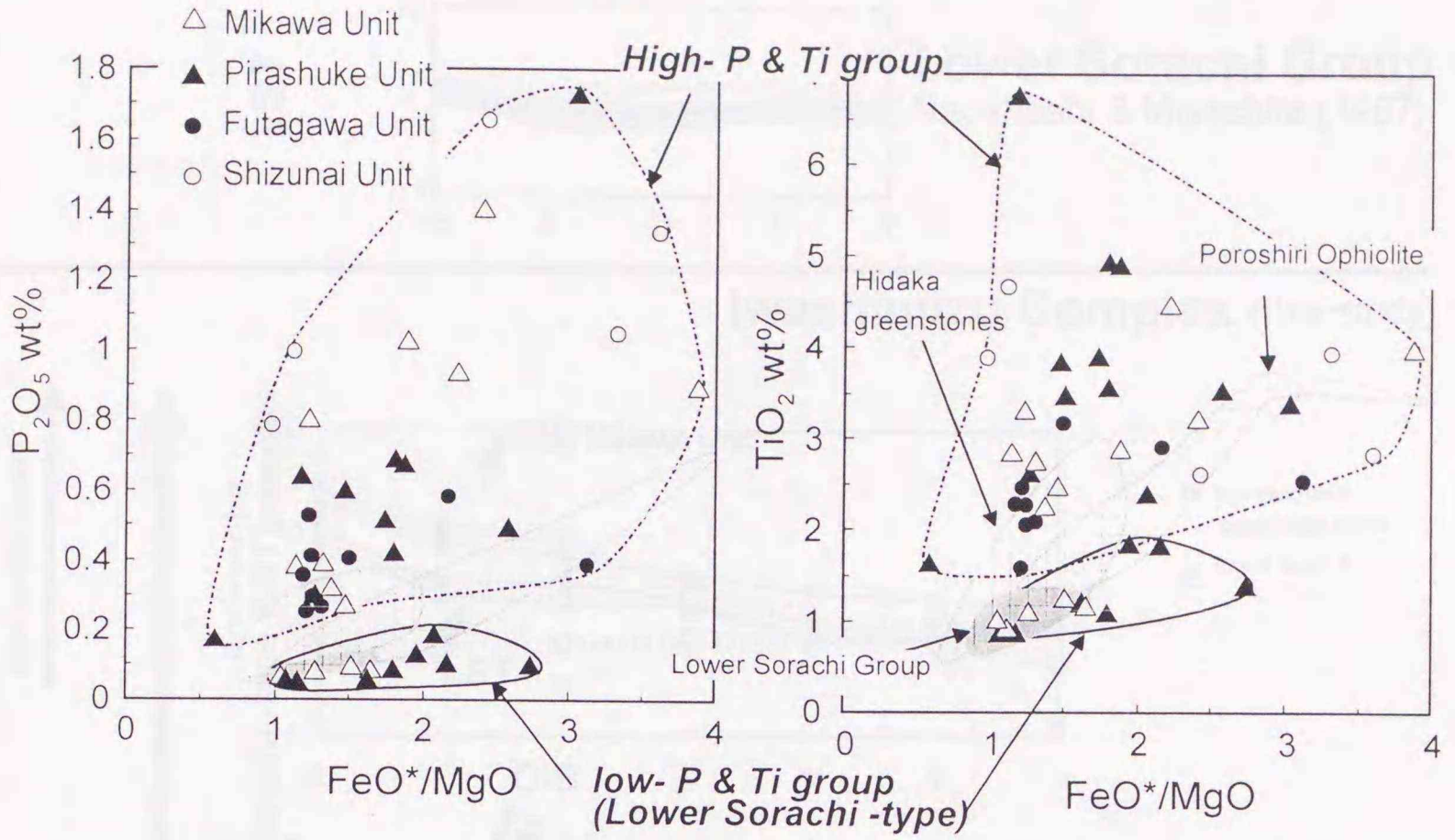


Fig. 42. Major element compositions of greenstones in the Iwashimizu Complex. Reference data: Lower Sorachi Group: Ishizuka (1981); Kiminami et al. (1985); Niida (1992), Hidaka greenstone: Kinugasa et al. (1981); Osanai et al. (1985); Miyashita & Katsushima (1986); Miyashita & Yoshida (1994), Poroshiri Ophiolite: Miyashita et al. (1994).

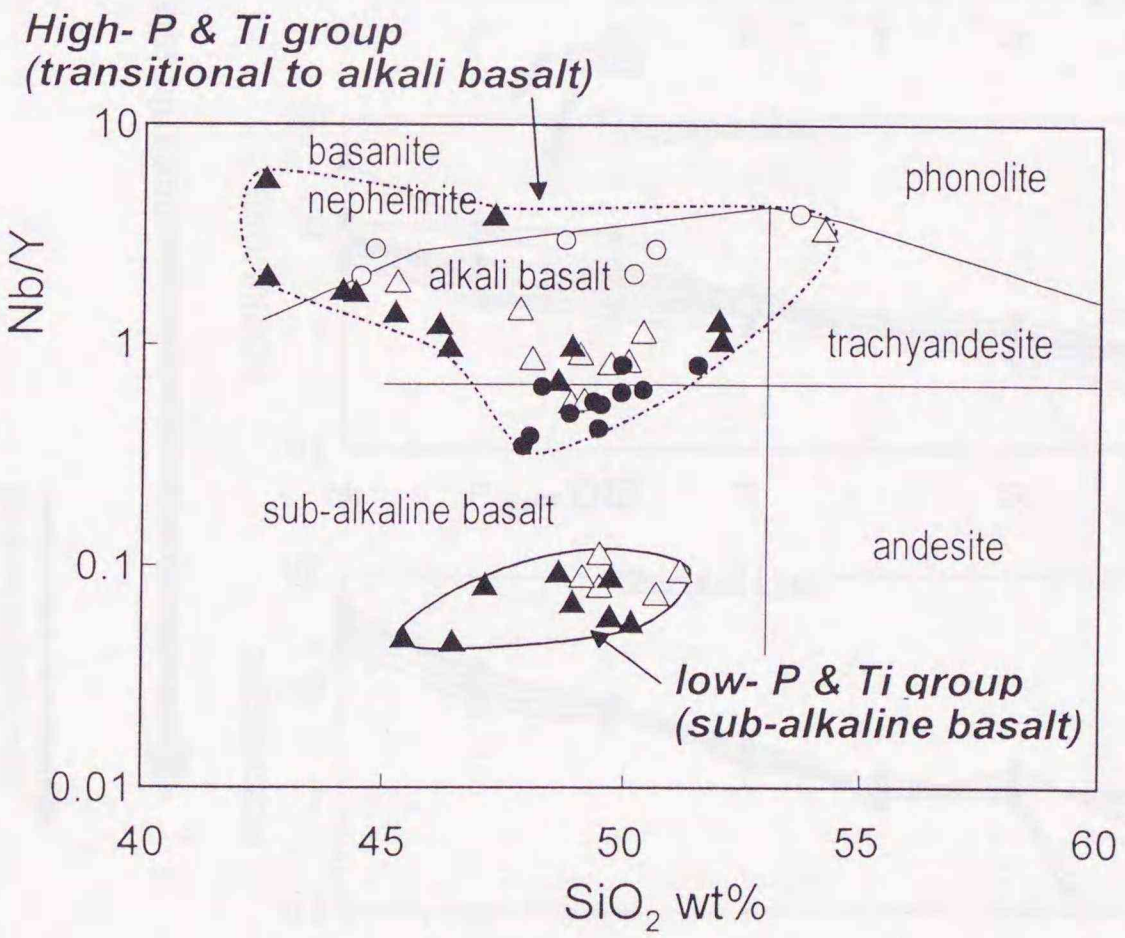


Fig. 43. Nb/Y ratios of greenstones in the Iwashimizu Complex. Alkaline / sub-alkaline discriminant fields after Winchester & Floyd (1977). Symbols as in Fig. 42.

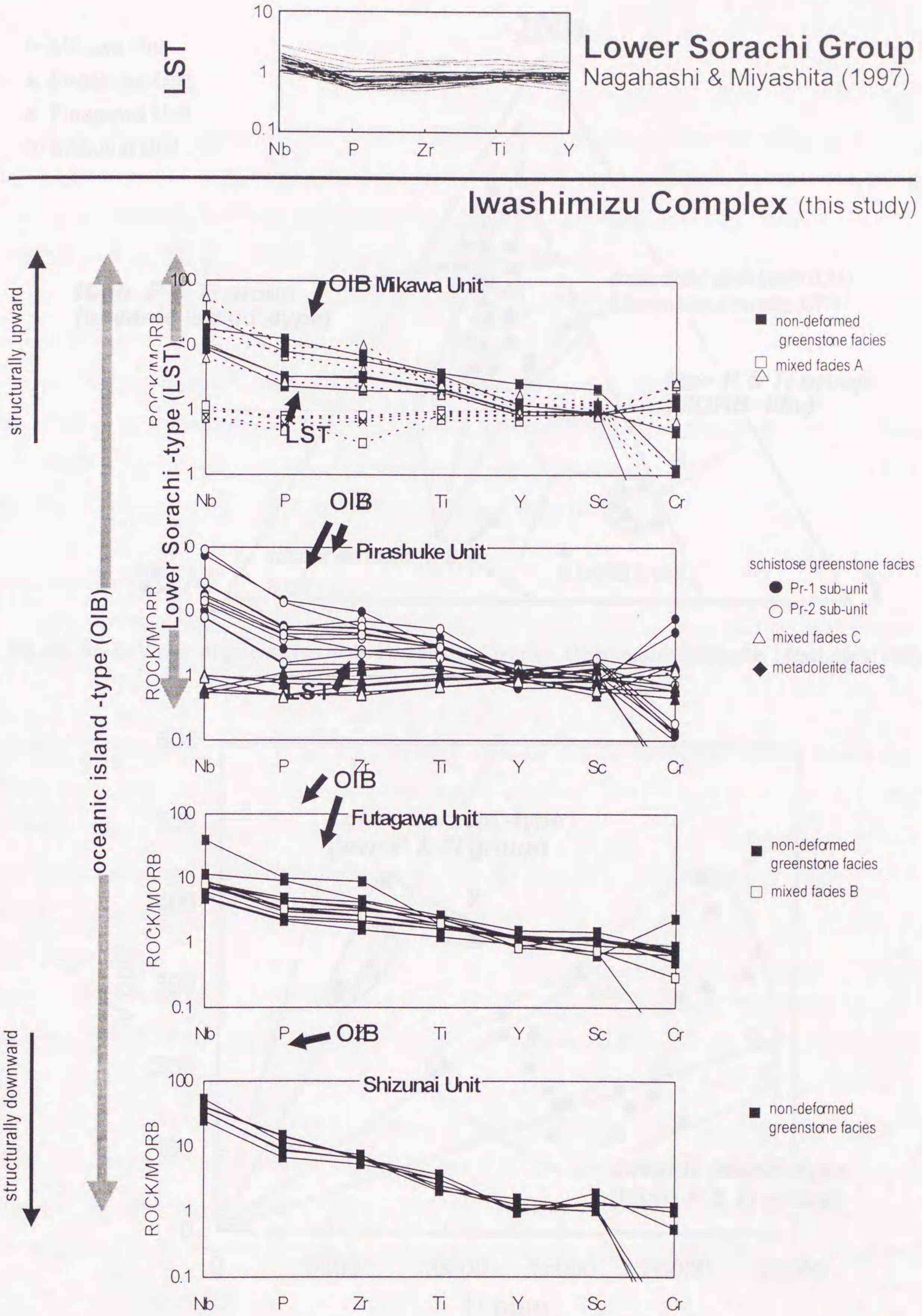


Fig. 44. MORB-normalized trace-element patterns of greenstones in the Iwashimizu Complex. MORB-normalizer after Sun & McDonough (1989), except Cr after Pearce (1982).

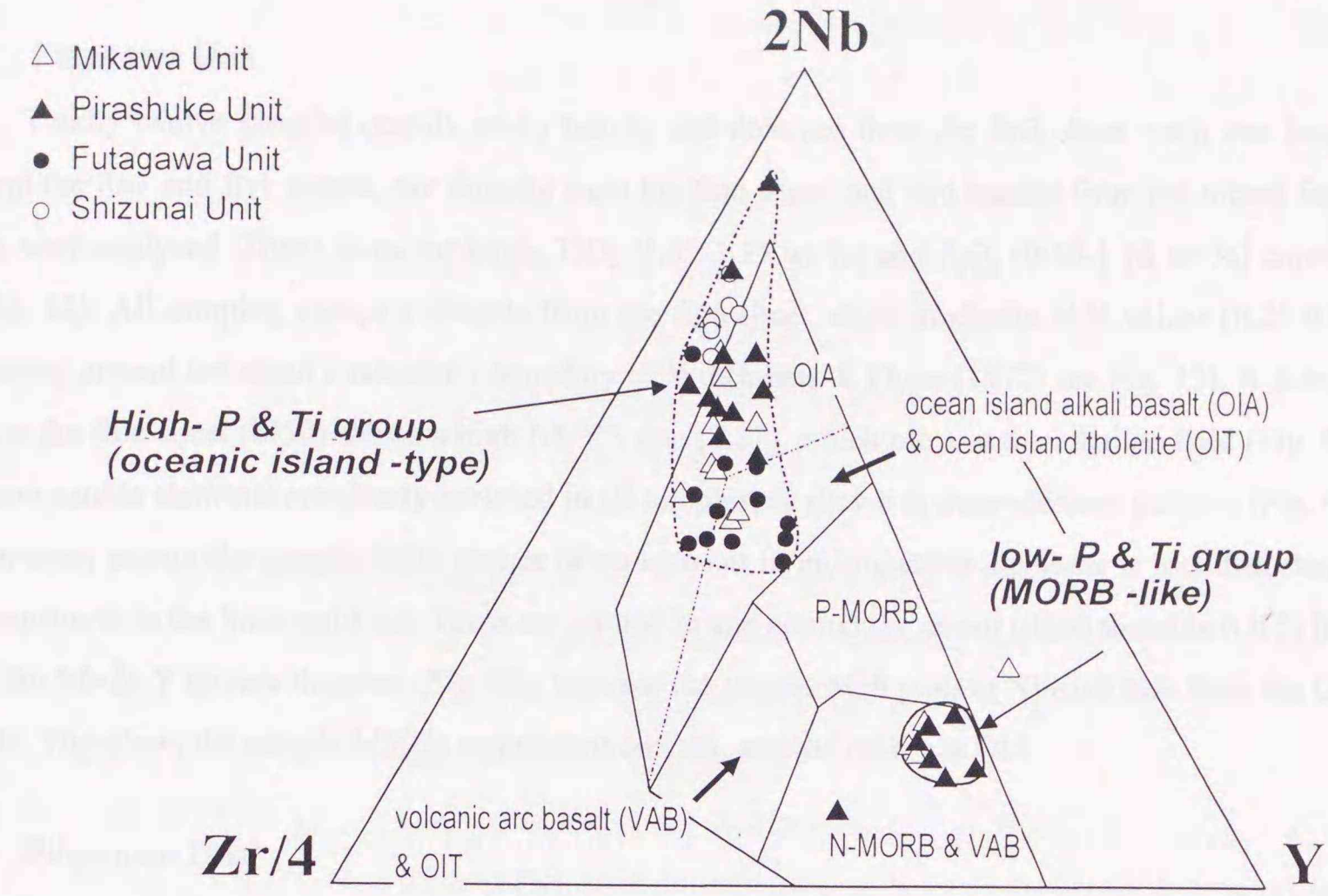


Fig. 45. Nb-Zr-Y plot of greenstones in the Iwashimizu Complex. Discriminant fields after Meschede (1986).

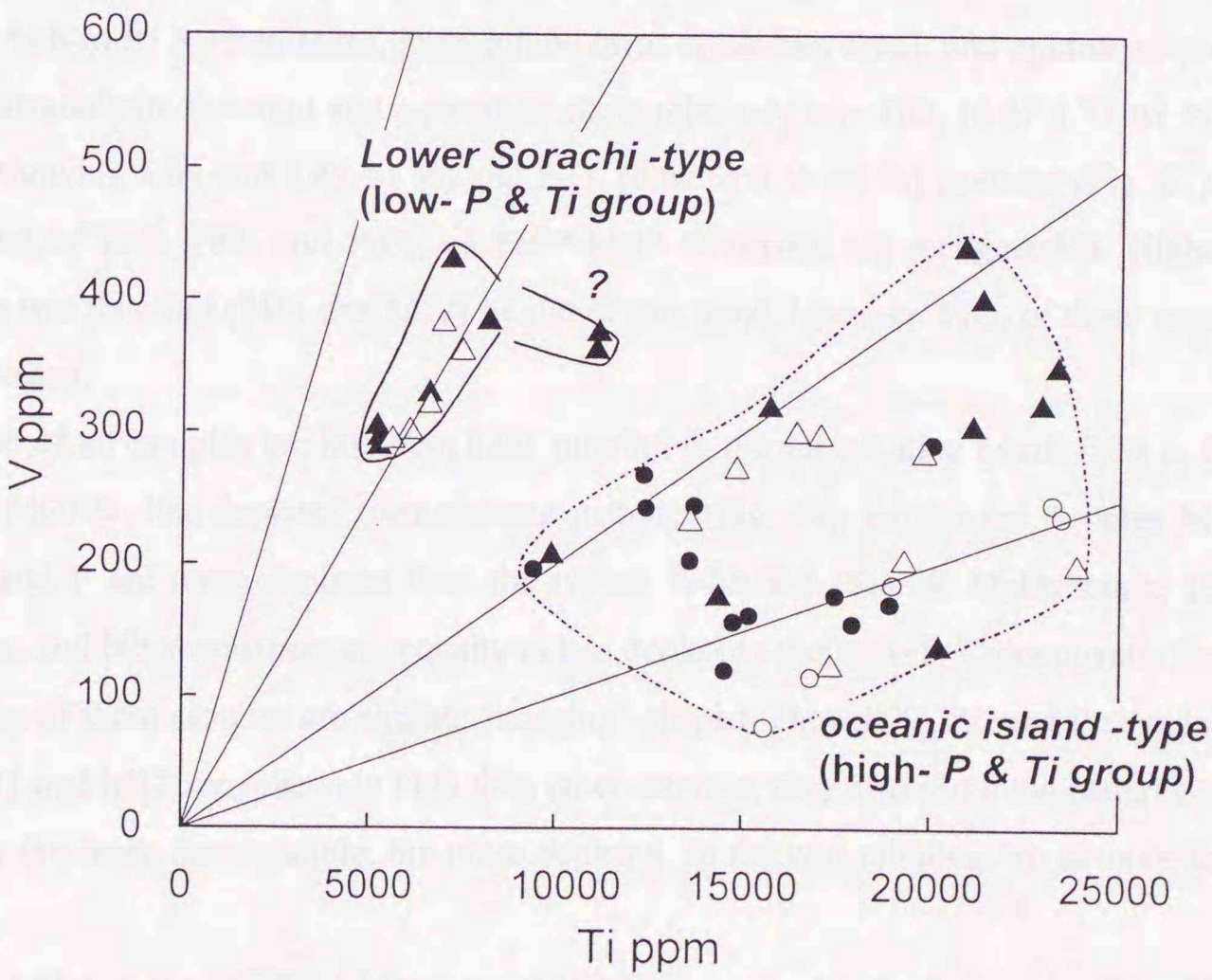


Fig. 46. Ti-V plot of greenstones in the Iwashimizu Complex. Discriminant fields after Shervais (1982). Symbols as in Fig. 45.

concluded to be oceanic island -type alkali basalts (OIA).

2. Futagawa Unit

Totally twelve samples (totally seven basalts and dolerites from the ftn3 sheet, each one basalts form the ftn1 and fts1 sheets, one dolerite from the ftn6 sheet, and two basalts from the mixed facies B), were analyzed. These show moderate TiO_2 (1.57-3.35 wt %) and P_2O_5 (0.30-1.18 wt %) contents (Fig. 42). All samples, except a dolerite from the ftn6 sheet, show moderate N/Y values (0.35-0.81) plotting around the alkali / sub-alkali boundary of Winchester & Floyd (1977; see Fig. 43). A dolerite from the ftn6 sheet (M50) shows a high Nb/Y value (2.87), which plots in the alkaline field (Fig. 43). Incompatible elements are clearly enriched in all samples, as shown in trace-element patterns (Fig. 44). However, except the sample M50, degree of enrichment in incompatible elements is less than that of greenstones in the Shizunai Unit. These are plotted in and around the ocean island tholeiite (OIT) field on the Nb-Zr-Y ternary diagram (Fig. 45), whereas the sample M50 plots at Nb-rich side from the OIA field. Therefore, the sample M50 is regarded as an OIA, and the others as OIT.

3. Pirashuke Unit

Totally twenty samples from the Pirashuke Unit were analyzed: seven from the Metadolerite Sub-unit; seven from the Pr-1 Sub-unit; and six from the Pr-2 Sub-unit.

Metadolerite Sub-unit: Metadolerites, meta-pillow lavas (Nukabira area), and epidote amphibolite, all from the Metadolerite Sub-unit and equivalent show relatively low TiO_2 (0.87-1.37 wt % except two dolerites showing 1.84 and 1.85 wt %) and P_2O_5 (0.06 to 0.13 wt %) contents (Fig. 42). Slight increasing trend of both TiO_2 and P_2O_5, as FeO*/MgO increases, are recognizable. Higher TiO_2 contents of the two dolerites (M11 and M12) lie out of this trend, however, P_2O_5 of these samples lie on the general trend.

Nb/Y ratios of all samples are less than 0.09, plotting in the sub-alkaline basalt field in Fig. 43. They show N-MORB -like depleted trace-element patterns (Fig. 44). Except the samples M11 and M12, Ti, Zr, and P are more depleted than the typical N-MORB (Sun & McDonough, 1989) in ascending order, and Nb abundances are equally to less depleted relative to P. Consequently the trace-element patterns of these samples are slightly "hanging"-shaped. Though Ti, Zr, and P abundances in the sample M11 and M12 are relatively high than other samples, they also show the patterns slanting to the left, *i.e.*, the more incompatible, the more depleted. In the two samples, Nb is more depleted than P.

All samples plot in the MORB / island arc (IAB) field on the Nb-Zr-Y diagram (Fig. 45). The samples M10 and M12 plot in the MORB field, and the others plot around the boundary between

MORB and IAB fields on the Ti-V diagram (Shervais, 1982: Fig. 46). The lower Ti group (M13, M30-31, and M55-56) is thus regarded as MORB-IAB intermediate -type basalts. Indistinct increasing trends of TiO_2 and P_2O_5 (Fig. 42) and depleted trace-element patterns relative to N-MORB (Fig. 44) are the common characteristics of the Lower Sorachi Group (Nagahashi & Miyashita, 1997). Therefore, these characteristics are regarded as the Lower Sorachi -type tholeiite (LST). The samples M11 and M12 are more similar to N-MORB in terms of higher HFS element abundances, except that Nb is evidently depleted. However, the samples M12 (higher HFS) and M13 are considered to comprise a single dolerite body based on mapping. Hence, a possibility is also left that the chemical characteristics of the samples M11 and M12 are variations of LST.

Pr-1 and Pr-2 Sub-units: The dolerite sample M06, collected from the mixed facies C, show low TiO_2 and P_2O_5 abundances (Fig. 42), and Nb/Zr ratio (Fig. 43). It shows a slight depleted trace-element pattern except Nb (Fig. 44), as much as the typical greenstones of the Metadolerite facies and the Lower Sorachi Group. This sample is thus identified as LST.

The other samples are all from the schistose greenstone facies. They have high TiO_2 (2.4 to 6.7 wt %) and P_2O_5 (0.18 to 1.72 wt %), except an undifferentiated ankaramite (M59; see Fig. 42). Trace-element patterns (Fig. 44) show that incompatible elements are distinctly enriched, indicating that these greenstones are oceanic island -type basalts (OIB). Nb-Zr-Y (Fig. 45) and Ti-V (Fig. 46) plots also show that they are of OIB -origin. Nb/Y ratio of the sample M35 is transitional between alkaline and non-alkaline basalts (Fig. 43), and within the range of OIT in the Futagawa Unit. Therefore, the M35 basalt is probably an OIT. The others have high Nb/Y ratios enough to be classified as OIA.

4. Mikawa Unit

Greenstones of the Mikawa Unit are also classified into two groups: OIA and LST. Samples M04-M05, M09, M25,and M54 have low TiO_2 (0.9-1.2 wt %) and low P_2O_5 (0.06-0.09 wt%) concentrations (Fig. 42), both slightly increasing as FeO*/MgO increases, and have low Nb/Y ratio classified as non-alkaline basalts (Fig. 43). They show depleted trace-element patterns (Fig. 44). These samples are thus concluded to be LST.

The other greenstones, both from the non-deformed greenstone facies and the mixed facies A, show high concentrations of TiO_2 (2.2-4.4 wt%) and P_2O_5 (0.3-1.5 wt%; Fig. 42). These greenstones show pronounced enrichment in incompatible elements (Fig. 44), and plot in the OIB fields on both Nb-Zr-Y and Ti-V diagrams (Figs. 45 and 46). Nb/Y ratios show that both OIT and OIA are contained in these greenstones (Fig. 43).

5. Relation between petrochemical types, petrography and mode of occurrences

Greenstones in the Iwashimizu Complex are petrochemically classified into three types: OIA, OIT, and LST. Field occurrences, petrographic and petrochemical characteristics are summarized in Table 7. OIA and OIT greenstones mainly occur as mappable tectonic slices several hundred meters thick and several kilometers in extent. They also occur as smaller slices and blocks in the inter-slice mixed facies. To compare basalts between Futagawa and Pirashuke Units, olivine (-plagioclase) basalt is common in the OIT -type. Whereas in the OIA-type, basalts containing cpx (typically titanaugite) are more common, and ankaramite (cpx- highly phyric basalt) is not rare. Both OIT and OIA contain ilmenite more common than magnetite in groundmass. There is no clear petrographic difference between OIT and OIA dolerites, though apatite, biotite, kaersutite and aegirine seem to be more common in OIA than in OIT. The OIT-type basalts tend to occur as uniform Pillow lava, less vesicular, close packed, without hyaloclastite, and occasionally with chert. Whereas the occurrences of OIA basalts are highly variable: non to extremely vesicular, with and without hyaloclastite, as close-packed to isolated pillow lavas, and with chert or micrite limestone or bioclastic limestone.

The LST greenstones are all non-vesicular, and dominantly aphyric. They are never accompanied by chert and limestone. The LST greenstones contained in the Mikawa Unit (mixed facies A) were characteristically metamorphosed under the zeolite to prehnite-pumpellyite facies, inconsistent with the metamorphic grades of OIA and OIT greenstones as described in the next section. The LST greenstones in the Pirashuke Unit (Metadolerite Sub-unit) were metamorphosed under pumpellyite-actinolite facies to epidote-amphibolite facies.

Metamorphism

Previous studies

In Mitsuishi - Shizunai area, Nakano (1978, 1981, and 1999) described metamorphic minerals and their assemblages in metabasites. He classified the assemblages into three types (Fig. 47): type-Ia characterized by pumpellyite + sodic pyroxene assemblage (high-pressure part of prehnite-pumpellyite facies); type-Ib by the occurrence of lawsonite (lawsonite-albite facies); type-II by the occurrence of epidote (glaucophane-schist facies); and type-III as epidote-amphibolite. He described that metabasites of each type comprise blocks separated by faults. Hence, it is important to describe the relation between metamorphic grade and the new lithologic division proposed in this study. Previously reported radiometric ages are displayed in Fig. 36. Nakagawa and Nakano (1987) reported a K-Ar age: 125±6 Ma from white mica in mafic schist of the Pirashuke Unit. Ota et al. (1993) reported K-Ar ages of white mica from metapelite (107.6±2.3 Ma) and siliceous schist (124.1±2.7 Ma) from the Futagawa Unit. Iwasaki and Ueda (1993) and Watanabe et al. (1994) reported K-Ar ages of white

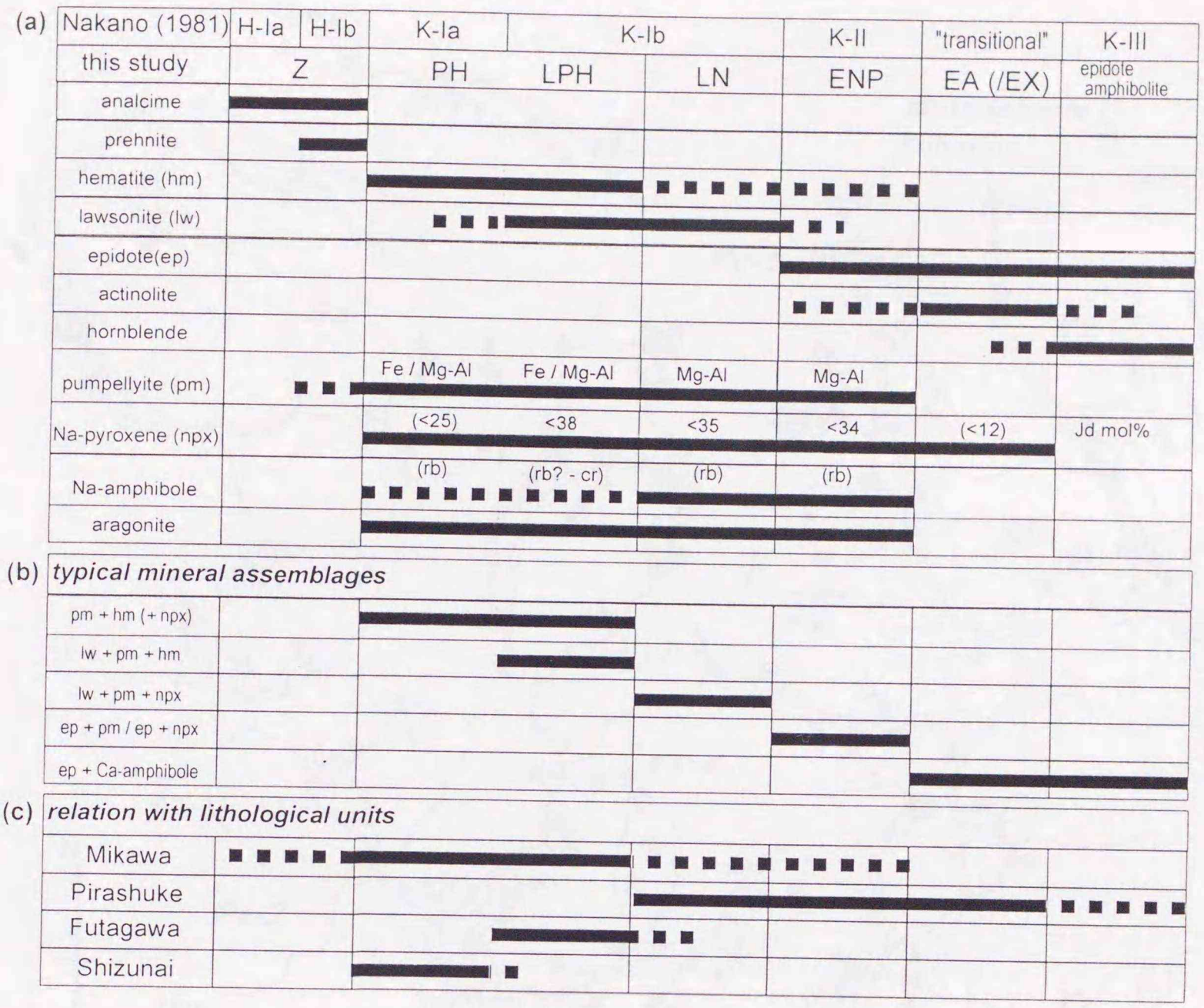


Fig. 47. Metamorphic mineral assemblages of metabasites in the Iwashimizu Complex. (a) Occurrence of metamorphic minerals and metamorphic grade. (b) Representative metamorphic mineral assemblages. (c) Relation between mineral assemblages and lithological units.

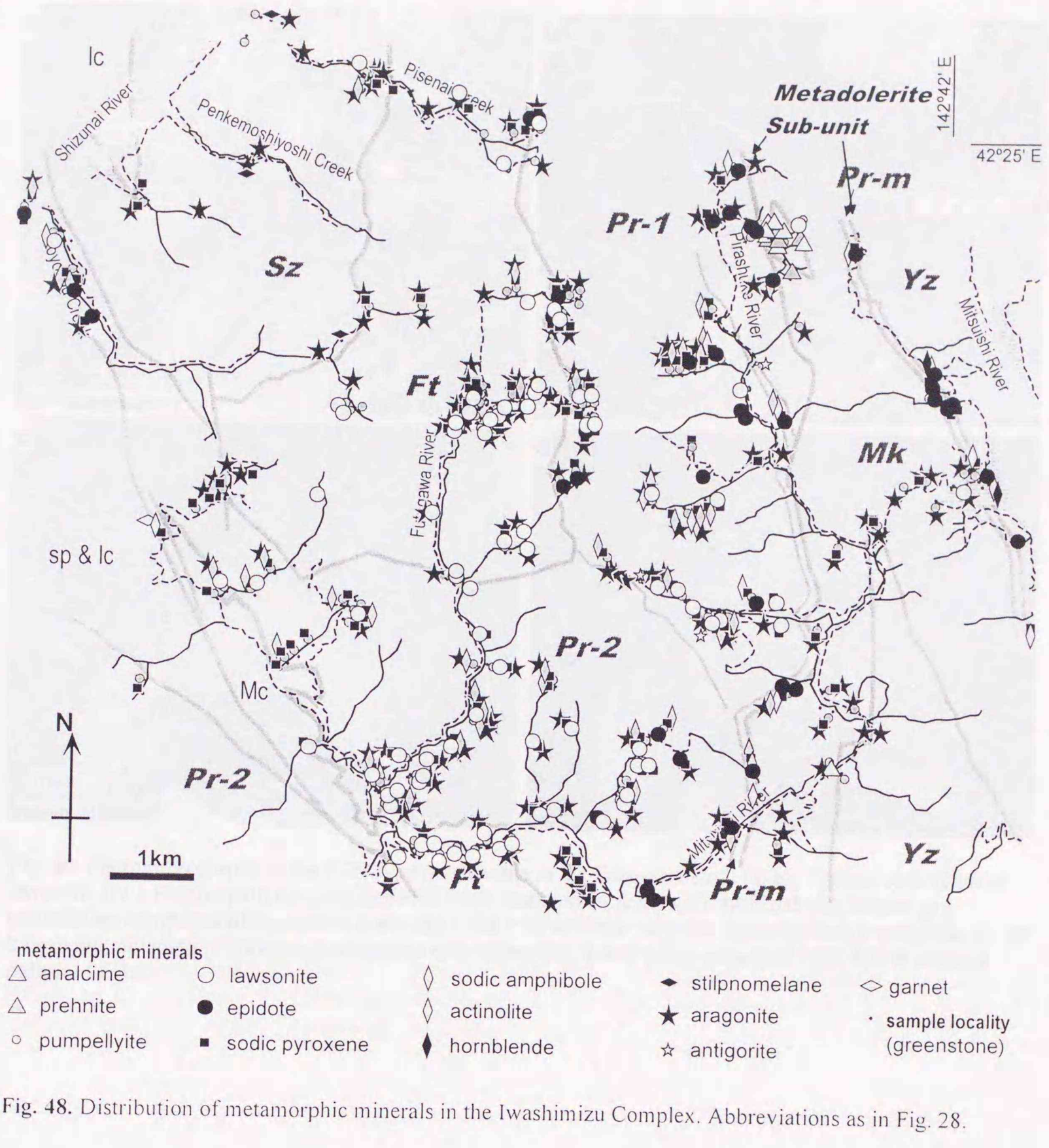


Fig. 48. Distribution of metamorphic minerals in the Iwashimizu Complex. Abbreviations as in Fig. 28.

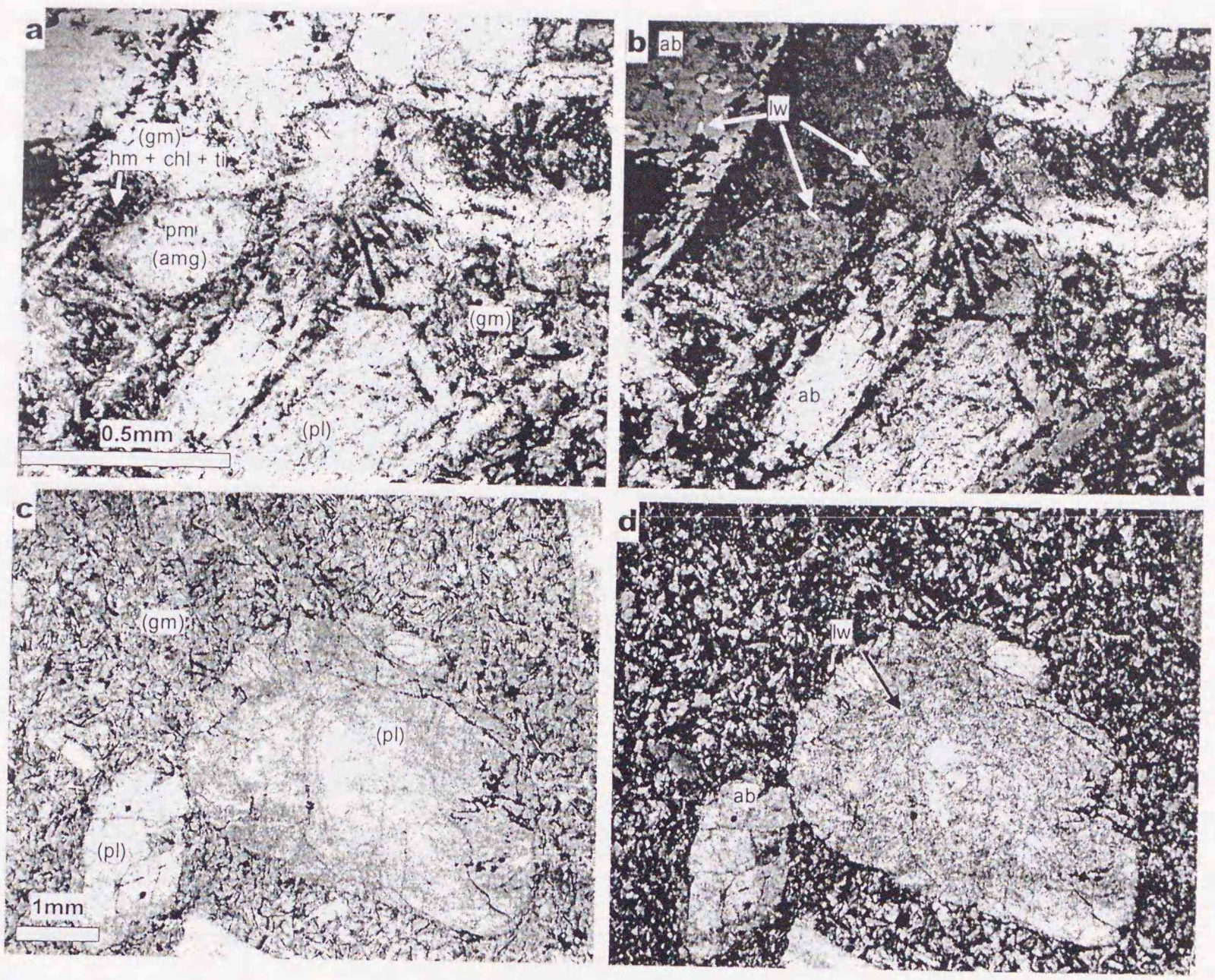


Fig. 49. Photomicrographs of the LPH-type metabasalts in the Futagawa Unit. (a, b): Typical occurrence of lawsonite (lw), Fe-pumpellyite (pm), hematite (hm), and chlorite (chl). (pl): albitized plagioclase, gm: groundmass composed of devitrified glass (chl + hm + ti) and relict acicular ilmenite, (amg): amigdule. (c, d): Lawsonite replacing plagioclase phenocrysts with albite (ab). a & c: plane-polarized light, b & d: crossed polarized light.

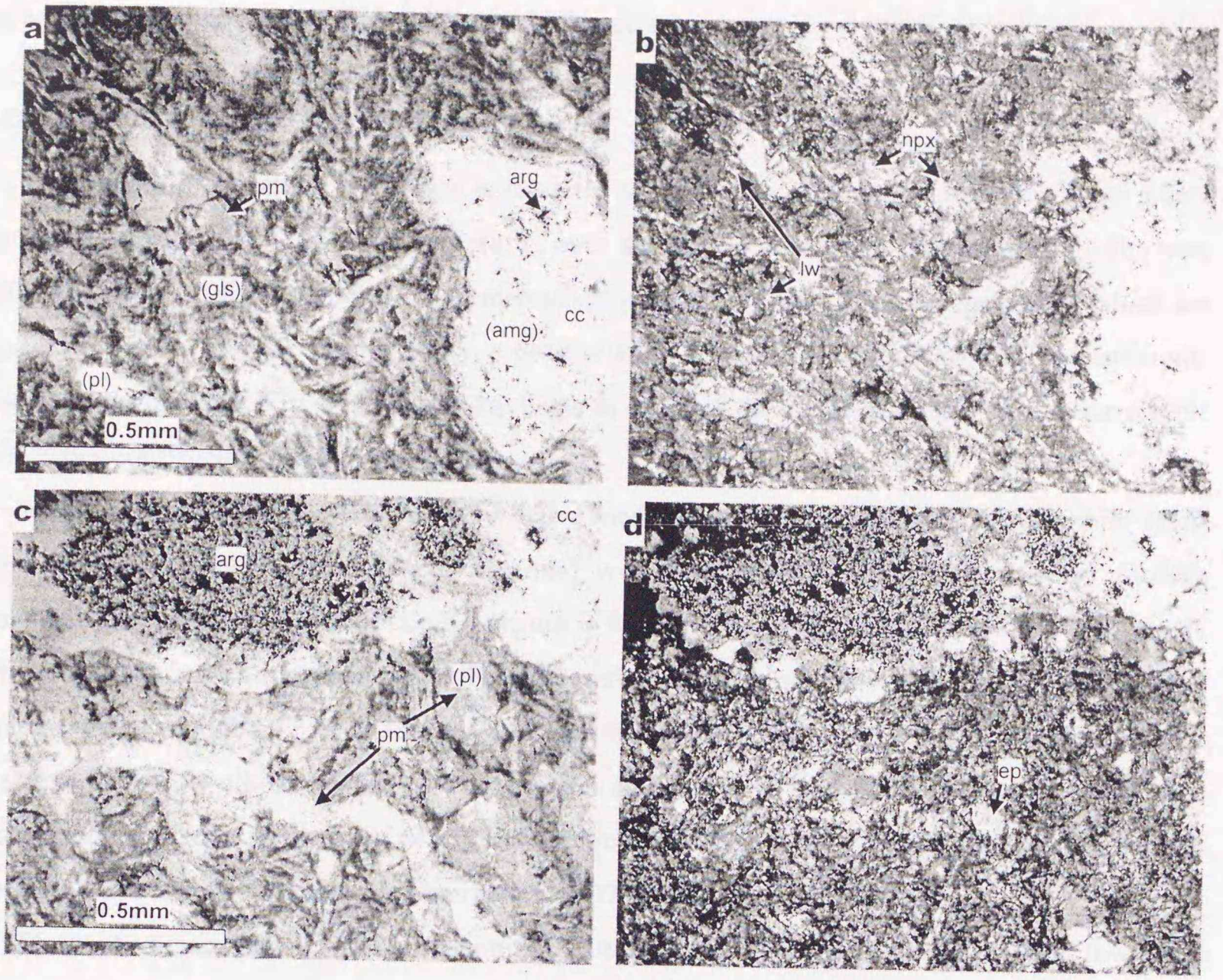


Fig. 50. Photomicrographs of metabasalts in the Pirashuke Unit. (a, b): A LN-type metabasalt in the Pr-2 Sub-unit. Both lawsonite and sodic pyroxene (npx) occur scattered in groundmass, replacing glass. Lawsonite also occur replacing plagioclase microlites with albite. Aragonite (arg) occupies an amigdule, mostly replaced by calcite (cc). (c, d): An ENP-type metabasalt in the Pr-1 Sub-unit. Pumpellyite (pm) replaces both plagioclase microlite and glass, and also occur in vein. Epidote is seen in vein in this sample. Aragonite occur in vein with calcite. (gls): devitrified glass. The other abbreviations as in Fig. 49. a & c: plane-polarized light, b & d: crossed polarized light.

mica ranging 107 - 113 Ma, except one locality showing 90-94 Ma near serpentinite, from black and tuffaceous mudstones of the Shizunai Unit in Niikappu area.

Examination on metamorphic grade

Description of metamorphic grades is expected to derive the information about the depth where each unit was initially formed. In this study, over 432 thin sections of metabasites (Fig. 48) were optically described for determination of metamorphic grade, typical photomicrographs of which are shown in Figs. 49 and 50. Consequently, a good relation between the unit division and metamorphic grade was recognized (Fig. 47), which also helps to evaluate the significance of tectonostratigraphic framework constructed in the former section.

Metamorphic minerals were optically determined. Most silicate minerals (except white mica, stilpnomelane, smectite, zeolites, and prehnite) were confirmed by EPMA in selected sections (analcime and prehnite in clasts of conglomerate in Middle Yezo Group were chemically confirmed). Almost all sections were stained by the Feigl's solution for determination of aragonite. Four selected samples were examined for XRD analysis, in which lawsonite, hematite, white mica, smectite, chlorite, analcime, natrolite, albite, quartz, calcite, and relict augite were confirmed. Aragonite peaks were recognized from the sample, in which thin section carbonate was typically stained. Pyrite was confirmed by reflective microscope observation on 32 selected polished sections.

Most of metabasites in the Iwashimizu Complex are recrystallized under very low-grade metamorphic conditions. In such rocks, it is difficult to presume the areas where metamorphic minerals were crystallized in equilibrium. This study only provides the description under a rough assumption that all minerals were in equilibrium within the area of a thin section, except the extreme case that assemblages are obviously different by parts of a thin section. In spite of such rough examination, the assemblages seem to be classified into four major groups and three or possibly four minor groups, which distribute consistently with lithological units (Fig. 47). However, more careful and precise description is to be achieved in future study.

Description of minerals

Aragonite

Aragonite mainly occurs as infill of veins (Figs 50a,b), vesicles (Fig. 50c, d), and pores of hyaloclastite, and as patched irregular crystals on groundmass of lava. Most aragonite is irregularly shaped surrounded by calcite, which occurrences mean that these aragonites were partly (and probably fully in other cases) replaced by calcite along their margin and cracks. Zeolite- and/or prehnite-bearing greenstones (restrictively occurs in the mixed facies A of the Mikawa Unit) never contain aragonite. Except that case, aragonite is commonly contained in all units in the study area.

Lawsonite

Lawsonite occurs as euhedral, tiny rectangular crystals or aggregates of fan-shaped crystals. In the Futagawa Unit, lawsonite mainly occurs replacing plagioclase phenocrysts and microlites, and grown in veins and amigdules (Figs. 49a-d). In the Pirashuke Unit, lawsonite also occurs replacing glass (Figs. 50a, b) as common as the occurrences above. In both the Futagawa and Pirashuke Units, lawsonite occasionally coexists with quartz in veins.

Epidote group

Epidote occurs as granular crystals. They are commonly pale yellow-colored, showing high birefringence and weakly anomalous interference color. Rarely they show pale yellowish green to pale yellow pleochroism. Hence, some of them resemble to yellowish-colored sodic pyroxene. In this study, ones which show both positive and negative elongation is identified as epidote, distinguished from sodic pyroxenes (aegirine-augite to aegirine-jadeite) showing only negative elongation throughout. This identification is supported by selective EPMA analysis. Allanite is contained in several Na-amphibole schist samples. It is dark brown- colored, showing strong anomalous interference color. EPMA-analysis shows that it is poor in Ca than epidote, probably because of containing trace elements in place of Ca.

The epidote group is observed only in Pr-1 and Metadolerite Sub-units, with a few exceptions in the Pr-2 Sub-unit, the Futagawa Unit, and the Mikawa Unit. In the Pr-1 Sub-unit, epidote occurs in glassy matrix and in veins (Figs. 50c, d). In the Metadolerite Sub-unit, it also occurs replacing plagioclase.

Pumpellyite

Pumpellyite occurs as aggregates of microcrystals or fan-shaped crystals. They mainly occur in amigdules and veins, and replacing olivine, plagioclase and glass matrix (Figs. 49a, b and 50a-d). Color under plane-polarized light is variable: the most commonly with pale green to non-colored pleochroism; less commonly with non-colored (and no pleochroism); bluish green to non-colored and deep green to pale yellow pleochroism. Pumpellyite with yellow to pale-yellow pleochroism is also not rare in hematite-bearing assemblages. Selected EPMA analysis (Fig. 51) show that deep-green and yellow pumpellyites, observed in the Shizunai and Futagawa Units, are rich in FeO* up to 20 wt%, clearly classified as Fe-pumpellyite (Schiffman & Liou, 1983). Whereas pale-green and non-colored pumpellyites, occurring in all units, are poor in FeO* (<10 wt%) and rich in Al_2O_3, classified as Mg-Al pumpellyite.

Sodic pyroxene

Sodic pyroxenes are common in all units, except the zeolite- and/or prehnite-bearing greenstone bodies. There are several types in their occurrences.

One of the common occurrences is that sodic pyroxenes partly to fully replace igneous

Table 8. Representative major element compositions of metamorphic minerals in the Iwashimizu Complex. ab: albite, chl: chlorite, cr: crossite, f-act-hb: ferro-actinolitic-hornblende, m-rb: magnesio-riebeckite, qz: quartz, sub-act: subcalcic-actinolite. Nomenclature of amphiboles after Leake (1978). Jadeite component: Jd = 100 × (Al^{VI} - Al^{IV}), acmite component: Ac = 100 × (Na - Al^{VI} - Ti + Al^{IV}), augite component: Au = 100 - Jd -

mineral	pyroxene											amphibole					
unit	Sz	Sz	Ft	Ft	Pr2	Pr2	Pr1	Pr1	PrM	PrM	Mk	Sz	Ft	Pr2	Pr1	PrM	PrM
remarks	*+ab*	*+ab*	*+qz+ab*	*+qz+ab*	*+qz+ab*	*+ab*	*+qz+ab*	*+qz*	*+ab*	*+chl*	*+qz*	*m-rb*	*cr*	*cr*	*m-rb*	*sub-act*	*f-act-hb*
SiO_2	53.57	53.46	55.37	53.94	55.57	58.91	55.45	54.91	53.26	53.79	52.70	53.92	53.00	55.34	53.57	50.93	48.95
TiO_2	0.21	0.12	0.35	0.34	0.10	0.00	0.00	0.08	0.12	0.08	0.01	0.49	0.28	0.25	0.34	0.66	0.50
Al_2O_3	6.39	3.78	9.13	7.84	8.18	24.24	7.96	5.15	4.32	1.78	3.01	2.26	5.64	4.63	2.44	4.15	5.05
FeO*	19.18	17.22	17.71	18.76	20.51	0.73	19.68	22.02	19.42	7.16	22.23	25.36	23.91	20.97	22.18	19.43	20.21
MnO	0.14	1.10	0.11	0.42	0.06	0.08	0.06	0.07	0.12	0.16	0.14	0.17	0.52	0.10	0.10	0.19	0.24
MgO	2.98	5.05	1.65	1.83	0.39	0.29	1.15	0.96	3.72	12.58	2.66	6.81	6.39	8.14	9.36	10.77	10.75
CaO	5.05	9.76	2.61	4.48	0.68	0.44	1.45	1.66	7.40	20.58	6.52	1.10	1.00	0.49	1.43	7.73	11.04
Na_2O	11.15	8.26	12.56	10.97	14.21	14.94	12.79	12.90	10.35	2.60	10.32	6.84	5.94	7.13	6.85	3.37	1.02
K_2O	0.00	0.00	0.00	0.00	0.00	0.09	0.00	0.00	0.00	0.00	0.00	0.00	0.00	0.00	0.00	0.00	0.00
total	98.66	98.76	99.48	98.57	99.68	99.72	98.53	97.74	98.71	98.72	97.57	96.94	96.68	97.06	96.26	97.22	97.76
	O=6	O=6	O=6	O=6	O=6	O=6	O=6	O=6	O=6	O=6	O=6	O=23	O=23	O=23	O=23	O=23	O=23
Si	1.968	1.992	1.997	1.993	2.001	1.996	2.028	2.039	1.969	1.993	1.990	7.872	7.822	7.915	7.790	7.532	7.332
Ti	0.006	0.003	0.010	0.009	0.003	0.000	0.000	0.002	0.003	0.002	0.000	0.054	0.031	0.027	0.037	0.073	0.057
Al	0.277	0.166	0.388	0.341	0.347	0.968	0.343	0.225	0.188	0.078	0.134	0.389	0.982	0.781	0.418	0.724	0.892
Fe^{3+}	0.570	0.440	0.477	0.441	0.618	0.021	0.509	0.621	0.600	0.118	0.641	1.655	0.781	1.252	1.589	0.388	0.000
Fe^{2+}	0.019	0.096	0.057	0.139	0.000	0.000	0.093	0.063	0.000	0.104	0.061	1.440	2.169	1.256	1.108	2.014	2.532
Mn	0.004	0.035	0.003	0.013	0.002	0.002	0.002	0.002	0.004	0.005	0.004	0.021	0.065	0.012	0.012	0.023	0.031
Mg	0.163	0.280	0.089	0.101	0.021	0.014	0.063	0.053	0.205	0.695	0.150	1.481	1.406	1.735	2.028	2.374	2.401
Ca	0.199	0.390	0.101	0.178	0.026	0.016	0.057	0.066	0.293	0.818	0.264	0.171	0.158	0.075	0.222	1.227	1.774
Na	0.794	0.597	0.878	0.786	0.992	0.981	0.907	0.928	0.742	0.187	0.755	1.936	1.700	1.978	1.932	0.966	0.295
K	0.000	0.000	0.000	0.000	0.000	0.004	0.000	0.000	0.000	0.000	0.000	0.000	0.000	0.000	0.000	0.000	0.000
total	4.000	4.000	4.000	4.000	4.010	4.002	4.000	4.000	4.004	4.000	4.000	15.020	15.115	15.031	15.136	15.321	15.313
Jd	21.3	40.6	38.2	22.3	34.7	96.0	34.3	7.4	12.6	6.5	11.4	Mg#	0.5	0.4	0.6	0.6	0.5	0.5
Ac	57.6	44.4	48.7	45.0	64.3	2.2	56.4	70.1	61.3	12.0	64.1	XFe^{3+}	0.9	0.5	0.6	0.9	0.6	0.0
Au	21.1	15.0	13.1	32.6	1.0	1.8	9.3	22.5	26.1	81.5	24.5	Al^{IV}	6.3	7.2	6.7	6.4	7.6	8.0

Fe^{3+} in amphiboles are estimated as Fe^{3+} = Na + K - Al + 2Ti + Cr

mineral	pumpellyite							lawsonite					epidote			
unit	Sz	Sz	Ft	Ft	Pr1	Pr1	Mk	Sz	Ft	Ft	Pr2	Pr2	Pr1	Pr1	PrM	PrM
SiO_2	34.84	37.97	36.37	36.37	37.00	37.36	36.29	39.58	39.58	39.96	39.72	38.89	37.37	37.80	37.46	37.72
TiO_2	0.09	0.05	0.05	0.24	0.07	0.04	0.08	0.46	0.28	0.08	0.04	0.02	0.01	0.09	0.07	0.06
Al_2O_3	11.05	24.22	19.03	22.31	21.02	22.58	22.94	30.26	30.63	30.31	30.95	29.47	22.10	22.71	21.83	22.35
FeO*	21.22	4.97	11.81	6.02	8.28	6.31	7.50	2.02	1.33	2.07	1.74	2.94	13.20	12.64	13.82	12.61
MnO	0.25	0.64	0.59	0.37	0.26	0.17	0.17	0.15	0.00	0.04	0.01	0.02	0.36	1.16	0.11	0.10
MgO	1.75	3.07	1.84	2.88	2.53	3.06	1.52	0.03	0.02	0.05	0.00	0.02	0.04	0.04	0.00	0.04
CaO	20.80	21.21	20.96	20.82	21.79	21.81	22.49	15.76	16.37	16.10	16.45	16.31	22.21	21.19	23.17	22.85
Na_2O	0.06	0.18	0.09	0.19	0.09	0.09	0.14	0.00	0.02	0.13	0.00	0.00	0.00	0.00	0.02	0.04
K_2O	0.00	0.00	0.00	0.00	0.00	0.00	0.00	0.00	0.00	0.00	0.00	0.00	0.00	0.00	0.00	0.00
total	90.06	92.32	90.73	89.19	91.03	91.41	91.14	88.25	88.23	88.75	88.90	87.66	95.28	95.63	96.47	95.75
	O=24.5	O=24.5	O=24.5	O=24.5	O=24.5	O=24.5	O=24.5	O=8	O=8	O=8	O=8	O=8	O=12.5	O=12.5	O=12.5	O=12.5
Si	6.13	6.14	6.15	6.11	6.15	6.13	6.02	2.07	2.07	2.08	2.06	2.06	3.03	3.06	3.00	3.04
Ti	0.01	0.01	0.01	0.03	0.01	0.01	0.01	0.02	0.01	0.00	0.00	0.00	0.00	0.01	0.00	0.00
Al	2.29	4.62	3.79	4.42	4.12	4.37	4.48	1.87	1.89	1.86	1.89	1.84	2.11	2.16	2.06	2.12
Fe^{3+}	2.44	0.14	0.92	0.36	0.60	0.40	0.51	0.09	0.06	0.09	0.08	0.13	0.83	0.71	0.92	0.80
Fe^{2+}	0.68	0.53	0.75	0.49	0.55	0.47	0.54	---	---	---	---	---	0.07	0.14	0.00	0.04
Mn	0.04	0.09	0.08	0.05	0.04	0.02	0.02	0.01	0.00	0.00	0.00	0.00	0.02	0.08	0.01	0.01
Mg	0.46	0.74	0.46	0.72	0.63	0.75	0.38	0.00	0.00	0.00	0.00	0.00	0.01	0.00	0.00	0.01
Ca	3.93	3.68	3.80	3.75	3.88	3.84	4.00	0.88	0.92	0.90	0.92	0.93	1.93	1.84	1.99	1.97
Na	0.02	0.06	0.03	0.06	0.03	0.03	0.05	0.00	0.00	0.01	0.00	0.00	0.00	0.00	0.00	0.01
K	0.00	0.00	0.00	0.00	0.00	0.00	0.00	0.00	0.00	0.00	0.00	0.00	0.00	0.00	0.00	0.00
total	16.00	16.00	16.00	16.00	16.00	16.00	16.00	4.94	4.95	4.95	4.95	4.96	8.00	8.00	8.00	8.00

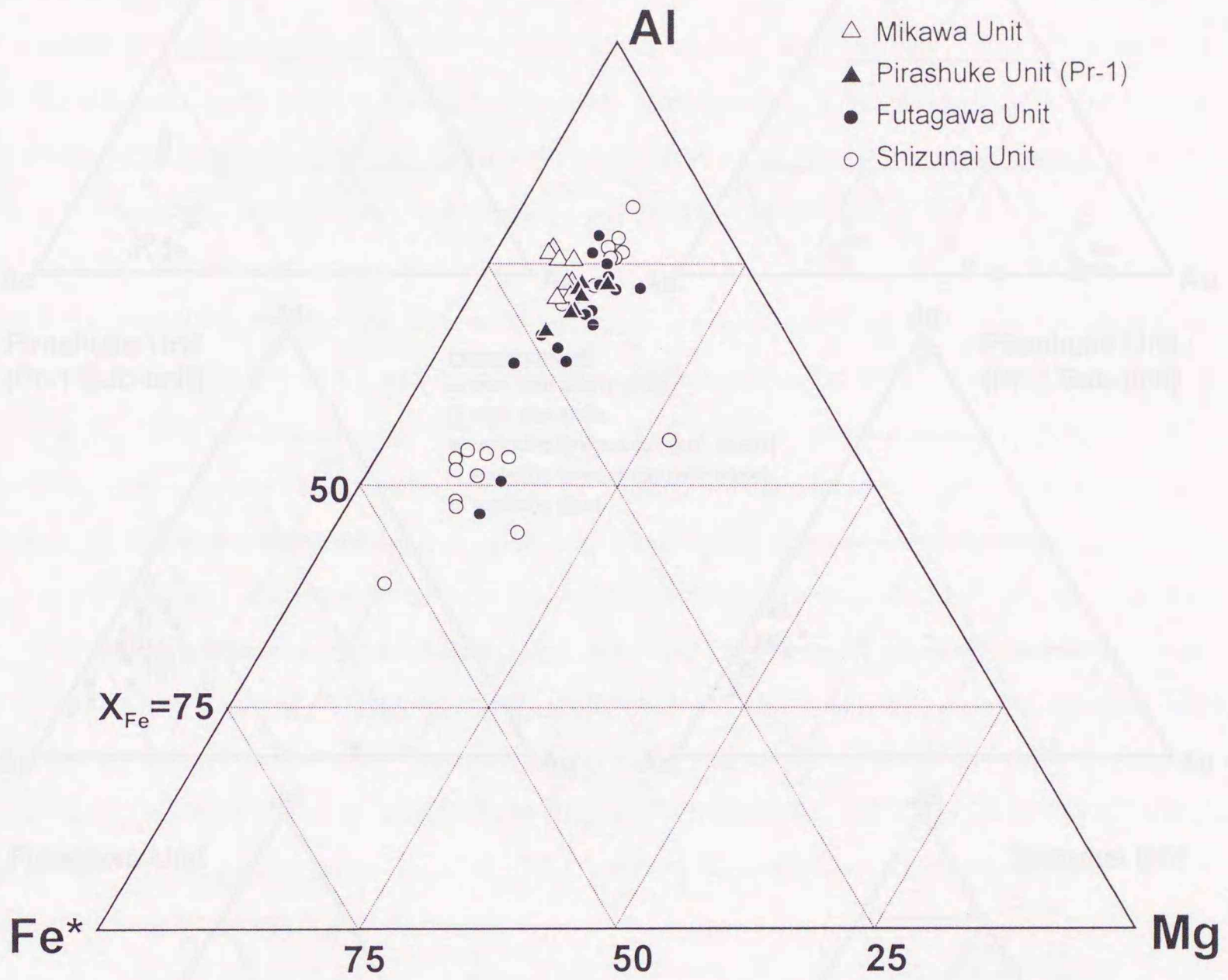


Fig. 51. Chemical composition of pumpellyite in selected metabasite samples of the Iwashimizu Complex.

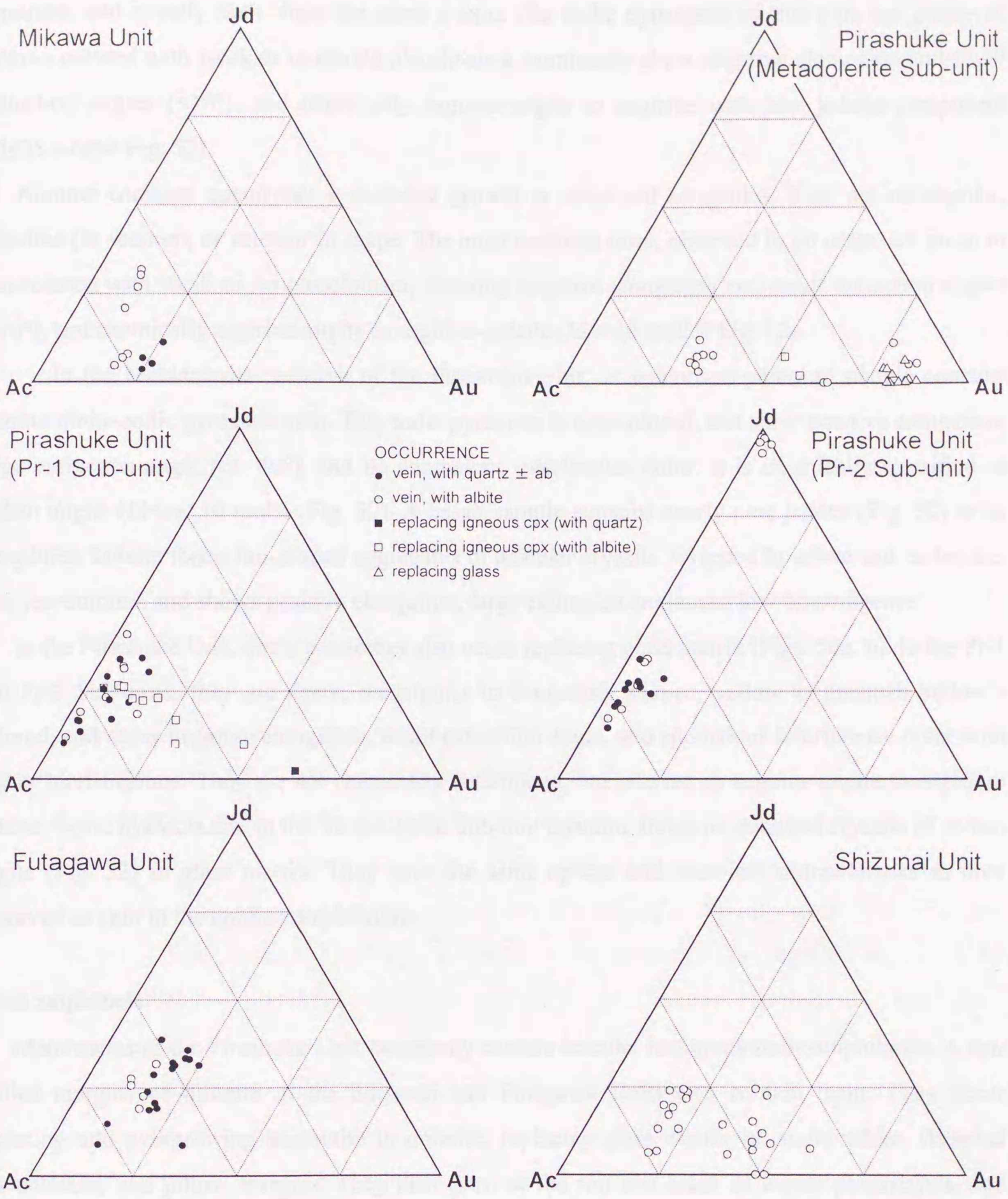


Fig. 52. Chemical composition of metamorphic sodic pyroxenes in the Iwashimizu Complex.

clinopyroxenes (augite and aegirine), dominantly irregularly replace along rim and crack of igneous pyroxene, and usually both share the same c-axis. The sodic pyroxenes of this type are green- or yellow- colored with weak to moderate pleochroism, commonly show negative elongation and small extinction angles (<10°), and chemically aegirine-augite to aegirine with low jadeite component (Jd<25 mol%: Fig. 52).

Another common occurrence is euhedral growth in veins and amigdules. They are rectangular, lobe-like (in section), or acicular in shape. The most common ones, observed in all units, are green to non-colored with weak to no pleochroism, showing negative elongation and small extinction angles (<10°), and chemically aegirine-augite to aegirine-jadeite (Jd < 40 mol%: Fig. 52).

In the Metadolerite Sub-unit of the Pirashuke Unit, an epidote-amphibolite sample contains epidote-albite-sodic pyroxene vein. This sodic pyroxene is non-colored, and show positive elongation, large extinction angle (ca. 40°), and no anomalous interference color. It is chemically classified as sodian augite (Jd<ca. 10 mol%: Fig. 52). A basalt sample contains nearly pure jadeite (Fig. 52) in its amigdules. Jadeite forms fan-shaped aggregates of acicular crystals, wrapped by albite and carbonate. It is non-colored, and shows positive elongation, large extinction angle, and low birefringence.

In the Pirashuke Unit, sodic pyroxenes also occur replacing glass matrix (Figs. 50a, b). In the Pr-1 and Pr-2 Sub-units, they are dusty, rectangular to irregularly shaped, yellow to greenish yellow - colored, and show negative elongation, small extinction angle, and anomalous interference color with higher birefringence. They are not chemically determined, but inferred as aegirine-augite to aegirine-jadeite. Some hyaloclastite in the Metadolerite Sub-unit contains abundant euhedral crystals of sodian augite (Fig. 52) in glass matrix. They have the same optical and chemical characteristics as ones observed as vein in the epidote amphibolite.

Sodic amphibole

Metabasites in the Pirashuke Unit commonly contain acicular to fibrous sodic amphiboles. A few chilled margins of dolerite in the Shizunai and Futagawa Units also contain them. They occur replacing and overgrowing kaersutite in dolerite, replacing glass matrix of mafic schist, flattened hyaloclastite, and pillow margins. They also grow at the rim and crack of augite phenocrysts, and rarely observed in veins.

Most sodic amphiboles show both positive and negative elongation in each thin section, and samples containing amphiboles with thoroughly negative elongation are also seen. Both show blue to violet or purple pleochroism, and strong anomalous interference color. Chemically determined crystals were mostly magnesio-riebeckite (and riebeckite). A sample from the Futagawa Unit contains crossite.

Actinolite

Actinolite occurs only in the Pirashuke Unit (mainly in Pr-1 and Metadolerite Sub-unit). It forms acicular to fibrous crystals. These crystals are non-colored to very weakly green-colored, grown over relict augite or rarely in glass matrix of hyaloclastite. Some of analyzed actinolite in the Metadolerite Sub-unit is sub-calico.

Hornblende

Hornblende only occurs in the Metadolerite Sub-unit. Two modes of occurrence are observed: one is bluish green hornblende in epidote amphibolite, and the other is pale brownish green hornblende (to actinolitic hornblende) partly replacing igneous augite. The latter ones are partly replaced by sodic amphibole.

Relict augite

Relict augite is common in all units. There are some tendencies in occurrence of relict augite.

(1) Metabasites with abundant hematite occasionally contain sodic pyroxene, and tend not to contain relict augite except large-size phenocrysts. Whereas metabasites containing relict augite commonly contain sodic pyroxene and/or pumpellyite, and tend not to contain hematite. The tendency suggests that augites were oxidized until either augite or hematite was consumed up in the metamorphic conditions. For reference, the relict augite + hematite assemblage is common in the Idonnappu Zone, where sodic pyroxene never occurs.

(2) Metabasites containing lawsonite and/or epidote tend scarcely to contain relict augites. Relict augites favor to contact with sodic pyroxene, pumpellyite, sodic amphibole, actinolite, and chlorite. Whereas they tend not to contact with lawsonite nor epidote, except in the Metadolerite Sub-Unit where they commonly contact with epidote. The tendency suggests that augite could selectively survive in relatively Al-poor rocks. Probably they either fully decomposed, or were not initially contained, in aluminous rocks or part of rocks enough to produce lawsonite and/or epidote, except in the Metadolerite Sub-unit (epidote commonly contact with relict augite in the Idonnappu Zone).

These tendencies suggest that the occurrence of relict augite is controlled by local paragenesis under each metamorphic condition. Probably, common occurrence of pumpellyite + sodic pyroxene + chlorite assemblage obstructs the existence of both relict augite + hematite and relict augite + lawsonite/epidote, as displayed in Fig. 53. Probably because sodic pyroxene was unstable in the Idonnappu Zone, such assemblages could be common.

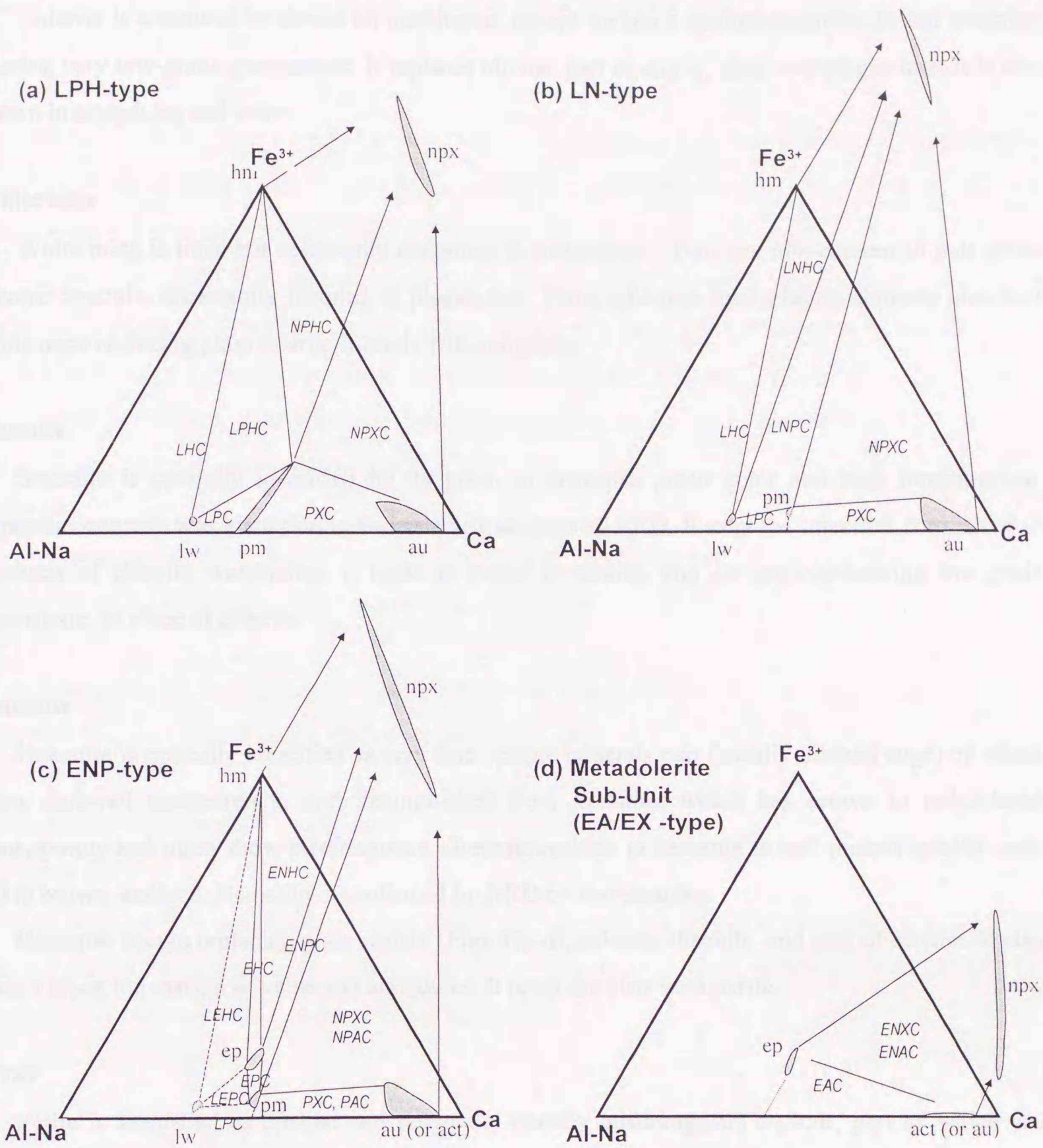


Fig. 53. Fe^{3+} - (Al-Na) - Ca diagrams explaining occurrences of major metamorphic minerals (except sodic amphibole) in metabasites of the Iwashimizu Complex. All assemblages contain chlorite + albite ± quartz : each plot can be roughly approximated as Fe^{3+} - (Al-Na) - Ca - Fe^{2+}+Mg tetrahedron projected from the chlorite-side. Shadows indicate the analyzed compositional ranges. lw & L: lawsonite, pm & P: pumpellyite, hm & H: hematite, npx & N: sodic pyroxene, ep & E: epidote, au & X: relict augite, act & A: actinolite, and C: chlorite.

Chlorite

Chlorite is contained in almost all metabasite, except for some epidote-amphibolite and smectite-bearing very low-grade greenstones. It replaces olivine, part of augite, glass and plagioclase. It is also grown in amigdules and veins.

White mica

White mica is trace but commonly contained in metabasites. They are non-colored to pale-green colored crystals, dominantly forming in plagioclase. Some schistose hyaloclastite contains abundant white mica replacing glass matrix. It rarely fills amigdules.

Smectite

Smectite is optically identified by its green to brownish green color and high birefringence. Saponitic smectite was identified in two selected samples by XRD. Except the smectites considered as products of chlorite weathering, it tends to occur in zeolite- and /or prehnite-bearing low-grade greenstone, in place of chlorite.

Hematite

Hematite is optically identified as very fine opaque minerals part (usually thinned edge) of which show dark-red transparency, and distinguished from limonite, which has brown to red-colored transparency and often show birefringence. Greenstones rich in hematite is also mesoscopically dark red to brown -colored. Hematite is confirmed by XRD on two samples.

Hematite occurs replacing glass matrix (Figs 49a-d), acicular ilmenite, and part of olivine. It also occurs along the margin of veins and amigdules. It never coexists with pyrite.

Pyrite

Pyrite is identified as opaque and polygonal (mostly quadrangular) crystals, part of which are confirmed by reflective microscope observation. It commonly occurs in veins, and more rarely in glass matrix.

Quartz

Quartz mainly occurs in vein and amigdules. It rarely occurs replacing olivine and clinopyroxene phenocrysts with chlorite, pumpellyite, and sodic pyroxene. It is difficult to distinguish fine-grained quartz from albite, because it cannot be decided whether optically uniaxial or biaxial.

Albite

The most common occurrence of albite is to replace igneous plagioclase. Such albite crystals are seen almost all the sample, except some zeolite-facies rocks in which Ca-rich plagioclase is preserved.

Albite is distinguished from plagioclase richer in Ca by small extinction angle (5-10°) and lower refractive index (than quartz). Albite also occurs in veins and amigdules.

Analcime and other zeolites

Analcime restrictively occurs in several greenstone bodies in the mixed facies A. It is optically identified by its low refractive index and almost no birefringence. It occurs filling veins, occasionally showing euhedral polyhedral shape. Most of analcime-bearing samples also contain albitized plagioclase, and are scarcely accompanied by quartz.

Nakano (1981) reported analcime which wraps jadeite, both grown in vesicles of greenstones in the Pirashuke Unit. Such occurrence has not been observed in the examined samples, by this study.

In the analcime-bearing greenstone bodies in the Mikawa Unit, some unidentifiable fine-grained felsic minerals inferred as zeolite, partly replacing plagioclase, are rarely observed. A XRD analysis detected natrolite peaks from one of these rocks.

Prehnite

Prehnite occurs in the greenstone bodies containing analcime. Prehnite occurs tabular to blocky crystals filling veins, occasionally together with analcime.

Garnet

Garnet is observed in one picritic sample from the Pirashuke Unit. It is granular shaped, showing slight birefringence, hence is considered as Ca-garnet.

Mineral assemblages in each unit

1. Shizunai Unit

Ten samples from the Shunbetsu River area, neighboring north from the study area, are added for examination on the Shizunai Unit. Observed assemblages are as follows (+ ab + ti ± qz ± arg ± wm; numbers in parenthesis indicate number of samples):

①lw + chl + hm (1)

②pm + npx + chl + hm (2)

③pm + npx + chl ± py (2)

④pm + npx + rb + chl + hm (1)

⑤pm + npx + rb + chl (1)

⑥pm + chl + hm (1)

⑦pm + chl ± py (2)

⑧npx + chl + hm (1)

⑨npx + chl (2)

⑩stp + chl + hm (3)

⑪stp + chl + lim (py?) (1)

⑫ chl + hm (21)

⑬ chl ± py (10) total: n=48 samples

Most samples of the dominant assemblages ⑫ and ⑬ contain carbonate, hence, it is inferred that Ca-Al silicates tend to be unstable in the Shizunai Unit. The rest assemblages suggest that the pumpellyite + hematite is stable, and lawsonite is also stable. The characteristics are common with the metabasites in the Futagawa Unit described below, however, lawsonite is far less common (found in only one sample) in the Shizunai Unit. These can thus be grouped as "PH-type". Sodic pyroxene occurring as vein minerals, which does not coexist with quartz, contain jadeite component ranging 0 to 25 mol% (Fig. 52).

2. Futagawa Unit

The metamorphic mineral assemblage typical in the Futagawa Unit is lawsonite + pumpellyite + chlorite + hematite, with albite, titanite, quartz and aragonite. Mineral assemblages observed in this unit are listed as follows (+ ab + ti ± qz ± arg ± wm; numbers in parenthesis indicate number of samples):

① lw + chl + hm (11)

② lw + chl ± py (4)

③ lw + pm + chl + hm (10)

④ lw + pm + chl ± py (3)

⑤ pm + npx + chl ± py (4)

⑥ pm + npx + chl + hm (2)

⑦ pm + chl ± py (3)

⑧ pm + chl + hm (2)

⑨ pm + npx + rb + chl + py? (1)

⑩ npx + rb + chl (1)

⑪ npx + chl + hm (1)

⑫ npx + chl ± py (4)

⑬ chl ±py (9)

⑭ chl + hm (20)

⑮ lw + pm + npx + chl + hm (3)

⑯ lw + pm + npx + chl ± py (5)

⑰ lw + pm + rb + chl + py (1)

⑱ ep + pm + npx + rb + chl + py? (1) total: n=85 samples

In assemblages ⑮ and ⑯, either lawsonite or sodic pyroxene is rarely contained, and generally both do not coexist. Lawsonite never coexist with sodic amphibole in ⑰. Therefore, it is possible to

consider that these assemblages are mix of the other assemblages sector by sector in single section. Assemblages ⑮-⑯ are rather common in the Pirashuke Unit, therefore, it is also possible that they are of transitional type. Based on the assumptions of these exception, and with additional exception of chlorite + carbonate assemblages (⑬ and ⑭) which may be strongly controlled by fCO_2, the rest assemblages are comprehensive under Al_2O_3 - CaO - RO (FeO + MgO) - Fe_2O_3 system with excess albite, quartz, and white mica, and simply displayed in Fig. 53a. The characteristic of the Futagawa Unit is the existence of pumpellyite - hematite join, and the absence of lawsonite + sodic pyroxene join, with common occurrence of lawsonite and aragonite. Thus, the assemblages are herein grouped as "LPH -type".

Sodic pyroxenes which occur in veins with quartz show jadeite contents ranging 8 to 38 mol% (Fig. 52).

3. Pirashuke Unit

Pr-2 Sub-unit:

The metamorphic mineral assemblage typical in the Pr-2 Sub-unit is lawsonite + sodic pyroxene + pumpellyite + chlorite, with albite, titanite, quartz and aragonite. Mineral assemblages observed in this unit are listed as follows (+ ab + ti ± qz ± arg ± wm; numbers in parenthesis indicate number of samples):

① lw + chl + hm (2)
② lw + pm + chl + py (1)
③ lw + npx + chl + hm (4)
④ lw + npx + chl ± py (9)
⑤ lw + pm + npx + chl ± py (10)
⑥ lw + pm + npx + chl + hm (1)
⑦ lw + npx + rb + chl + py (4)
⑧ lw + pm + npx + rb + chl + py (2)
⑨ pm + npx + chl ± py (7)
⑩ pm + npx + rb + chl ± py (7)
⑪ npx + rb + chl + hm (2)
⑫ npx + rb + chl ± py (5)
⑬ pm + rb + chl ± py (2)
⑭ npx + chl + hm (3)
⑮ npx + chl ± py (5)
⑯ pm + chl + py (1)
⑰ rb + chl + hm (1)

⑱ rb + chl ± py (2)

⑲ chl + hm (1)

⑳ chl ± py (3)

21 ep + lw + pm + npx + chl + py (1)

22 ep + pm + npx + rb + chl + py (1)

23 act + gar + chl + py (1) total: n=75 samples

The epidote-bearing assemblages 21 and 22 are rather common in the Pr-1 Sub-unit, hence are considered as transitional samples to the Pr-1 Sub-unit. One of the characteristics of the Pr-2 Sub-unit is the absence of pumpellyite + hematite -bearing assemblage, except one sample showing ⑥ in which hematite occur as vein. Another characteristic is the common occurrence of lawsonite + sodic pyroxene -bearing assemblages ③-⑧. In addition, a few samples containing lawsonite + sodic amphibole are also seen (⑦ and ⑧). These characteristics may be explained on the FAC plot (Fig. 53b), in which the lawsonite - sodic pyroxene join exists in place of the pumpellyite-hematite join. Thus, the association can be grouped as "LN-type".

Sodic pyroxenes which occur in veins with quartz show jadeite contents ranging 15 to 35 mol% (Fig. 52). A sample contains nearly pure jadeite which grew in amigdules, wrapped in albite and carbonate.

Pr-1 Sub-unit

The characteristic of this sub-unit is the occurrence of epidote-bearing assemblages. Mineral assemblages observed in this unit are listed as follows (+ ab + ti ± qz ± arg ± wm; numbers in parenthesis indicate number of samples):

① lw + npx + chl + hm (1)

② lw + npx + chl ± py (5)

③ lw + pm + npx + chl + hm (1)

④ lw + pm + npx + chl ± py (8)

⑤ lw + pm + npx + rb + chl (1)

⑥ lw + npx + rb + chl (1)

⑦ ep + lw + pm + npx + chl + hm (1)

⑧ ep + lw + npx + rb + chl + py (1)

⑨ ep + lw + pm + npx + chl (1)

⑩ ep + lw + pm + chl + py (1)

⑪ lw + chl + py (1)

⑫ ep + pm + chl + py (2)

⑬ ep + npx + chl + hm (2)

⑭ ep + npx + chl ± py (4)

⑮ ep + npx + rb + chl (1)

⑯ ep + pm + npx + rb + act + chl + py (1)

⑰ ep + pm + npx + rb + chl + py (1)

⑱ ep + pm + act + chl + py (1)

⑲ ep + chl + py (4)

⑳ all + npx + chl (1)

21 all + rb + chl (1)

22 all + chl + hm (1)

23 pm + chl + py (5)

24 pm + npx + chl + py (4)

25 pm + npx + rb + chl ± py (4)

26 pm + rb + chl ± py (2)

27 pm + rb + act + chl + py (1)

28 npx + chl + hm (1)

29 npx + chl ± py (5)

30 npx + rb + act + chl (1)

31 npx + rb + chl ± py (5)

32 rb + chl ± py (7)

33 act + chl + py (1)

34 chl + hm (8)

35 chl ± hm (6)

total: n=91 samples

Assemblages ① to ⑥ are common with the LN-type metabasites in the Pr-2 Sub-unit, characterized by the lawsonite + sodic pyroxene pair. Assemblages ⑦ to ⑩ and ⑫ to ⑲ are characterized by the occurrence of epidote, most of which co-occur with sodic pyroxene and/or pumpellyite. The assemblages (⑪ to 35) which does not contain lawsonite + sodic pyroxene pair may be roughly explained in Fig. 53c, in which the epidote-hematite join, the epidote-sodic pyroxene join, and the epidote-pumpellyite join exist, whereas the lawsonite-sodic pyroxene join and the pumpellyite-hematite join are absent. Thus, these assemblages can be grouped as "ENP-type". However, more local and detailed description will be needed because relation between sodic amphibole and other minerals has not been explained.

Sodic pyroxenes which occur in veins with quartz show jadeite contents ranging 11 to 34 mol% (Fig. 52). Sodic pyroxenes replacing igneous augite show relatively low jadeite contents ranging 2 to 19 mol%.

Metadolerite Sub-unit

No sample in this sub-unit contains aragonite.

①ep + hb ± act ± chl (7)

②ep + pm + npx + act + hb + chl + py (1)

③ep + pm + npx + chl + py (1)

④ep + pm + chl (1)

⑤ep + pm + act + chl + py (1)

⑥ep + npx + chl + py (9)

⑦ep + npx + act ± hb + chl ± py (3)

⑧ep + act + chl + py? (2)

⑨npx + act + chl + py (1)

⑩npx + chl ± py (2)

⑪act + chl ± py (4) total: n=25

Epidote is common in the Metadolerite Sub-unit. The assemblage ① is composed dominantly of epidote + albite + bluish-green hornblende, with/without retrogressive actinolite, thus showing an epidote-amphibolite assemblage. These epidote-amphibolites occur only as floated blocks in Holocene landslide debris in the study area. Nakano (1981), however, reported epidote-amphibolite from north extension of the sub-unit.

The assemblages ② to ⑤ contain epidote + pumpellyite ± sodic pyroxene, identical to the EN-type. The assemblages ⑦ and ⑧ contain epidote + actinolite without pumpellyite. They suggest that both pumpellyite-sodic pyroxene and pumpellyite-chlorite joins are absent (Fig. 53d), which are the characteristic of the greenschist facies (here termed as EA-type). The assemblages ⑥ and ⑨-⑪ can be identified as EN-type. However, epidote commonly contact with relict augite in the assemblage ⑨, unlike in the Pr-1 Sub-unit. Hence, it is also possible to consider ⑨ as a variation of the pumpellyite-free, greenschist facies (temporarily termed as "EX"-type), if relict augite is treated as a metastable Al-poor, Ca-Fe-Mg bearing phase in place of actinolite (Fig. 53).

Sodic pyroxenes occurring in this sub-unit usually do not coexist with quartz. Analyzed pyroxenes are sodian augite to aegirine augite with low jadeite contents ranging 0 to 12 mol% (Fig. 52).

4. Mikawa Unit

Greenstones of the Mikawa Unit are divided into two major groups. The LST greenstones contain zeolite and/or prehnite, and never contain aragonite. The OIB greenstones contain aragonite, lawsonite, sodic pyroxene etc.

LST type

Mineral assemblages observed in this type are listed as follows (± ti ± cc ± wm; numbers in parenthesis indicate number of samples):

① anc ± ab + smc/chl ± py (3)

② anc + pm + ab + smc ± chl ± py (3)

③ anc + nat + pm + ab + smc/chl (1)

④ anc + prh ± ab + smc ± chl + py (4)

⑤ prh ± ab + smc + py (2)

⑥ prh + pm + ab + smc + chl? + py (1)

⑦ pm + qz + ab + smc (1) total: n=15 samples

Common occurrences of prehnite and the absence of any high-pressure type minerals suggest that they were metamorphosed under low-pressure conditions, *i.e.* the zeolite facies to prehnite-pumpellyite facies. Thus, they can be grouped as "Z-type". Analcime + quartz assemblage has not been observed in the examined thin sections. However, there are three samples in which plagioclase is not albitized, hence some are possibly metamorphosed under lower temperature than the stability field of albite (Thompson, 1971).

OIB type

①ep + pm + chl + py (1)

②ep + pm + npx + py (2)

③lw + npx + chl (1)

④lw + pm + chl (1)

⑤lw + chl + py (1)

⑥lw + pm + chl + hm (1)

⑦pm + npx + chl + hm (1)

⑧pm + npx + chl ± py (6)

⑨pm + npx + rb + chl ± py (2)

⑩pm + chl + hm (1)

⑪pm + chl ± py (9)

⑫npx + chl + hm (2)

⑬stp + py (1)

⑭chl + hm (11)

⑮chl ± py (11) total: n=51 samples

Among these assemblages, ① and ② contain epidote, which is the characteristic of the ENP-

type greenstone. The assemblages ③ to ⑥ contain lawsonite, and ③ shows lawsonite + sodic pyroxene + pumpellyite (LN-type), and ⑥ shows lawsonite + pumpellyite + hematite(LPH-type). The assemblages ⑦ and ⑩ contain pumpellyite + hematite, also identical to the LPN-type. The rest assemblages (relatively poor in Al or high variant) are common in all of EN, LN, and LPH types.

Sodic pyroxenes occurring in veins contain jadeite contents ranging 4 to 32 mol%, however, ones coexisting quarts show relatively low jadeite contents (4-11 mol%; Fig. 52).

Metamorphic condition

Metamorphic mineral assemblages in metabasites of the Iwashimizu Complex are classified as major LPH, LN, EN -types, with minor epidote - calcic amphibole assemblages such as greenschist (EA-type) and epidote-amphibolite. Though detailed paragenetic analysis reflecting mineral chemistry in the Iwashimizu Complex has not been achieved on the three major types, they are consistent with paragenetic study on the Mariana Forearc by Maekawa et al. (1995: Fig. 54). Based on his analysis, the epidote-free LPH assemblage occurs in the low-temperature and low-pressure side in the pressure-temperature space relative to the other assemblages, because the assemblage can only exist between the univariant lines (E) and (N). The epidote-free LN assemblage can exist between the univariant lines (E) and (P) if saturated with chlorite, hence occupies the low-temperature and high-pressure side. The ENP-type at the high-temperature side, between the univariant lines (N) and (P). Thus, it is suggested that the Shizunai and Futagawa Units were metamorphosed under lower temperature and lower pressure condition than the Pirashuke Unit.

This application is consistent with analyzed chemical compositions of pumpellyite and sodic pyroxene. The Shizunai and Futagawa Units contain Fe-rich pumpellyite, suggesting a low-temperature condition (Schiffman and Liou, 1983). Sodic pyroxenes of the Shizunai Unit contain less jadeite component (though they do not coexist with quartz) than other units, suggesting lower pressure condition (Popp and Gilbert, 1972) than other units.

The jadeite-poor sodic pyroxenes, though which do not coexist with quartz, implies that much metabasites of the Metadolerite Sub-unit were metamorphosed under higher temperature (and also possibly lower pressure) conditions than the Pr-1 and Pr-2 Sub-units. Absence of aragonite, and the existence of the EA, EX and epidote-amphibolite assemblages without pumpellyite support this interpretation.

Based on above discussion, the metamorphic condition of each unit can be roughly estimated as displayed in Fig. 55.

1. Shizunai Unit

The coexistence of jadeite-poor (Jd<25 mol%) pyroxenes and aragonite is only allowed by very low-temperature and medium-pressure condition (<200℃ and <5kb). The condition is restricted

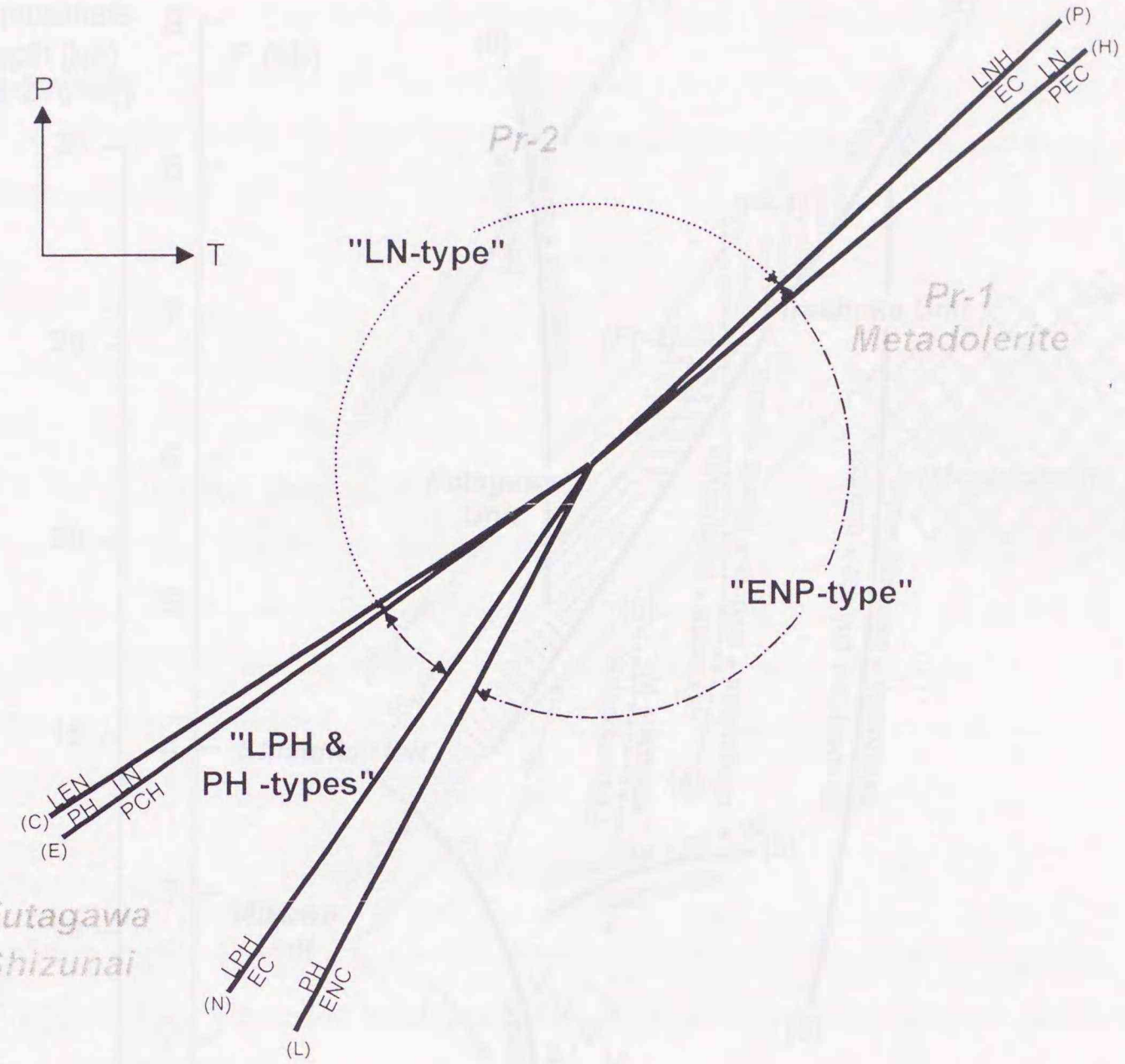


Fig. 54. Metamorphic mineral assemblages applied to the Schreinemakers' bundle for six-phase equilibrium system by Maekawa et al. (1995) L: lawsonite, C: chlorite, N: Na-pyroxene, E: epidote, H: hematite, P: pumpellyite.

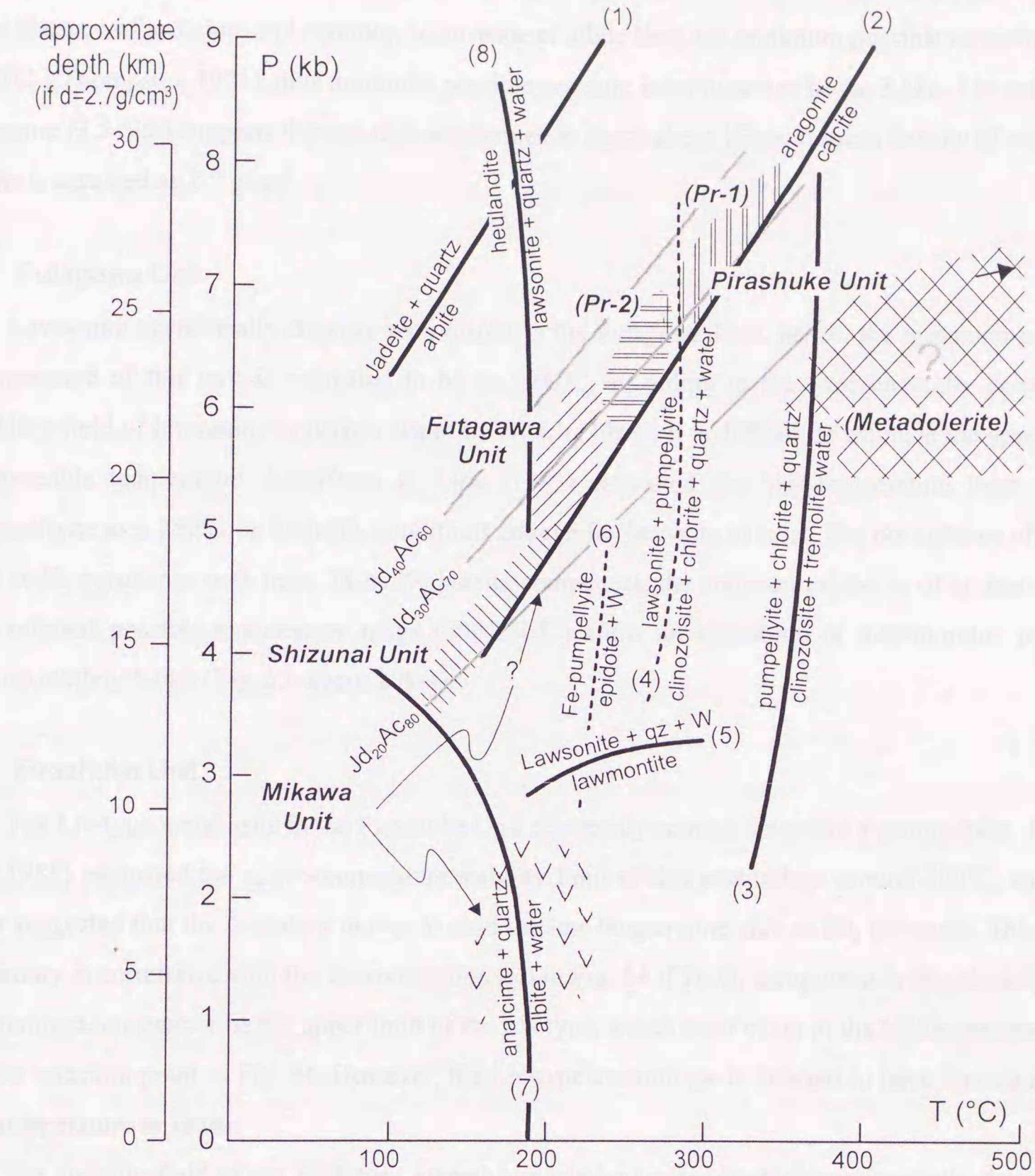


Fig. 55. Inferred P-T conditions for the units / sub-units in the Iwashimizu Complex. Solid lines: determined by experimental studies; dashed lines: estimated by natural paragenesis. References : (1) Popp & Gilbert (1972), (2) Johannes & Puchan (1971), (3) Nitsch (1971), (4) Liou et al. (1985), (5) Liou (1971), (6) Schiffman & Liou (1983), (7) Thompson (1971), (8) Nitsch (1968). Jadeite isopleths: calculated by the method after Popp & Gilbert (1972).

between the stability field of aragonite (Johannes & Puhan, 1971) and the jadeite-acmite isopleth calculated by the method after Popp and Gilbert (1972), as discussed in Maruyama and Liou (1985). The absence of analcime and common occurrence of albite limit the minimum possible temperature as 100℃ (Thompson, 1971), thus minimum possible pressure is estimated to be ca. 3.5kb. The estimated pressure (3.5-5kb) suggests that the unit was formed at depth about 15km, if mean density of overlying units is assumed as 2.7 g/cm^3.

2. Futagawa Unit

Lawsonite occasionally coexists with quartz in the Futagawa Unit, hence, the minimum possible temperature of this unit is estimated to be ca. 200℃, according to the experimentally determined stability field of lawsonite + quartz + water by Nitsch (1968). It is difficult to estimate the upper limit of possible temperature. Schiffman & Liou (1983) estimated the high-temperature limit of Fe-pumpellyite as ≤ 250℃ in high-fO_2 conditions enough for hematite to exist. The coexistence of quartz and sodic pyroxenes with max. 38 mol% jadeite component, the common existence of aragonite, and the inferred possible temperature range (200-250℃) allow an estimation of metamorphic pressure approximately 5-6kb (Fig. 55; about 20km).

3. Pirashuke Unit

The LN-type metabasite in the Pirashuke Unit commonly contain lawsonite + pumpellyite. Liou et al. (1985) estimated the upper-temperature stability limit of this assemblage around 300℃, and they also suggested that the boundary moves toward the low-temperature side as fO_2 increases. This phase boundary is correlative with the univariant line (N) in Fig. 54 if Fe_2O_3 component is introduced. Thus, the temperature cannot be the upper limit of the LN-type, which must occur at the higher-pressure side of the invariant point in Fig. 54. However, the LN-type assemblage is inferred to have formed around the temperature or lower.

The stability field of the ENP-type assemblage can be limited by the experimentally determined stability limit of pumpellyite by Nitsch (1971: about 350℃). Sodic pyroxene (Jd=ca.35) and aragonite cannot coexist at higher temperature than about this phase boundary. The low-temperature limit of the ENP-type assemblage can be determined by the univariant line (N) in Fig. 54, thus correlative with the phase boundary (4) in Fig. 55 (300℃ or lower). The lower temperature limit of epidote (Schiffman and Liou, 1983; boundary (4) in Fig. 55) may also help the restriction.

The Pr-1 and Pr-2 Sub-units are thus inferred to have been metamorphosed at the temperature ranging about 250-350℃. Probably, the LN-type formed at lower temperature than ca. 300℃, and the ENP-type higher than that. To take the coexistence of sodic pyroxene (Jd=ca.35) and aragonite into account, the depth where the Pr-1 and Pr-2 Sub-units were formed is inferred to be 7-8kb and 6-7kb,

respectively (Fig. 55).

It is difficult to estimate metamorphic condition of the Metadolerite Sub-unit. EA-type (greenschist) and epidote-amphibolite were formed at higher temperature than the stability limit of pumpellyite (ca. 350℃: Nitsch, 1971; boundary (3) in Fig. 55). Much of the rest metabasites are also pumpellyite free (EX-type), possibly formed at higher temperature of the limit as greenschist. Jadeite-poor sodic pyroxenes (Jd<12 mol%) imply relatively lower P/T conditions as high-pressure intermediate series.

4. Mikawa Unit

The LST greenstones never contain aragonite, lawsonite, sodic pyroxene, and other high-P/T type minerals. This Z-type characteristic suggests that the greenstones were metamorphosed at pressure lower than both aragonite/calcite boundary (Johannes and Puhan, 1971) and the lower-pressure stability limit of lawsonite + quartz + water determined by Liou (1971). They are thus considered to have been metamorphosed at lower pressure than ca. 3kb (Fig. 55). This condition is notably lower than the other metabasites in the Iwashimizu Complex.

The rest OIB greenstones commonly contain aragonite. Most of them seem to be PH- or LPH-type assemblages without obvious deformation. The low jadeite contents in sodic pyroxene suggest that the metamorphic condition of them is correlative with that of the Shizunai Unit. A few greenstones containing epidote or lawsonite + sodic pyroxene imply a possibility that a small amount of higher-grade rocks are also mixed.

Discussion

Origin of constituent lithofacies

Both OIA and OIT -type greenstones (together as OIB-type), the main constituent of the Iwashimizu Complex, are interpreted to originate oceanic intra-plate seamounts. Common occurrence of pillow lava, hyaloclastite, intercalation of chert and limestone, all support this interpretation. The absence of any terrigenous clastic rocks or even particles within coherent greenstone sequence also indicates that the basalts erupted in a pelagic circumstance. These greenstones were cut by faults and shear zones to be tectonic slices, suffered the high-P/T type metamorphism, and now comprises a part of continental crust of Hokkaido. Therefore, the occurrences are best explained that the OIB -type basalts erupted within oceanic crust, then subducted beneath the continental margin to the mid- to lower crustal level, tectonically sliced and accreted to the continental margin, and finally exhumed to the earth's surface. Greenstones are variably deformed, depending on metamorphic grade and original position, to be non-deformed or schistose greenstone facies, or greenstone lenses/layers in the mixed

Table 9. Summary of characteristics of units in the Iwashimizu Complex. The units are arranged in accordance with tectonostratigraphic order (see Fig. 30), except the Naizawa Complex for reference. Bold lines: major fault.

unit / sub-unit		constituent lithologic facies	fossil age of mudstone	greenstone chemistry	metamorphic type	inferred original depth
Mikawa		mixed facies A non-deformed greenstone	late Valanginian - Hauterivian	OIA > OIT >> LST	Z, PH / LPH (+LN, ENP?)	15-20 km? & <10 km
Pirashuke	Metadolerite	metadolerite	?	LST (+OIB?)	ENP, EA / EX, >> ep-amp	20-25 km???
	Pr-1	schistose greenstone mixed facies C	?	OIA > OIT >> LST	LN, ENP	25-30 km
	Pr-2	schistose greenstone mixed facies B	?	OIA (+OIT?)	LN	20-25 km
Futagawa		non-deformed greenstone mixed facies B	Early Cretaceous	OIT > OIA	LPH (>>LN)	~ 20 km
Shizunai		non-deformed greenstone clastic facies chert / tuffaceous mudstone	late Valanginian - Hauterivian	OIA	PH	~ 15km
(Naizawa Complex)		non-deformed LST (B-Unit) mixed facies (MN-Unit)	late Valanginian - early Barremian	LST>OIA (>>OIT?)	Z, pp	<10 km

facies B, or mafic schists in the mixed facies C.

The chert-tuffaceous mudstone facies and the clastic facies occur as sheet bodies in the Shizunai Unit, alternating with greenstone slices. Some of them comprise greenstone - chert - tuffaceous mudstone - clastic rocks sedimentary succession, as first reported by Hori & Sakakibara (1994), showing typical oceanic crust to trench-fill sequence ranging late Triassic to Early Cretaceous. Along the Pisenai and Penkemoshiyoshi Creeks, the chert-clastic sequence overlies an alternation of chert and OIA-type dolerite, intercalating hyaloclastite. Therefore, these sedimentary rocks are considered to have deposited on and around the seamounts.

The mixed facies B is also composed of greenstone, chert, tuffaceous mudstone, and clastic sedimentary rocks. Though they completely lost their original sedimentary sequence because of severe shearing, the same constituent lithofacies as the greenstone-chert-clastic sequence suggests that they originally comprised oceanic crust - trench-fill sequences. Mafic schist and metachert of the mixed facies C may also originate from seamounts and covering sediments.

The LST-type greenstone bodies in the Pirashuke and Mikawa Units are inconsistent with the interpretation discussed above, because of their depleted chemical features. These chemical characteristics are common with the Lower Sorachi Group. Unlike the OIB-type greenstones, the LST-type ones are not accompanied by typical oceanic sediments such as red chert nor pelagic limestone as the Lower Sorachi Group are not. Therefore, it is considered that the LST-type greenstones originate from the Lower Sorachi Group, which structurally overlies the Kamuikotan Metabasites in the northern Kamuikotan Zone.

Inner structure of a seamount collision-type accretionary complex

As described in the former sections, and according to the preliminary mapping in northern extension of the study area (Fig. 27), the most fundamental structure of the Iwashimizu Complex is the slab-stack structure. There is no difference in metamorphic grade between the slices in a single unit (or sub-unit; Fig. 48). The structure thus suggests that the subducted seamounts were tectonically sliced and stacked by thrusts, forming the units at each depth.

These units, each of which formed individual depth, are in fault contact to form the pile-nappe structure. From the Shizunai Unit to the Pirashuke Unit, metamorphic grade (and inferred metamorphic pressure) increases structurally upward bounded by the unit-boundary faults (Summarized in Table 9). Because original sedimentary structures all face normally, the pile-nappe structure displays an inverted arrangement of metamorphic grade. Thus the unit-boundary faults,

which divide the Shizunai, Futagawa, and Pirashuke Units are of reverse type: the higher-grade units overlie the lower-grade units by the faults. This type of thrust structure can only be achieved with contemporaneous unroofing in the hanging wall unit, because without the unroofing, the underthrust unit must have suffered equal to or higher pressure metamorphism than the hanging wall. There may be another notable point: if we consider the seamount accretion occurred as underplating, the inverted arrangement of metamorphic grade suggests that the depth of underplating decreased gradually. Hence, it is possible to consider that the Futagawa Unit underplated the already exhuming Pirashuke Unit (formed at 25-30km depth) at the depth of ca. 20km; The Shizunai Unit underplated both the exhuming Futagawa and Pirashuke Units, at ca. 15km depth. According to this interpretation, the underplated seamount slices immediately turned up to be exhumed.

Metamorphic grade of the Mikawa Unit, is evidently lower than the structurally underlying Pr-1 and Metadolerite Sub-units (Pirashuke Unit). The dominant assemblage in the Mikawa Unit is the PH and LPH types, and zeolite/prehnite-bearing (Z-type) greenstones are also contained. Hence bounded by the Mikawa / Pirashuke unit-boundary fault, the low-grade (PH-type) greenstones structurally overlie the high-grade (ENP-type to epidote-amphibolite) rocks. Along a branch of Pirashuke River, a low-pressure Z-type greenstone of the Mikawa Unit is in fault contact with a ENP-type greenstone of the Pr-1 Sub-Unit. Thus, there is a pressure gap up to 3-4 kb across the unit-boundary fault between the Mikawa and Pirashuke Units. Geometrically, there may be two possible ways to produce this type of fault: one is normal faulting, by which a low-grade rocks can relatively slip down over a high-grade rocks; the other is thrust faulting cutting tilted units, by which a low-grade rocks can be laterally displaced to overlie a high-grade rocks (Ring et al., 1999). More information is needed to determine the nature and origin of this fault. However, this boundary fault seems to be the most likely candidate which contributed unroofing of the Pirashuke Unit, because it is the only known fault in this area, which implies a large vertical displacement with normal sense.

Mode of seamount accretion

1. Shizunai Unit

According to the examination on metamorphism, the depth where Shizunai Unit was formed is roughly estimated as ca. 15 km. In this unit, slices composed of chert, tuffaceous mudstone, and clastic rocks occur as internally near-coherent slices. They alternate with OIB-type greenstone slices bounded by faults and impassable shear zones. Therefore, both the subducted seamounts and covering sediments were sliced, and tectonically stacked together bounded by inter-slice faults or thin shear zones.

2. Futagawa Unit

The Futagawa Unit is inferred to have formed at depth of ca. 20 km. In this unit, chert, tuffaceous mudstone, and siliciclastic rocks were dissected and sheared to be mappable shear zones (mixed facies B), which divide internally coherent and non-deformed greenstone slices. The occurrence indicate that the sedimentary rocks, which originally covered the subducting seamount, could not keep its sedimentary sequence, and wholly acted as shear zone for greenstone slices to be stacked. There may be two reasons for the difference in occurrences of sedimentary rocks between the Futagawa and Shizunai Units:

- Difference in degree of strain. Strain may be accumulated internally as sediments succeed to subduct. Hence, for instance, the sediments of the Futagawa Unit, which subducted to the deeper level, lost their original sequence more than those of the Shizunai Unit. However, it may be difficult to quantify the degree of strain in rocks with numerous slip surfaces.
- Difference in physical property of sediments by subduction depth. The layered mixed fabric of sheared mudstone and greenstone in the Futagawa Unit indicates that there was a little (or no) competency contrast between the two lithofacies. This fabric suggest that mudstone had been consolidated enough to break and pulverize greenstones. If such consolidation was achieved by increasing crystallinity of phyllosilicates as subduction depth increased, initial thin shear zone could propagate to the entire thickness of the sediments. In the Shizunai Unit, such mappable thick shear zone is absent, and the mudstone / greenstone layered mixed rocks are very thin and rare. This means that strain was kept constricted to the immappable thin zone at shallower depth. Detailed deformation structure and mica crystallinity should be described to test the idea.

3. Pirashuke Unit

The Pirashuke Unit is considered to have formed at the depth of ca. 25 km (Pr-2 Sub-Unit) to up to 30 km (Pr-1 Sub-unit). It is regarded as a tectonic pile of schistose greenstone slices and inter-slice shear zones (mixed facies B and C), part of which display a duplex-like distribution (Fig. 32).

In the Pr-2 Sub-unit, the constituent lithofacies are similar to the Futagawa Unit, *i.e.* greenstone slices (schistose greenstone facies) and inter-slice sheared sediments (mixed facies B), except that greenstones show ductile deformation such as flattening and stretching accompanied by recrystallization. The difference in deformation style suggest that the brittle-ductile transition of greenstones was placed between the Pirashuke and Futagawa Units, presumably at depth of 20-25 km (around 6kb) and at temperature of around 250℃. Greenstone slices kept their internal cohesion in spite of the ductile deformation, whereas no original sedimentary sequence was kept in the inter-slice mixed facies. Therefore, it is considered that major strain was still relatively concentrated to the mixed facies, in which numerous slip surfaces still existed. It is inferred that the phase transition from the

LPH-type assemblage to the LN-type assemblage caused the reduction in resistance against the stress, and greenstones thus began to deform ductile. However, the ductile deformation carried by recrystallization might be able to reduce a part of the stress only by a slow strain rate in such low-temperature condition. Thus, a large part of the strain may have concentrated within the inter-slice shear zones, which contain numerous slip surfaces.

The Pr-1 Sub-unit characteristically lacks terrigenous siliciclastic sedimentary rocks. The absence can be explained if clastic sediments did not deposited around the protolith seamount of the Pr-1 sub-unit. This idea, however, has a problem that this sub-unit lacks not only coarse clastic sediments but also hemipelagic mudstone such as varicolored shale or tuffaceous siliceous mudstone. Subducting oceanic plates are commonly covered by either hemipelagic mudstone or terrigenous turbidite in the recent trenches, and chert never crops out on the surface of subducting oceanic plate. Therefore the alternative explanation is more easily considered: all clastic sediments, which might have cover the greenstone and chert, had been accreted out until the oceanic plate subducted to the depth over 25km. Only greenstone and a small amount of chert could reach to the depth. This option suggest a progressive accretion by depth: much of clastics were accreted at shallower level of subduction zone, and hardly able to reach the lower crustal level; the relative abundance of accreted mafic rocks thus increased in proportion to depth.

The Pr-1 Sub-unit also characteristically contain small serpentinite bodies in the inter-slice mixed facies C. Microscopically observed samples are originally dunite containing euhedral chromian spinels, which suggest them as cumulate. Olivines were entirely replaced mainly by antigorite. Because no gabbroic rock is contained in the sub-unit, it is difficult to consider that the serpentinite bodies were derived from oceanic plate. Another interpretation is that the serpentinite bodies were derived from wedge mantle, which possibly comprised the hanging wall at the depth where greenstones of the Pr-1 sub-unit were accreted. If a duplex of sliced oceanic basalt was formed between underthrusting oceanic crust and hanging wall wedge mantle, tectonic fragment of serpentinite can be dragged within its ramp faults. The limited occurrence of serpentinite in the inter-slice mixed facies C supports the idea. Similar style in emplacement of serpentinite has been proposed by Maekawa (引用).

Hyaloclastite schists in the Metadolerite Sub-unit are considered to originate from subducted seamounts as in the other sub-units. However, metadolerites and epidote amphibolites, which are the major constituent of this sub-unit, are considered to originate from the Lower Sorachi Group in terms of their depleted LST-type chemical composition, not from subducted seamount. They suffered high-pressure part of the pumpellyite-actinolite facies to epidote-amphibolite facies metamorphism, thus are considered to have subducted to the depth up to 30 km, as the OIB-type metabasites in the Pirashuke Unit. They are considered as fragments of the upper-plate ophiolite, tectonically eroded by the collision between subducting seamount and forearc, as ones in the Naizawa Complex. These

fragments were dragged to the lower crustal level as the seamount subducts. The LST-type greenstone also rarely occur in the mixed facies C in the Pr-1 Sub-unit, suggesting that some of the fragments were dragged into the duplex of accreted seamount slices.

4. Mikawa Unit

The Mikawa Unit does not show typical slab-stack structure unlike other units in the Iwashimizu Complex. The non-deformed greenstone slices are of OIB-type, thus simply originates from subducted seamount.

The mixed facies A contains both high-P metamorphosed (aragonite-bearing) OIB greenstones and low-P type (zeolite and/or prehnite-bearing) LST greenstones. This occurrence indicates that the origin of the unit cannot be explained by a simple subduction model. It suggests a process in which the high-P greenstone exhumed and mixed with the low-P ones at shallow structural level (*i.e.* the zeolite facies condition). These LST-type greenstones are considered to originate from the Lower Sorachi Group based on chemistry. However, the mode of their emplacement may be quite different from those in the Pirashuke Unit and the Naizawa Complex (B-Unit), because the LST greenstones did not subducted to the depth where OIB greenstones were metamorphosed. The Lower Sorachi Group is considered to have lain at base of the forearc basin Nitarachi-Yezo Sequence, as discussed in the former chapter. If the Iwashimizu Complex exhumed in the forearc basin, it may be possible to have occurred that the exhumed high-P rocks and the overlying low-P ophiolite mixed. Chert blocks in the mixed facies A are recrystallized seemingly compatible to the high-P type OIB greenstones. However, sandstone and tuffaceous mudstone are very weakly consolidated compared to those in other units, and rather resembles to the Nitarachi-Yezo Sequence. Hence, I speculate that the sandstone and mudstone of the mixed facies A may originate from the forearc basin sequence as the LST greenstones, not from trench-fill deposits. Metamorphic examination on these sediments will be needed to test the interpretation.

Correlation with the northern Kamuikotan Zone

In the northern Kamuikotan Zone, greenstones dominantly occur in Horokanai area as blueschists (Shibakusa, 1989), and in Biei area as low-grade metabasalts (Unit C: Kawamura et al., 1998). Sakakibara & Ota (1994) suggested that these metabasite units (Horokanai and Biei Units, respectively) structurally overlie the pelitic schist -dominant units (Pankehoronai Unit; Unit A of Kawamura et al., 1998). These metabasites consist mainly of OIA, and intercalate smaller amount of chert, siliciclastic rocks, and depleted tholeiitic greenstone (Maekawa, 1983, 1986; Kawamura et al., 1998; Sakakibara et al., 1999).

Metabasites of the Horokanai Unit suffered the lawsonite-blueschist and epidote-blueschist facies

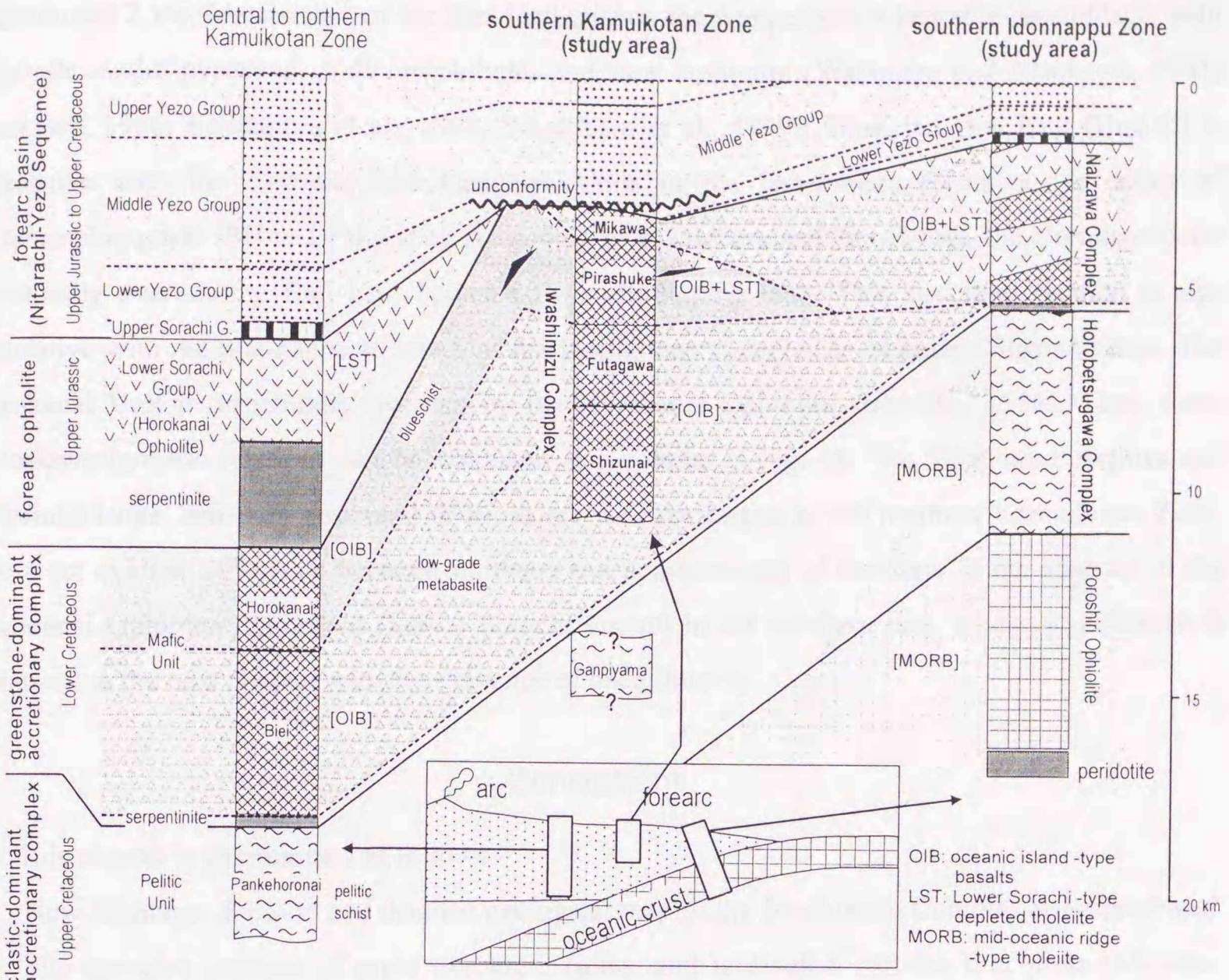


Fig. 56. Comparison of tectonostratigraphic columns of the southern Idonnappu Zone and the southern Kamuikotan Zone with that of the northern Kamuikotan Zone, and reconstruction of the Cretaceous forearc system in central Hokkaido. Reference data: Igi et al. (1958); Ishizuka (1980, 1981), Miyashita (1983); Sakai and Kanie (1986); Wada et al. (1992); Sakakibara and Ota (1994); Kawamura et al. (1998, in press); Sakakibara et al. (1999); and this study.

metamorphism (Shibakusa, 1989), thus correlative with the Pirashuke Unit in the southern Kamuikotan Zone. Metabasites of the Biei Unit contain the pumpellyite + hematite assemblage, with aragonite, sodic pyroxene, sodic amphibole, and rare lawsonite (Watanabe and Maekawa, 1985; Maekawa, 1986; Kawamura et al., 1998; Sakakibara et al., 1999). Thus, the Biei Unit (Unit C) is correlative with the Shizunai and Futagawa Units in the Iwashimizu Complex., in terms of metamorphic grade (PH to LPH -type). According to Sakakibara and Ota (1994), the Horokanai Unit structurally overlies the Biei Unit bounded by north-dipping fault. This structural relation is also correlative with the pile-nappe structure of the Iwashimizu Complex in Mitsuishi-Shizunai area. The Horokanai Unit is structurally overlain by the Horokanai Ophiolite (Ishizuka, 1980). Thus, these tectonostratigraphic relations can be expressed as a column in Fig. 56. The Shizunai, Futagawa and Pirashuke Units, and their structural relations are well correlative to the northern Kamuikotan Zone. The most evident difference between northern and southern part of the zone is the absence of the Horokanai Ophiolite equivalent (Lower Sorachi Group) in the southern part, whose significance is discussed in the next chapter with the existence of unconformity.

Conclusions

This chapter is summarized as follows

(a) New lithologic division and detailed geological map of the Iwashimizu Complex were presented. The complex consists of eight lithologic facies, and is divided into the four units (Shizunai, Futagawa, Pirashuke, and Mikawa Units), based on unique assemblages of the lithologic facies.

(b) Each unit represents tectonic stack of greenstone slices of presumably Triassic to Jurassic, intercalating sheared mixed facies ± Triassic to Lower Cretaceous sedimentary slices.

(c) The four units, bounded by faults, comprised a pile-nappe as a whole, and were bent by later folds.

(d) Greenstones are dominantly of oceanic island -type (OIB) alkali basalt and tholeiite. A small amount of depleted tholeiite showing the common characteristics with the Lower Sorachi Group (Lower Sorachi -type: LST) is also contained in the Pirashuke and Mikawa Units.

(e) A relation between lithologic unit division and metamorphic grade of greenstones is described, which helps to estimate the accretion depth of each unit. Greenstones of the Iwashimizu Complex are metamorphosed at estimated depth ranging ca. 15 km (Shizunai Unit) to 25-30km (Pirashuke Unit).

(f) The pile-nappe structure display an inverted arrangement of metamorphic grade, and at the upper structural horizon, metamorphic grade decreases upward with a gap. These structures are considered to have formed by contemporaneous thrusting and unroofing in the Iwashimizu

Complex.

(g) Modes of occurrence of constituent lithofacies are different by units, which is considered reflecting the difference in accreted depth. Weakly deformed sedimentary slices were stacked along with greenstone slices at shallower level (ca. 15 km); greenstone slices intercalate thin and severely sheared clastic rocks at medium level (20-25 km); and any terrigenous rock is absent, and serpentinite occur between deformed greenstone slices at deepest level observable (25-30 km).

(h) The Iwashimizu Complex is correlative with the metabasites of the Horokanai and Biei areas in the northern Kamuikotan Zone. Age and lithologic assemblage suggest that both the Iwashimizu Complex and the Naizawa Complex were originally parts of the single Lower Cretaceous accretionary body: deep part and shallow part, respectively.

Chapter IV. Yezo Supergroup in the Mitsuishi area: Blueschist-bearing fluvial conglomerate and unconformity in the Cretaceous forearc sequence

Introduction

Inner trench slope tectonically acts sensitively in response to the change of tectonic conditions in subduction zone, such as development of accretionary body, tectonic erosion, and collision / subduction of seamounts and oceanic plateaus. It is expected that forearc basin sequence has recorded the change in its stratigraphic succession.

In central Hokkaido, mid-Cretaceous (Albian) unconformity has been recognized in the forearc basin sequence of the Yezo Supergroup since Hashimoto (1936), and called "Intra-Yezo (*Naka-Yezo*) Disturbance" (Inoma, 1969). The event is considered implying the uplift of high-P/T metamorphic rocks in the Kamuikotan Zone (Kiminami *et al.*, 1978). However, poor evidence has obstructed characterization of the exhumation process, and some recent studies (Motoyama *et al.*, 1991; Takashima *et al.*, 1997a, b; Takashima and Nishi, 1999) denied existence of the unconformity.

This chapter reports fluvial conglomerate in the mid-Cretaceous forearc basin strata unconformably overlying the Early Cretaceous high-P/T metamorphosed accretionary complex in the Mitsuishi River district, southern Kamuikotan Zone. The conglomerate consists dominantly of greenstone clasts, some of which contain high-P/T metamorphic minerals. The unconformity is signified as a record of rapid exhumation of the high-P/T metamorphosed accretionary complex (Iwashimizu Complex) in response to the subduction condition of oceanic plate.

Stratigraphy of the Nitarachi-Yezo Sequence

The Nitarachi-Yezo Sequence of the Mitsuishi River area occurs separately in the south area (routes C to F: Fig. 57) and north area (routes A and B). The south area is located in the middle reaches of the Mitsuishi River to the Sakubai River, extending to the Urakawa district in the southeast. The sequence of the north area is isolated in the eastern slope of the Pirashuke River.

The sequence of the south area is monoclinic, showing a wedge-shaped distribution. It comprises the Nitarachi Formation (Upper Sorachi Group), the Tsukenai Formation (Lower Yezo Group), and the Utafue Formation (Middle Yezo Group) of Sakai and Kanie (1986). The sequence of the north area comprises sandstone of the Utafue Formation, showing a small-scale syncline.

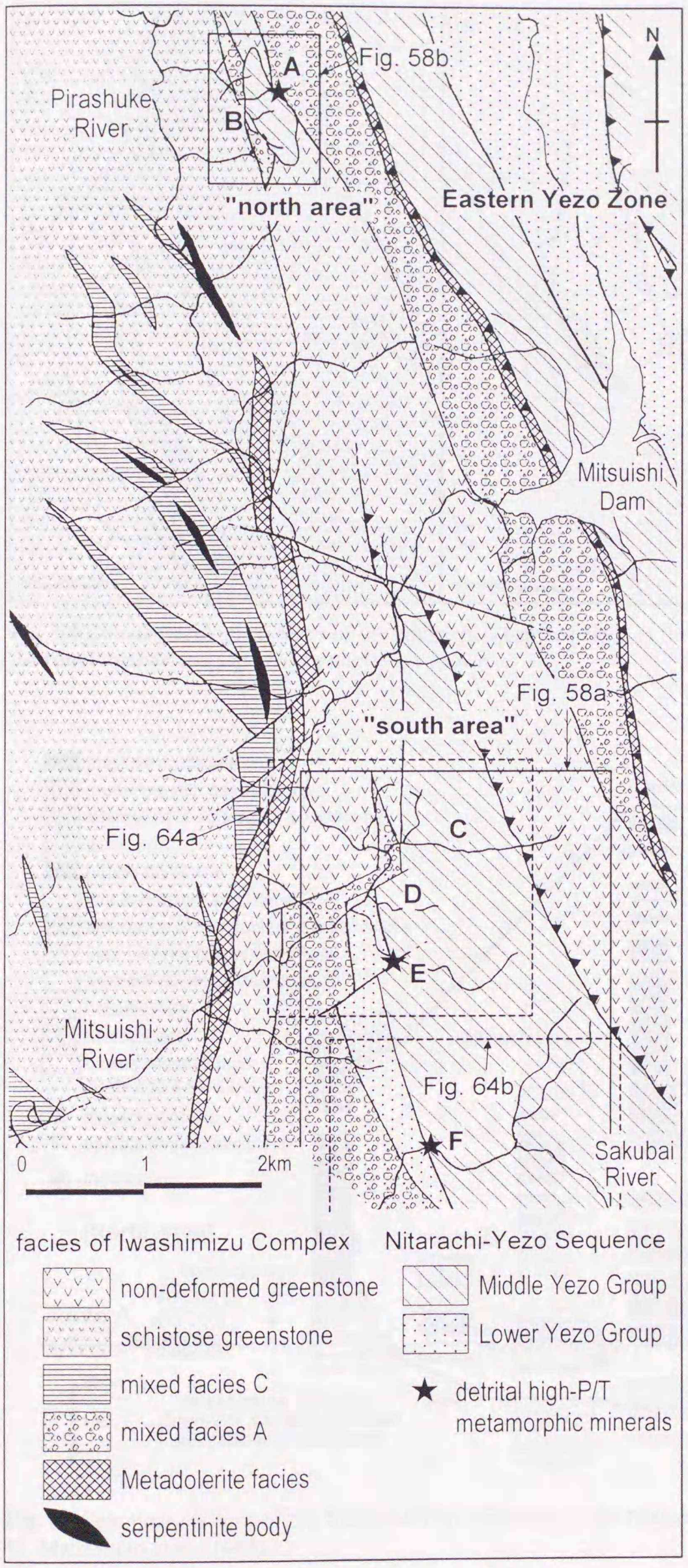


Fig. 57. Geologic map of the eastern marginal part of the southern Kamuikotan Zone in the Mitsuishi River area. Facies of the Iwashimizu Complex correspond to those of Table 1. A-F: routes of which columnar sections are shown in Fig. 59.

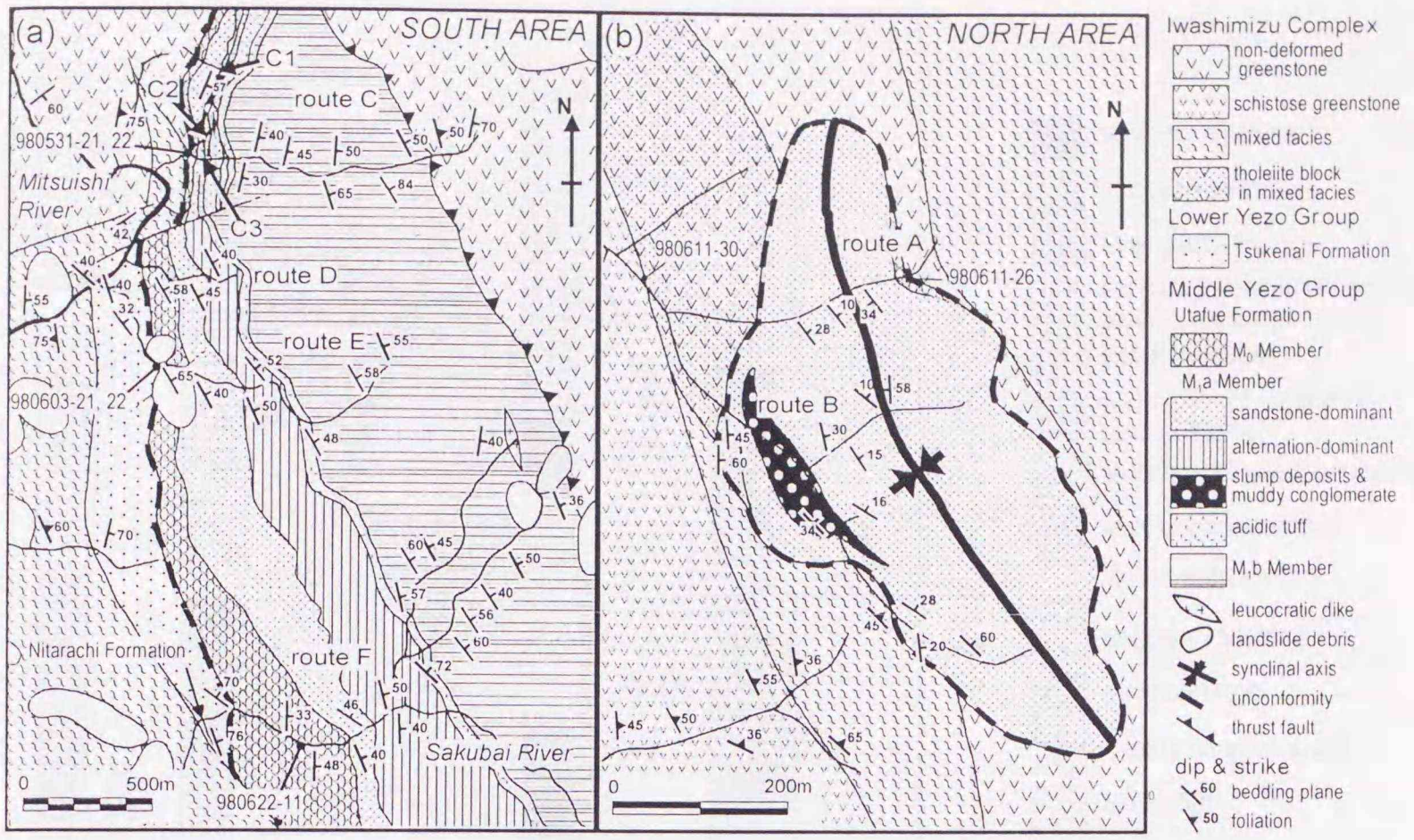


Fig. 58 Detailed geological maps of the Nitarachi-Yezo Sequence in the south and north areas. Localities of the conglomerate and sandstone samples are shown.

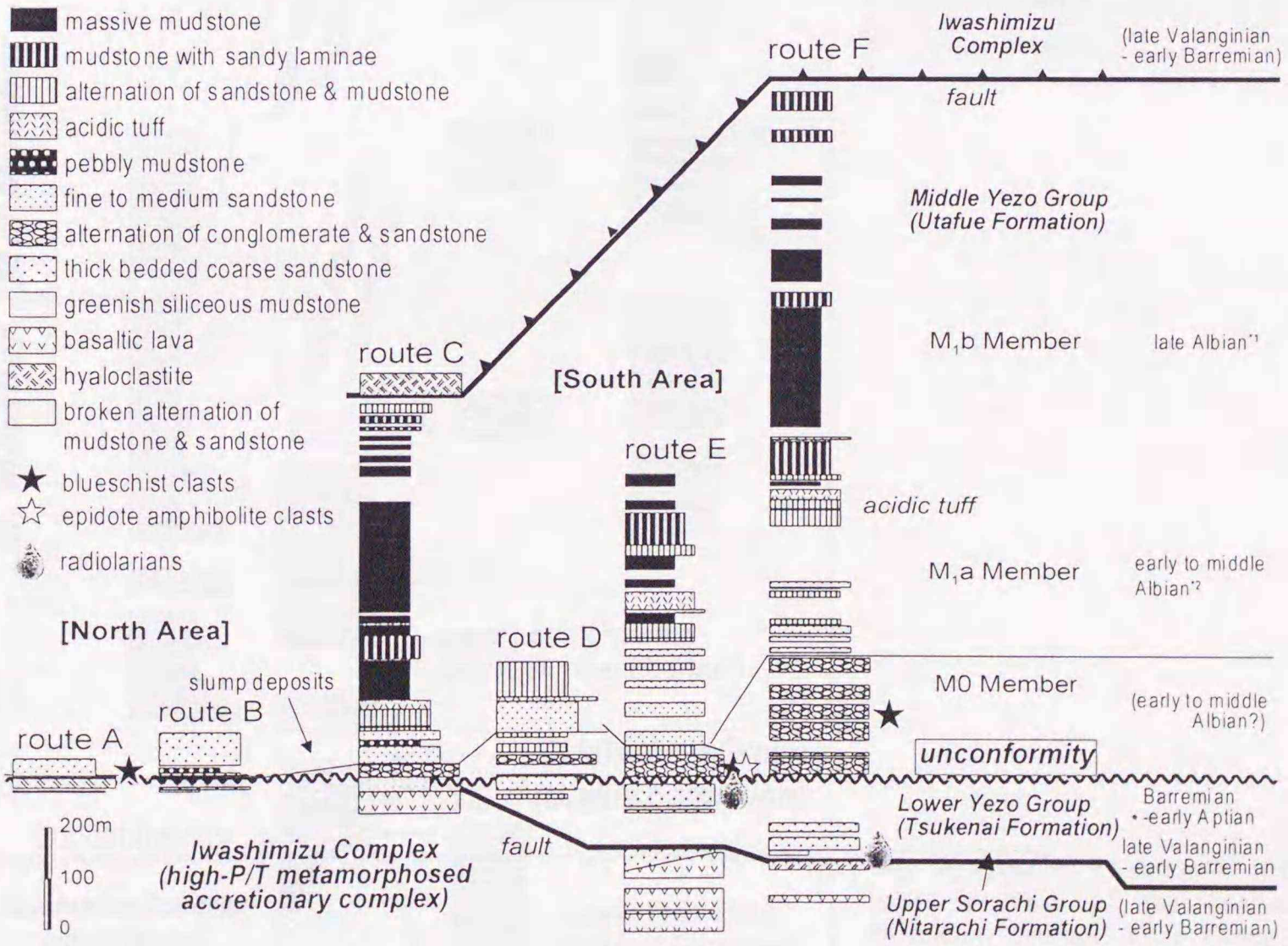


Fig. 59 Columnar sections of the Nitarachi-Yezo Sequence in the Mitsuishi River area. *1: Taketani (1982), *2: Matsumoto et al. (1984).

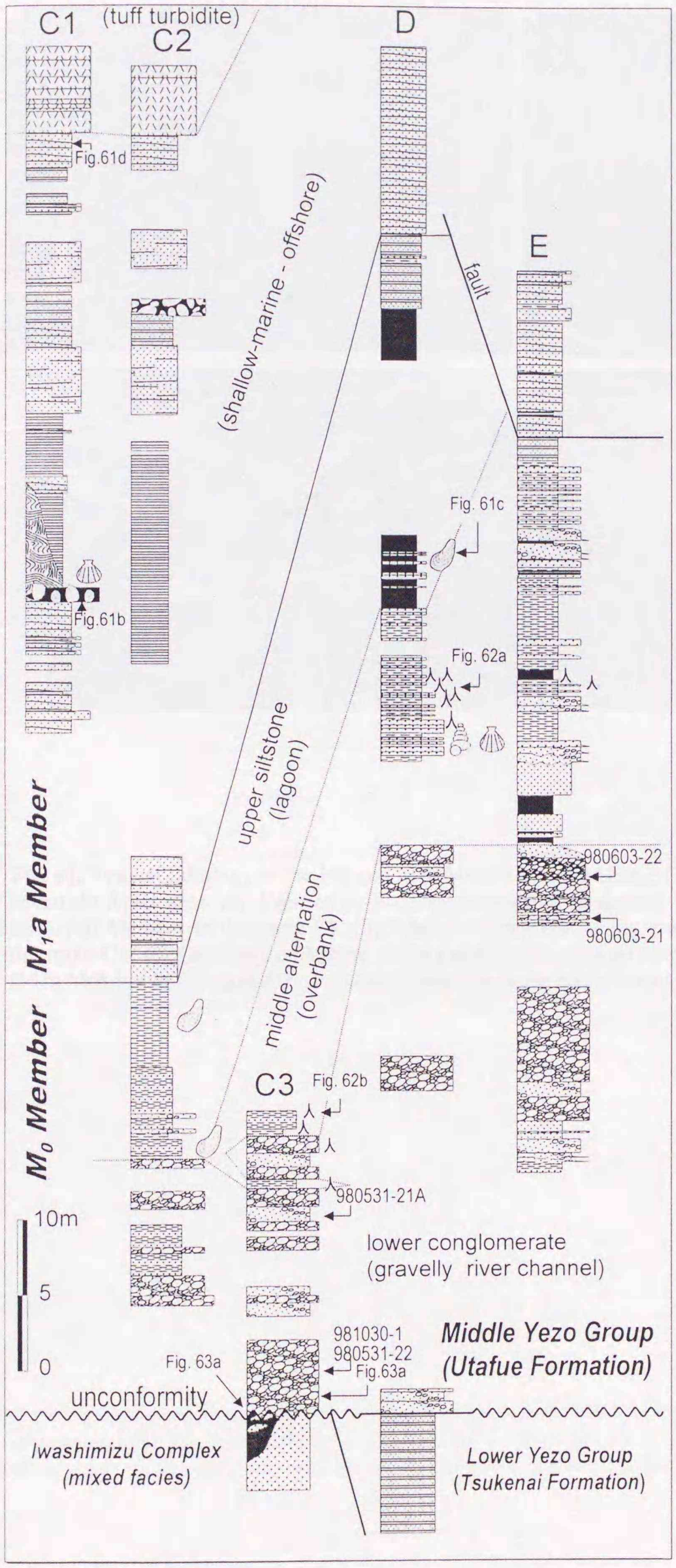


Fig. 60 Detailed columns of the lower sections of the Utafue Formation (Middle Yezo Group) in the south area. Routes C1-C3, D, and E are shown in Fig. 58.

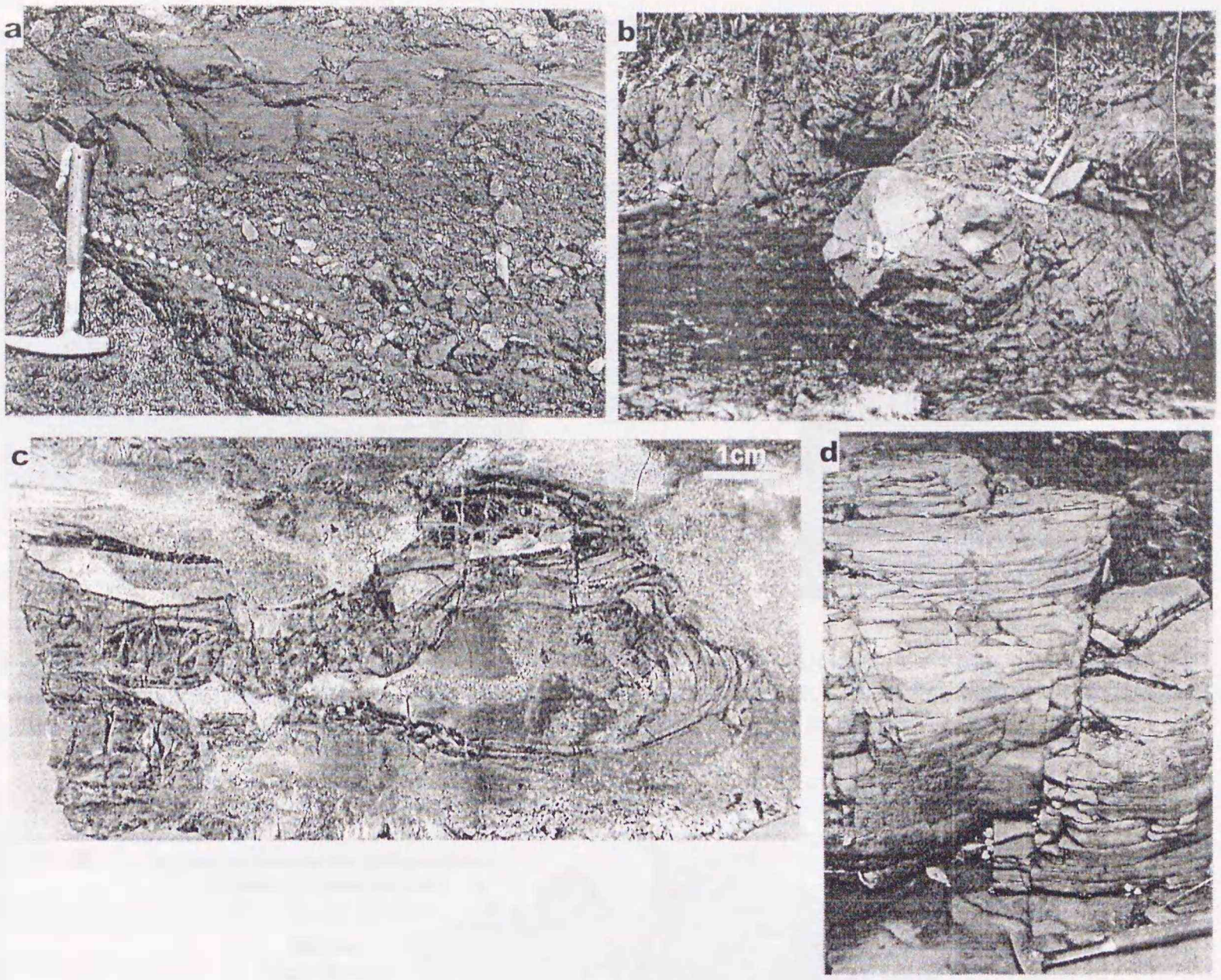


Fig. 61. Typical lithology of the M0 and M1a Members of the Utafue Formation (Middle Yezo Group) in the Mitsuishi River area. (a) Alternation of conglomerate and sandstone, with crude cross-stratification (dotted line). M0 Member in the route C3. (b) Pebbly siltstone containing greenstone blocks (bs). M1a Member in the route C1. (c) Calcareous siltstone of the route D including an "*Ostrea*" fossil. (d) Laminated sandstone (M1a Member in the route C1). Parallel to very low-angle coaly lamination is thoroughly observed.

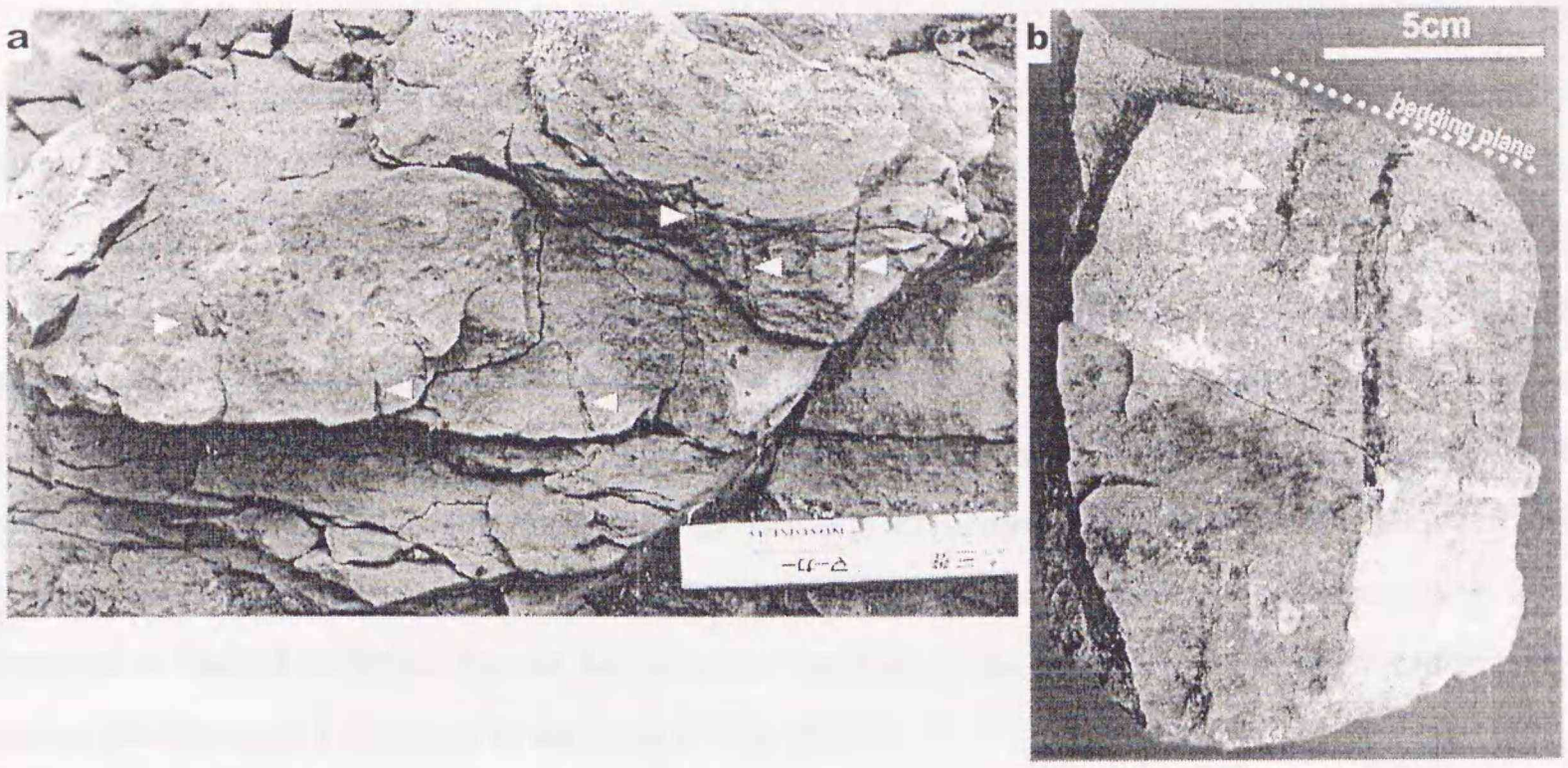


Fig. 62. Occurrence of rootlets (white arrows) in the M0 member, Utafue Formation. (a) Rootlets in a massive sandy siltstone of the route D. Orientation of a marker pen (1.5cm width) indicating the bedding plane. (b) Hand specimen of a fine sandstone bed with rootlets, from the route C.

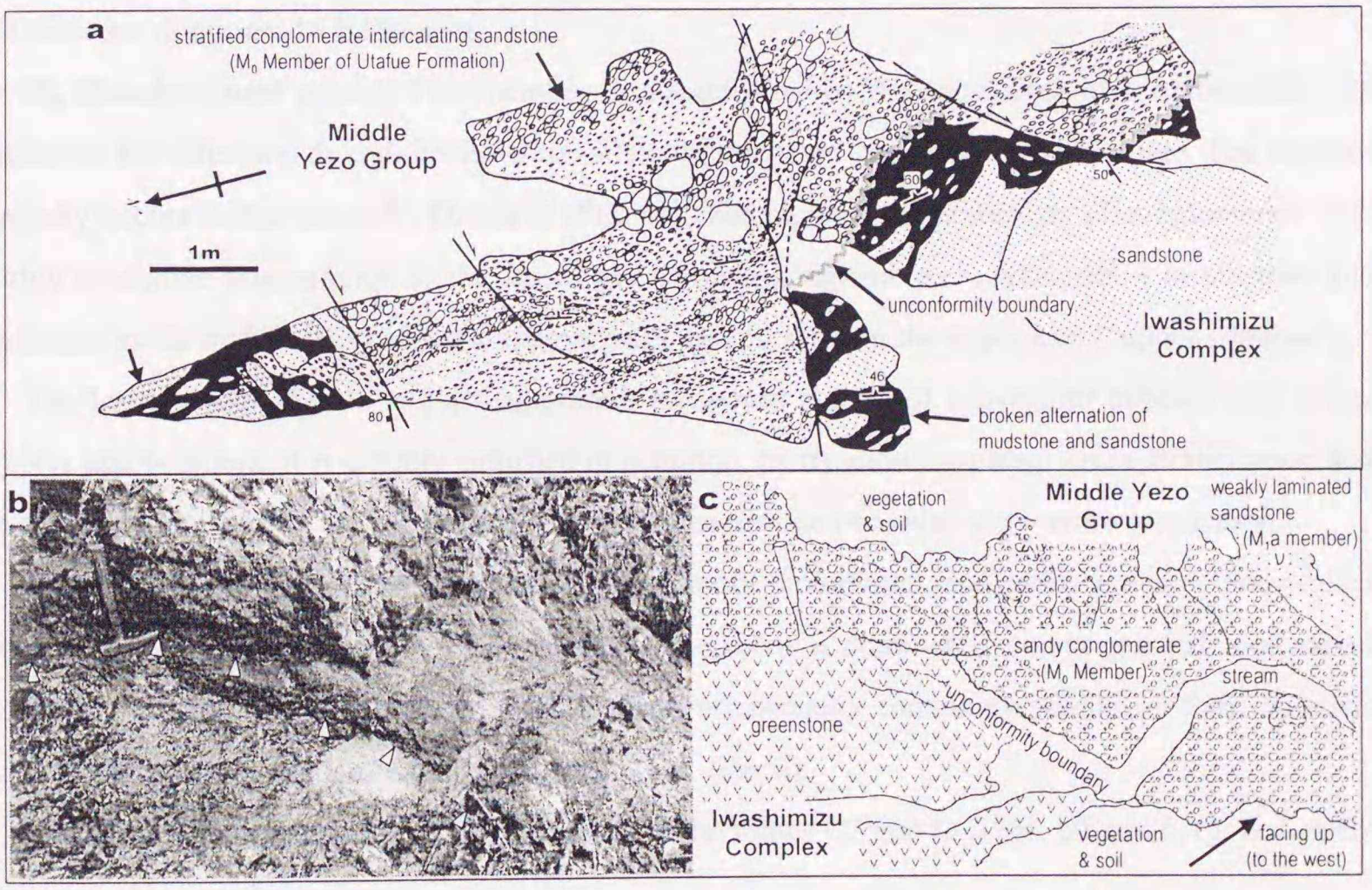


Fig. 63. Unconformity contact between the basal conglomerate (M0) of the Utafue Formation (Middle Yezo Group) and the Iwashimizu Complex. (a) Sketch in horizontal view in the route C3. (b-c) In the route A (a: photograph, b: sketch). A hammer gives scale, and white arrows indicate the unconformity plane.

Nitarachi Formation

Greenish siliceous mudstone with acidic tuff crops out in the Sakubai River (route F in Figs. 58 and 59), though recognized at only one outcrop. It overlies the Iwashimizu Complex presumably separated by a fault.

Tsukenai Formation

Thick-bedded (ca. 0.4 to 1m) coarse to very coarse sandstone, with subordinate amount of mudstone and thin acidic tuff, occurs between the routes D and F (Figs. 58 and 59). Bedding planes generally strike NS, dipping 30-70° to the east. Base of each sandstone bed is sharp, and top of it usually grades to laminated fine sandstone or siltstone of several centimeters thick, showing the signature of turbidite. They are weakly deformed, partly showing pinch-and-swell structure. The formation is faulted underlain by the Iwashimizu Complex in the routes D and E, and conformably overlies the Nitarachi Formation in the route F (Fig. 59).

Utafue Formation

The Utafue Formation of this area unconformably overlies both the Iwashimizu Complex and the Tsukenai Formation, and is thrust by the Iwashimizu Complex at the top. The formation can be divided into three members; conglomerate-bearing M_0 Member, sandstone-dominant M_1a Member, and siltstone-dominant M_1b Member.

(1) **M_0 Member (new name)**: This member is characterized by the occurrence of conglomerate with sandstone and siltstone, though it shows considerable lithologic variations route by route. The member typically occurs in the routes C, D, and E (Fig. 60). The member there consists of conglomerate with pebbly sandstone intercalation in the lower part ("lower conglomerate"), alternation of siltstone and sandstone in the middle part ("middle alternation"), and siltstone in the upper part ("upper siltstone").

The lower conglomerate is clast-supported, composed mainly of subangular pebbles with a few cobbles and boulders. It is crudely stratified in common, partly showing planar cross-stratification and clast imbrication (Fig. 61a). The intercalated pebbly sandstone beds also show cross-lamination.

The siltstone in the middle alternation is commonly bioturbated, and rarely contains thin-walled shells of bivalves and gastropods. The alternating sandstone is dominantly coarse grained, well sorted and poorly graded. It is 5 to 100 cm thick bedded, occasionally containing pebbles at base. Rootlets occur in the siltstone and alternating sandstone (Figs. 62a, b).

The upper siltstone contains "*Ostrea*" shells in the routes C2 and D (Figs. 60 and 61c), and partly intercalates thin sandstone beds.

The three parts described above comprises a conformable succession with no tectonic gap. Lithologic transitions between the parts are observed: the middle alternation overlies the lower conglomerate in the routes C3 and E; the middle alternation is absent and the upper siltstone

conformably overlies the lower conglomerate in the routes C2.

In the route A (Figs. 57 and 58), the M_0 Member consists only of an ill-sorted sandy conglomerate bed 1.2m thick, composed of subangular pebbles and cobbles. The member is absent in the route B. In the route F, the member consists of ill-sorted and matrix-supported conglomerate interbedded with cross-laminated coarse sandstone.

The unconformable sedimentary contact between the M_0 Member and the underlying Iwashimizu Complex or the Tsukenai Formation is observed in the routes A and C3. In the route C3 (Fig. 63a), stratified and cross-bedded conglomerate bed overlies the sheared broken alternation of sandstone and mudstone, which partly contains greenstone lenses belonging to the mixed facies of the Iwashimizu Complex. The contact is weakly argillized but coherent without obvious shear deformation, though cut almost perpendicularly by later normal faults. In the route A (Figs. 63b, 63c), an ill-sorted thin conglomerate bed coherently overlies a greenstone body of the mixed facies of the Iwashimizu Complex without any slip surface.

(2) M_1a Member (Sakai and Kanie, 1986): This member is dominated by fine to medium sandstone, and sandy alternation of sandstone and siltstone. Sandstones often show characteristic dense parallel lamination (Fig. 61b) and very low angle cross-lamination with coaly fragments. Graded turbidite sandstone bed with Bouma sequence (Ta-b-c) is sometimes observed. Ripple marks, trace fossils, and molluscan fossils occasionally occur in the sandstones.

A siltstone-dominated part consisting of laminated siltstone and muddy alternation of siltstone and sandstone occurs in the middle horizon of the member in the route C. The sandstone laminae and beds are sharp-based, normally graded into siltstone.

In the sandstone and siltstone of the routes B and C, matrix-supported muddy conglomerate and/or pebbly mudstone containing greenstone blocks up to 120cm diameter, occur with slumped siltstone and sandstone (Fig. 61b).

Acidic tuff beds more than 5m thick in total, which comprise a key horizon, lies in the upper part of this member.

The M_1a Member conformably overlies the M_0 Member, and their transition is observed in the routes A, C2, and D.

(3) M_1b Member (Sakai and Kanie, 1986): This member is dominated by massive and laminated siltstones with subordinate amount of muddy alternation of sandstone and mudstone. They are occasionally bioturbated. Sandstone laminae and beds have sharp base, normally graded into siltstone. Thin acidic tuff beds are occasionally intercalated.

Age

Radiolarian fossils are extracted from the Tsukenai Formation and underlying Nitarachi Formation (Figs. 64, 65 and Table 10). Fossil ages from the Utafue Formation were reported by Taketani (1982) and Matsumoto *et al.* (1984).

(1) Nitarachi Formation: Greenish siliceous mudstone (980622-16A) contains radiolarians *Cecrops septemporatus* and *Stichocapsa altiformina,* both indicating late Valanginian to early Barremian age (Schaaf, 1985; Sanfilippo and Riedel, 1985; Jud, 1994). The sample also contains *Podobursa triacantha*, *Sethocapsa uterculus*, and *S. trachyostraca*, all of which are common in this age range. The age of this mudstone is thus concluded to be late Valanginian to early Barremian, consistent with that of the type Nitarachi Formation in the Urakawa area (Kanie *et al.*, 1981).

(2) Tsukenai Formation: The gray mudstone sample 981030-5B was collected from the uppermost part of the Tsukenai Formation, just below the basal conglomerate (M_0) of the Utafue Formation. It contains radiolarian fossils: *Eucyrtis* cf. *tenuis*, *Sethocapsa orca*, and *Pseudodictyomitra leptoconica*. *E. tenuis* ranges from early Hauterivian to late Aptian (Sanfilippo and Riedel, 1985; Schaaf, 1985), *S. orca* from early Hauterivian to early Aptian, and *P. leptoconica* from Barremian to earliest Aptian (Schaaf, 1981; Jud, 1994). The mudstone is thus concluded to be of Barremian to lower Aptian, compatible to the type Tsukenai Formation in the Urakawa area (Mitsugi and Hirano, 1997). This age also indicates that only lower part of the Lower Yezo Group occurs in the Mitsuishi River area, and muddy upper part (Aptian to lower Albian Becchari Formation: Sakai and Kanie, 1986) is lacked.

(3) Utafue Formation: Matsumoto *et al.* (1984) reported early to middle Albian nautiloid from the M_1a Member in the Sakubai River. Taketani (1982) reported late Albian to early Cenomanian radiolarians from M_1b Member along the Sakubai River. Although no fossil age has been determined from the M_0 Member, it is inferred as lower to middle Albian based on its stratigraphic position.

Petrological features of basal conglomerate

Clast composition

Basal conglomerate (M_0 Member) of the Middle Yezo Group usually contains abundant greenstone clasts (40 to over 60 modal %, see Figs. 66 and 67). The rests are clasts of sandstone, mudstone, greenish siliceous mudstone, acidic tuff, chert, with minor limestone and pelitic schist, and scarce sand-sized clasts of acidic volcanics and granitic rock. Schistose greenstone clasts commonly occur, and several clasts are of folded schist. Sandy matrix contains grains of quartz, clinopyroxene, metamorphic minerals (described later), minor plagioclase, zircon, and scarce K-feldspar and chromian spinel.

Table 10. List of radiolarian fossils from the Nitarachi-Yezo sequence of the Mitsuishi area. Nt: Nitarachi Formation, Ly: Tsukenai Formation, M0: Utafue Formation, grn-silsh: greenish siliceous mudstone, grn-gray md: greenish gray mudstone, cl: clast in conglomerate.

Sample No.	980622-16B	981030-5B	981030-1A	981030-1B	980603-22A
Lithological unit	Nt	Ly	M_0	M_0	M_0
Lithology	grn-silsh	grn-gray md	grn-silsh cl.	grn-silsh cl.	grn-silsh cl.
Acaeniotyle diaphorogona FOREMAN	+				
Acanthocircus trizonalis RUST	+				
Alievium helenae SCHAAF	+			+	
Archaeodictyomitra excellens (TAN)			+		
Archaeodictyomitra simplex PESSAGNO	+	+			
Archaeodictyomitra spp.	+	+	+	+	
Cecrops septemporatus (PARONA)	+				
Crucella cachensis PESSAGNO			+		
Dibolachras tytthopora FOREMAN					+
Dictyomitra spp.	+		+	+	
Eucyrtidium manokawaensis TUMANDA	+				
Eucyrtis cf. *tenuis* (RUST)		+			
Hemicryptocapsa capita TAN			+		
Hemicryptocapsa sp.			+		
Holocryptocanium japonicum NAKASEKO & NISHIMURA	+				
Homoeoparonaella cf. *speciosa* (PARONA)			+		
Pantanellium squinaboli (PARONA)	+				
Parvicingula boesii (PARONA)	+		+		
Parvicingula cf. *sphaerica* STEIGER	+				
Parvicingula usotanensis TUMANDA	+		+	+	
Podobursa triacantha (FISCHLI)	+				
Podobursa cf. *tricola* FOREMAN				+	
Pseudodictyomitra carpatica LOZYNIAK	+		+	+	
Pseudodictyomitra leptoconica (FOREMAN)		+			
Pseudodictyomitra lilyae (TAN)	+				
Pseudodictyomitra nuda SCHAAF	+	+	+	+	
Pyramispongia barmsteinensis STEIGER	+		+		
Sethocapsa kaminogoensis AITA			+		
Sethocapsa orca (FOREMAN)		+			
Sethocapsa simplex TAKETANI	+	+	+		
Sethocapsa trachyostraca FOREMAN	+				
Sethocapsa uterculus (PARONA)	+		+		
Sethocapsa sp. aff. *S. uterculus*		+			
Spongotripus cf. *satoi* TUMANDA		+	+		
Stichocapsa altiformina TUMANDA	+		+		
Stichocapsa pulchella RUST	+		+		
Syringocapsa cf. *spinosa* (SQUINABOL)			+		
Thanarla conica (ALIEV)	+	+	+	+	
Thanarla elegantissima (CITA)			+		
Wrangellium columnum (RUST)				+	
Wrangellium puga (SCHAAF)				+	
Xitus gifuensis (MIZUTANI)	+				
Xitus spicularius (ALIEV)	+	+	+		

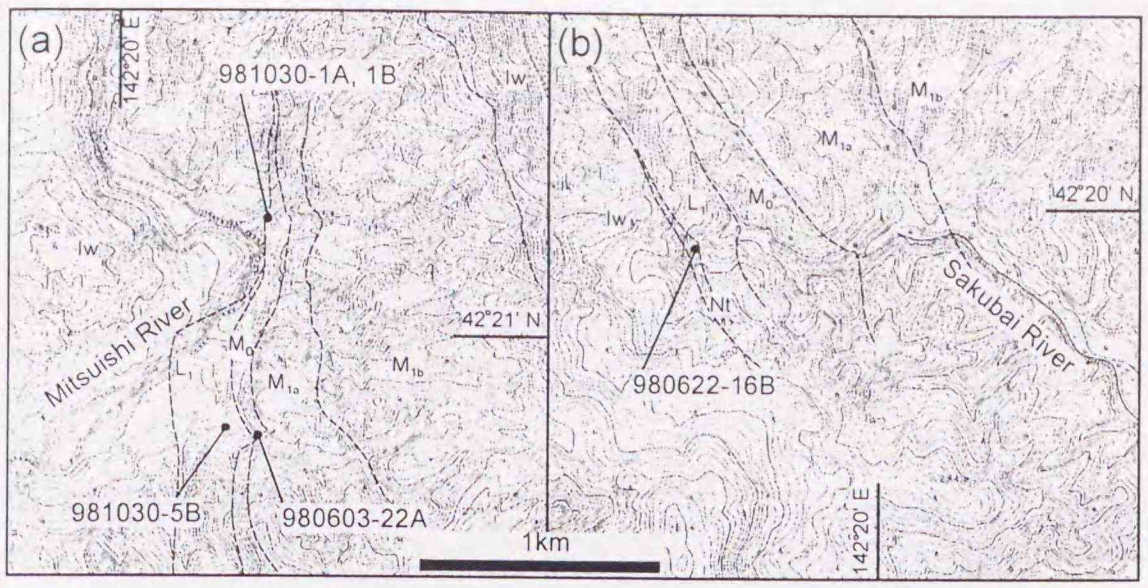


Fig. 64. Sample localities of radiolarian fossils.

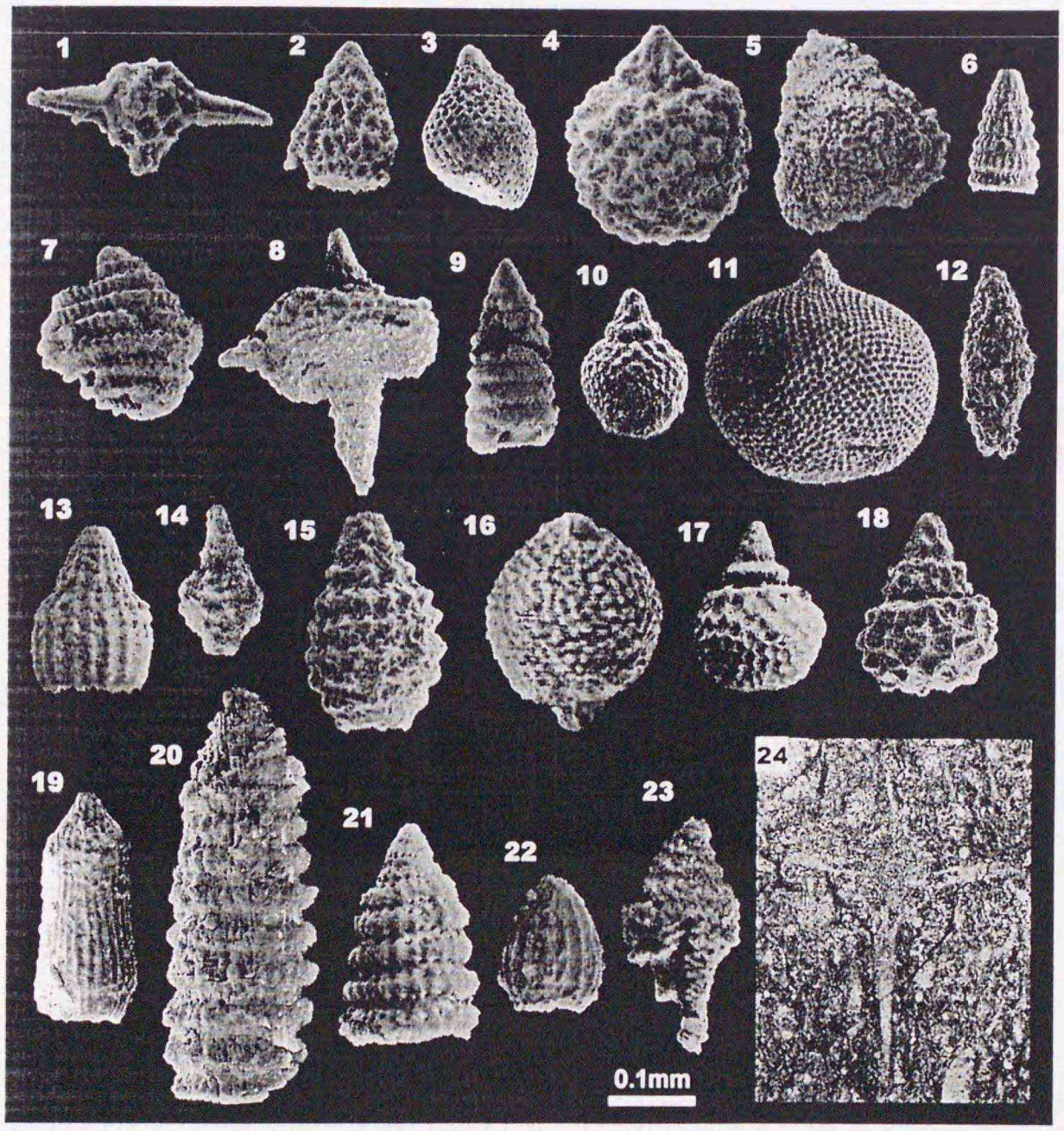


Fig. 65. Radiolarian fossils from the Nitarachi-Yezo Sequence in the Mitsuishi River area. 1-8: From sample 980622-16B in the Nitarachi Formation (1: *Cecrops septemporatus*, 2: *Stichocapsa altiformina*, 3: *Stichocapsa pulchella*, 4: *Sethocapsa trachyostraca*, 5: *Pyramispongia barmsteinensis*, 6: *Pseudodictyomitra leptoconica*, 7: *Parvicingula* cf. *sphaerica*, 8: *Podobursa triacantha*). 9-12: From sample 981030-5B in the Tsukenai Formation, Lower Yezo Group (9: *Pseudodictyomitra lilyae*, 10: *Sethocapsa* aff. uterculus, 11: *Sethocapsa orca*, 12: *Eucyrtis* cf. *tenuis*). 13-24: From siliceous mudstone clasts in the basal conglomerate of the Utafue Formation, Middle Yezo Group. 13-19: From sample 981030-1A (13: *Thanarla elegantissima*, 14:*Syringocapsa* cf. *spinosa*, 15: *Parvicingula usotanensis*, 16: *Hemicryptocapsa capita*, 17: *Sethocapsa uterculus*, 18: *Sethocapsa kaminogoensis*, 19: *Archaeodictyomitra excellens*). 20-23: Sample 981030-1B (20: *Wrangellium columnum*, 21: *Wrangellium puga*, 22: *Thanarla conica*, 23: *Podobursa* cf. *tricola*). 24: Sample 980603-22A, *Dibolachras tytthopora*.

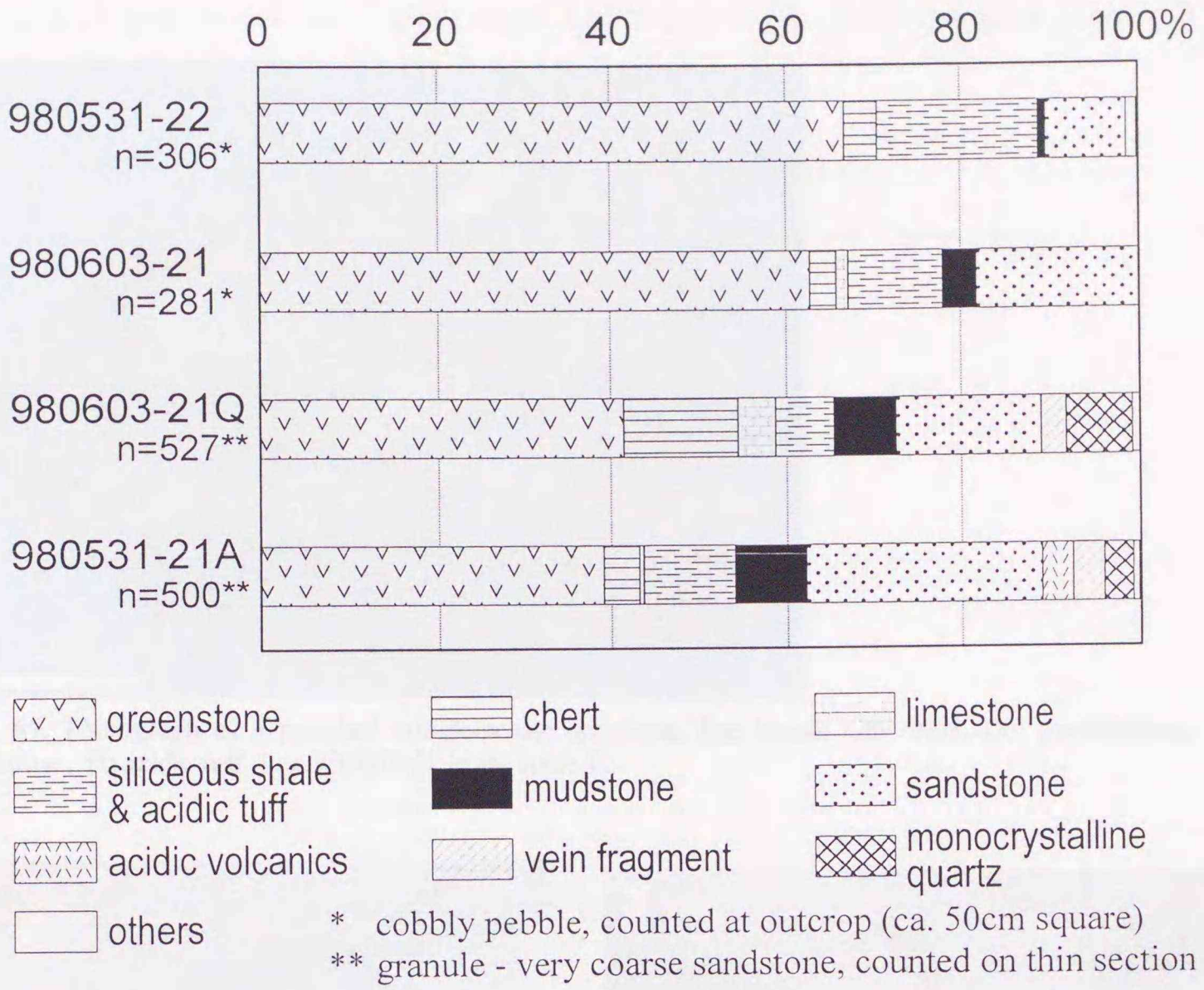


Fig. 66. Modal compositions of the greenstone conglomerate and very coarse sandstone from the M0 Member, Utafue Formation.

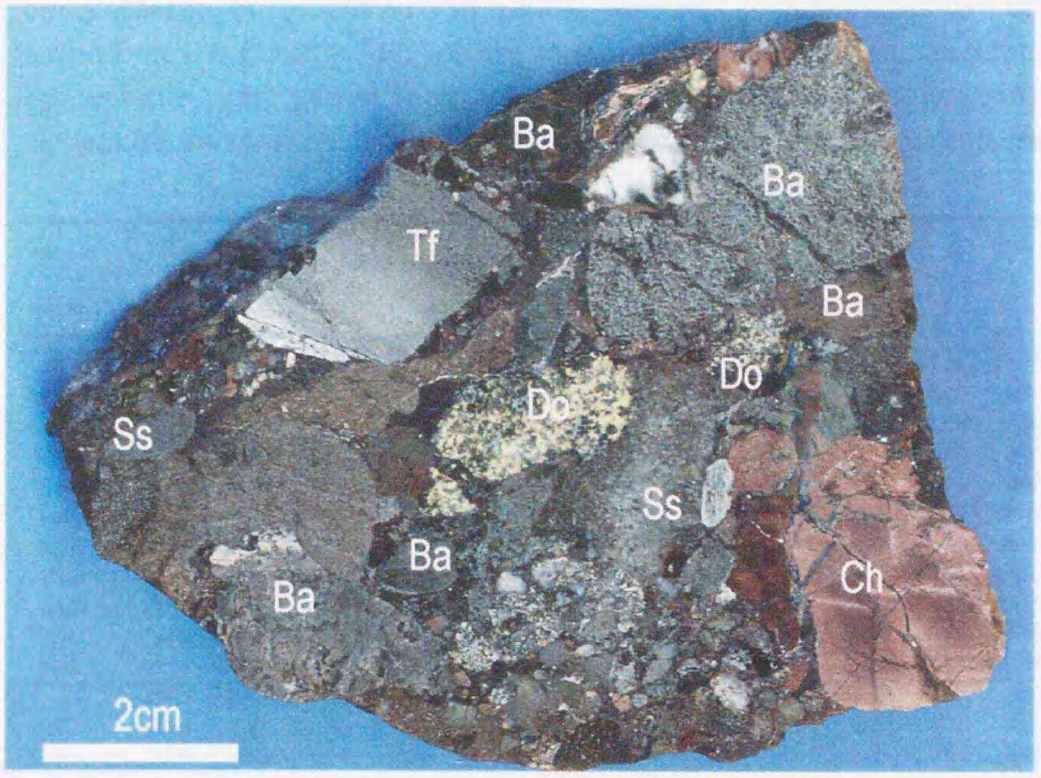


Fig. 67. Photograph of a polished conglomerate specimen. Ba: basalt, Ch: chert, Do: metadolerite, Ss: sandstone, Tf: acidic tuff. Loc.980603-21 in the route E.

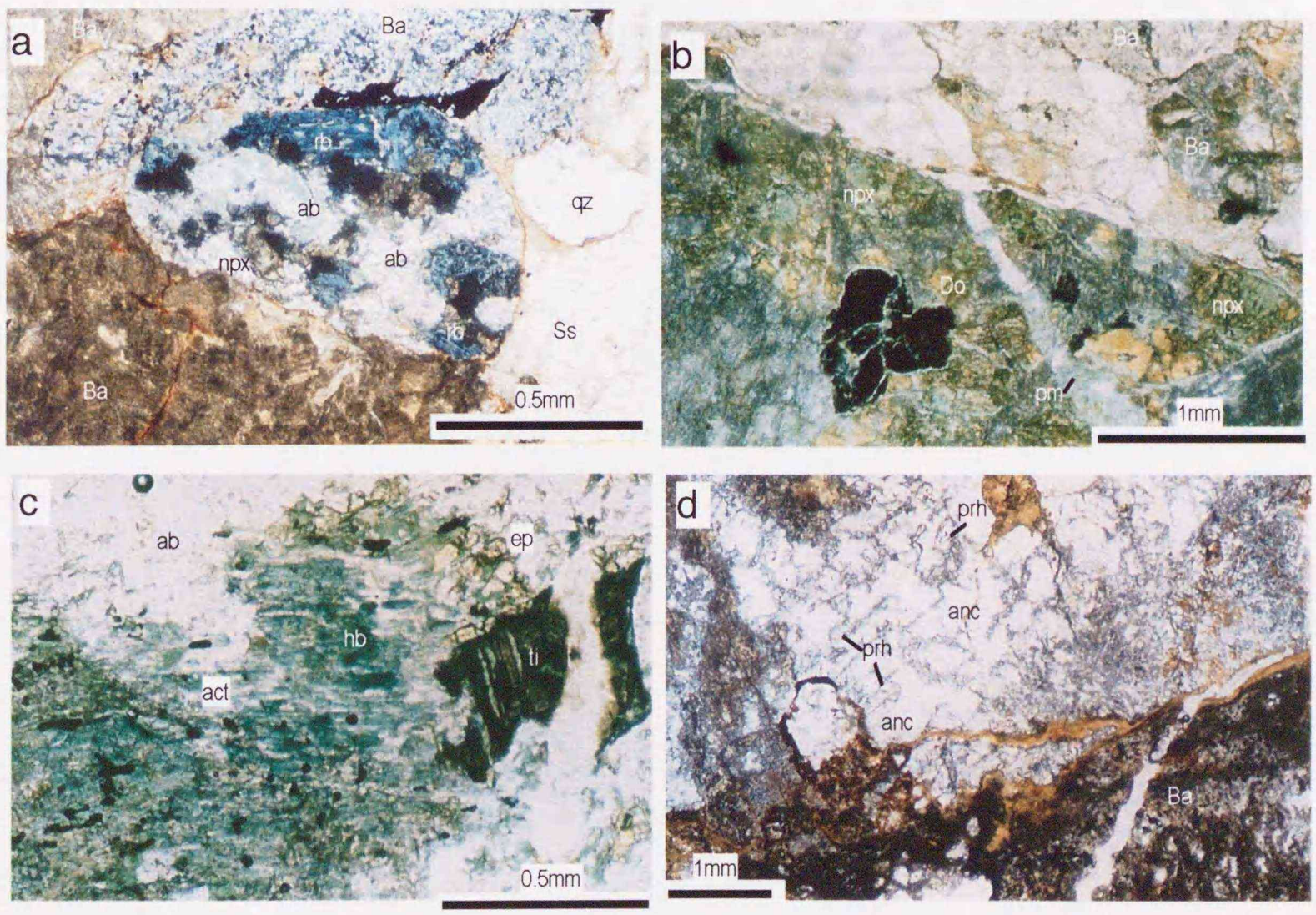


Fig. 68. Photomicrographs of the greenstone conglomerate under plane-polarized light. (a): Clast of sodic pyroxene - riebeckite - albite metadolerite. (b): Dolerite clast with sodic pyroxene and pumpellyite. (c): Epidote - amphibolite clast. (d): Clast of analcime - prehnite vein. Ba: basalt, Ch: chert, Do: metadolerite, Ss: sandstone, ab: albite, act: actinolite, anc: analcime, ep: epidote, hb: hornblende, npx: sodic pyroxene, pm: pumpellyite, prh: prehnite, qz: quartz, rb: (magnesio-?) riebeckite, ti: titanite. (c): Loc.980603-21 in the route E, (a, d): Loc. 980611-26 in the route A, (b) Loc. 980611-30, a drift along a stream of the route B.

Table 11. Representative major element compositions of metamorphic minerals in clasts of the basal conglomerate of the Utafue Formation. Numbers of cations per unit cell at max Fe^{3+}/Fe^{2+} are shown for amphiboles. act: actinolite, act-hb: actinolitic hornblende, anc: analcime, cr: crossite, ed-f: ferro-edenite, ep: epidote, gar: garnet, npx: sodic pyroxene (aegirine augite), pm: pumpellyite, prh: prehnite, rb: riebeckite, rb-m: magnesio-riebeckite, win: winchite. A-E in parentheses indicates the route, from which

Sample	980603-21AMP epidote amphibolite clast (D)					980603-21A9 (D)				980622-11 (E)	980611-26 (A)				980611-26T (A)		980611-30T (A)	
point	3	14	22	2	16	62	60	50	49	74	30	35	43	44	393	394	127	163
mineral	*act*	*act-hb*	*ed-f*	*win*	*ep*	*cr*	*rb-m*	*pm*	*gar*	*rb-m*	*rb*	*npx*	*npx*	*npx*	*anc*	*prh*	*npx*	*npx*
SiO_2	53.29	51.30	45.44	53.40	38.03	54.60	54.77	37.13	39.06	56.81	52.16	53.73	51.35	54.24	59.79	42.12	53.94	55.11
TiO_2	0.00	0.29	0.09	0.01	0.02	0.09	0.01	0.00	0.02	0.25	0.50	0.06	0.12	0.09	0.00	0.02	0.40	0.08
Al_2O_3	2.30	4.54	8.21	1.50	22.41	3.43	2.56	20.48	22.12	1.97	2.98	1.06	3.95	2.28	22.24	22.46	3.43	4.83
Cr_2O_3	0.00	0.00	0.00	0.02	0.03	0.01	0.00	0.03	0.07	0.01	0.00	0.04	0.01	0.10	0.00	0.02	0.05	0.03
FeO*	20.02	16.59	23.90	23.00	12.71	24.60	24.11	9.26	31.42	19.59	26.74	17.52	21.73	22.85	0.04	0.68	21.99	22.76
MnO	0.34	0.29	0.30	0.28	0.16	0.34	0.32	0.09	0.74	0.08	0.74	0.40	0.12	0.14	0.04	0.02	0.23	0.14
MgO	10.41	12.42	7.52	8.89	0.00	6.25	7.44	3.08	7.59	10.80	5.80	6.95	6.07	3.64	0.00	0.00	2.29	1.57
CaO	9.46	10.88	9.03	5.14	23.23	1.20	1.84	21.56	0.74	0.82	2.28	15.28	7.42	6.14	0.01	24.74	3.54	3.42
Na_2O	2.15	2.21	3.33	4.54	0.00	6.56	6.49	0.01	0.06	6.87	6.02	5.25	8.32	10.32	8.91	0.13	12.39	12.66
K_2O	0.00	0.00	0.44	0.12	0.00	0.00	0.00	0.00	0.00	0.00	0.00	0.00	0.00	0.00	0.04	0.00	0.00	0.00
Total	97.98	98.52	98.26	96.90	96.58	97.08	97.54	91.64	101.82	97.20	97.21	100.30	99.13	99.81	91.10	90.21	98.28	100.60
	O=23	O=23	O=23	O=23	O=12.5	O=23	O=23	O=24.5	O=12	O=23	O=23	O=6	O=6	O=6	O=6	O=11	O=6	O=6
Si	7.85	7.49	6.96	7.88	3.04	7.96	7.94	6.13	2.99	8.00	7.75	2.01	1.91	2.00	2.14	3.06	2.00	1.99
Ti	0.00	0.03	0.01	0.00	0.00	0.01	0.00	0.00	0.00	0.03	0.06	0.00	0.00	0.00	0.00	0.00	0.01	0.00
Al	0.40	0.78	1.48	0.26	2.11	0.59	0.44	3.99	2.00	0.33	0.52	0.05	0.17	0.10	0.94	1.93	0.15	0.21
Cr	0.00	0.00	0.00	0.00	0.00	0.00	0.00	0.00	0.01	0.00	0.00	0.00	0.00	0.00	0.00	0.00	0.00	0.00
Fe^{3+}	0.21	0.00	0.00	1.07	0.81	1.29	1.39	0.75	0.01	1.60	1.33	0.31	0.60	0.63	0.00	0.00	0.68	0.69
Fe^{2+}	2.25	2.03	3.06	1.77	0.04	1.71	1.53	0.53	2.00	0.70	2.00	0.24	0.08	0.08	0.00	0.04	0.00	0.00
Mn	0.04	0.04	0.04	0.03	0.01	0.04	0.04	0.01	0.05	0.01	0.09	0.01	0.00	0.00	0.00	0.00	0.01	0.00
Mg	2.29	2.70	1.72	1.96	0.00	1.36	1.61	0.76	0.87	2.27	1.29	0.39	0.34	0.20	0.00	0.00	0.13	0.08
Ca	1.50	1.70	1.48	0.81	1.99	0.19	0.29	3.82	0.06	0.12	0.36	0.61	0.30	0.24	0.00	1.93	0.14	0.13
Na	0.61	0.62	0.99	1.30	0.00	1.86	1.83	0.00	0.01	1.88	1.73	0.38	0.60	0.74	0.62	0.02	0.89	0.89
K	0.00	0.00	0.09	0.02	0.00	0.00	0.00	0.00	0.00	0.00	0.00	0.00	0.00	0.00	0.00	0.00	0.00	0.00

Fe^{3+} in amphiboles are estimated as $Fe^{3+} = Na + K - Al + 2Ti + Cr$

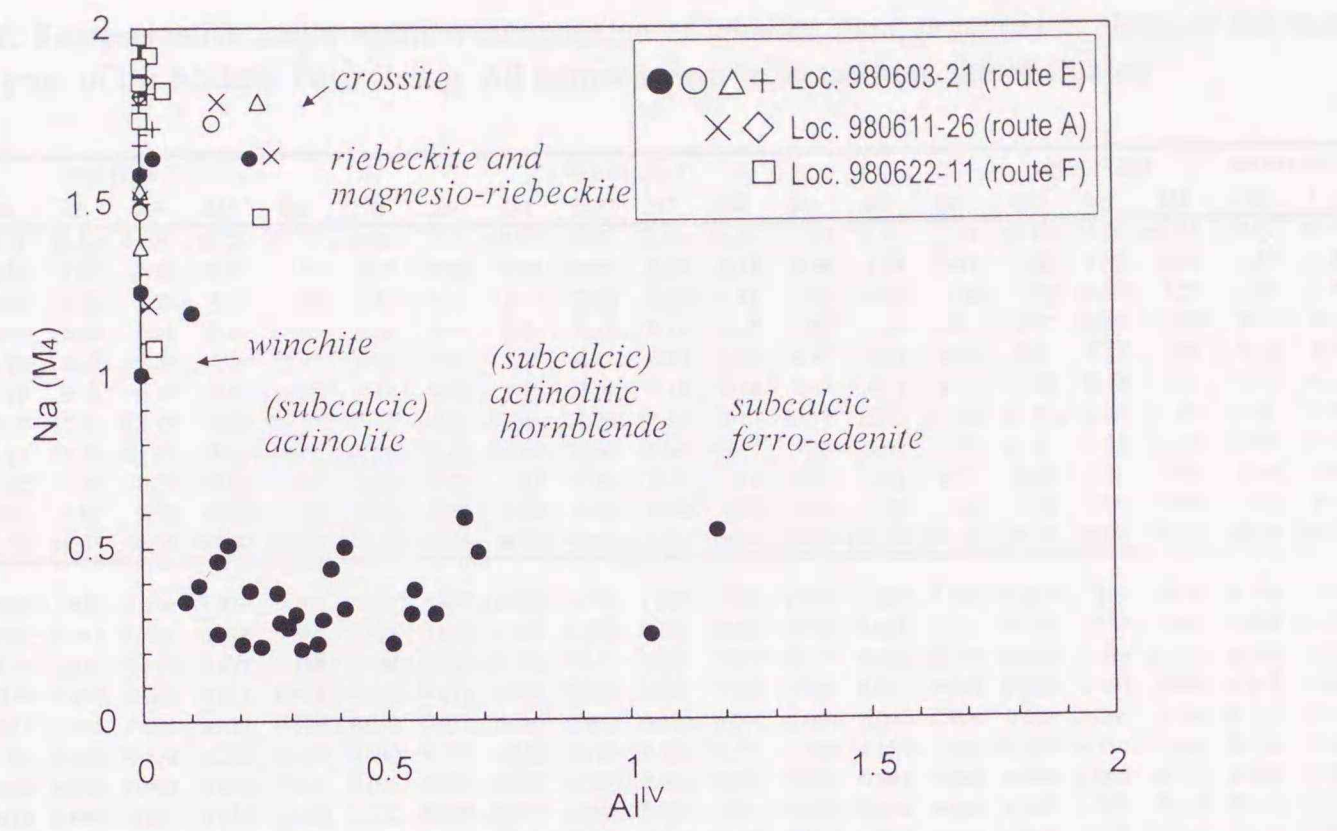


Fig. 69. Al^{IV}-Na(M4) plot of metamorphic amphiboles in clasts of the basal conglomerate. Possible compositional ranges between maximum and minimum Fe^{3+}/Fe^{2+} are tie-lined. Nomenclature after Leake (1978). Amphiboles in each clast are plotted as same symbol.

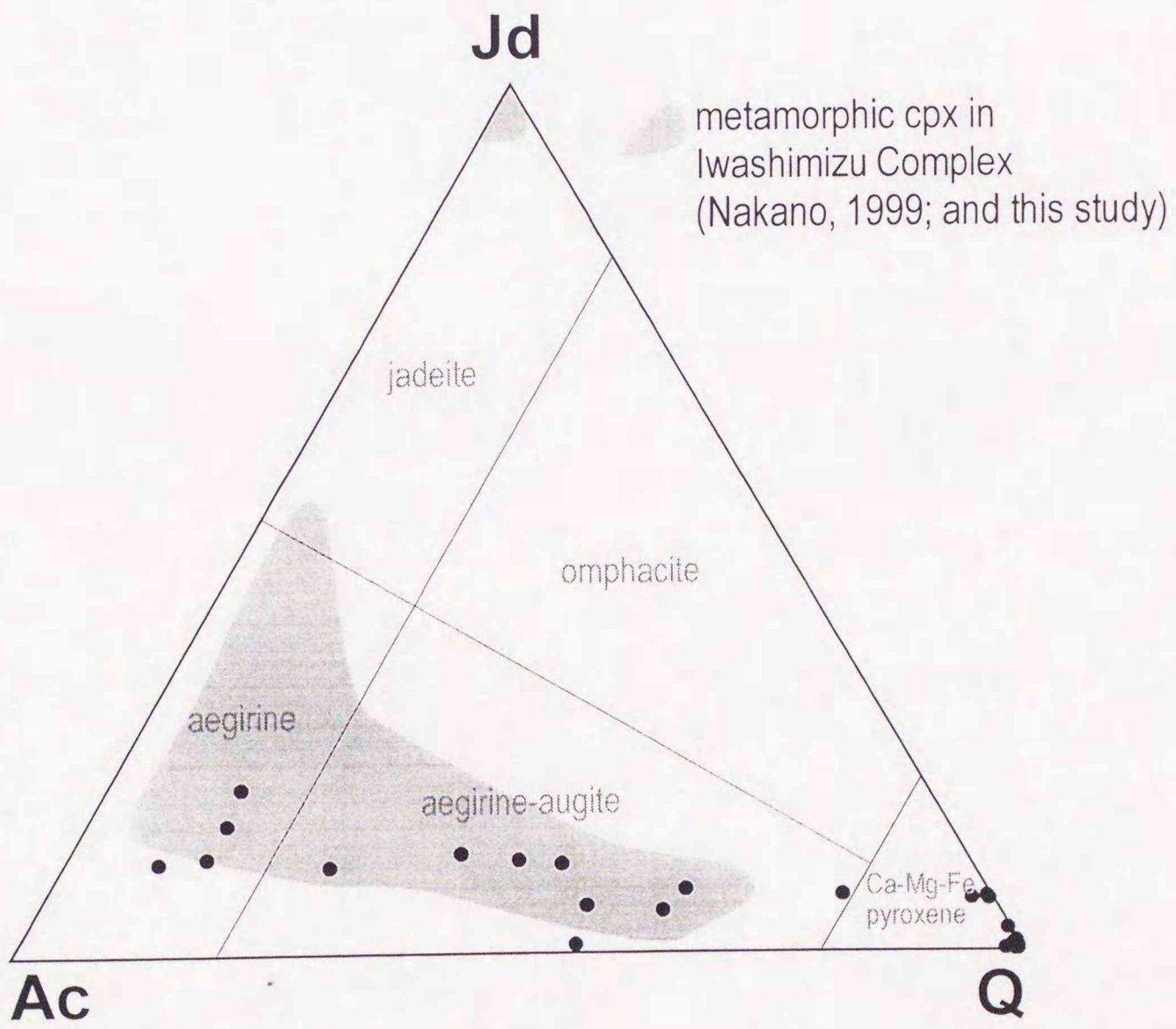


Fig. 70 Chemical composition of detrital clinopyroxenes from the basal conglomerate of the Middle Yezo Group. Nomenclature after Morimoto et al. (1988). Jd: jadeite component, Ac: aegirine component, Q: wollastonite + enstatite + ferrosilite component.

Table 12. Representative major element composition of igneous clinopyroxenes in clasts of the basal conglomerate of the Middle Yezo Group. All samples were collected from the north area.

Sample	980611-26				980611-26A1										980611-26T			980611-30T	
point	36	41	419	421	227	228	229	232	240	247	256	261	267	268	407	417	418	170	171
SiO_2	52.92	48.55	51.07	52.22	50.71	51.06	50.92	51.97	52.88	52.19	54.28	53.80	52.05	53.14	50.78	48.23	45.81	47.23	46.39
TiO_2	0.23	1.55	0.50	0.50	0.71	0.89	0.58	0.26	0.30	0.39	0.16	0.38	1.03	0.43	1.00	1.08	2.13	2.33	3.26
Al_2O_3	2.94	5.23	4.53	3.23	3.42	4.34	4.13	2.21	2.62	2.32	1.81	2.76	4.02	3.26	4.02	6.34	7.27	6.74	7.37
Cr_2O_3	0.73	0.00	1.08	0.27	0.85	0.22	0.45	0.21	0.52	0.12	0.22	0.23	1.26	0.09	0.97	0.24	0.00	0.05	0.02
FeO*	5.23	8.65	5.20	7.29	5.41	7.28	6.01	5.85	4.72	6.40	5.57	6.47	3.93	6.88	6.01	7.15	9.56	8.60	8.91
MnO	0.14	0.17	0.14	0.19	0.15	0.16	0.12	0.16	0.14	0.18	0.16	0.18	0.13	0.13	0.12	0.17	0.21	0.14	0.18
MgO	17.47	12.25	15.77	17.44	16.37	15.23	15.36	16.49	17.29	16.27	17.12	15.51	15.92	15.60	15.71	13.60	11.84	11.91	11.90
CaO	21.19	21.98	21.42	18.62	21.22	21.06	21.22	21.50	21.05	20.69	19.17	19.98	21.52	21.52	21.10	21.82	21.30	21.84	22.38
Na_2O	0.22	0.56	0.27	0.25	0.34	0.28	0.22	0.17	0.15	0.25	0.16	0.25	0.41	0.31	0.40	0.26	0.64	0.98	0.65
K_2O	0.00	0.00	0.00	0.00	0.00	0.00	0.00	0.00	0.00	0.00	0.00	0.00	0.00	0.00	0.00	0.00	0.00	0.00	0.00
Total	101.07	98.93	99.99	100.00	99.16	100.53	99.00	98.82	99.66	98.81	98.66	99.56	100.29	101.36	100.11	98.90	98.77	99.80	101.05
O=6																			
Si	1.906	1.829	1.866	1.909	1.866	1.871	1.887	1.925	1.931	1.937	1.993	1.971	1.887	1.928	1.858	1.801	1.730	1.760	1.716
Ti	0.006	0.044	0.014	0.014	0.020	0.025	0.016	0.007	0.008	0.011	0.005	0.010	0.028	0.012	0.028	0.030	0.061	0.065	0.091
Al	0.125	0.232	0.195	0.139	0.148	0.188	0.180	0.096	0.113	0.101	0.079	0.119	0.172	0.139	0.173	0.279	0.324	0.296	0.321
Cr	0.029	0.000	0.044	0.011	0.035	0.009	0.018	0.009	0.021	0.005	0.009	0.009	0.051	0.004	0.039	0.010	0.000	0.002	0.001
Fe^3	0.037	0.063	0.021	0.022	0.070	0.032	0.011	0.043	0.000	0.016	0.000	0.000	0.000	0.000	0.044	0.066	0.142	0.124	0.112
Fe^2	0.120	0.210	0.138	0.200	0.097	0.190	0.175	0.138	0.144	0.182	0.171	0.198	0.119	0.209	0.140	0.157	0.160	0.144	0.164
Mn	0.004	0.005	0.004	0.006	0.005	0.005	0.004	0.005	0.004	0.006	0.005	0.006	0.004	0.004	0.004	0.005	0.007	0.004	0.006
Mg	0.938	0.688	0.859	0.950	0.898	0.832	0.849	0.911	0.942	0.900	0.937	0.847	0.860	0.844	0.857	0.757	0.667	0.661	0.656
Ca	0.819	0.888	0.840	0.730	0.838	0.828	0.844	0.854	0.825	0.824	0.755	0.785	0.837	0.838	0.828	0.874	0.863	0.873	0.888
Na	0.015	0.041	0.019	0.018	0.024	0.020	0.016	0.012	0.011	0.018	0.012	0.018	0.029	0.021	0.028	0.019	0.047	0.071	0.046
K	0.000	0.000	0.000	0.000	0.000	0.000	0.000	0.000	0.000	0.000	0.000	0.000	0.000	0.000	0.000	0.000	0.000	0.000	0.000

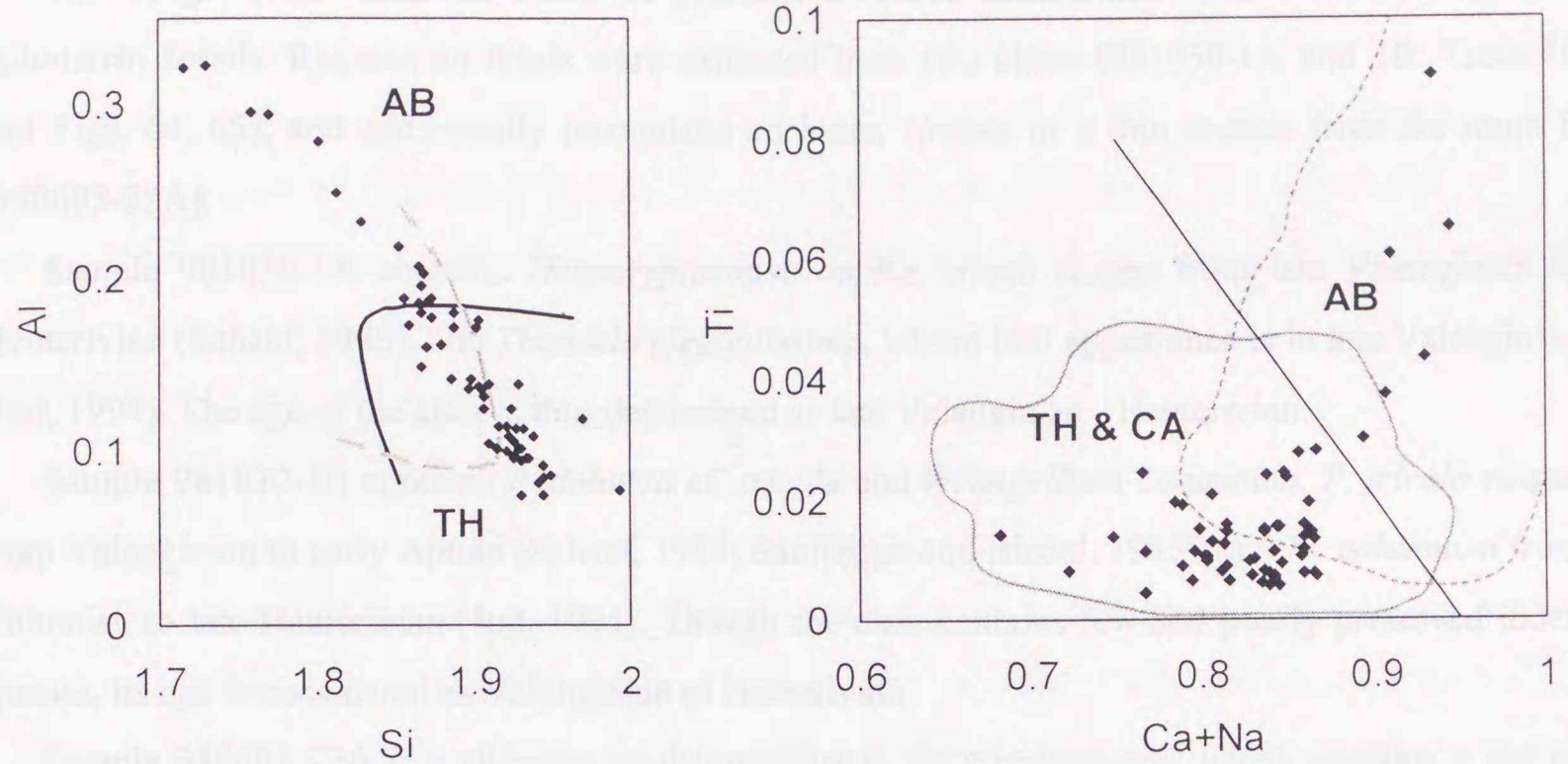


Fig. 71. Si - Al (Maruyama, 1976) and Ca + Na - Ti (Leterrier *et al.*, 1982) plots of detrital augite (Mg#>0.75) in the basal conglomerate of the Utafue Formation (Middle Yezo Group). TH: tholeiitic, AB: alkaline, and CA: calc-alkaline.

Radiolarian ages of the siliceous mudstone clasts

The conglomerate contains clasts of greenish siliceous mudstone, which commonly contain radiolarian fossils. Radiolarian fossls were extracted from two clasts (981030-1A and 1B: Table 10 and Figs. 64, 65), and additionally recognized an index species in a thin section from the route E (980603-22A).

Sample 981030-1A contains *Hemicryptocapsa capita*, which ranges from late Valanginian to Hauterivian (Schaaf, 1985), and *Thanarla elegantissima*, whose first appearance is in late Valanginian (Jud, 1994). The age of the clast is thus determined as late Valanginian - Hauterivian.

Sample 981030-1B contains *Podobursa* cf. *tricola* and *Wrangellium columnum*. *P. tricola* ranges from Valanginian to early Aptian (Schaaf, 1985; Sanfilippo and Riedel, 1985), and *W. columnum* from Tithonian to late Hauterivian (Jud, 1994). Though the clast contains few and poorly preserved index species, its age is considered as Valanginian to Hauterivian.

Sample 980603-22A is a siliceous mudstone clast in the conglomerate, which contains a test of *Dibolachras tytthopora* (Fig. 65). The species indicates late Valanginian to early Aptian (Sanfilippo and Riedel, 1985; Jud, 1994).

The ages of the three clasts are compatible with the Valanginian - Barremian Nitarachi Formation.

Detrital metamorphic minerals

Metamorphic minerals occur within the greenstone clasts, and separately in sandy matrix as detrital mineral fragments (Fig. 68): they are sodic amphibole, actinolite, sodic pyroxene, epidote, pumpellyite, and scarce hornblende, lawsonite, prehnite, analcime, garnet, and stilpnomelane. Aragonite was also recognized in a cobble of riebeckite-albite metabasalt by staining method. A pebble comprising albite, epidote, and hornblende with retrogressive actinolite, showing epidote-amphibolite assemblage has been found (Fig. 68c).

Representative major element composition of the metamorphic minerals is shown in Table 11. The analyzed sodic amphibole grains are mostly of riebeckite to magnesio-riebeckite, with one crossite grain. The epidote-amphibolite pebble (980603-21AMP) contains calcic amphiboles (ferro-edenite, actinolitic hornblende, and actinolite, see Fig. 69), some of which show subcalcic composition. This pebble also contains retrogressive vein of riebeckite and winchite (point 2 in Table 11).

Pale green to yellowish green clinopyroxene and a few non-colored clinopyroxene grains show sodian augite, aegirine-augite, and aegirine compositions, containing less than 20% jadeite component (Fig. 70). Jadeite and aegirine-jadeite, which are seen in the Iwashimizu Complex (Fig. 52), have not been detected.

Garnet grains are contained in sandy matrix, and show almandine - pyrope series compositions (*e.g.* Table 11 point 49): some are pyrope-rich containing 7.0-7.6 wt% MgO (27-29 mol% pyrope).

Ca-garnet is also seen in chloritized glassy matrix of a clinopyroxene-phyric basalt (ankaramite) clast.

Metamorphic minerals described above show that greenstone clasts of all metamorphic grades described by Nakano (1981) and this study are contained in the conglomerate. The majority is the clasts correlative to the type K-Ia (PH-type); the clasts of the type K-II (ENP-type) is subordinate. The only one sand grain of aggregated lawsonite is correlative with the types K-Ib (either LPH or LN - type), and one epidote-amphibolite pebble is correlated with the type K-III. The clasts of analcime and prehnite vein (type H-Ib; Z-type) were found from the route A.

Detrital igneous clinopyroxene

Igneous clinopyroxenes are contained in basaltic clasts and as sand grains in the basal conglomerate, especially in the north area. Major element composition of them is shown in Table 12 and Fig. 71. Analysis was made on the pyroxenes as phenocrysts and dolerite groundmass in basaltic clasts, and as medium to coarse sand grains of same origins. Mg# (Mg / Mg+Fe^{2+}) range from 0.76 to 0.90. Si, Al, Ca+Na and Ti atomic ratios (O=6) show considerable variation (Fig. 71): some have low Ti (less than 0.015 per unit cell) and low Al (less than 0.15) plotting in the tholeiitic fields of Maruyama (1976) and Leterrier *et al.* (1982), whereas others have high Ti (more than 0.015) and Al (more than 0.15), plotting in the alkaline fields. Such different types of basaltic clasts are also petrographically recognized, *i.e.*, non-vesicular aphyric basalt and dolerite suggesting tholeiitic, which contain magnetite and non-colored augite, vs. ol- and cpx-phyric basalt (often vesicular) and dolerite suggesting alkaline, which contain ilmenite, titaniferous augite, minor kaersutite and aegirine.

Discussion

Sedimentological interpretation for the Utafue Formation

(1) M_0 Member: The stratified and clast-supported lower conglomerates with planar cross bedding and clast imbrication, occurring in the routes C to E, are clearly traction current deposits. They are correlative to the channel facies of gravelly river deposits as typified by Miall (1992). Overlying middle alternation commonly contains rootlets indicating non-marine environments. This lithofacies is interpreted as overbank deposits. The upper siltstone is interpreted as brackish lagoon deposits, because it contains "*Ostrea*" shells.

The typical M_0 Member is thus explained by a gravelly river system, consisting of gravelly channel deposits and silty overbank deposits. This is the first report of fluvial deposits at the base of the Middle Yezo Group. The M_0 Member of the route A is a very thin (1.2 m) sandy conglomerate bed with subangular clasts overlain by the sandstone of the M_1a Member. This conglomerate is interpreted as shallow marine deposits, as well as a part of the M_1a sandstone.

(2) M_1a Member: The sandstone of this member, occasionally containing shell fossils, sometimes

shows dense coaly lamination, and beds are generally not graded (Fig. 61d). These characteristics suggest that the sandstone beds are traction current deposits, not turbidites. They are considered as shallow-marine deposits including shoreface sandstone. This part, however, also includes sandy turbidite beds suggesting offshore and/or slope environments. Their succession is not sufficiently revealed as well as each facies interpretation.

The siltstone-dominant part, which is intercalated in the laminated sandstone, is accompanied by sharp-based and normally graded sandy laminae and beds. They are interpreted as offshore deposits dominated by fine-grained turbidite.

The slump bodies containing greenstone blocks suggest that the basement Iwashimizu Complex was exposed and collapsed in shallow-marine areas with some topographic instability.

(3) M_1b Member: This member is dominated by siltstone with sharp-based and graded sandy laminae and beds. The laminae and beds are interpreted as offshore fine-grained turbidite, as those in the muddy part in the M_1a Member.

Clastic composition of the conglomerate

Greenstone and mafic schist, chert, limestone, and pelitic schist, all of which are seen in the basal conglomerate as sedimentary clasts, are the major constituent lithofacies of the Iwashimizu Complex. Metamorphic mineral assemblages in the clasts are also well consistent with those of metabasites in the Iwashimizu Complex, from analcime- and prehnite-bearing low-grade rocks, through sodic pyroxene- and sodic amphibole-bearing rocks, to epidote-amphibolite. These lithologic and metamorphic correlations lead a simple consequence that much of the clasts in the basal conglomerate was directly provided from the underlying Iwashimizu Complex. They also suggest that almost all the lithofacies observed in the present Iwashimizu Complex had already been accomplished until the formation of the unconformity.

The Iwashimizu Complex contains both oceanic island-type alkaline volcanics and depleted tholeiite (Nakano, 1985; Watanabe and Niida, 1987; Kimura *et al.*, 1994). Augites in clasts of the basal conglomerate, which show both alkaline and tholeiitic affinities, are reflecting the two contrastive types of greenstones in the source Iwashimizu Complex.

Greenish siliceous mudstone clasts are interpreted to originate from the Nitarachi Formation in terms of age and lithology. Sandstone clasts may have been derived from the Lower Yezo Group.

Composition of the basal conglomerate thus indicates the erosion of the Iwashimizu Complex and lower part of the Nitarachi-Yezo Sequence. Minor sand grains of granitic rock, acidic volcanics, and pyrope-rich garnet may originate from other source such as continental arc and continental margin (Oshima Belt or farther west).

Significance of unconformity

Occurrence of the unconformity in the Nitarachi-Yezo Sequence clearly shows that the high-P/T metamorphosed Iwashimizu accretionary complex, which formed in the mid-Early Cretaceous (Valanginian - Barremian), rapidly exhumed and suffered subaerial erosion in the late Early Cretaceous (early to middle Albian). Metamorphic pressure of 7 - 8 kb is estimated for the Pirashuke Unit, so that the highly metamorphosed unit of the Iwashimizu Complex was uplifted from the depth of more than 20 km. The interval between the accretion and exhumation is estimated as ca. 20 m.y. This interval is abnormally short for exhumation of high-P/T metamorphic complex in subduction zone, except the case that continental crust is subducting (Maruyama *et al.*, 1996). This evidence strongly suggests that the unconformity was formed by the exhumation event, rather than by an eustatic sea-level change.

The Iwashimizu Complex was subsequently subsided since the late Albian covered by more than 1.4 km thick fining-upward succession of the Utafue Formation. The unconformity indicates a change in tectonic movement of the Iwashimizu Complex from rapid exhumation to gentle subsidence.

Although early workers recognized the existence of Albian unconformity mainly from south part of the Sorachi-Yezo Belt (Hashimoto, 1936; Osanai and Matsushita, 1959, 1960; Kimura, 1979), Takashima *et al.* (1997a, 1997b) and Takashima and Nishi (1999) denied the existence of the unconformity based on conformable successions in central part of the belt. Kawamura *et al.* (1999) reconfirmed the existence of the unconformity, which restrictively occurs along the eastern margin of the south Kamuikotan Zone (Fig. 72). This work provided a new locality and the clear information on the Albian unconformity, directly indicating the subaerial exhumation of the Kamuikotan Metamorphics (Iwashimizu Complex) in Mitsuishi area. High-P/T minerals also occur in conglomerate and pebbly mudstone of the other area in the south Sorachi-Yezo Belt (Fig. 72: Kawamura et al., 2000; this study). The difference in local depositional history is considered to reflect the lateral variation in regional forearc tectonics, *i.e.* degree of unroofing of the high-P/T metamorphosed accretionary complex.

Exhumation process of the Iwashimizu Complex

Serpentinite diapirism was formerly considered as the critical process for exhumation of the Kamuikotan Metamorphics (Niida and Kito, 1986). However, the basal conglomerates of the Middle Yezo Group in this area contain no serpentinite clasts, and eastern part of the present Iwashimizu Complex also contains only scarce serpentinite. These occurrences indicate that the exhumation process of the high-P/T metamorphosed rocks in this area was not serpentinite diapirism, unlike that in the present Mariana forearc (Maekawa *et al.*, 1992). The Iwashimizu Complex was exhumed as a

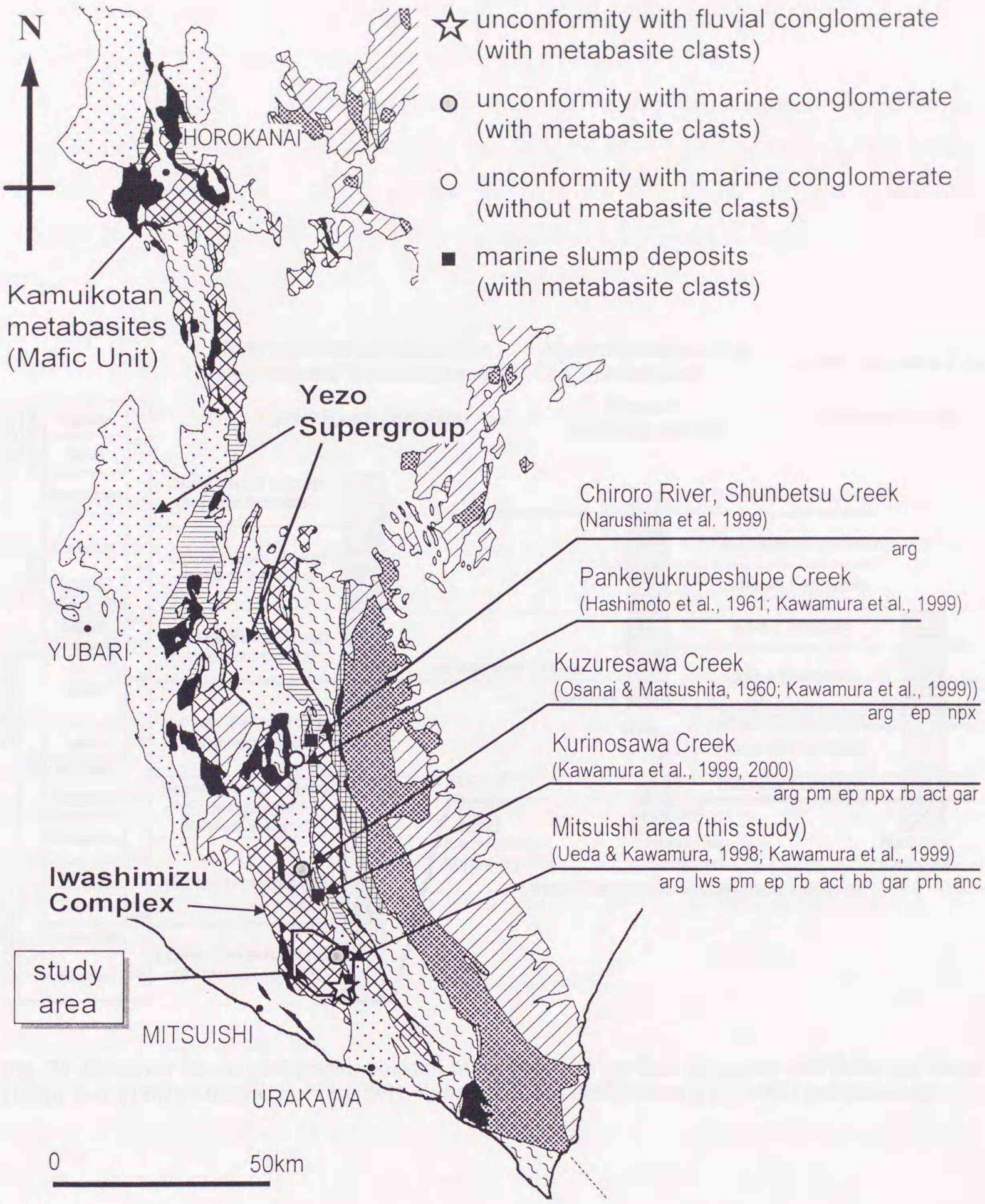


Fig. 72. Distribution of unconformity and metabasite-bearing conglomerates. Metamorphic minerals in metabasite clasts: this study.

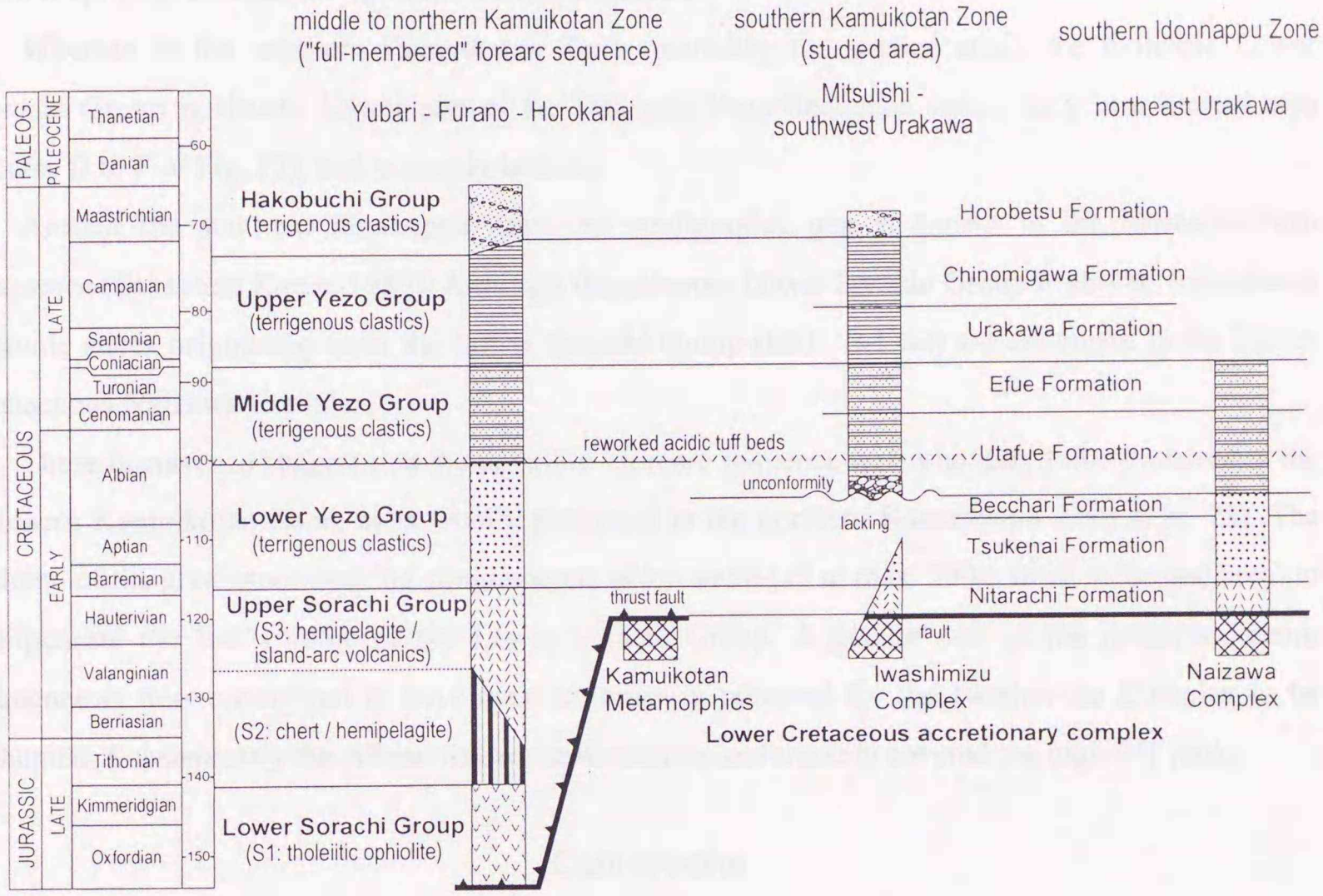


Fig. 73. Schematic tectonostratigraphic columns of the Sorachi-Yezo Belt. Compiled after Sakai and Kanie (1986), Kito (1987), Motoyama *et al.* (1991), Kiminami *et al.* (1992), Wada *et al.* (1992) and this work.

coherent mass of tectonic pile, not as blocks.

Fig. 73 displays a summarized stratigraphic column of this area, compared with that around the central to northern Kamuikotan Zone and the southern Idonnappu Zone.

In the central to northern Kamuikotan Zone, the forearc Nitarachi-Yezo Sequence without internal stratigraphic gap conformably overlies 0.5 to 5 km thick tholeiitic ophiolite of the Lower Sorachi Group (Ishizuka, 1980; Kito, 1987; Kiminami *et al.*, 1992; Kawaguchi, 1997). The high-P/T Kamuikotan accretionary complex tectonically underlies this ophiolite-forearc sequence (Asahina and Komatsu, 1979; Ishizuka, 1980). These occurrences imply that the accretionary complex was metamorphosed beneath the ophiolite-forearc sequence.

Whereas in the southern Kamuikotan Zone (including the studied area), the tholeiitic Lower Sorachi Group is absent. Lower part of the Nitarachi-Yezo Sequence occurs only in a limited area (routes D to F in Fig. 57), and is mostly lacked.

Around the southern Idonnappu Zone, no stratigraphic gap is known in the Nitarachi-Yezo Sequence (Sakai and Kanie, 1986). Although the coherent Lower Sorachi Group is absent, voluminous tectonic slices originating from the Lower Sorachi Group (LST: B-Unit) are contained in the Lower Cretaceous Naizawa Complex.

These occurrence suggest that the ophiolite - forearc sequence was originally full-membered in the southern Kamuikotan Zone, as is wholly preserved in the northern Kamuikotan Zone (Fig. 73). The volume of the greenstone-bearing conglomerate is too small (15 to max. 200m thick in limited area) to compensate the lost volume of the Lower Sorachi Group. A greater part of the ophiolite-forearc sequence is thus considered to have been tectonically removed for the Iwashimizu Complex to be exhumed. Subsequently the Albian forearc sediments unconformably covered the high-P/T rocks.

Conclusions

This chapter is summarized as follows.

(a) Forearc basin deposits of the Nitarachi-Yezo Sequence in the Mitsuishi area comprise the Valanginian-Barremian Nitarachi Formation (Upper Sorachi Group), the Barremian-Aptian Tsukenai Formation (Lower Yezo Group), and the Albian Utafue Formation (Middle Yezo Group).

(b) M_0 Member of the basal Utafue Formation contains fluvial conglomerate, which unconformably overlies the Tsukenai Formation and the high-P/T metamorphosed Iwashimizu accretionary complex.

(c) The conglomerate contains greenstone clasts accompanied by high-P/T metamorphic minerals, and Lower Cretaceous siliceous mudstone clasts. The clastic composition indicates the erosion of both the Iwashimizu Complex and lower part of the Nitarachi-Yezo Sequence.

(d) The Iwashimizu Complex rapidly uplifted over 20 km during 20 m.y. since its accretion, to be

exhumed subaerially. Subsequently it turned to subside gently.

(e) Forearc exhumation of the high-P/T rocks in this area was not due to serpentinite diapir as discussed formerly, but was due to uplift of a coherent accretionary body.

Chapter V. Tectonic evolution of Cretaceous forearc in south central Hokkaido

Comparison of accreted greenstones in central Hokkaido

Petrological types of greenstones in central Hokkaido

Miyashita & Yoshida (1988) and Niida (1992) classified the chemical types of greenstones in central Hokkaido, based mainly on the Sorachi Group and the Hidaka Supergroup. This study described greenstones in the Cretaceous accretionary complexes in the Idonnappu and Kamuikotan Zones (Table 13), and four chemical types (OIA, OIT, LST, and N-MORB) were identified. To summarize previous studies and this work, greenstones in central Hokkaido are classified as follows.

- High-Na/K alkali basalt (Upper Sorachi type basalt: USB)
- Low-TiO_2 tholeiitic basalt (Lower Sorachi type tholeiite: LST)
- Oceanic island type basalt / trachyte (both alkali basalt and tholeiite: OIB)
- N-MORB type tholeiitic basalt (Hidaka type: MORB)

Each geological complex can be characterized by unique assemblages and occurrences of the greenstones of above types. For example, the Sorachi Group is typified by basal ophiolite of LST + autochthonous USB in the forearc sequence, the Iwashimizu Complex by abundant OIB with minor LST both as tectonic slices, and the Hidaka Supergroup by autochthonous MORB ± minor blocks of OIB in the accretionary complex. The Naizawa Complex contains tectonic slices and blocks of LST + OIB; The Horobetsugawa Complex contains sheared MORB + OIB/LST as sedimentary blocks. The Iwashimizu Complex consists mainly of tectonic slices of OIB, partly containing scarce LST. They are all compatible with the above categories. Although these geologic complexes contain greenstones of partly common chemical types with others, they display differing assemblages and modes of occurrence unit by unit, depending mainly on geologic age. Thus, the nature of greenstones can be a key to correlate geological units, as much as other kinds of data such as fossil ages.

Correlation of geological units in the Sorachi-Yezo Belt

1. Late Jurassic to Early Cretaceous forearc sequence (Sorachi Group)

One of the important characteristics of the Sorachi Group in typical sections (Furano and Horokanai areas) is to comprise conformable successions with the forearc basin Yezo Supergroup (Kito, 1987; Kiminami et al., 1992): from Jurassic LST ophiolite, through island-arc volcano-sedimentary complex or hemipelagic mudstone, to siliciclastic sedimentary sequence. Though several sear zones have been reported within the ophiolite (Ishizuka, 1980), no mixed facies made up of different origins (e.g. oceanic basalt, pelagic sediments, and terrigenous clastic sediments), nor thrust

Table 13. Characterization and comparison of petrological types and occurrences of greenstones in central Hokkaido

classification			*occurrences*				
			Sorachi Group	Kamuikotan Zone	Idonnappu Zone		Hidaka Supergroup
				Iwashimizu Complex	**Naizawa Complex**	**Horobetsugawa Complex**	
			forearc basin sequence	accretionary complex			
TYPE	CHEMISTRY	emplacement / eruption AGE	Jurassic - Early Cretaceous[*3, 4]	Early Cretaceous		Late Cretaceous	Early Paleogene[*7,8]
Upper Sorachi type	high-Na_2O/K_2O alkali basalt [*1], island-arc tholeiite[*2]	Early Cretaceous[*3]	*in-situ* in forearc sequence[*3]				
Lower Sorachi -type (LST)	tholeiitic basalt HFS -poor	Late Jurassic[*3, 4]	basal ophiolite of forearc sequence[*5]	small tectonic slices and blocks	large tectonic slices (B)	sedimentary blocks	
oceanic island -type (OIB)	alkali basalt / tholeiite HFS & LIL -rich	(Permian?-) Triassic to Cretaceous[*6,9]		large tectonic slices	tectonic slices and blocks (MN)	sedimentary blocks	sedimentary blocks?[*8, 9]
MORB -type	tholeiite basalt HFS -moderate	Cretaceous to early Paleogene[*7]				tectonic slices in chert-clastic successions	*in-situ* in accretionary complex [*10]

*1: Niida (1992). *2: Nagahashi (1998). *3: Kito (1987). *4: Ishizuka et al. (1983); Kiminami et al. (1992). *5: Asahina & Komatsu (1979); Ishizuka (1980); Kiminami et al. (1985). *6: Sakakibara et al. (1997); and inferred from accompanying chert & limestone ages (see Fig. 36). *7: Watanabe & Iwata (1987: revised age interpretation), Kiminami et al. (1990). *8: Nanayama (1992); Owada et al. (1992). *10: Mariko (1984), Miyashita & Katsushima (1986); Tajika & Iwata (1994); Kiminami et al. (1999).

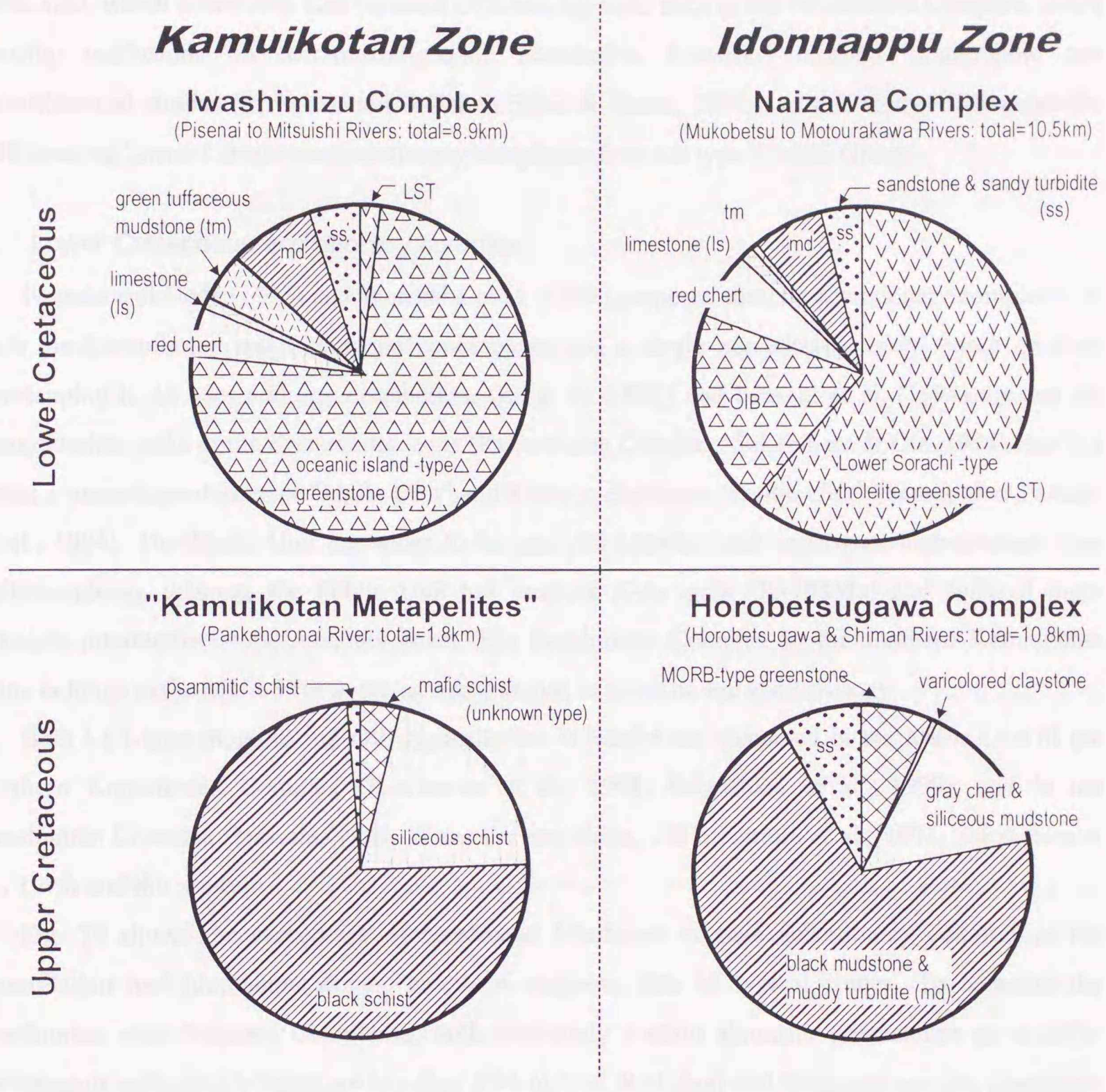


Fig. 74. Volume percentage of constituent lithofacies of accretionary complexes in the Kamuikotan and Idonnappu Zones, based on mapping data along transverse routes. All lithofacies are assumed to occur as sheeted bodies.

imbrication structure such as duplex, have not been reported. Another notable feature is the absence of typical red chert, OIB, and Permo-Triassic pelagic sedimentary rocks such as limestone and chert. The name "Sorachi Group" has been traditionally used for the greenstone-dominant units in central Hokkaido, which sometimes also included OIB-bearing units such as the Iwashimizu Complex, hence causing confusions on tectonostratigraphic correlation. However, detailed stratigraphic and petrochemical studies (引用 Kontani & Sakai; Sakai & Kanie, 1986; and this study) distinguish the OIB-bearing Lower Cretaceous accretionary complexes from the type Sorachi Group.

2. Lower Cretaceous accretionary complex

Iwasaki and Ueda (1993) and Watanabe et al. (1994) proposed that the accretionary complexes in both the Kamuikotan and Idonnappu zones comprised a single accretionary body, based on their overlapping K-Ar ages and age distribution. Ota et al. (1993) and Iwasaki et al. (1994) divided the metamorphic rocks of the Kamuikotan zone (Kamuikotan Complex: Sakakibara & Ota, 1994) into two units; a greenstone-dominant "Mafic Unit" and a clastic-dominant "Pelitic Unit" (names after Iwasaki et al., 1994). The Mafic Unit has older K-Ar ages (90-135Ma), and underwent high-pressure type metamorphism, whereas the Pelitic Unit has younger K-Ar ages (50-108Ma) and suffered high-pressure intermediate type metamorphism. The Iwashimizu Complex in the southern Kamuikotan Zone belongs to the Mafic Unit in the category above, in terms of age and lithology.

Both LST-type tholeiite and OIB-type alkaline volcanics are contained in the Mafic Unit of the northern Kamuikotan Complex (Kawamura et al., 1998; Sakakibara et al., 1999), and in the Iwashimizu Complex (Nakano, 1985; Watanabe and Niida, 1987; Kimura et al., 1994; Sakakibara et al., 1999; and this study).

Fig. 74 shows the percentage of constituent lithofacies in each accretionary complex in the Kamuikotan and Idonnappu Zones, based on mapping data of typical routes. To compare the Iwashimizu with Naizawa Complexes, both commonly contain abundant greenstones up to 80%. Terrigenous sedimentary rocks are less than 20% in total. Red chert and limestone are also commonly contained. Thus, the constituent lithofacies and their proportions are quite similar. The difference between the two complexes is their LST/OIB ratios. It is possible to consider that it reflects the difference in structural depth where they formed: re-accreted volume of tectonically eroded material (LST) decreases in proportion to the subducted depth if based on the tectonic erosion model (Fig. 25).

Both complexes contain chert and clastic sediments ranging Triassic to Lower Cretaceous (See Fig. 36). The radiolarian ages from terrigenous clastic rocks, regarded as the timing of accretion, range in the late Valanginian - early Barremian time in both complexes. Therefore, the Iwashimizu and Naizawa Complex are concluded to have formed simultaneously.

Radiolarian and K-Ar ages, lithological assemblage, and chemical types of contained greenstones,

all are thus common in the two complexes, clearly supporting the correlation of Iwasaki and Ueda (1993). In detail, the study area, the OIB-type greenstones commonly occur in all units in the Iwashimizu Complex, whereas the LST greenstones limitedly occur in the Pirashuke and Mikawa Units. Thus, these two units are likely to be more closely correlative to the Naizawa Complex than the rest Shizunai and Futagawa Units.

This correlation suggests that the Naizawa Complex in the Idonnappu Zone represents the shallower (low-grade metamorphosed) and near-toe part of a Cretaceous accretionary prism, and the Iwashimizu Complex and the "Mafic Unit" of the Kamuikotan Zone the deeper (high-grade metamorphosed) part nearer the arc (Fig. 56). Moriya et al. (1998) described a P-wave velocity model across the Urakawa area, in which ca. 5.4 km/sec layer consisting of the Iwashimizu Complex in the Kamuikotan Zone also underlies the Nitarachi-Yezo Sequence in the Eastern Yezo Zone, and extends to the Idonnappu Zone. I thus consider that the Cretaceous accretionary complexes are widely distributed beneath the forearc basin sequence in the Sorachi-Yezo Belt (Fig. 75), and the present "Kamuikotan Zone" and the "Idonnappu Zone" represents the sectors where they are exhumed. Since the accretionary complex in the Kamuikotan Zone is one of the main constituents of the Sorachi-Yezo Belt, that in the Idonnappu Zone is also its constituent. The Idonnappu Zone is thus regarded as a sub-belt of the Sorachi-Yezo Belt. The eastern margin of the Idonnappu Zone is defined by the Hidaka Western Boundary Thrust or the Hidaka Main Thrust in southern Hokkaido. However, this margin is not clear in central to northern Hokkaido.

3. Upper Cretaceous accretionary complex

Greenstones in deformed chert-clastic facies of the PT-Unit, Horobetsugawa Complex show the MORB-type chemical characteristics common with greenstones in the Hidaka Belt (*e.g.* Tomuraushi), in having higher TiO_2 (1.6-2.0 wt%), which increases with differentiation (Fig. 17). In the Hidaka Belt, *in-situ* occurrences of N-MORB greenstones are reported from the Paleogene clastic complex, being attributed to subduction of an oceanic spreading center (Miyashita *et al.*, 1997).

Most greenstones in the PT-Unit are severely sheared occurring at the basal part of chert-clastic successions. The radiolarian age from reddish siliceous mudstone overlying the greenstone suggests that the age of the greenstone is approximately Albian, 20-30Ma older than the age of the accretion. It is thus considered that the N-MORB and related sediments in the Horobetsugawa Complex were emplaced by accretion in the Late Cretaceous, and by *in-situ* eruption in the early Paleogene.

Greenstone compositions in the PT-Unit are also similar to those of the Poroshiri Ophiolite (Fig. 17). The Poroshiri Ophiolite displays an almost complete ophiolitic sequence (Miyashita, 1983), neighboring east from the northern extension of the Horobetsugawa Complex (Koiboku Sub-belt; Kiyokawa, 1992), namely, the former originally underlay the latter. Miyashita *et al.* (1997)

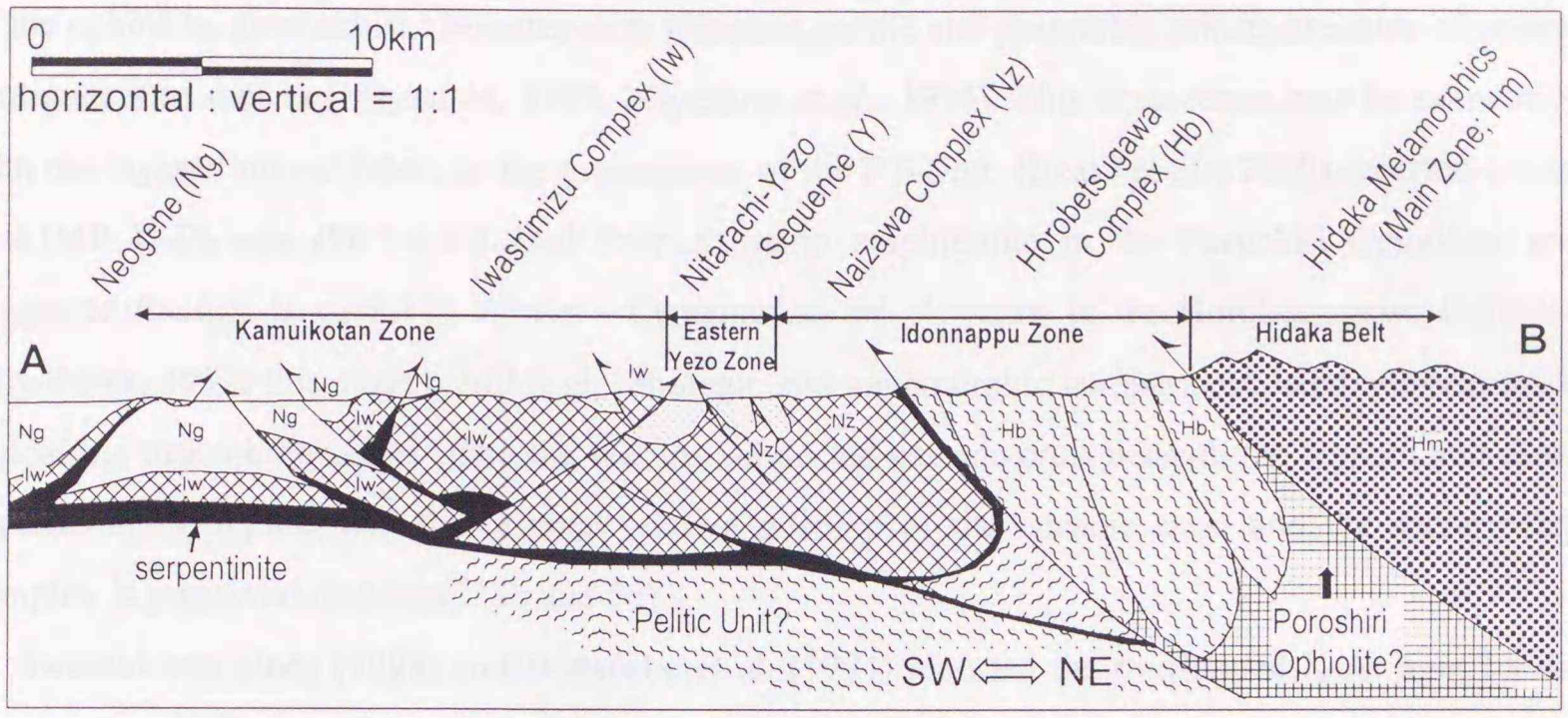


Fig. 75. Cross section of the southern Sorachi-Yezo Belt. Section line shown in Fig. 1. Reference data: Sakai and Kanie (1986), Wada et al. (1992); Arita et al. (1998), Moriya et al. (1998), and this study.

demonstrated a lithologic transition from the Poroshiri Ophiolite to the Koiboku Sub-belt. At the top of the ophiolite, greenschist alternates with siliceous, pelitic and psammitic schists at scales of several centimeters to meters (Miyashita, 1983, Miyashita *et al.*, 1994). This occurrence may be correlative with the layered mixed fabric in the greenstones of the PT-Unit. Kizaki et al. (2000) reported zircon SHRIMP U-Pb age (96.7±2.6 Ma) from a quartz amphibolite in the Poroshiri Ophiolite, and suggested the age is coeval to Albian - Cenomanian red claystone in the Horobetsugawa Complex (Kiyokawa, 1992; this study). Although lithologic and metamorphic comparisons need more study, It is possible that the Poroshiri Ophiolite was the subducted oceanic crust beneath the Upper Cretaceous accretionary complex, and the original relative position of the oceanic crust and the accretionary complex is preserved (see Figs. 25b and 56).

Iwasaki and Ueda (1993) and Watanabe et al. (1994) reported the overlapped K-Ar ages (white mica) of pelitic rocks from the Horobetsugawa Complex (PT-Unit) and the Pelitic Unit along Pankehoronai River in Biei-Ashibetsu area (northern Kamuikotan Zone). They considered that the both units comprised a single Upper Cretaceous accretionary body. The Pelitic Unit consists mainly of pelitic schist, but also contains intercalated chert and greenschist layers and rare limestone (Maekawa, 1983; Iwasaki et al., 1994). The assemblage and percentage of constituent lithofacies (Fig. 74) are very similar to those of the PT-Unit in the Horobetsugawa Complex, supporting their idea. Thus, this study also correlates the Pelitic Unit and the Horobetsugawa Unit as displayed in Fig. 56. Chemical data of metabasites in the Pelitic Unit, and age of sedimentation also, are needed to verify this correlation in future.

The southern Kamuikotan Zone is mostly occupied by the Iwashimizu Complex, and there is no pelitic schist directly correlated with the Pelitic Unit. However, recently Kawamura et al. (in press) reported aragonite + sodic pyroxene + pumpellyite assemblage from the "undivided Hidaka Group" (Takahashi and Suzuki, 1978) occurring in the north part of the southern Kamuikotan Zone. This unit, emended as the Ganpiyama Complex by Kawamura et al. (in press), consists dominantly of foliated mudstone and broken alternation of sandstone and mudstone, with subordinate amount of chert, varicolored siliceous mudstone, and greenstone. Latest Albian to Cenomanian radiolarian fossils have been reported from black mudstone and red claystone by Agency of Natural Resources and Energy of Japan (1989). One analyzed greenstone shows the MORB-type chemical feature (Katoh et al., unpublished data). This Ganpiyama Complex is considered to be a lower-grade facies of the Pelitic Unit, in terms of lithologic feature, younger age, and existence of high-P/T metamorphic minerals. Tectonostratigraphic relation between the Ganpiyama and Iwashimizu Complex is not yet understood.

Reconstruction of Cretaceous forearc wedge

The correlation discussed above is summarized in Fig. 56. Tectonostratigraphic comparison between Idonnappu Zone, both the northern and southern Kamuikotan Zone, and the Nitarachi-Yezo Sequence in adjacent areas allow a reconstruction of the forearc crust in the Late Cretaceous time (Fig. 76c: please compare with Fig. 56).

The uppermost part of the forearc is covered by the Nitarachi-Yezo Sequence several kilometers thick. The sequence is underlain by ophiolite of the Lower Sorachi Group in the northern Kamuikotan Zone (ca. 5km: Ishizuka, 1980). Whereas it is underlain by the greenstone-dominant Lower Cretaceous accretionary complex (Naizawa and Iwashimizu Complexes: 4 to over 6km) in the southern Kamuikotan and the Idonnappu Zones. In the northern Kamuikotan Zone, Lower Cretaceous accretionary complex underlies the Lower Sorachi Ophiolite. The difference in units underlying the Nitarachi-Yezo Sequence may reflect two factors. One is the effect of disruption of the ophiolite due to the seamount collision/subduction, which were prominent at near-toe side of the wedge, *i.e.* the Idonnappu Zone. Another is degree of exhumation of the Iwashimizu Complex equivalents, which selectively progressed in the southern Kamuikotan Zone.

In the Idonnappu Zone and the northern Kamuikotan Zone, the clastic-dominant Upper Cretaceous accretionary complex structurally underlies the Lower Cretaceous accretionary complex (5-5.5km thick in the Idonnappu Zone). Thus, the upper 15 to 20km sections of the forearc crust are reconstructed, as displayed in Figs. 56 and 76. The scheme indicate that the forearc was composed of three nappe sheets; the Jurassic Lower Sorachi Ophiolite, Lower Cretaceous accretionary complex, and Upper Cretaceous accretionary complex in descending order. Each nappe sheet is ca. 5km thick or more, and is bounded by faults accompanied by serpentinite (Fig. 56).

Kiyokawa (1992) showed an eastward younging trend of fossil aged in the Idonnappu Zone, and considered it indicating a trench-ward growth of accretionary complex. He considered that the Iwashimizu Complex was older than accretionary complexes in the Idonnappu Zone. However, Recent radiolarian data (Hori & Sakakibara, 1994; this study) indicate that formation of both the Iwashimizu Complex and the Naizawa Complex are coeval. The examination of illite crystallinity and radiolarian ages in this study, with K-Ar ages by Iwasaki & Ueda (1993) and Watanabe et al. (1994) together, revealed that the trend rather indicates younging structurally downward. A structurally downward-younging trend of K-Ar ages is reported within the northern Kamuikotan Zone (Sakakibara and Ota, 1994; Ota, 1999). Therefore, The pile-nappe structure discussed above is considered suggesting a forearc crustal evolution structurally downward by underplating, rather than ocean-ward frontal accretion (Fig. 76).

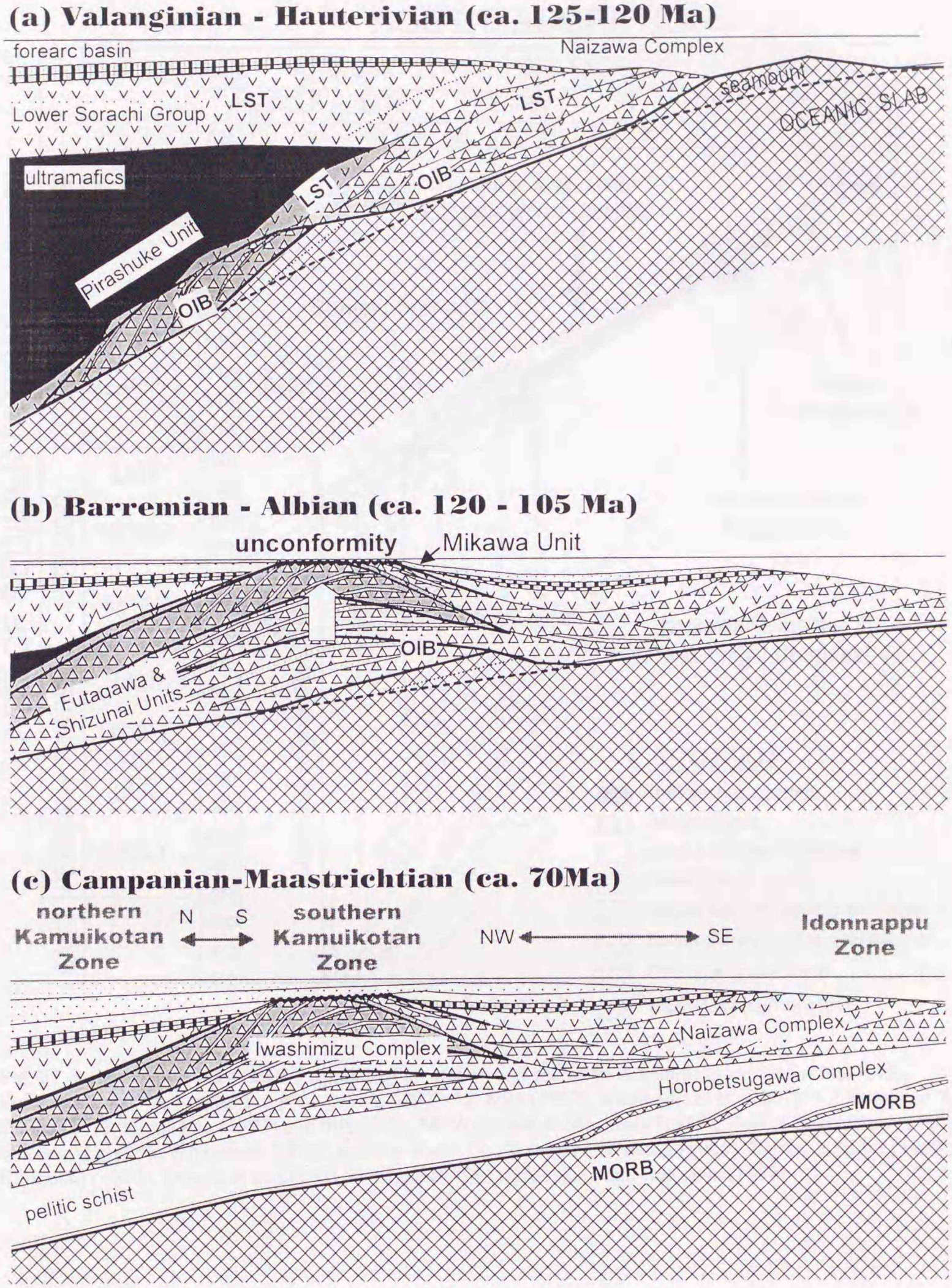


Fig. 76. Restored cross section of the Cretaceous forearc in south central Hokkaido

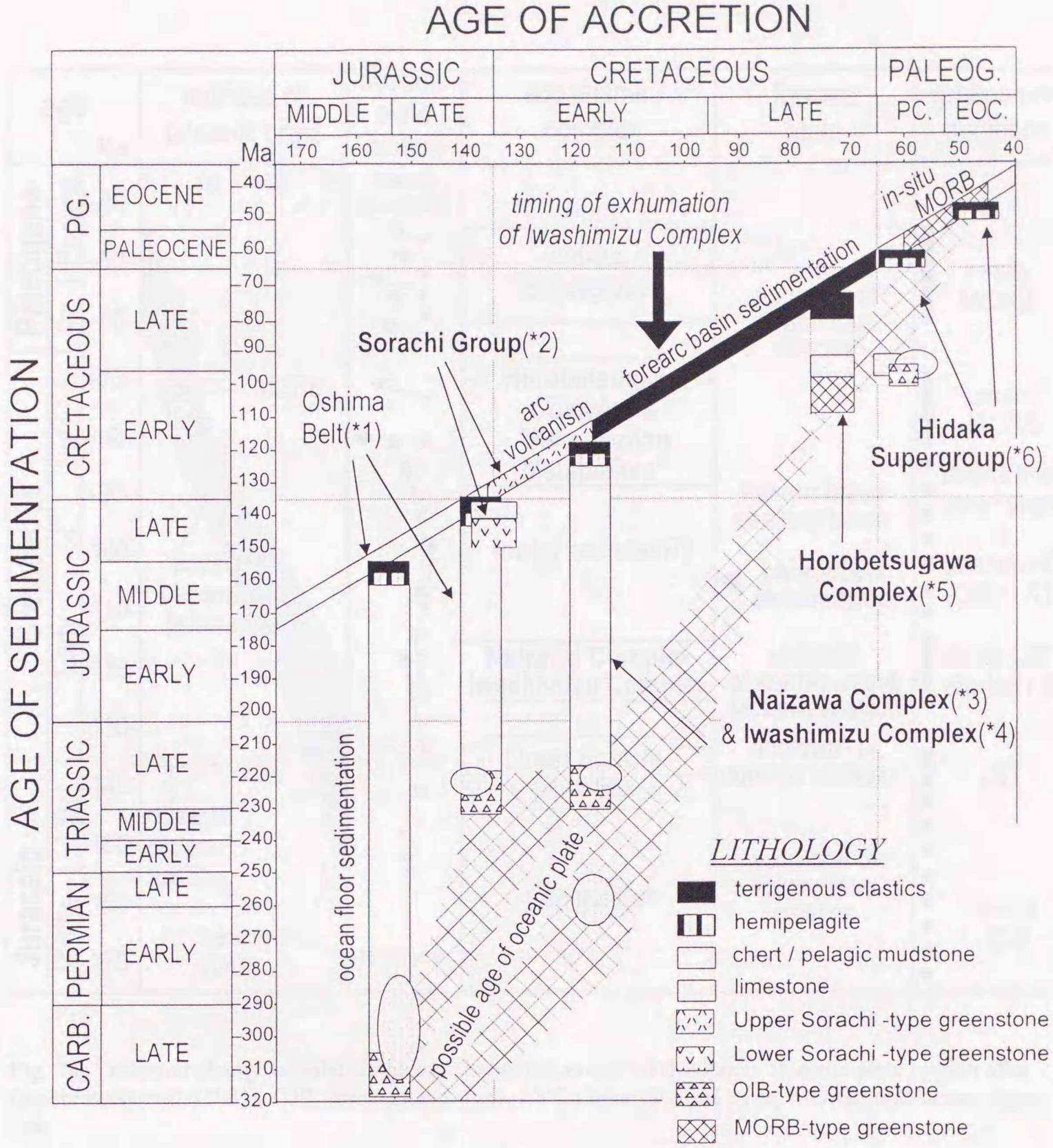


Fig. 77. Relationships between the age of sedimentation and accretion in central to southwest Hokkaido. Reference data: *1: Kawamura et al. (1986, 1997), *2: Kito (1987), Kiminami et al. (1992), *3: Sakagami & Sakai (1979), Kiyokawa (1992) and this study, *4: Watanabe & Maekawa (1985), Hori & Sakakibara (1994) and this study, *5: Kiyokawa (1992) and this study, *6: Watanabe & Iwata (1985), Tajika & Iwata (1990), Kiminami (1990), Owada et al. (1992), Nanayama, 1992, Nanayama and Ganzawa (1997).

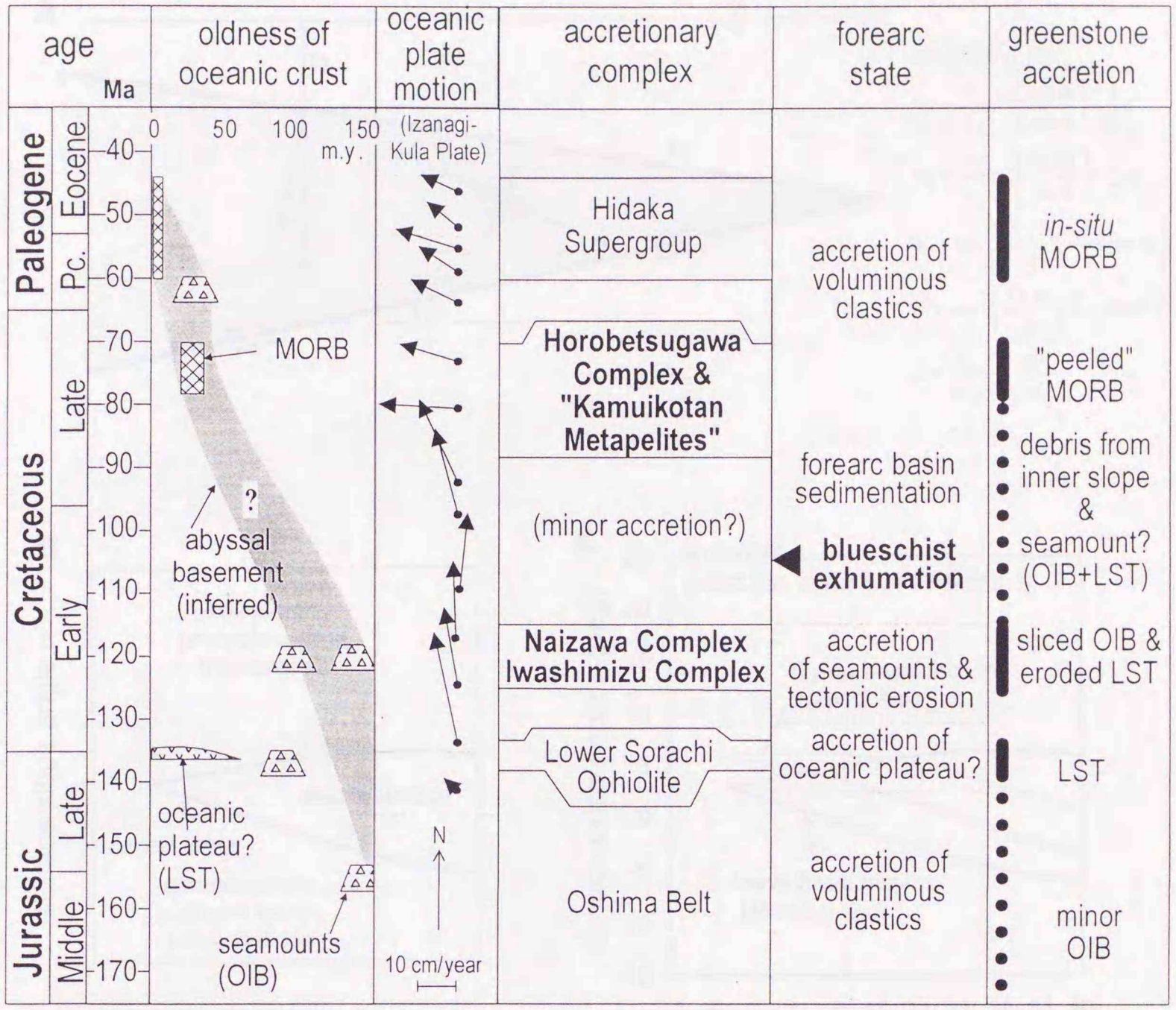
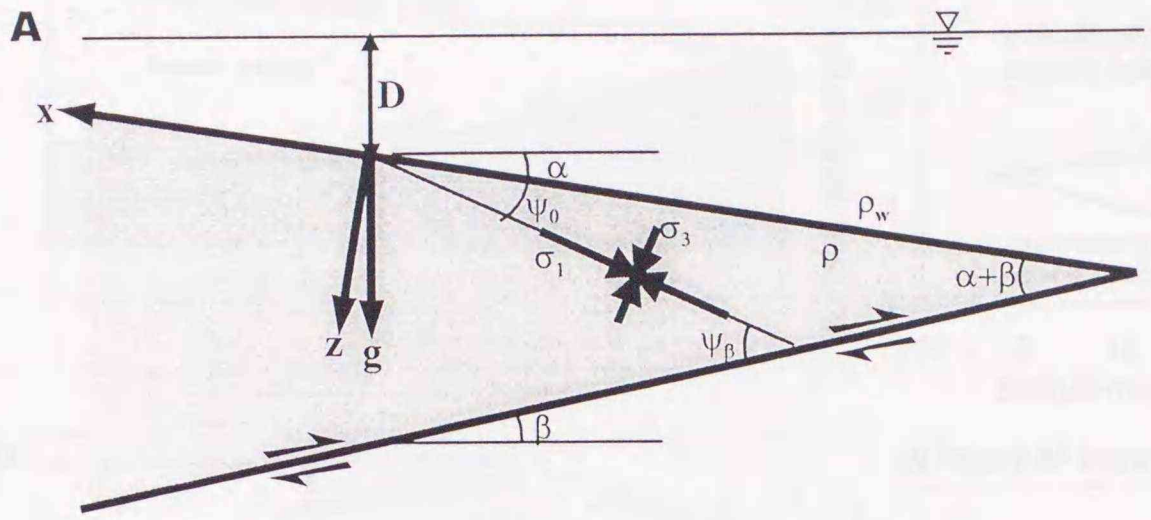


Fig. 78. Temporal change in subduction zone condition in central Hokkaido. Oceanic plate motion after Engebretson et al. (1985). OIB: ocean island -type, LST: Lower Sorachi -type, MORB: mid-ocean ridge -type



$$\alpha + \beta = \Psi_b - \Psi_0$$

$$\Psi_0 = \frac{1}{2}\sin^{-1}\left(\frac{\sin\alpha}{\sin\phi}\right) - \frac{1}{2}\alpha'$$

$$\Psi_b = \frac{1}{2}\sin^{-1}\left(\frac{\sin\phi_b}{\sin\phi}\right) - \frac{1}{2}\phi_b'$$

$$\phi_b' = \tan^{-1}\left(\frac{1-\rho_w/\rho}{1-\lambda}\times\tan\phi_b\right)$$

$$\alpha' = \tan^{-1}\left(\frac{1-\rho_w/\rho}{1-\lambda}\times\tan\alpha\right)$$

$$\lambda = \frac{p_f - \rho_w g D}{|\sigma_z| - \rho_w g D}$$

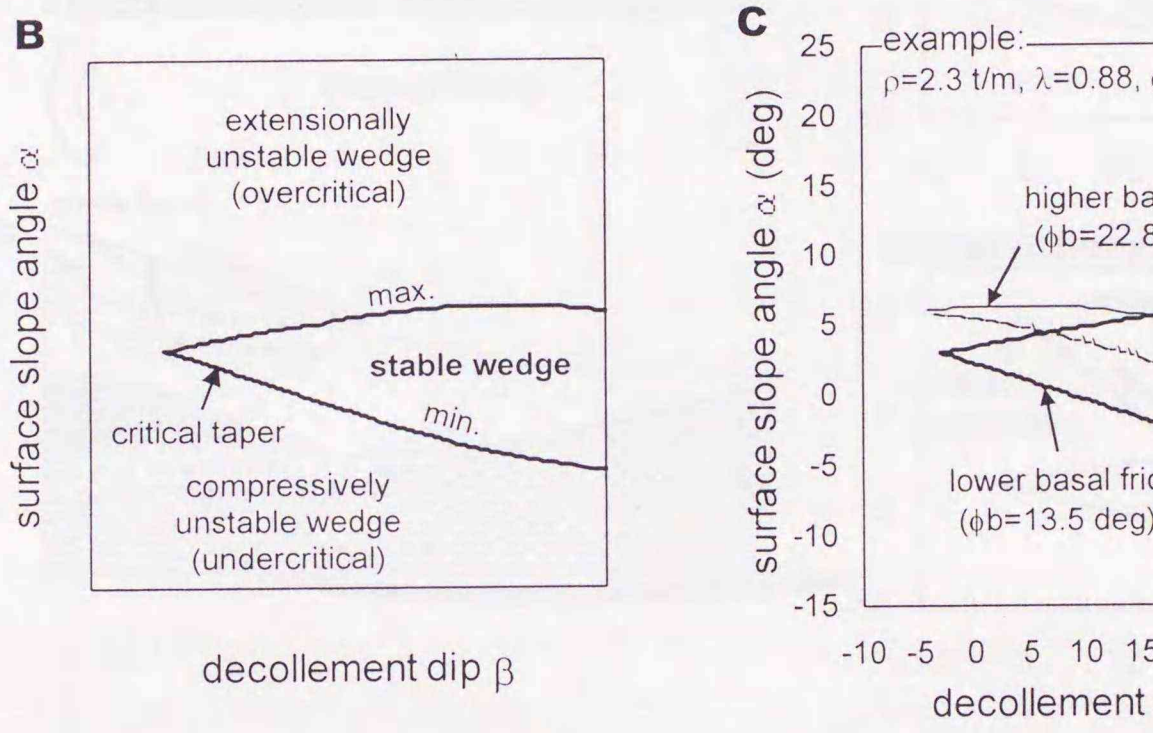


Fig. 79. Outline of the non-cohesive critical Coulomb-wedge model by Dahlen (1984). (A) Cross-sectional sketch of a submarine noncohesive critical wedge (modified from Dahlen, 1984). Critical taper ($\alpha+\beta$) depends on density of the wedge material (ρ) and water (ρ_w), pore pressure ratio (λ), internal friction angle in wedge (ϕ) and in decollement (ϕb). p_f: pore pressure, g: constant acceleration of gravity, D: depth from the sea surface, and $|\sigma_z|$: lithostatic pressure. (B): Stable and unstable slope angle (α), at given decollement dip (β) and other parameters ρ, λ, ϕ. and ϕ_b. (C) Comparison of stability fields at different ϕb and constant ρ, λ, and ϕ. The example values of the latter three parameters and ϕb=13.5 deg are after Lallement et al. (1996).

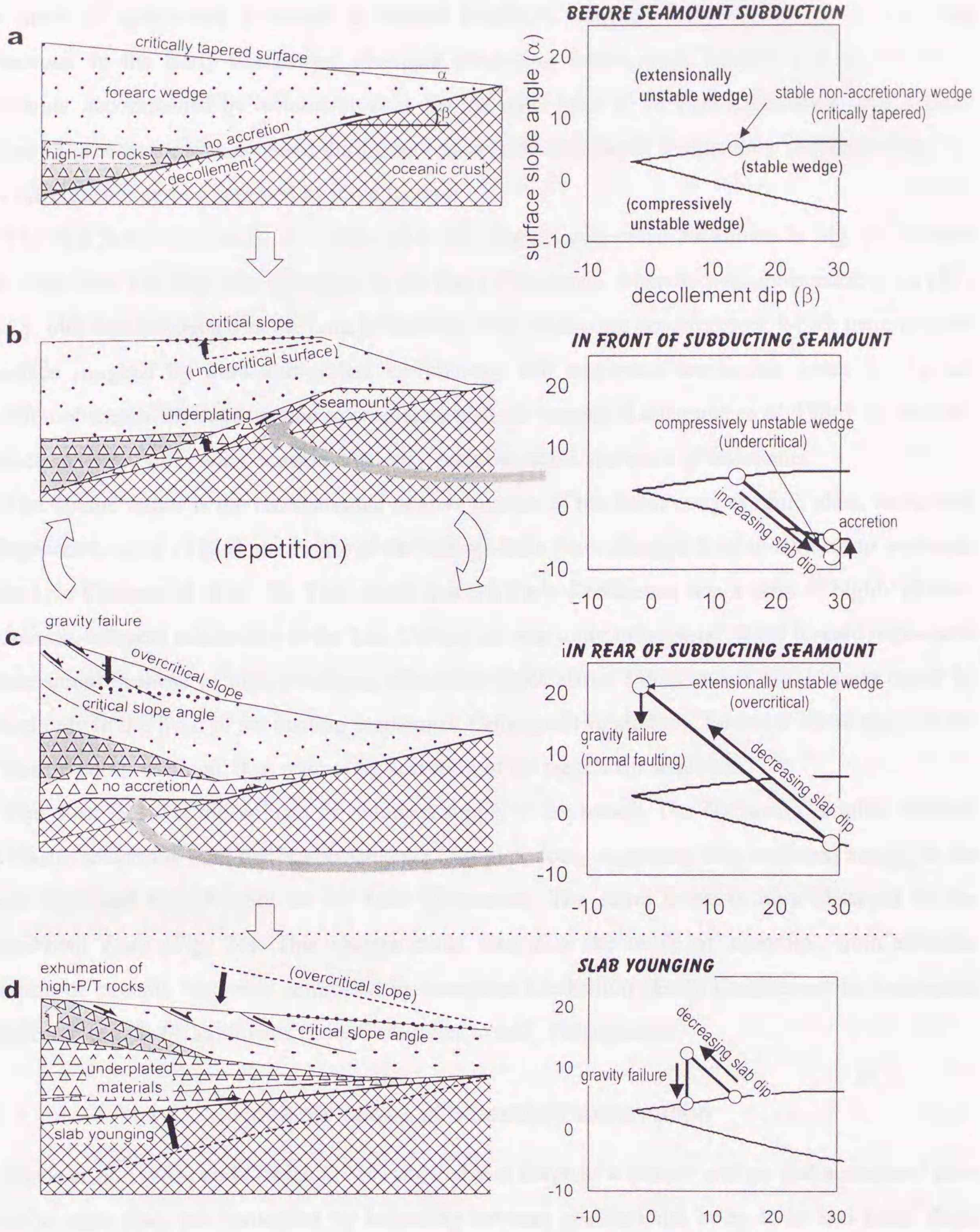


Fig. 80. "Seamount-jack-up" model for accretion and exhumation of the Iwashimizu Complex, explained by the Coulomb-wedge model (Dahlen, 1984). Topographic change are calculated based on kink-geometry (Suppe, 1983), with roughly assumed volume of accreted materials. Note that the Coulomb-wedge geometry does not depend on the scale (Davis et al., 1983), and need an assumption that the wedge wholly lies within the brittle field. Example of stable field shown is calculated after Dahlen (1984), using the parameters (Fig. 79C with ϕ_b=13.5 deg) proposed by Lallement et al. (1996) based on bathymetry and thrust geometry of present forearc wedges.

Temporal change in mode of greenstone accretion

The mode of greenstone accretion in central Hokkaido contrasts between the Early and Late Cretaceous. In the Early Cretaceous, abundant greenstone bodies were accreted via subduction of seamounts, accompanied by tectonic erosion. On the other hand in the Late Cretaceous, only a small volume of greenstone was accreted during accretion of the trench-fill sedimentary sequence (Fig. 74). This difference may be explained by three factors.

The first factor is contrast in oldness of subducting oceanic crust. As shown in Fig. 77, oceanic crust older than 100 m.y. was subducted in the Early Cretaceous, whereas younger oceanic crust (20 - 30 m.y. old) was subducted in the Late Cretaceous. Old subducting oceanic crust, which generally has a surface roughed by horst-and-graben morphology and numerous seamounts, tends to obstruct accretion of trench-fill deposits and to accelerate tectonic erosion (Lallemand *et al.* 1996). In contrast, subduction of smooth young oceanic crust may promote stable accretion of sediments.

The second factor is the reconstructed relative motion of the subducting oceanic plate. According to Engebretson *et al.* (1985), the vector of the Izanagi-Kula Plate changed from northward to westward in the Late Cretaceous (Fig. 78). This shows that the Early Cretaceous was a time of highly oblique subduction, whereas subduction in the Late Cretaceous was more orthogonal. If the forearc region was transtensional because of highly oblique subduction (McCaffrey 1992), thrust faults could easily be formed only in the front of subducting seamounts. Orthogonal subduction, however, more easily make the forearc compressional, thus promoting accretion of the trench-fill sequence.

The third factor is the volume of sediment supply to the trench. The Naizawa Complex contains less clastic sediments than the Horobetsugawa Complex does, suggesting that sediment supply to the trench increased considerably in the Late Cretaceous. The same trend is also observed in the Kamuikotan Zone (Fig. 74). This change could also alter the mode of accretion, from episodic accretion of oceanic materials controlled by seamount subduction (Early Cretaceous) to continuous accretion of trench-fill sediments (Late Cretaceous to early Paleogene).

Possible cause of blueschist exhumation

Davis *et al.* (1983) and Dahlen (1984) showed that shape of a forearc wedge, and accretion / non-accretion state also, are controlled by balancing between gravitational body force and basal shear traction by subducting slab. The balanced and stable wedge taper has been called as "critical taper" (Fig. 79). Their theory indicated that decrease of slab dip, which is usually caused by younging of subducting oceanic crust, promotes forearc overcritical (unstable with too thick wedge for newly given decollement dip). Thus, an extensional tectonics is to be dominated thinning the wedge (Fig. 80d). Iwasaki *et al.* (1995) described that metamorphic pressure of the Kamuikotan Metamorphics decreased

from Early Cretaceous to early Paleogene whereas temperature increased simultaneously, and considered that the occurrence was due to younging of subducting oceanic crust. The pile-nappe structure with inverted metamorphic grade in the Iwashimizu Complex implies more short-time decrease in slab dip accompanied by unroofing. Hence, decrease of slab dip is considered to be one of the critical processes for exhumation of the Iwashimizu Complex. Similar style of exhumation process is known in the modern Cascadia Margin, North America, where high-P/T rocks of the Miocene Olympic Core Complex is currently exhumed and uplifting, beneath which Wadachi-Benioff zone is shallower than surrounding area (Brandon and Calderwood, 1990). The decrease of slab dip also simply lifts up the wedge materials. A decrease of orthogonal convergence rate, which reduces basal shear traction, may help the overcritical extensional tectonics.

McCaffrey (1992) indicated that oblique subduction of oceanic plate can promote trench-parallel extension, and pointed out a possibility for exhumation of high-P/T rocks. Although modern highly oblique convergent margins such as Sunda, Aleutian, and Kurile arcs are extensional, but depression is dominated in forearc region (Huchon and Le Pichon, 1984; Kimura, 1986; Geist *et al.*, 1988). Hence, even if high-P/T rocks could be unroofed, they might not be able to reach to sea surface by oblique subduction alone.

Another important possible cause is the "jack-up model" proposed by Platt (1986). After this model, continuous underplating thickens the wedge and increases the surface slope dip, causing a gravity failure of the overcritically tapered wedge. Hence, a high-P/T unit can be detached from the wedge bottom, lifted up by younger underplated materials, then able to reach to the wedge surface among extensionally torn forearc basin deposits.

Kawamura *et al.* (1999) considered that the unconformity was formed by uplifting of the forearc basin due to the local underplating of subducted seamount volcanics. If voluminous greenstones were underplated successively, the Pirashuke Unit accreted earlier may have been “jacked up” by subsequently underplated greenstones (Fig. 76), and overlying low-grade unit (probably the Lower Sorachi Ophiolite) can be tectonically removed by gravity failure of the forearc wedge, as proposed by Platt (1986). The south Kamuikotan Zone (Iwashimizu Complex) is characterized by the abundant occurrence of oceanic island-type greenstones. The Shizunai Unit in Niikappu area shows K-Ar ages ranging 90- 110 Ma (white mica in pelitic rocks from the Niikappu area; Iwasaki *et al.*, 1995; see Fig. 36), which overlaps the Albian unconformity event. These occurrences may support application of the "seamount jack-up model" to the Iwashimizu Complex exhumation. The model can also explain the local and abnormally rapid exhumation, considering subduction of a seamount chain.

Thus the model seems to well explain the tectonostratigraphic occurrence of units in central Hokkaido (Fig. 76). However, it still has a problem that it is hard for the trust-driven underplating to occur beneath such overcritically extensional wedge, because decollement may also be extensional

and thrust faults could not form (Dahlen, 1984). The problem may be solved if considering overcritical / undercritical regime during seamount subduction proposed by Lallement and Le Pichon (1987). They applied the critical Coulomb-wedge model to comprehend the bathymetric features around the currently subducting Daiichi-Kashima and Erimo Seamounts in Japan Trench. This theory can also explain accretion and exhumation of greenstones during repetitive seamounts subduction (Fig. 80). Initially critical wedge (Fig. 80a) becomes undercritical (unstable with too thin wedge for newly given decollement dip) in front of a subducting seamount (Fig. 80b), allowing underplating mainly of greenstones cut by thrust faults. Subsequently, the wedge immediately becomes overcritical in rear of the seamount (Fig. 80c), suffering extensional failure. This "seamount jack-up model" can thus promote nearly simultaneous faulting of both reverse and normal sense, *i.e.* underplating and unroofing. Probably a repetition of such process in several times is needed for a high-P/T metamorphosed unit to reach to the sea surface. This process may be accelerated if there are scarce sediments above the seamounts, because the stability field of wedge gets narrower as its basal friction increases (Fig. 79C). Hence, the oscillatory change between compressive and extensional states must be achieved more easily.

This theory can be applied only to brittle field, at most the depth where the Futagawa unit was formed. To explain the exhumation of whole Iwashimizu Complex, introduction of ductile deformation to this theory is needed for future study.

Conclusions

(1) There is a relation between age of accretionary complex and mode of occurrence / chemical character of greenstones. The Lower Cretaceous Naizawa and Iwashimizu Complex contain both OIB and LST greenstones as tectonic slices and blocks. The Upper Cretaceous Horobetsugawa Complex contains a small amount of MORB greenstones severely sheared. These greenstones are distinguished from basal ophiolite of forearc basin (Jurassic Lower Sorachi Group) and *in-situ* MORB greenstones in the Paleogene Hidaka Supergroup.

(2) These correlation and tectonostratigraphic comparison between the Kamuikotan and Idonnappu Zones leads a reconstruction of the Cretaceous forearc wedge of the Sorachi-Yezo Belt (Fig. 76). The wedge is considered to comprise a pile-nappe structure made up of Jurassic ophiolite, Lower Cretaceous accretionary complex, and Upper Cretaceous accretionary complex, suggesting a structurally downward growth by underplating accretion.

(3) The difference indicates a temporal change in accretion style of greenstones, which may reflect change in conditions of subducting oceanic crust during the Cretaceous time. The highly oblique subduction of the old oceanic crust, with limited sediment supply, led to

dominant seamount accretion and tectonic erosion in the Early Cretaceous. Contrasting near-orthogonal subduction of young oceanic crust, coupled with voluminous sediment supply, promoted accretion of thick sediments with minor MORB and olistostrome in the Late Cretaceous.

(4) The exhumation event of the Iwashimizu Complex occurred during the transition between two styles described above. To take age, petrologic, and stratigraphic data into account, there are two major possible causes for the exhumation. The younging of oceanic crust may shallow the accretion depth, decrease the slab dip, and consequently cause an extensional thinning of overlying units. Another cause is repetitive subduction of seamounts: the voluminous underplating of greenstones in front of subducting seamounts lift up the earlier accreted units; and gravity failure in rear of seamounts thins the overlying forearc sequence.

Acknowledgments

This study stands on various supports by following people. Dr. M. Kawamura of Hokkaido University led me to study accretion tectonics, and gave many suggestions as the primary supervisor. Prof. H. Okada and Emeritus Prof. M. Kato of Hokkaido University gave me many suggestions during this study. Prof. T. Watanabe of Hokkaido University lectured on metamorphic petrology and petrography, and gave many suggestions on K-Ar ages and relationship to the Kamuikotan Complex. Prof. S. Miyashita of Niigata University gave many suggestions on greenstones in Hokkaido and "greenstonology", and I had fruitful discussions with members of the petrology and structural geology seminar of Niigata University. Dr. K. Niida of Hokkaido University gave many suggestions on greenstones in the Sorachi-Yezo Belt, an on structural framework of the Kamuikotan Zone. Dr. K. Iwata suggested me to determine radiolarian ages. Dr. K. Yoshida (Shinshu Univ.) and Mr. G. Kawakami (Hokkaido Univ.) gave many suggestions on sedimentology of the Yezo Supergroup. Mr. T. Narushima (Hokkaido Univ.) gave me many informations about stratigraphy of the Nitarachi-Yezo Sequence. Dr. B. Roser of Shimane University had critical readings on the chapter of Idonnappu Zone, and gave me suggestions during our field work, his readings, and also my stay in his home. Dr. M. M. Buslov of the United Institute of Geology, Geophysics and Mineralogy, Novosibirsk for his very useful suggestions on post-accretion tectonics, and perhaps taught me the spirits of field workers during two-weeks excursion in Gorny Altai. Dr. K. Arita of Hokkaido University gave me much information on deep structure of Hidaka Mountains. Mr. A. Sakai (Geological Survey of Japan) gave his advice during my fieldwork. Drs. Y. Hikida (Nakagawa Museum of Natural History) and M. Kano (Mikasa City Museum) gave suggestions on molluscan fossils. Dr. M. Nakagawa of Hokkaido University gave many facilities for XRF analysis. Messrs. S. Terada and M. Ikeda of Hokkaido University gave many facilities and helps for XRF, EPMA, and XRF analysis. Mr. T. Kudo and Dr. M. Miyasaka (Amma) of Hokkaido University, and Mr. S. Sato of Hokkaido Doshitsu Consultant Co. Ltd. also lectured me on XRF and EPMA analysis. Messrs. T. Kuwajima and H. Nomura of Hokkaido University helped and advised me on thin section preparation.

I had fruitful discussions with: Dr. I. Iwasaki of Tokyo University on evolution of both the Kamuikotan and Idonnappu Zones, and Cretaceous subduction zone in central Hokkaido (he invited me into the Kamuikotan Zone), Drs. T. Katoh (Earth Science Co. Ltd.), M. Nakagawa (Geological Survey of Japan), and members of the Hidaka Convergent Margin Research Group on geology and tectonics of the southern Sorachi-Yezo Belt, Dr. K. Kizaki (Earth Science Co. Ltd.) on relation between the Poroshiri Ophiolite and the Idonnappu Zone. He also lectured me on amphibole chemistry. Thanks are also due to: Dr. F. Nanayama of Geological Survey of Japan for his suggestions on tectonics in Hokkaido; Mr. T. Terada of Ministry of agriculture, forestry and fisheries of Japan for

many overnight discussions on structural geology. Messrs. T. Higake (Deceased in 1999), M. Yamazaki (Shin Engineering Consultant co. ltd.) and members of the Earth Science Co. Ltd. encouraged me during my study.

References

A

Agency of Natural Resources and Energy of Japan, 1989, Report of the research on storage conditions of rare-metal mineral resources: the south Hidaka district. Ministry of International Trade and industry, 119p.

Aita, Y. and Okada, H., 1986, Radiolarians and calcareous nannofossils from the uppermost Jurassic and Lower Cretaceous strata of Japan and Tethyan regions. *Micropaleontology*, **32**, 97-128.

Aita, Y., 1987, Middle Jurassic to Lower Cretaceous Radiolarian Biostratigraphy of Shikoku with reference to selected sections in Lombardy Basin and Sicily. *Tohoku Univ. Sci. Rep. 2nd Ser. (Geol.)*, **58**, 1-91.

Arita, K., Ikawa, T., Ito, T., Yamamoto, A., Saito, M., Nishida, Y., Satoh, H., Kimura, G., Watanabe, T., Ikawa, T., and Kuroda, T., 1998, Crustal structure and tectonics of the Hidaka Collision Zone, Hokkaido (Japan), revealed by vibroseis seismic reflection and gravity surveys. *Tectonophysics*, **290**, 197-210.

Arita, K., Toyoshima, T., Owada, M., Miyashita, S. and Jolivet, L., 1986, Tectonic movements of the Hidaka metamorphic belt, Hokkaido, Japan. *Monogr. Assoc. Geol. Collab. Japan*, no. 31, 247-263.**

Asahina, T. and Komatsu, M., 1979: The Horokanai ophiolitic complex in the Kamuikotan Tectonic Belt, Hokkaido, Japan. *Jour. Geol. Soc. Japan.*, **85**, 317-330.

Awan, M. A. and Kimura, K., 1996, Thermal structure and uplift of the Cretaceous Shimanto Belt, Kii Peninsula, Southwest Japan: An illite crystallinity and illite b_0 lattice spacing study. *The Island Arc*, **5**, 69-88.

B

Baumgartner, P. O., Bartolini, A., Carter, E. S., Conti, M., Cortese, G., Danelian, T., De Wever, P., Dumitrica, P., Dumitrica-Jud, R., Gorican, S., Guex, J., Hull, D. M., Kito, N., Marcucci, M., Matsuoka, A., Murchey, B., O'Dogherty, L., Savary, J., Vishnevskaya, V., Widz, D. and Yao, A., 1995, Middle Jurassic to Early Cretaceous radiolarian biochronology of Tethys based on Unitary Associations. *Mém. Géol. (Lausanne)*, no. 23, 1013-1048.

Baker P. E., Castillo P. R. & Condliffe E. 1995. Petrology and geochemistry of igneous rocks from Allison and Resolution guyots, Site 865 and 866. *In* Winterner E. L., Sager W. W., Firth J. V. & Sinthon J. M. eds. *Proceedings of the Ocean Drilling Program, Scientific Results* **143**, pp. 245-61. College Station, Texas.

Ballance P. F., Scholl D. W., Vallier T. L., Stevenson A. J., Ryan H. & Herzer R. H. 1989. Subduction of a Late Cretaceous seamount of the Louisville Ridge at the Tonga Trench: A model of normal and accelerated tectonic erosion. *Tectonics* **8**, 953-62.

Bloomer S. H. 1983. Distribution and origin of igneous rocks from the landward slopes of the Mariana Trench: Implications for its structure and evolution. *Journal of Geophysical Research* **88**, 7411-28.

Bloomer S. H. & Fisher R. L. 1987. Petrology and geochemistry of igneous rocks from the Tonga Trench - a non-accreting plate boundary. *Journal of Geology* **95**, 469-5.

Brandon, M. T., and Calderwood, A. R., 1990: High-pressure metamorphism and uplift of the Olympic subduction complex. *Geology*, **18**, p.1252-1255.

Brewer T.S., Batch W. & Furnes H. 1996. Geochemistry of lavas from Hole 896A. *In* Alt J. C., Kinoshita H., Stokking L. B. & Michael P. J. eds. *Proceedings of the Ocean Drilling Program, Scientific Results* **148**, pp. 9-19. College Station, Texas.

C

Cambon P., Joron J. L., Bougault H., and Treuil M. 1980. Leg 55, Emperor Seamounts: Trace Elements in transitional tholeiites, alkaline basalts, and hawaiites - mantle homogeneity or heterogeneity and magmatic process. *In* Jackson E. D. & Koizumi I. eds. *Initial Reports of the Deep Sea Drilling Project* **55**, pp. 585-97. U.S. Government Printing Office, Washington.

Cristie D. M., Dieu J. J. & Gee J. S. 1995. Petrologic studies of basement lavas from Northwest Pacific Guyots. *In* Haggerty J. A., Silva P., Rack F. & McNutt M. K. eds. *Proceedings of the Ocean Drilling Program, Scientific Results* **144**, pp. 495-512. College Station, Texas.

D

Dahlen, F. A., 1984, Noncohesive critical Coulomb wedges: An exact solution. *Jour. Geophys. Res.*, **89**, 10125-10133.

Davis, D., Suppe, J., and Dahlen, F. A., 1983, Mechanics of fold-and-thrust belts and accretionary wedge. *Jour. Geophys. Res.*, **88**, 1153-1172.

Drake N. E., Rhodes J. M. & Autio L. K. 1985. Geochemistry of basalts from Deep Sea Drilling Project Hole 556-564. *In* Bougault H., Cande S. C. *et al.* eds. *Initial Reports of the Deep Sea Drilling Project* **82**, pp. 421-38. U.S. Government Printing Office, Washington.

E

Engebretson D. C., Cox A. & Gordon R. C. 1985. Relative motions between oceanic and continental plates in the Pacific Basin. *Geological Society of America Special Paper* **206**, 59pp.

F

Fisher M. A., Collot J. Y. & Geist E. L. 1991. Structure of the collision zone between Bougainville Guyot and the accretionary wedge of the New Hebrides island arc, Southwest Pacific. *Tectonics* **10**, 887-903.

Floyd P. A. 1986. Petrology and geochemistry of oceanic intraplate sheet-flow basalts, Nauru Basin, Deep Sea Drilling Project Leg 89. *In* Moberly R., Schlanger S. O. *et al.* eds. *Initial Reports of the Deep Sea Drilling Project* **89**, pp. 471-97. U.S. Government Printing Office, Washington.

Foreman, H. P., 1978, Mesozoic Radiolaria in the Atlantic Ocean off the Northwest coast of Africa, Deep Sea Drilling Project, Leg 41. *Initial Report of Deep Sea Drilling Project*, **41**, 739-761.

Fryer P. & Smoot C. 1985. Processes of seamount subduction in the Mariana and Izu-Bonin Trenches. *Marine Geology* **64**, 77-90.

G

Geist, E. L., Childs, J. R., and Scholl, D. W., 1988, The origin of summit basins of the Aleutian Ridge: Implication for block rotation of an arc massif. *Tectonics*, 7, 327-341.

Geological Survey of Japan, 1978, *1/500,000 geologic map "Kushiro".*

Geological Survey of Japan, 1984, *1/500,000 geologic map "Abashiri".*

Geological Survey of Japan, 1986, *1/500,000 geologic map "Sapporo".*

Geological Survey of Japan, 1990, *1/500,000 geologic map "Asahikawa".*

H

Hasegawa, K., Osanai, H., Suzuki, M. and Matsushita, K., 1961, Pre-Yezo Group in the Axial Zone of Hokkaido –Proposal on the classification of the Group–, *Rep. Geol. Surv. Hokkaido*, no. 25, 108-115.**

Hashimoto, S., Suzuki, M., and Osanai, H., 1961, Explanatory text of the geological map of Japan, 1/50,000 "Poroshiridake", Geological Survey of Hokkaido, 46pp.**

Hashimoto, W., 1936, Geology of western mountains of the Furano Basin, Sorachi District, Ishikari Province, Hokkaido, Japan. *Jour. Geol. Soc. Japan*, **43**, 493-530.*

Hori, R. S. and Sakakibara, M., 1994, A chert-clastic sequence spanning the late Triassic - early Cretaceous period of the Kamuikotan Complex in the Shizunai area, south-central Hokkaido, Japan. *Jour. Geol. Soc. Japan*, **100**, 575-583.

Huchon, P. and Le Pichon, X., 1984, Sunda Strait and Central Sumatra fault. *Geology*, **12**, 668-672.

Humphris S. E., Thompson R. N., Gibson I. L. & Marriner G. F. 1980. Comparison of geochemistry of basalts from the East Pacific Rise, OCP Rise, and Siqueiros Fracture Zone, Deep Sea Drilling Project Leg 54. *In* Natland J. H. & Powell R. eds. *Initial Reports of the Deep Sea Drilling Project* **54**, pp. 635-49. U.S. Government Printing Office, Washington.

I

Igi, Y., Tanaka, K., Hata, M., and Sato, H., 1958, Explanatory text of the geological map of Japan, 1/50,000 "Horokanai" (Asahikawa-39), Geological Survey of Japan, 64p.**

Igo, Hy., Igo, Hh., Adachi, S. and Sato, Y., 1980, On the geologic age of the Hidaka and Sorachi Groups. *Studies of geosynclines and tectonic division of the northern part of the Japan Islands. Report of Scientific*

Project, Grant-in-aid for Scientific Research (*A*), 69-75.*

Igo, Hy., Koike, T., Igo, Hh. and Kinoshita, T., 1974, On the occurrence of Triassic conodonts from the Sorachi Group in the Hidaka Mountains, Hokkaido. *Jour. Geol. Soc. Japan*, **80**, 135-136.*

Inoma, A., 1969, The Intra-Yezo disturbance and sedimentation of the Middle Yezo Group. *Jour. Japanese Assoc. Petrol. Techn.*, **34**, p.11-10 and p.21-25.**

Ishizuka H. 1980. Geology of the Horokanai Ophiolite in the Kamuikotan Tectonic Belt, Hokkaido, Japan. *The Journal of the Geological Society of Japan* **86**, 119-34.

Ishizuka H. 1981. Geochemistry of the Horokanai ophiolite in the Kamuikotan Tectonic Belt, Hokkaido, Japan. *The Journal of the Geological Society of Japan* **87**, 17-34.**

Ishizuka, H., Okamura, M. and Saito, Y., 1983, Latest Jurassic radiolarians from the Horokanai Ophiolite in the Kamuikotan Zone, Hokkaido, Japan. *Jour. Geol. Soc. Japan*, **89**, 731-732.

Iwasaki, I., Shibakusa, H., Gouchi, N. and Watanabe, T., 1994, Kamuikotan Belt (Central Part). *Excursion Guidebook, 101st Annu. Meet. Geol. Soc. Japan*, 139-160.*

Iwasaki, I. and Ueda, H., 1993, The metamorphic ages of accretionary complex in the central axial part of Hokkaido. *Abst. 100th Annu. Meet. Geol. Soc. Japan*, 232.*

Iwasaki, I., Watanabe, T., Itaya, T., Yamazaki, M. and Takigami, Y., 1995, Paleogene K-Ar ages from the Kamuikotan metamorphic rocks, southern area of the Kamuikotan Gorge, central Hokkaido, northern Japan. *Geol. Jour.*, **30**, 281-295.

J

Johannes, W. and Puhan, D., 1971, The calcite-aragonite transition, reinvestigated. *Contrib. Mineral. Petrol.*, **31**, 28-38.

Jud, R., 1994, Biochronology and systematics of Early Cretaceous Radiolaria of the Western Tethys. *Mém. Géol.* (*Lausanne*), no. 19, 1-147.

K

Kanie, Y., Taketani, Y., Sakai, A. and Miyata, Y., 1981, Lower Cretaceous deposits beneath the Yezo Group in the Urakawa area, Hokkaido. *Jour. Geol. Soc. Japan*, **87**, 527-553.**

Kawabe, F., Hirano, H., and Takagi, K., 1996, Biostratigraphy of the Cretaceous System in the northern Oyubari area, Hokkaido. *Jour. Geol. Soc. Japan*, **102**, 440-459.

Kawaguchi, M., 1997, Lower Cretaceous strata around the River Onisashi, northern Hokkaido. *In* Kawamura, M., Oka, T. and Kondo, T., eds., *Commemorative Volume for Prof. Makoto Kato*, 121-134.**

Kawamura, M., Nakagawa, M., Katoh, T., Toda, H., Kon, H., Yoshida, K., Yamamoto, K., Terada, T., Nagata, H., Kokubu, H., Sakakibara, M., Ohtsu, S. and the Kamuikotan Belt Research Group, 1998, Geologic structure of the metamorphosed Mesozoic accretionary complex in the Sorachi-Yezo Belt, central Hokkaido, Japan. - Unit-classification of the Biei Complex and proposal of Oichan Nappe - . *Earth Sci.* (*Chikyu Kagaku*), **52**, 433-452.**

Kawamura, M., Narushima, T., Hayato, U., and Kawakami, G., 2000, Pebbly mudstone including the clasts of high-P/T metamorphic rocks in the Middle Yezo Group. *Abst. 107th Annu. Meet. Geol. Soc. Japan*, 261.*

Kawamura, M., Ozawa, S., Kameyama, S. and Iwata, K., 1997, Supplemental data for the Kamiiso and Toi Complexes of the East Oshima Belt, SW Hokkaido. *In* Kawamura, M., Oka, T. and Kondo, T., eds., *Commemorative Volume for Prof. Makoto Kato*, 111-120.**

Kawamura, M., Tajika, J., Kawamura, T. and Kato, Y., 1986, Constitution and occurrences of the Paleozoic and Mesozoic formations in S. W. Hokkaido, northern Japan. *Monogr. Assoc. Geol. Collab. Japan*, no. 31, 17-32.**

Kawamura, M. and Ueda, H., 1997, "Sand diapir" in the Idonnappu Belt, central Hokkaido, northern Japan. *In* Kawamura, M., Oka, T. and Kondo, T., eds., *Commemorative Volume for Prof. Makoto Kato*, 209-214.**

Kawamura, M., Ueda, H., Nakagawa, M., Katoh, T. and the Research Group of Hidaka Convergent Zone (in press), High P/T metamorphic minerals found from the "undivided Hidaka Supergroup" in the Sorachi-Yezo Belt, Hokkaido. *Jour. Geol. Soc. Japan.***

Kawamura, M., Ueda, H., and Narushima, T., 1999, Unconformities and slump bodies recognized in forearc

sediments - stratigraphic phenomena at the basal part of the Middle Yezo Group, Sorachi-Yezo Belt, central Hokkaido-. *Mem. Geol. Soc. Japan*, **52**, 37-52.**

Kiminami, K., 1987, Radiolarian ages of the Hidaka Supergroup along Hidaka-Horobetsu-gawa river and Samani-gawa river, southern Hidaka Belt. *HSG Newsletter*, no. 2, 11-14.*

Kiminami, K., 1989, Several new proposals on tectonics around Hokkaido. *Monthly Earth*, **11**, 309-315.*

Kiminami, K., Kawabata, S. and Miyashita, S., 1990, Discovery of Paleogene radiolarians from the Hidaka Supergroup and its significance with special reference to the ridge subduction. *Jour. Geol. Soc. Japan*, **96**, 323-326.

Kiminami, K., Komatsu, M. and Kawabata, K., 1992, Composition of clastics of the Sorachi Group and the Lower Yezo Group in the Inushibetsu-gawa area, Hokkaido, Japan, and their significance. *Mem. Geol. Soc. Japan*, no. 38, 1-11.**

Kiminami, K., Komatsu, M., Niida, K. and Kito, N., 1986, Tectonic divisions and stratigraphy of the Mesozoic rocks of Hokkaido, Japan. *Monogr. Assoc. Geol. Collab. Japan*, no. 31, 1-15.**

Kiminami K., Kontani Y. & Miyashita S. 1985. Lower Cretaceous strata covering the abyssal tholeiite (the Hidaka Western Greenstone Belt) in the Chiroro area, central Hokkaido, Japan. *The Journal of the Geological Society of Japan* **91**, 27-42.

Kiminami, K., Miyashita, S. and Kawabata, K., 1999, Occurrence and significance of *in-situ* basaltic rocks from the Rurochi Formation in the Hidaka Supergroup, northern Japan. *Mem. Geol. Soc. Japan*, no. 52, 103-112.**

Kiminami, K., Takahashi, K., and Maniwa, K., 1978, The Cretaceous system in Hokkaido – Yezo and Nemuro Groups -. *Monograph Assoc. Geol. Collab. Japan*, **21**, 111-126.**

Kimura, G., 1986, Geologic section of north Hokkaido. *Tectonic belts in Hokkaido - petrology and tectonics. Newsletter for Scientific Project, Grant-in-aid for Scientific Research (A)*, no. 1, 107-111.*

Kimura G. 1986. Oblique subduction and collision: Forearc tectonics of the Kuril Arc. *Geology* **14**, 404-7.

Kimura, G., Sakakibara, M. and Okamura, M., 1994, Plumes in central Panthalassa? Dedications from accreted oceanic fragments in Japan. *Tectonics*, **13**, 905-916.

Kimura K & Hori R. 1993. Offscraping accretion of Jurassic chert-clastic complexes in the Mino-Tamba Belt, central Japan. *Journal of Structural Geology* **15**, 145-61.

Kimura, T., 1979, *Japan Islands - until its building* - , vol. **2**-first, Kokin-Syoin, Tokyo, 578pp.*

Kinugasa, I., Hashimoto, S. and Arai, S., 1981, Geology and metamorphism of the Hidaka Belt of Ochiai area, Hokkaido. *Geosci. Rep. Shizuoka Univ.*, no. 6, 1-10.

Kisch, H. J., 1987, Correlation between indicators of very low-grade metamorphism. *In* Frey, M., ed., *Low Temperature Metamorphism*, Blackie & Sun, London, 227-300.

Kisch, H. J. and Frey, M., 1987, Effect of sample preparation on the measured 10 Å peak width of illite (illite 'crystallinity'). *In* Frey, M., ed., *Low Temperature Metamorphism*, Blackie & Sun, London, 301-304.

Kito, N., 1987, Stratigraphic relation between greenstones and clastic sedimentary rocks in the Kamuikotan Belt, Hokkaido, Japan. *Jour. Geol. Soc. Japan*, **93**, 21-35.**

Kiyokawa, S., 1989, Geologic section of central Hokkaido –special reference to the Idonnappu Belt-. *Monthly Earth*, **11**, 316-322.*

Kiyokawa, S., 1992. Geology of the Idonnappu Belt, Central Hokkaido, Japan: Evolution of a Cretaceous accretionary complex. *Tectonics*, **11**, 1180-1206.

Kizaki, K., Watanabe, T., Fanning, C. M. and S., Miyashita, 2000, Formative age of the Poroshiri Ophiolite by zircon U-Pb SHRIMP dating. *Abst. Annu. Meet. Geol. Soc. Japan Hokkaido Branch 1999*, 18-20.*

Koitabashi, S., Endo, H. and Katagawa, H., 1978, Greenstones in the middle stream area of the River Niikappu and the upper stream area of the River Ribira, southern Kamuikotan belt. *Earth Science* ("*Chikyu Kagaku*"), **32**, 299-300.*

Komatsu, M., Miyashita, S. and Arita, K., 1986, Composition and structure of the Hidaka Metamorphic belt, Hokkaido - historical review and present status -. *Monogr. Assoc. Geol. Collab. Japan*, no. 31, 189-203.**

Kubler, B., 1968. Évaluation quantitative du métamorphisme par la cristallinité de l'illite. *Bull. Centre de*

Recherches - SNPA., **2**, 39-40.

L

Lallemand, S. and Le Pichon, X., 1987, Coulomb wedge model applied to the subduction of seamounts in the Japan Trench. Geology, **15**, 1065-1069.

Lallemand S. E., Schnürle P. & Malavieille J. 1994, Coulomb theory applied to accretionary and nonaccretionary wedges: Possible causes for tectonic erosion and/or frontal accretion. *Journal of Geophysical Research* **99**, 12033-55.

Leake, B. E., 1978, Nomenclature of amphiboles. *The Canadian Mineralogist*, **16**, 501-520.

Leterrier, J., Maury, R., Thonon, P., Girard, D., and Marchal, M., 1982, Clinopyroxene composition as a method of identification of the magmatic affinities of paleo-volcanic series. *Earth Plan. Sci. Letters*, **59**, 139-154.

Liou, J. G., 1971, P-T stabilities of laumontite, wairakite, lawsonite, and related minerals in the system $CaAl_2Si_2O_8$-SiO_2-H_2O. *Jour. Petrol.*, **12**, 379-411.

Liou, J. G., Maruyama, S. and Cho, M., 1985, Phase equilibria and mineral parageneses of metabasites in low-grade metamorphism. *Mineral. Magazine*, **49**, 321-333.

M

Maeda, J., Suetake, S., Ikeda, Y., Tomura, S., Motoyoshi, Y. and Okamoto, Y., 1986, Tertiary plutonic rocks in the axial zone of Hokkaido - distribution, age, major element chemistry, and tectonics -. *Monogr. Assoc. Geol. Collab. Japan*, no. 31, 223-246.**

Maekawa, H., 1983, Submarine sliding deposits and their modes of occurrence of the Kamuikotan Metamorphic rocks in the Biei area, Hokkaido, Japan. *Jour. Fac. Sci. Univ. Tokyo, sec. II*, **20**, 489-507.

Maekawa, H., 1986, Processing formation of the kamuikotan metamorphic rocks from the Biei and surrounding areas, central Hokkaido. *Monogr. Assoc. Geol. Collab. Japan*, no. 31, 107-117.**

Maekawa, H., Fryer, P. and Ozaki, A., 1995, Incipient blueschist-facies metamorphism in the active subduction zone beneath the Mariana Forearc. *In* Taylor, B. and Natland, J. eds, *Active margins and marginal basins of the Western Pacific, Geophysical Monograph*, **88**, American Geophysical Union, Washington, DC ,281-289.

Maekawa, H., Shozui, M., Ishii, T., Saboda, C., and Ogawa, Y., 1992, Metamorphic rocks from the serpentinite seamounts in the Mariana and Izu-Ogasawara forearcs. In *Fryer, P., Pearce, J. A., Sotkking, L. G. eds. Proceedings of the Ocean Drilling Program, Scientific Results*, College Station, TX.

Mahoney J. J., Storey M., Duncan R. A., Spencer K. J., and Pringle M. 1993. Geochemistry and geochemistry of Leg 130 basement lavas: Nature and origin of the Ontong Java Plateau. *In* Berger W. H., Kroenke L. W., Mayer L. A. *et al.* eds. *Proceedings of the Ocean Drilling Program, Scientific Results* **130**, pp. 3-22. College Station, Texas.

Mariko, T., 1984, Sub-sea hydrothermal alteration of basalt, diabase and sedimentary rocks in the Shimokawa Copper Mining area, Hokkaido, Japan. *Mining Geology*, **34**, 307-321.

Maruyama, S., 1976, Chemical natures of the Sawadani Greenstone Complex in the Chichibu Belt, eastern Shikoku. *Jour. Geol. Soc. Japan*, **82**, 183-197.

Maruyama, S. and Liou, J. G., 1985, Clinopyroxene - a mineral telescoped through the process of blueschist facies metamorphism. *Jour. Metamorph. Geol.*, **5**, 529-552.

Maruyama, S., Liou, J. G., and Terabayashi, M., 1996, Blueschists and eclogites of the world and their exhumation. *Intern. Geol. Review*, **38**, 485-594.

Matsumoto, T., Miyauchi, T., Kanie, Y., Miyata, Y., and Ueda, Y., 1984, Cretaceous Nautiloids from Hokkaido-V. *Trans. Proc. Palaeont. Soc. Japan*, **134**, 335-346.

Matsushita, K., and Suzuki, M., 1962, *Explanatory text of the Geological Map of Japan*, 1/50,000 *Noya* (*Kushiro-61*). Hokkaido Development Agency, pp.38.

Matsuoka, A., 1992, Jurassic and early Cretaceous radiolarians from Leg 129, Sites 800 and 801, western Pacific Ocean. *In* Larson, R. L. and Lancelot, Y., eds., *Proceedings of the Ocean Drilling Program, Scientific Results*, **129**, College Station, Texas, 203-220.

McCaffrey R. 1992. Oblique plate convergence, slip vectors, and forearc deformation. *Journal of Geophysical*

Research **97**, 8905-15.

Meschede M. 1986. A method of discriminating between different types of Mid-Ocean Ridge Basalts and continental tholeiites with the Nb-Zr-Y diagram. *Chemical Geology* **56**, 207-18.

Miall, A. D., 1992, Alluvial deposits. *In Walker, R. G. and James, N.P. eds., Facies Models 3rd edition*, Geological Association of Canada, pp.119-142.

Mitsugi, T. and Hirano, H., 1997, Cretaceous Radiolaria from the Lower Yezo Group, central Hokkaido, Japan. *Jour. Geol. Soc. Japan*, **103**, 113-125.**

Miyashiro A. 1973. The Troodos ophiolitic complex was probably formed in an island arc. *Earth and Planetary Science Letters* **19**, 218-24.

Miyashita S. 1983. Reconstruction of the ophiolite succession in the western zone of the Hidaka Metamorphic Belt, Hokkaido. *The Journal of the Geological Society of Japan* **89**, 69-86.**

Miyashita, S., Arai, T. and Nagahashi, T., 1997, Significance of greenstones in the Hidaka Belt, Hokkaido: Evidence for polycollision of ocean ridges. *Mem. Geol. Soc. Japan*, no. 47, 307-323.**

Miyashita S. & Katsushima T. 1986. The Tomuraushi greenstone complex of the central Hidaka zone: contemporaneous occurrence of abyssal tholeiite and terrigenous sediments. *The Journal of the Geological Society of Japan* **92**, 535-57.

Miyasita, S., Kizaki, K., Arai, T., and Toyoshima, T., 1994, *The Poroshiri Ophiolite of the hidaka Zone, central Hokkaido, Japan.* IGCP project 283, 321, 359 in Japan, Field Trip Guidebook, Kyobunsha, Sapporo, 82 p.

Miyashita, S. and Yoshida, A, Geology and petrology of the Shimokawa ophiolite (Hokkaido, Japan): ophiolite possibly generated near R-T-T triple junction. *In* Ishiwatari, A. ed., *Circum-Pacific ophiolites: Proc. 29th IGC Ophiolite Symposium, Part D,* VSP Pub., Netherland, 163-182.

Miyashita, S. and Yoshida, A., 1988, Pre-Cretaceous and Cretaceous ophilites in Hokkaido, Japan. *Bull. Soc. Geol. France.*, (8), 251-260.

Morimoto, N., Fabries, J., Ferguson, A.K., Ginzburg, I.V., Ross, M., Seifert, F.A., Zussman, J., Aoki, K. and Gottardi, G., 1988, Nomenclature of pyroxenes. *Amer. Mineral.*, **73**, 1123-1133.

Moriya, T., Okada, H., Matsushima, T., Asano, S., Yoshii, T. and Ikami, A., 1998, Collision structure in the upper crust beneath the southwestern foot of the Hidaka Mountains, Hokkaido, Japan as derived from explosion seismic observations. *Tectonophysics*, **290**, 181-196.

Motoyama, I., Fujiwara, O., Kaiho, K., and Murota, T., 1991, Lithostratigraphy and calcareous microfossil biochronology of the Cretaceous strata in the Oyubari area, Hokkaido, Japan. *Jour. Geol. Soc. Japan.*, **97**, 507-527.

N

Nagahashi, T., 1998, The geochemistry of greenstones occurrenced in Upper Sorachi Group in Hokkaido, Japan (Abstract). *105th Annual Meeting of the Geological Society of Japan* 228.*

Nagahashi T. & Miyashita S. 1997. The origin of greenstones in the Lower Sorachi Group in Hokkaido, Japan (Abstract). *104th Annual Meeting of the Geological Society of Japan* 220.*

Nagahashi T. & Miyashita S. 1997. The origin of greenstones in the Lower Sorachi Group in Hokkaido, Japan *Significance of greensones on formation of accretionary Complex: Report of Scientific Project, Grant-in-aid for Scientific Research (A)*, no. 2, 117-124.*

Nakagawa M., Goto Y., Funayama J. & Aramaki S. 1994. Trace element analysis of GSJ rocks reference samples "igneous rock series" by XRF fluorescence spectrometry. *In* S. Aramaki ed. *Temporal and spatial transition of Cenozoic magmatism at arc-arc junctions*, pp.148-55. Hokkaido University, Sapporo.*

Nakagawa, M. and Nakano, N., 1987, K-Ar dating and its significance of Kamuikotan mafic schist from Mitsuishi River, southern central Hokkaido, Japan. *Earth Science* (*"Chikyu-Kagaku"*), **41**, 244-247.

Nakano, N., 1978, Stratigraphy of basic rocks in the Shizunai - Mitsuishi district, Hokkaido. *Earth Science* ("*Chikyu Kagaku*"), **32**, 293-298.

Nakano, N., 1981. Metamorphism of the greenstones in the Kamuikotan zone and the Hidaka western marginal

tectonic zone in the Shizunai - Mitsuishi district, Hokkaido. *Jour. Geol. Soc. Japan.*, **87**, 211-224.**

Nakano, N., 1985, Petrological character of metabasalts in the southern Kamuikotan belt, Hokkaido, Japan. *Jour. Tokyo Univ. Agricult. Daiichi High School*, no. 3, 33-64.*

Nakano, N., 1999, Occurrence and paragenesis of aragonite in low-grade metamorphic rocks. *Jour. Tokyo Univ. Agricult. Daiichi High School*, no. 17, 37-64.*

Nanayama, F., 1992, Stratigraphy and facies of the Paleocene Nakanogawa Group in the southern part of central Hokkaido, Japan. *Jour. Geol. Soc. Japan*, **98**, 1041-1059.**

Nanayama, F. and Ganzawa, Y., 1997, Sedimentary stratigraphy, environment and age of the northern unit of Nakanogawa Group in the Hidaka belt, central Hokkaido, Japan. *Mem. Geol. Soc. Japan*, no. 47, 279-293.**

Narushima, T., Kawamura, M. and Ueda, H., 1999, "Basal conglomerate" of the Middle Yezo Group around Hidaka-cho area, and its tectonic implication. *Abst. 106th Annu. Meet. Geol. Soc. Japan*, 308.*

Niida K. 1992. Basalts and dolerites in the Sorachi - Yezo Belt, central Hokkaido, Japan. *Journal of Faculty of Science, Hokkaido University, Ser. IV* **23**, 301-19.

Niida, K. and Katoh, T., 1978, Ultra mafic rocks in Hokkaido. *Monogr. Assoc. Geol. Collab. Japan*, no. 21, 61-81.**

Niida, K. and Kito, N., 1986, Cretaceous arc-trench system in Hokkaido. *Monogr. Assoc. Geol. Collab. Japan*, no. 31, 379-402**

Nitsch, K. H., 1968, Die Stabilität von Lawsonit. *Naturwissenschaften*, **55**, 388.

Nitsch, K. H., 1971, Stabilitätsbeziehungen von Prehnit- und Pumpellyit haltigen Paragenesen. *Contib. mineral. petrol.*, **30**, 240-260.

O

Osanai, H., and Matsushita, K., 1959, Some problems of the Cretaceous system at the western wing of the Hidaka Mountain Range -I: The stratigraphies of the Cretaceous system at Soshubetsu, Chiroro, Shunbetsu districts. *Reports Geol. Sur. Hokkaido*, **21**, 17-28.**

Osanai, H., and Matsushita, K., 1960, Some problems of the Cretaceous system at the western wing of the Hidaka Mountain Range -II: The stratigraphies of the Cretaceous system at Usappu, the Nukabira-gawa, the Niikappu-gawa and the Shukushubetsu-gawa, the Idonnappu-gawa, the Abukasanpe-gawa, the Mitsuishi-gawa and the Kerimai-gawa districts. *Reports Geol. Surv. Hokkaido*, **24**, 19-37.**

Osanai, Y., Owada, M. and Takasu, I., 1985, Original rock constitution of the Main Zone of the Hidaka metamorphic belt, Hokkaido, Japan. *Sci. Rep. Fukuoka Univ. Edu.*, no. 38, 71-91.

Ota, T., Sakakibara, M. and Itaya, T., 1993, K-Ar ages of the Kamuikotan metamorphic rocks in Hokkaido, Japan. *Jour. Geol. Soc. Japan*, **99**, 335-345.**

Owada, M., Nanayama, F., Shimura, T. and Osanai, Y., 1992, Lamprophyre from the Nakanogawa group in the central zone of Hokkaido, northern Japan. *Jour. Mineral. Petrol. Econ. Geol.*, **87**, 62-67.**

Owada, M., Osanai, Y. and Kagami, H., 1991, Timing of anatexis in the Hidaka metamorphic belt, Hokkaido, Japan. *Jour. Geol. Soc. Japan*, **97**, 751-754.

P

Pearce J. A. 1982. Trace element characteristics of lavas from destructive plate boundaries. *In* Thorpe R. S. ed. *Andesites*, 525-48. John Wiley & Sons, Chichester.

Pearce J. A., Rogers N., Tindle A. J. & Watson J. S. 1986. Geochemistry and petrogenesis of basalts from Deep Sea Drilling Project Leg 92, Eastern Pacific. *In* Leinen M., Rea D. K. *et al.* eds. *Initial Reports of the Deep Sea Drilling Project* **92**, pp. 435-57. U.S. Government Printing Office, Washington.

Pessagno, E. A. Jr., 1976, Radiolarian zonation and stratigraphy of the California Coast Ranges. *Spec. Publ. Micropaleont.*, no. 2, 1-95.

Platt, J. P., 1986, Dynamics of orogenic wedges and the uplift of high-pressure metamorphic rocks. *Geol. Soc. America Bull.*, **97**, 1037-1053.

Popp, R. K. and Gilbert, M. C., 1972, Stability of acmite-jadeite pyroxenes at low pressure. *Amer. Mineral.*, **57**, 1210-1231.

R

Rhodes J. M., Blanchard D. P., Dungan M. A., Rogers K. V. & Brannon J. C. 1979. Chemistry of Leg 45 basalts. *In* Natland, J. H. & Shambach, J. D. eds. *Initial Reports of the Deep Sea Drilling Project* **45**, pp. 447-59. U.S. Government Printing Office, Washington.

Ring, U., Brandon, M. T., Willet, S. D. and Gordon, S., 1999, Exhumation processes. *In* Ring, U., Brandon, M. T., Willet, S. D. and Lister, G. S. eds. *Exhumation processes: normal faulting, ductile flow and erosion.* (*Spec. Pub. Geol. Soc. London*, **154**), Cambridge University Press, Cambridge UK, 1-27.

S

Sakagami, S. and Sakai, A., 1979, Triassic Bryozoans from the Hidaka Group in Hokkaido, Japan. *Trans. Proc. Palaeontol. Soc. Japan*, no. 114, 77-86.

Sakai, A., 1976, The Hidaka Supergroup in the Motourakawa river area, Hokkaido. *Abst. 83rd Annu. Meet. Geol. Soc. Japan*, 39*

Sakai, A. and Kanie, Y., 1986. *1/50000 quadrangle series: Geology of the Nishicha district.* Geological Survey of Japan.**

Sakakibara, M., Hori, R., Ikeda, R. and Umeki, M., 1997, Petrologic characteristics and geologic age of green rocks including chert xenoliths in the Pippu area, central Hokkaido, Japan. *Jour. Geol. Soc. Japan*, **103**, 953-961.**

Sakakibara, M., Hori, R., Kimura, G., Ikeda, M., Koumoto, T. and Kato, H., 1999, The age of magmatism and petrochemical characteristics of the Sorachi plateau reconstructed in Cretaceous accretionary complex, central Hokkaido, Japan. *Mem. Geol. Soc. japan*, no. 52, 1-15.

Sakakibara, M., and Ota, T., 1994, Metamorphic evolution of the Kamuikotan high-pressure and low-temperature metamorphic rocks in central Hokkaido, Japan. *Jor. Geophys. Res.* **99**, 22,221-22,235.

Sanfilippo, A. and Riedel, W. R., 1985, Cretaceous Radiolaria. *In* Bolli, H. M., Saunders, J. B. and Perch-Nielsen, K., eds., *Plankton Stratigraphy*, Cambridge University Press, Cambridge, 573-630.

Saunders A. D. 1986. Geochemistry of basalts from the Nauru Basin, Deep Sea Drilling Project Legs 61 and 89: Implications for the origin of oceanic flood basalts. *In* Moberly R., Schlanger S. O. *et al.* eds. *Initial Reports of the Deep Sea Drilling Project* **89**, pp. 499-517. U.S. Government Printing Office, Washington.

Schaaf, A., 1985, Un nouveau canevas biochronologique du Crétacé inférieur et moyen: les biozones à radiolaires. *Bull. Sci. Géol.*, **38**, 227-269.

Schiffman, P. and Liou, J. G., 1983, Synthesis of Fe-pumpellyite and its stability relations with epidote. *Jour. Metamorph. Geol.*, **1**, 91-101.

Shervais J. W. 1982. Ti-V plots and the petrogenesis of modern and ophiolitic lavas. *Earth and Planetary Science Letters* **59**, 101-18.

Shibakusa, H., 1989, Lawsonite-pumpellyite-epidote stabilities in glaucophane schists in the Horokanai-Kamietanbetsu area of Kamuikotan Zone, Hokkaido, Japan. *Mineral. Petrol.*, **40**, 241-256.

Stakes D. S. & Franklin J. M. 1994. Petrology of igneous rocks at Middle Valley, Juan de Fuca Ridge. *In* Mottl M. J., Davis E. E., Fisher A. T. & Slack J. F. eds. *Proceedings of the Ocean Drilling Program, Scientific Results* **139**, pp. 79-102. College Station, Texas.

Sun S. & McDonough W. F. 1989. Chemical and isotopic systematics of oceanic basalts: implications for mantle composition and processes. *In* Saunders A. D. & Norry M. J. eds. *Magmatism in the Ocean Basins*, pp. 313-45. Geological Society, London.

Suppe, J., 1983, Geometry and kinematics of fault-bend folding. *Amer. Jour. Sci.*, 283, 684-721.

Suzuki, M., Osanai, H., Matsui, K., and Watanabe, J., 1961, *Explanatory text of the Geological Map of Japan, 1/50,000 Idonnappudake (Kushiro-56)*, Hokkaido Development Agency, pp.64.**

Suzuki, S., Sakai, A. and Uozumi, S., 1983, Molluscan fossils from the Neogene deposits scattered along the western wing of the Hidaka Mountains, Hokkaido. *Jour. Fac. Sci. Hokkaido Univ., ser. IV*, **20**, 1-154.

T

Tajika, J. and Iwata, K., 1990, Paleogene melange of the nothern Hidaka Belt -Geology and radiolarian age of the Kamiokoppe Formation-. Jour. Hokkai-Gakuen Univ., no. 66, 35-55.*

Tajika, J. and Iwata, K., 1994, Eruptive field of greenstones in the Hidaka Supergroup from the viewpoint of sedimentary stratigraphy - an example of Tatsuushi area in the northern Hidaka Belt, Hokkaido-. *Monthly Earth*, **16**, 495-499.

Takahashi, K., and Suzuki, M.,1978, Explanatory text of the geological map of Japan, 1/50,000 Iwachishi (Sapporo-45), Geological Survey of Hokkaido, 46pp.**

Takashima, R., and Nishi, T., 1999, Re-evaluation of the intra-Yezo disturbance and the Cretaceous tectonics in Hokkaido, Japan. *Jour. Geol. Soc. Japan*, **105**, 711-728.

Takashima, R., Nishi, H., Saito, T., and Hasegawa T., 1997a, Geology and planktonic foraminiferal biostratigraphy of Cretaceous strata distributed along the Shuparo River, Hokkaido, Japan. *Jour. Geol. Soc. Japan*, **103**, 543-563**

Takashima, R., Suzuki, N., Koike, T., and Saito, T., 1997b, Reexamination of the unconformity proposed at the boundary between the Lower and Middle Yezo Groups in the Soshubetsu area, Hokkaido, and its geological significance – reevaluation of the intra-Yezo disturbance. *Jour. Geol. Soc. Japan*, **103**, 489-492.

Taketani, Y., 1982, Cretaceous radiolarian biostratigraphy of the Urakawa and Obira areas, Hokkaido. *Sci. Rep. Tohoku Univ., 2nd Ser. (Geol.)*, **52**, 1-76.

Taketani, Y., 1995, A review of the Cretaceous radiolarian biostratigraphy in Japan - Some radiolarian biohorizons useful for international correlation -. *Jour. Geol. Soc. Japan*, **101**, 30-41.**

Taketani, Y. and Kanie, Y., 1992, Radiolarian age of the Lower Yezo Group and the upper part of the Sorachi Group in Hokkaido. *In* Ishizaki, K. and Saito, T., eds., *Centenary of Japanese Micropaleontology*, Terrapub, Tokyo, 365-373.

Tanabe, H. and Kano, K., 1996, Illite crystallinity study of the Cretaceous Shimanto Belt in the Akaishi Mountains, eastern Southwest Japan. *The Island Arc*, **5**, 56-68.

Tanaka, T. and Orihashi, Y., 1997, *HUPS Technical Report*, no.2..

Tatsumi Y., Shinjoe H., Ishizuka H., Sager W. W. & Klaus A. 1998. Geochemical evidence for a mid-Cretaceous superplume. *Geology* **26**, 151-4.

Thompson, A. B., 1971, Analcite-albite equilibria at low temperatures. *Amer. Jour. Sci.*, **271**, 79-92.

Tsuchiya N., Shibata T., Koide Y., Owada M., Takazawa E., Goto Y., Choi J. H., Terada S., and Hariya Y. 1989. Major element analysis of rock samples by X-ray fluorescence spectrometry, using scandium anode tube. *Journal of Faculty of Science, Hokkaido University*, *Ser IV* **22**, 489-502.

Tumanda, F. P., 1989, Cretaceous radiolarian biostratigraphy in the Esashi Mountain area, Northern Hokkaido, Japan. *Sci. Rep. Inst. Geosci. Univ. Tsukuba, Sec. B,* **10**, 1-44.

U

Ueda, H., Kawamura, M. and Iwata, K., 1993, Occurrence of the Paleocene radiolarian fossils from the Idonnappu Belt, central part of Hokkaido, Northern Japan. *Jour. Geol. Soc. Japan*, **99**, 565-568.*

Ueda, H., Kawamura, M. and Kato, M., 1994a, Structure and Metamorphism of the Mesozoic Accretionary Complex in North Pacific Rim - A study on the Idonnappu Belt, Hokkaido, Northern Japan. *In* Wu, H., Tian, B. and Liu, Y., eds., *IGCP Project 294 international symposium, Very low grade metamorphism: Mechanisms and geological application*, Seismological Press, Baijing, 132-144.

Ueda, H., Kawamura, M., Katoh, T. and Nakagawa, M., 1994b, Geology of accretionary complexes in the Southern Idon'nappu and Kamuikotan Belts, and "Nappe Tectonics". *Excursion Guidebook, 101st Annu. Meet. Geol. Soc. Japan*, 161-174.*

Underwood, M. B., Laughland, M. M. and Kang, S. M., 1993, A comparison among organic and inorganic indicators of diagenesis and low-temperature metamorphism, Tertiary Shimanto Belt, Shikoku, Japan. *Geol. Soc. Amer. Spec. Pap.*, no. 273, 45-61.

V

von Huene, R. and Scholl, D. W., 1993, The return of sialic material to the mantle indicated by terrigeneous material subducted at converggent margins. *Tectonophysics*, **219**, 163-175.

W

Wada, N., Takahashi, K., and Watanabe, J., 1992, *Explanatory text of the Geological Map of Japan, 1/50,000 Mitsuishi* (*Kushiro-65*), Geological Survey of Hokkaido, pp.73.

Watanabe, T., 1981, Idonnappu Formation in the Kamuikotan Belt as constituent of a Mesozoic subduction wedge. *In* Hara, I. ed., *Tectonics of paired metamorphic belts*, Tanishi Print Kikaku, Hiroshima.

Watanabe, T. and Maekawa, H., 1985: Early Cretaceous dual subduction system in and around the Kamuikotan Tectonic Belt, Hokkaido, Japan. *In* N. Nasu, K. Kobayashi, S. Uyeda, I. Kushiro and H. Kagami eds. *Formation of active Ocean margins*, Terrapub, Tokyo, 677-699.

Watanabe, K. and Niida, K., 1987, Greenstones in the Nukabiragawa area of the Kamuikotan Belt., *Earth Sci.* (*Chikyu Kagaku*), **41**, 151-164.**

Watanabe, T., Iwasaki, I., Ueda, H. and Koitabashi, S., 1994, K-Ar age and structure of Mesozoic accretionary prism in NW Pacific rim - a case study of the Kamuikotan metamorphic and Idonnappu belts. *In* Wu, H., Tian, B. and Liu, Y., eds., *IGCP Project 294 international symposium, Very low grade metamorphism: Mechanisms and geological application*, Seismological Press, Baijing, 145-155.

Watanave, Y. and Iwata, K., 1985, The Hidaka Supergroup in the Tomuraushi Region, Hidaka Belt, Hokkaido, Japan. "*Earth Science*" (*Chikyu Kagaku*), **41**, 35-47.

Weaver B. L., Tarney J. & Saunders A. D. 1985. Geochemistry and mineralogy of basalts recovered from the central North Atlantic. *In* Bougault H., Cande S. C. *et al.* eds. *Initial Reports of the Deep Sea Drilling Project* **82**, pp. 395-419. U.S. Government Printing Office, Washington.

Winchester J. A. & Floyd P. A. 1977. Geochemical discrimination of different magma series and their differentiation products using immobile elements. *Chemical Geol*ogy **20**, 325-43.

Y

Yoshida, T., Matsuno, K., Sato, H. and Yamaguchi, S.,1959, Explanatory text of the geological map of Japan, 1/50,000 Biu (Sapporo-56), Geological Survey of Hokkaido, 46pp.**

(*: In Japanese. **: In Japanese with English abstract)

[日本語要旨]

北海道空知－エゾ帯南部地域における白亜紀前弧テクトニクス
－とくに緑色岩類の付加・上昇プロセスについて－

植田勇人

近年海洋プレート沈み込み帯における付加体の実態が明らかになる一方，多様な付加様式の決定要因の特定について問題となっている．これらの問題を解決するためには，多くの付加体の比較を行う手法のみならず，単一の過去の沈み込み帯における付加様式の時代変遷を把握し，周辺環境（海洋プレートの性質など）の変化と比較することが重要である．本研究では中央北海道空知－エゾ帯南部に分布する白亜紀付加体および前弧海盆堆積物の地質構造・層序・年代・および岩石学的な解析をもとに，白亜紀に北海道に存在したプレート沈み込み帯における前弧域の地殻構造とテクトニクスを地史的に復元し，緑色岩の付加様式・付加体構成岩相の時代変化・およびこれらの変遷期における付加体深部相（高圧変成岩）の上昇イベントを捉えた．

本論文はＩ章の序説のほか，II～V 章で構成される．

II 章では，白亜系付加体の浅部相(<10km)である浦河地域のイドンナップ帯について新たな地質図と岩相区分を提示し，放散虫年代，イライト結晶度による弱変成作用，緑色岩の産状と岩石学的性質の記載を行った．イドンナップ帯の付加体は，緑色岩が卓越するナイ沢コンプレックスと，陸源砕屑岩が卓越する幌別川コンプレックスに大別される．

ナイ沢コンプレックスはソレイアイト質の緑色岩スラブと，前期白亜紀砂泥質岩・チャート・石灰岩・海山型緑色岩の構造的混合体がサンドイッチ状に積み重なった構造を示す．ソレイアイト緑色岩はジュラ紀末に付加した空知層群下部のオフィオライトと共通した化学組成を示す（下部空知型）．このためナイ沢コンプレックスは，海溝陸側斜面にあったオフィオライトと沈み込む海山が衝突することにより，両者が破壊・混合したと解釈される．一方幌別川コンプレックスは，後期白亜紀砂泥質岩に少量のチャート・中央海嶺型玄武岩のシートを挟在する PT-Unit を主体とし，石灰岩・緑色岩・チャートのブロックを混在する海底地すべり～土石流堆積物，および後期白亜紀～暁新世のの斜面海盆堆積物を含む．PT-Unit は海溝を充填したタービダイトと，海洋地殻表層の玄武岩・チャートが薄くそぎ取られて付加したものと解釈される．

イライト結晶度の分布から，構造的下位へ向かった変成度の連続的な上昇トレンドと，断層による繰り返し構造が認められた．この結果からイドンナップ帯は白亜紀付加体の断面と捉えられ，古第三紀後期以降に再配列を被ったと結論される．復元された断面から，ナイ沢・幌別川両コンプレックスが上下に積み重なり，それぞれ 3.5-4km および 5-5.5km の厚さであることが判明した．

III 章では，白亜紀付加体の深部相(15-30km)である三石－静内地域神居古潭帯の岩清水コンプレックスについて新たに詳細な地質図と岩相区分を提示し，放散虫年代・変成作用・緑色岩の産状および岩石学的性質を記載した．岩清水コンプレックスは低温高圧型変成作用を受けた緑色岩および少量のチャートや陸源砕屑岩のスライスが，混在相からなる剪断帯を挟んで繰り返すスラブ・スタック構造で構成されており，スライスや混在相の種類から 4 つのユニットに区分される．これらは初生的には低角な断層を境に構造的に累重したパイル・ナップ構造を示し，全体が褶曲している．3 ユニットの陸源砕屑岩部からは前期白亜紀の放散虫化石年代が得られた．構造的上位のユニットほど変成度が高く，最上部で断層を挟んで急に低変成度になる．緑色岩はほとんどが海山型のアルカリ岩乃至ソレイアイトであり，少量の下部空知型ソレイアイトを含む．

以上から，岩清水コンプレックスは前期白亜紀に海山沈み込みに伴って形成された付加体であると結論される．沈み込んだ海山は数 km×数百 m の板状にスライスされ，堆積物とともに積み重なったほか，イドンナップ帯同様空知層群の断片が沈み込み帯に引き込まれたと考えられる．変成度から推定される付加深度と岩相の間には対応関係が見られ，深度による付加メカニズムの違いを反映していると考えられ

る. 比較的浅部ではチャートや砕屑岩は緑色岩とともにスライスとなるが, より深部では堆積構造を失い剪断帯となる. 25km 以上の深部ではもはや陸源砕屑物は含まれない. 変成度の逆転構造から, 次第に沈み込む海洋地殻の傾斜が緩くなる環境下で底付け付加が進行したことや, 上位層の構造的欠層とパイルナップの形成が同時進行的であったことが示唆される.

IV 章では, 本研究で蝦夷累層群(前弧海盆堆積体)中に新たに発見された, 岩清水コンプレックスを覆う不整合と, 青色片岩礫を含む陸成基底礫岩の産状を記載し, 白亜紀中期における岩清水コンプレックスの上昇の実態を考察した. 不整合は三石地域の中部蝦夷層群基底部(前期白亜紀末 Albian)に見られ, ルートによって岩清水コンプレックスあるいは下部蝦夷層群(Barremian-Aptin)を覆っている. 基底礫岩に伴う砂泥質岩からは植物根化石やカキ化石が見られ, 礫岩とともに河川から汽水域にかけての堆積環境を示す. 基底礫岩には多量の緑色岩礫や前期白亜紀放散虫を含む珪質泥岩礫が含まれる. 緑色岩礫中には岩清水コンプレックスに見られる低温高圧型の変成鉱物がほぼ一通り見られた.

以上の産状から, 前期白亜紀(Hauterivian 頃)に下部地殻深度で付加した岩清水コンプレックスは約 20Ma の短期間に上昇し, 白亜紀中頃(Albian)には陸上に露出していたことを示している. 礫の構成から高圧変成岩類は蛇紋岩ダイアピルのブロックとしてではなく, ほぼ現在と同じ構成をもつ付加体全体として上昇したと考えられる.

V 章では, II〜IV 章で記述した付加体浅部および深部相・前弧海盆堆積物の構造層序を, おもに年代と含まれる緑色岩の組成・産状の特徴から中央北海道の他の地質体と対比した. その結果白亜紀の前弧地殻は, 構造的上位からジュラ紀オフィオライト・下部白亜系付加体・上部白亜系付加体のシート状地質体が累重した大規模なパイルナップとして復元され, 地殻が海洋プレートからの底付け付加により下方に成長したことを示した.

神居古潭帯・イドンナップ帯を通じて, 下部白亜系付加体は多量の緑色岩(とくに海山型)を含む一方陸源砕屑岩に乏しく, 上部白亜系は陸源砕屑岩優勢で少量の緑色岩(中央海嶺型)が含まれるという岩相上の特徴が見られた. これは化石年代から復元される沈み込み海洋地殻の年齢・既に復元されているプレートの運動方向・および陸源砕屑物供給量の変化に対応したと推定される. すなわち前期白亜紀には, 陸源砕屑物供給に乏しい環境下で古い海洋地殻の著しい斜め沈み込みに伴って, 付加体はおもに海山の沈み込みにコントロールされて形成された. 一方後期白亜紀には陸源砕屑物の供給量が増加するとともに若い海洋地殻が直交に近い向きで沈み込むようになり, 多量の陸源砕屑岩と少量の海洋地殻表層部が付加した.

岩清水コンプレックスの上昇過程はこの転換期に起こっている. Coulomb-wedge モデルを導入した定性的解析と併せると, 海洋地殻の若化に伴うスラブ傾斜角の低下と, 海山の頻繁な沈み込みによる局所的な圧縮場ー展張場の繰り返しが, 高圧変成岩上昇の原因として考えられる.

| 採取日 | 番 | 副番 | 薄片色 | ルート | unit | facies | 岩石名 | 補足 | 泡 | phenocryst | | | | | | | | | | groundmass | | | | | | | | | | | | | | metamorphic minerals | | | | | | | | | | | | | |

| 採取日 | 番 | 副番 | 色 | ルート | unit | facies | 岩石名 | 補足 | 泡 | phenocryst | | | | | | | | | | | groundmass | | | | | | | | | | | | | | | | | | metamorphic minerals | | | | | | | | | | | | | | | | | |

採取日	番	副番	岩色	ルート	unit	facies	岩石名	補足	泡	phenocryst ol	au	Ti-au	kaer	aeg	pl	sp	mt	Ti-mg	il	ap	groundmass texture	ol	au	Ti-au	hb	kaer	aeg	bi	mt	Ti-mg	ilm	pl	ap	glass	metamorphic minerals anl	prh	pm	lws	ep	all	npx	cpx	Na-amp	act	hb	gar	qz	ab	smc	chl	stp	wm	cc	arg	ti	opq	py	hm	ilm
980613	4 //	*		赤盤の沢	Pr1	sg	aph bas		A												ho											(*)	(*)		•		•				•						•	•		•			•				
980613	5	*		赤盤の沢	Pr1	sg	au-pl bas		f		•				(*)						is		•									(*)	(*)		•		•	•			•						•	•		•			•	•	?		
980613	6 A	*		赤盤の沢	Pr1	sg		rew HC																												•		•			•						•	•		•			•	•			
980613	6 B	*		赤盤の沢	Pr1	sg	aph bas		f												ig		(*)								(*)	(*)	(*)					•		•						•	•		•			•	•	?		
980613	7	*		赤盤の沢	Pr1	sg	aph bas		n												is											(*)	(*)		•		•				•						•	•		•			•			•	
980613	8 //	*		赤盤の沢	Pr1	sg	au-pl bas		C		•				(*)						pi		(D)									(*)	(*)		•		•				•						•	•		•			•	•	?		
980613	8	*		赤盤の沢	Pr1	sg	au bas		A		•										ho											(*)	(*)		•		•				•			•			•	•		•			•				
980613	11	*		赤盤の沢	Pr1	sg	aph bas		f												is		(*)									(*)	(*)	(?)			•		•			•						•	•		•			•	•			
980613	14	*		赤盤の沢	Pr2	MixB	aph bas		n												tr							•				(*)	(*)														•	•		•			•				
980613	16	*		赤盤の沢	Pr2	MixB	aph bas		C												sph										•	(*)	(*)														•	•		•			•			A	
980613	17	*		赤盤の沢	Pr1	sg	bas	rew HC																																								•	•		•			•			•	
980613	18	*		赤盤の沢	Pr1	sg	ol bas		C	(*)											crpt			•								(*)	(?)		•												•	•		•			•	•	?		
980707	5			ヒラシュケ左1	Pr1	sg	aph bas		f																											•		•		•						•	•		•			•		•		
980707	8			ヒラシュケ左1	Mk	MixA	ol bas		C	(*)											is	(*)	(*)									•	(*)	(*)							•						•	•	•	•			•			A	
980707	9			ヒラシュケ左1	Mk	MixA	ol-pl bas	HC	A	(*)					(*)						is											•	(*)	(*)							•						•	•	•	•			•			•	
980707	11			ヒラシュケ左1	Mk	MixA	pl bas		n	(?)					(*)						is											(*)	(*)														•	•	•	•			•	•			
980707	15			ヒラシュケ左3	Pr1	sg	ol?-pl-bas	HC	A																																							•	•	•	•			•			•	
980707	17			ヒラシュケ左3	Pr1	sg	bas	HC	A																																							•	•		•			•	•			
980707	17			ヒラシュケ左3	Pr1	sg	bas	sch																																							•	•		•			•				
980707	21			ヒラシュケ左3	Mk	鳥糞	ol?-au bas		-																													•	•									•	•	•	•			•	•			
980707	22			ヒラシュケ左3	Mk	鳥糞	aph bas		n		•										is										•	(*)	(*)			•										•	•		•			•	•			
980707	23			ヒラシュケ左3	Mk	鳥糞	ol bas		n	(*)	•										ig							•				(*)	(*)			•										•	•		•			•	•			
980710	7			二股一号林道	Pr2	sg	Ti-au bas		C																																						•	•		•			•				
980710	12			二股一号林道	Ft	nd	pl bas	phyric	f						(*)						ho											(*)	(*)														•	•		•			•			A	
980710	12			二股一号林道	Ft	nd	bas	スミ																																						•	•		•			•			•	
980710	16			二股一号林道	Ft	MixB	bas	スミ																																							•	•		•			•			•	
980711	2			二股一号左3	Ft	nd	aph bas																																								•	•		•			•			•	
980711	3			二股一号左3	Ft	MixB	bas	スミ																																							•	•		•			•			•	
980711	5 c			二股一号左3	Ft	MixB	aph bas		C						(m)						is		(*)									(*)	(*)			•	•				•						•	•		•			•				
980711	5			二股一号左3	Ft	MixB	aph bas		-																													•		?		•						•	•		•			•	•			
980711	5			二股一号左3	Ft	MixB	aph bas		-																																						•	•		•			•			•	
980711	6			二股一号左3	Ft	MixB	-	basic claystone																																							•	•		•			•			•	
980711	8			二股一号左3	Ft	MixB	bas	スミ																																							•	•		•			•			?	
980711	8			二股一号左3	Ft	MixB	bas	スミ																																							•	•		•			•				
980711	9 B			二股一号左3	Ft	MixB	bas	スミ																																							•	•		•			•			•	
980711	9			二股一号左3	Ft	MixB	bas	cata																																							•	•		•			•			•	
980711	12			二股一号左3	Pr1	sg	aph bas		n												ig		•								•	(*)														•	•	•	•			•			•	
980711	15			二股一号左3	Pr1	sg	bas	スミ																																								•	•		•			•			•	
980711	16			二股一号左3	Pr1	sg	aph bas	sch	n												is										(*)	(*)	(*)			•	•			•						•	•		•			•				
980711	17			二股一号左3	Pr1	sg	ankaramite		-																																							•	•		•			•				
980713	5			ヒラシュケ	Pr1	sg	pl bas	phyric	C																																							•	•		•			•	•			
980713	11			ヒラシュケ	Pr1	sg	bas	sch	A																																							•	•		•			•				
980713	12	*		ヒラシュケ	Pr1	sg	dolerite		n												oph		•				•				(*)	(*)														•	•		•			•			•	
980714	2			ヒラシュケ右1	Pr1	sg	ankaramite		r																																							•	•	•	•			•				
980714	3 B	*		ヒラシュケ右1	Pr1	sg	au bas		n		•										is		(*)									(*)	(*)	(*)													•	•		•			•			•	
980714	8	*		ヒラシュケ右1	Pr1	sg	aph bas	sch	n												is		(*)									•	(*)	(*)													•	•		•			•	•	?		late
980714	9	*		ヒラシュケ右1	Pr1	sg	au bas		n		•										is		•									(*)	(*)														•	•		•			•			•	
980714	11 A	*		ヒラシュケ右1	Pr1	sg	au-pl bas		n		(*)				(*)						tr		(*)							•			(*)														•	•		•			•	•			
980714	11 B	*		ヒラシュケ右1	Pr1	sg	au bas		C		•										ho		(*)										(*)	(*)													•	•		•			•	•	?		
980714	12	*		ヒラシュケ右1	Pr1	sg	ankaramite		A	(*)	•										ho		•	•								(*)	(*)													•	?		•			•	•	?		
980714	13 A	*		ヒラシュケ右1	Pr1	sg	ankaramite	HC sch	A		•										vit												(*)													•	•		•			•			•	
980714	14 A	*		ヒラシュケ右1	Pr1	sg	ankaramite		f		•	•									ig	(*)		•							(*)	(*)	(f)													•	late		•			•			•	

Appendix I. Petrographic data of greenstones.

| 採取日 | 番 | 副番 | 色 | ルート | unit | facies | 岩石名 | 補足 | 沿 | phenocryst | | | | | | | | | | | groundmass | | | | | | | | | | | | | | | | | metamorphic minerals | | | | | | | | | | | | | | | | |

| 採取日 | 番号 | 副番 | 薄片 | ルート | unit | facies | 岩石名 | 補足 | 泡 | phenocryst | | | | | | | | | | | | groundmass | | | | | | | | | | | | | | | | metamorphic minerals | | | | | | | | | | | | | | | |

| 採取日 | 番 | 副番 | 薄片 | ルート | unit | facies | 岩石名 | 補足 | 斑 | phenocryst | | | | | | | | | | | groundmass | | | | | | | | | | | | | | | | | | | | metamorphic minerals | | | | | | | | | | | | | | | | | | |

| 採取日 | 番 | 副番 | 薄片 | ルート | unit | facies | 岩石名 | 補足 | 沿 | phenocryst | | | | | | | | | | | groundmass | | | | | | | | | | | | | | | | | | | | metamorphic minerals | | | | | | | | | | | | | | | | | | |

| 採取日 | 番 | 副番 | 変色 | ルート | unit | facies | 岩石名 | 補足 | 色 | phenocryst | | | | | | | | | | | groundmass | | | | | | | | | | | | | | | | | | | | | metamorphic minerals | | | | | | | | | | | | | | | | | | |

unit	Sample No.	SITE	point	*min*	occ	SiO_2	TiO_2	Al_2O_3	FeO*	MnO	MgO	CaO	Na_2O	K_2O	Cr_2O_3	Total	remarks
cg	980603-21AMF	1	1	*amp*		53.56	0.03	1.89	19.44	0.40	10.97	9.76	1.86	0.00	0.00	97.91	
cg	980603-21AMF	1	2	*Na-amp*		53.40	0.01	1.50	23.00	0.28	8.89	5.14	4.54	0.12	0.02	96.90	
cg	980603-21AMF	1	3	*amp*		53.29	0.00	2.30	20.02	0.34	10.41	9.46	2.15	0.00	0.00	97.98	
cg	980603-21AMF	1	5	*ep*		37.89	0.04	22.98	12.23	0.82	0.00	21.38	0.00	0.00	0.01	95.35	
cg	980603-21AMF	2	6	*amp*		49.63	0.14	5.19	21.40	0.32	9.32	8.90	3.05	0.10	0.00	98.05	
cg	980603-21AMF	2	7	*amp*		49.00	0.04	5.06	20.21	0.24	10.06	9.47	3.00	0.15	0.00	97.23	
cg	980603-21AMF	2	8	*amp*		51.63	0.09	3.70	19.07	0.38	10.79	10.63	1.71	0.00	0.03	98.03	
cg	980603-21AMF	2	10	*ep*		37.92	0.09	21.50	13.53	0.17	0.00	22.87	0.00	0.00	0.05	96.14	
cg	980603-21AMF	3	11	*Na-amp*		54.21	0.10	0.81	27.58	0.39	6.27	2.33	5.72	0.00	0.03	97.44	
cg	980603-21AMF	3	12	*amp*		52.63	0.06	2.30	19.69	0.39	11.00	10.37	1.52	0.00	0.02	97.96	
cg	980603-21AMF	3	13	*Na-amp*		52.67	0.13	1.93	26.34	0.32	7.20	2.33	5.75	0.00	0.02	96.68	
cg	980603-21AMF	3	14	*amp*		51.30	0.29	4.54	16.59	0.29	12.42	10.88	2.21	0.00	0.00	98.52	
cg	980603-21AMF	3	16	*ep*		38.03	0.02	22.41	12.71	0.16	0.00	23.23	0.00	0.00	0.03	96.58	
cg	980603-21AMF	4	17	*ab*		70.65	0.01	18.57	0.70	0.01	0.27	0.11	10.32	0.03	0.00	100.67	
cg	980603-21AMF	4	18	*amp*		51.69	0.03	3.49	18.18	0.33	11.20	10.79	1.51	0.00	0.02	97.23	
cg	980603-21AMF	4	19	*amp*		51.80	0.09	3.27	19.42	0.34	11.07	9.53	2.27	0.00	0.00	97.78	
cg	980603-21AMF	2	20	*amp*		52.67	0.07	3.27	18.11	0.44	11.93	10.05	1.95	0.01	0.00	98.50	
cg	980603-21AMF	2	21	*amp*		53.59	0.05	2.20	19.36	0.39	11.25	10.42	1.51	0.00	0.02	98.78	
cg	980603-21AMF	2	22	*amp*		45.44	0.09	8.21	23.90	0.30	7.52	9.03	3.33	0.44	0.00	98.26	
cg	980603-21AMF	2	23	*amp*		52.17	0.20	3.32	16.92	0.33	11.91	10.24	0.98	0.00	0.03	96.09	
cg	980603-21AMF	2	24	*amp*		43.02	0.07	5.38	21.22	0.32	3.67	8.68	0.86	0.25	0.00	83.46	
cg	980603-21AMF	6	27	*Na-amp*		55.00	0.10	2.17	20.54	0.17	10.79	1.77	6.25	0.00	0.03	96.82	
cg	980603-21AMF	7	28	*Na-amp*		53.87	0.08	2.49	24.87	0.18	8.36	1.37	6.51	0.00	0.01	97.73	
cg	980603-21AMF	7	29	*Na-amp*		55.68	0.07	1.45	22.18	0.31	8.91	2.75	5.44	0.00	0.01	96.81	
cg	980611-26	8	30	*Na-amp*		52.16	0.50	2.98	26.74	0.74	5.80	2.28	6.02	0.00	0.00	97.21	
cg	980611-26	8	31	*Na-amp*		53.47	0.37	2.47	26.16	0.76	6.36	1.35	6.83	0.00	0.00	97.77	
cg	980611-26	8	32	*chl*		34.77	3.14	14.36	20.70	0.52	13.63	3.37	0.08	1.06	0.00	91.64	
cg	980611-26	8.5	33	*Na-amp*		55.30	0.03	1.95	25.02	0.31	7.18	1.07	6.42	0.00	0.00	97.28	
cg	980611-26	8.5	34	*Na-amp*		55.47	0.15	2.57	23.96	0.33	7.60	0.95	6.77	0.05	0.00	97.85	
cg	980611-26	9	35	*Npx*		53.73	0.06	1.06	17.52	0.40	6.95	15.28	5.25	0.00	0.04	100.28	
cg	980611-26	9	36	*au*		52.92	0.23	2.94	5.23	0.14	17.47	21.19	0.22	0.00	0.73	101.07	
cg	980611-26	9	37	*au*		53.81	0.23	1.76	5.63	0.19	18.43	20.24	0.14	0.00	0.24	100.67	
cg	980611-26	10	38	*all?*		36.48	0.84	10.37	14.74	0.25	3.21	29.83	0.06	0.00	0.85	96.62	
cg	980611-26	10	39	*all?*		36.47	0.86	10.55	14.59	0.27	2.37	30.37	0.05	0.00	0.79	96.32	
cg	980611-26	12	40	*pm*		38.02	0.05	22.02	7.33	0.20	2.50	20.76	0.00	0.00	0.08	90.97	
cg	980611-26	12	41	*au*		48.55	1.55	5.23	8.65	0.17	12.25	21.98	0.56	0.00	0.00	98.93	
cg	980611-26	13	42	*pm*		37.37	0.08	21.69	8.50	0.17	2.41	21.19	0.04	0.00	0.04	91.48	
cg	980611-26	14	43	*Npx*		51.35	0.12	3.95	21.73	0.12	6.07	7.42	8.32	0.00	0.01	99.10	
cg	980611-26	14	44	*chl*		34.63	0.03	13.89	25.87	0.45	14.45	0.52	1.14	0.00	0.03	91.01	
cg	980611-26	14	44	*chl*		34.27	0.01	13.76	27.20	0.39	12.96	1.56	1.36	0.00	0.05	91.55	
cg	980611-26	14	44	*Npx*		54.24	0.09	2.28	22.85	0.14	3.64	6.14	10.32	0.00	0.10	99.78	
cg	980611-26	14	44	*chl*		28.17	0.83	16.51	27.39	0.41	14.34	0.81	0.08	0.00	0.00	88.54	
cg	9806603-21 A9	16	46	*gar*		37.73	0.00	21.42	35.15	2.60	3.06	1.04	0.00	0.00	0.04	101.03	
cg	9806603-21 A9	17	47	*chl*		26.93	8.53	15.01	23.94	0.54	12.53	0.48	0.03	0.00	0.09	88.09	
cg	9806603-21 A9	17	48	*chl*		31.13	2.34	15.37	25.40	0.61	13.83	0.51	0.01	0.00	0.08	89.25	
cg	9806603-21 A9	18	49	*gar*		39.06	0.02	22.12	31.42	0.74	7.59	0.74	0.06	0.00	0.07	101.82	
cg	9806603-21 A9	19	50	*pm*		37.13	0.00	20.48	9.26	0.09	3.08	21.56	0.01	0.00	0.03	91.64	
cg	9806603-21 A9	19	51	*pm*		37.22	0.04	20.70	8.68	0.11	2.84	21.58	0.04	0.00	0.05	91.26	
cg	9806603-21 A9	20	53	*cr-sp*		0.07	0.05	27.84	18.42	0.25	12.84	0.01	0.00	0.00	39.93	99.41	
cg	9806603-21 A9	20	54	*cr-sp*		0.05	0.03	28.05	17.98	0.23	12.68	0.01	0.04	0.00	40.67	99.73	
cg	9806603-21 A9	21	55	*gar*		39.10	0.01	22.03	30.70	0.93	7.08	1.75	0.01	0.00	0.00	101.61	
cg	9806603-21 A9	22	56	*gar*		38.08	0.04	21.38	34.08	2.62	3.31	1.54	0.01	0.00	0.03	101.07	
cg	9806603-21 A9	26	59	*Na-amp*		55.65	0.00	1.77	24.65	0.24	7.36	1.23	6.66	0.00	0.01	97.55	
cg	9806603-21 A9	27	60	*Na-amp*		54.77	0.01	2.56	24.11	0.32	7.44	1.84	6.49	0.00	0.00	97.54	
cg	9806603-21 A9	28	62	*Na-amp*		54.40	0.09	3.43	24.60	0.34	6.25	1.20	6.56	0.00	0.01	96.88	
cg	9806603-21 A9	30	64	*all?*		31.90	0.18	15.62	14.12	0.66	0.19	13.58	0.08	0.00	0.00	76.33	
cg	9806603-21 A9	31	65	*all?*		31.32	0.48	13.30	14.80	0.73	0.10	10.98	0.00	0.00	0.00	71.70	
Hb	SCH RT-3	34	68	*amp*		53.05	0.14	2.74	14.56	1.60	13.32	12.08	0.53	0.00	0.02	98.03	
Hb	SCH RT-3	34	69	*amp*		53.15	0.01	2.27	15.56	1.81	13.25	12.23	0.39	0.00	0.03	98.71	
Hb	SCH RT-3	34	71	*act*		52.81	0.06	2.72	15.31	1.85	12.65	12.09	0.55	0.00	0.02	98.06	
cg	980622-11咲梅	35	73	*Na-amp*		56.60	0.06	1.46	20.11	0.06	10.94	0.15	7.42	0.00	0.03	96.82	
cg	980622-11咲梅	35	74	*Na-amp*		56.81	0.25	1.97	19.59	0.08	10.80	0.82	6.87	0.00	0.01	97.20	
cg	980622-11咲梅	35	76	*Na-amp*		57.00	0.78	1.54	18.94	0.10	11.18	0.81	6.77	0.00	0.04	97.16	
cg	980622-11咲梅	37	83	*ab*		71.94	1.12	18.61	0.53	0.00	0.02	0.02	9.15	0.01	0.00	101.40	
cg	980622-11咲梅	38	84	*Na-amp*		55.91	0.63	1.53	21.95	0.15	10.04	0.98	6.60	0.00	0.02	97.80	
cg	980622-11咲梅	38	85	*Na-amp*		57.75	0.34	2.35	19.31	0.15	11.25	0.42	6.99	0.00	0.07	98.63	
cg	980622-11咲梅	38	86	*Na-amp*		54.95	1.54	0.87	24.33	0.15	7.96	0.48	6.86	0.00	0.03	97.17	
cg	980611-30転	55	112	*au*	g	52.55	0.39	3.18	4.92	0.11	16.79	21.78	0.21	0.00	1.08	101.01	c
cg	980611-30転	55	113	*au*	g	50.55	0.48	4.27	5.34	0.16	16.51	19.97	0.22	0.00	1.30	98.79	c
cg	980611-30転	56	114	*au*	g	52.49	0.28	2.36	4.78	0.11	17.22	21.53	0.23	0.00	0.78	99.78	c
cg	980611-30転	57	116	*au*	g	52.05	0.39	3.04	7.22	0.17	16.87	19.77	0.34	0.00	0.11	99.95	r
cg	980611-30転	58	118	*au*	g	52.63	0.25	2.21	4.96	0.13	17.15	20.93	0.23	0.00	0.62	99.12	r
cg	980611-30転	58	119	*au*	s	52.63	0.53	2.45	8.25	0.23	19.10	17.17	0.19	0.00	0.01	100.56	c
cg	980611-30転	58	120	*au*	g	52.99	0.23	2.53	5.35	0.13	17.36	20.37	0.23	0.00	0.42	99.62	c
cg	980611-30転	58	121	*au*	gp	52.48	0.33	2.10	7.78	0.18	16.18	20.05	0.23	0.00	0.00	99.33	r
cg	980611-30転	59	122	*au*	gp	53.62	0.12	1.22	14.97	0.53	7.68	13.56	6.39	0.00	0.01	98.10	c
cg	980611-30転	59	123	*au*	gp	46.98	2.05	6.62	11.69	0.23	10.58	18.48	2.25	0.00	0.06	98.94	r

Appendix II. EPMA-analysed mineral compositions.

unit	Sample No	SITE	point	*min*	occ	SiO_2	TiO_2	Al_2O_3	FeO*	MnO	MgO	CaO	Na_2O	K_2O	Cr_2O_3	Total	remarks
cg	980611-30転	60	124	*au*	gp	52.04	0.21	2.17	5.63	0.15	16.92	20.76	0.18	0.00	0.38	98.43	c
cg	980611-30転	60	125	*au*	gp	52.11	0.53	3.99	5.83	0.15	16.34	20.46	0.19	0.00	0.54	100.15	r
cg	980611-30転	60	126	*Npx*	s	53.12	0.52	3.03	21.52	0.18	2.02	2.80	12.82	0.00	0.14	96.16	c
cg	980611-30転	61	127	*Npx*	gp	53.94	0.40	3.43	21.99	0.23	2.29	3.54	12.39	0.00	0.05	98.26	c
cg	980611-30転	62	128	*Npx*	gp	53.58	0.74	2.43	23.88	0.22	1.81	2.23	12.96	0.00	0.27	98.11	c
cg	980611-30転	62	129	*au*	gp	51.28	0.70	4.72	6.56	0.19	16.54	19.73	0.23	0.00	0.41	100.36	c
cg	980611-30転	62	130	*au*	gp	50.71	0.89	4.79	8.55	0.19	15.75	18.88	0.29	0.00	0.09	100.14	c
cg	980611-30転	63	131	*au*	gp	53.12	0.29	2.71	4.84	0.13	17.00	21.92	0.25	0.00	0.80	101.04	c
cg	980611-30転	63	132	*au*	gp	52.30	0.43	3.35	5.95	0.21	16.95	21.37	0.22	0.00	0.55	101.33	r
cg	980611-30転	63	133	*au*	gp	52.00	0.36	2.50	6.53	0.14	16.59	20.38	0.30	0.00	0.19	99.01	c
cg	980611-30転	64	134	*au*	gp	54.01	0.30	1.99	6.26	0.17	19.10	18.40	0.15	0.00	0.55	100.93	c
cg	980611-30転	64	135	*npx*	gg	54.93	0.27	1.83	24.88	0.13	6.82	0.20	7.41	0.00	0.15	96.62	c
cg	980611-30転	65	136	*npx*	gg	53.27	0.09	4.37	10.51	0.13	8.59	13.66	6.75	0.00	0.31	97.67	c
cg	980611-30転	66	137	*Na-amp*	g	46.01	0.58	6.73	12.49	0.24	14.47	15.59	0.69	0.00	0.14	96.94	c
cg	980611-30転	67	138	*ep*	gp	36.04	0.02	19.36	11.81	0.07	2.06	22.07	0.09	0.00	0.04	91.56	c
cg	980611-30転	67	139	*chl*	gp	41.54	0.07	10.90	13.88	0.38	20.59	2.10	2.00	0.00	0.03	91.49	r
cg	980611-30転	68	140	*au*	g	50.18	0.75	4.08	8.58	0.22	15.63	18.30	0.26	0.00	0.07	98.06	c
cg	980611-30転	69	141	*au*	g	50.99	0.72	4.72	6.36	0.12	16.52	20.59	0.23	0.00	0.44	100.67	
cg	980611-30転	70	142	*au*	gp	50.60	0.58	3.69	6.20	0.19	16.57	20.07	0.21	0.00	0.27	98.39	c
cg	980611-30転	70	143	*au*	gp	52.31	0.35	3.32	5.42	0.16	16.84	21.27	0.25	0.00	0.56	100.49	c
cg	980611-30転	71	144	*au*	gp	51.33	0.55	3.73	6.36	0.19	16.52	21.03	0.19	0.00	0.54	100.44	c
cg	980611-30転	73	146	*au*	gp	49.58	0.85	4.28	9.06	0.24	14.30	20.18	0.38	0.00	0.12	98.99	c
cg	980611-30転	73	147	*au*	gp	52.81	0.29	2.48	4.94	0.18	17.18	21.07	0.20	0.00	0.77	99.91	r
cg	980611-30転	73	148	*au*	s	51.14	0.76	4.17	7.75	0.22	16.15	20.13	0.25	0.00	0.17	100.73	c
cg	980611-30転	74	151	*au*	gp	51.18	0.67	7.84	7.88	0.17	14.66	16.32	1.41	0.00	0.18	100.32	r
cg	980611-30転	75	152	*au*	gp	50.29	2.09	5.91	20.23	0.20	8.71	5.56	5.48	0.23	0.00	98.68	c
cg	980611-30転	75	153	*au*	gp	47.72	1.34	6.74	9.94	0.16	12.18	22.16	0.34	0.00	0.10	100.68	r
cg	980611-30転	77	154	*au*	gp	48.27	1.12	6.61	9.79	0.26	12.10	20.40	0.69	0.00	0.09	99.33	c
cg	980611-30転	77	155	*au*	gp	52.87	0.29	2.54	7.76	0.33	15.82	19.69	1.24	0.00	0.44	100.98	c
cg	980611-30転	77	156	*au*	gp	52.21	0.72	3.19	9.07	0.24	16.03	19.61	0.24	0.00	0.01	101.32	r
cg	980611-30転	78	157	*au*	gp	52.81	0.21	2.35	5.54	0.19	17.36	21.23	0.23	0.00	0.29	100.21	c
cg	980611-30転	81	159	*au*	gp	54.50	0.36	2.07	4.97	0.18	17.72	21.25	0.17	0.00	0.53	101.75	c
cg	980611-30転	81	160	*au*	gp	53.43	0.27	2.26	4.95	0.16	17.41	21.25	0.23	0.00	0.67	100.64	r
cg	980611-30転	82	161	*au*	gp	53.64	0.27	1.75	6.29	0.19	17.87	21.08	0.21	0.00	0.12	101.42	c
cg	980611-30転	84	163	*Npx*	gp	55.11	0.08	4.83	22.76	0.14	1.57	3.42	12.66	0.00	0.03	100.60	r
cg	980611-30転	85	164	*au*	g	51.08	0.53	4.12	5.72	0.14	15.60	21.45	0.29	0.00	0.95	99.88	c
cg	980611-30転	86	166	*chl*	gp	27.69	0.04	17.32	25.70	0.64	15.88	0.04	0.02	0.00	0.01	87.33	c
cg	980611-30転	86	167	*au*	g	51.11	0.59	4.33	6.84	0.20	15.52	21.27	0.26	0.00	0.17	100.28	c
cg	980611-30転	87	168	*au*	g	54.03	0.09	1.87	7.63	0.16	12.11	19.95	3.07	0.00	0.27	99.17	c
cg	980611-30転	88	169	*au*	gg	52.61	0.46	2.27	7.44	0.27	16.75	20.24	0.25	0.00	0.04	100.34	c
cg	980611-30転	89	170	*au*	gp	47.23	2.33	6.74	8.60	0.14	11.91	21.84	0.98	0.00	0.05	99.80	c
cg	980611-30転	89	171	*au*	gp	46.39	3.26	7.37	8.91	0.18	11.90	22.38	0.65	0.00	0.02	101.05	c
cg	980611-30転	89	173	*chl*	gp	32.18	0.02	16.89	11.24	0.07	27.04	0.23	0.00	0.00	0.34	88.02	r
cg	980611-30転	91	175	*au*	g	52.61	0.35	2.88	4.74	0.16	17.47	20.86	0.24	0.00	0.91	100.22	c
cg	980611-30転	94	177	*au*	gp	51.36	1.01	2.29	11.15	0.27	13.87	20.53	0.43	0.00	0.00	100.91	c
cg	980611-30転	95	178	*Npx*	g	53.25	0.02	0.78	20.22	0.38	5.40	14.25	6.39	0.00	0.03	100.73	c
cg	980611-30転	95	179	*au*	gd	51.65	0.54	4.40	5.32	0.18	16.22	21.14	0.20	0.00	1.13	100.77	c
cg	980611-30転	97	181	*Npx*	gp	54.25	0.21	2.65	23.94	0.12	1.76	3.58	12.75	0.00	0.04	99.29	c
cg	980611-30転	98	183	*Npx*	g	55.03	0.04	2.51	17.21	0.18	6.22	11.58	7.90	0.00	0.01	100.68	c
Pr1	980609-8	100	186	*Npx*	au	53.42	0.01	0.68	15.20	0.31	8.28	16.14	5.29	0.00	0.01	99.34	qz
Pr1	980609-8	100	187	*Npx*	au	54.81	0.04	2.40	18.43	0.20	5.57	10.74	8.48	0.00	0.00	100.68	qz
Pr1	980609-8	104	188	*au*	R	50.62	1.10	4.26	6.72	0.10	15.98	20.21	0.29	0.00	0.32	99.60	c
Pr1	980609-8	104	189	*au*	R	50.91	1.61	4.53	6.86	0.20	15.23	20.89	0.30	0.00	0.06	100.57	c
Mk	980503-21	105	191	*au*	R	51.83	1.20	4.08	6.50	0.15	16.03	21.04	0.27	0.00	0.10	101.20	r
Mk	980503-21	106	192	*au*	R	52.11	0.75	3.58	5.53	0.13	16.70	20.92	0.30	0.00	0.61	100.63	c
Mk	980503-21	107	194	*au*	R	53.81	0.56	2.29	5.24	0.11	17.26	21.64	0.30	0.00	0.48	101.67	c
Mk	980501-17	111	207	*au*	R	54.22	0.65	2.38	5.74	0.15	17.97	20.26	0.32	0.00	0.26	101.95	c
Mk	980501-17	111	208	*au*	R	53.33	0.69	4.18	10.44	0.13	12.92	15.11	4.22	0.03	0.48	101.54	r
Mk	980501-17	112	209	*au*	R	52.44	0.79	3.16	6.63	0.18	16.46	21.16	0.29	0.00	0.39	101.49	c
Mk	980501-17	113	211	*au*	R	53.77	0.72	2.11	6.05	0.22	18.94	18.53	0.28	0.00	0.38	101.00	c
Mk	980501-17	114	213	*au*	R	50.78	1.44	3.28	10.84	0.21	14.49	19.71	0.28	0.00	0.02	101.04	c
Pr1	980506-18	115	215	*au*	R	53.32	0.93	1.68	11.61	0.27	15.63	18.15	0.27	0.00	0.01	101.86	c
Pr1	980506-18	117	219	*au*	R	53.98	0.76	2.85	3.87	0.20	17.32	21.65	0.26	0.00	0.24	101.13	c
Pr1	980506-18	118	221	*au*	R	52.68	1.03	1.99	6.85	0.24	15.54	19.56	0.23	0.00	0.00	98.13	c
Pr1	980506-18	119	223	*au*	R	50.61	1.34	3.33	11.06	0.27	13.66	20.37	0.32	0.00	0.00	100.95	c
Pr1	980506-18	119	224	*au*	R	48.07	1.60	3.87	12.18	0.37	13.32	18.61	0.31	0.00	0.06	98.38	c
cg	980611-26A1	121	227	*au*	gp	50.71	0.71	3.42	5.41	0.15	16.37	21.22	0.34	0.00	0.85	99.16	c
cg	980611-26A1	122	228	*au*	s	51.06	0.89	4.34	7.28	0.16	15.23	21.06	0.28	0.00	0.22	100.53	c
cg	980611-26A1	123	229	*au*	s	50.92	0.58	4.13	6.01	0.12	15.36	21.22	0.22	0.00	0.45	99.00	c
cg	980611-26A1	125	232	*au*	s	51.97	0.26	2.21	5.85	0.16	16.49	21.50	0.17	0.00	0.21	98.82	r
cg	980611-26A1	126	233	*npx*	s	53.40	0.06	2.45	18.58	0.19	5.61	10.09	8.79	0.00	0.03	99.20	c
cg	980611-26A1	127	237	*npx*	s	52.78	0.11	4.28	21.11	0.21	7.21	3.63	9.10	0.00	0.00	98.43	c
cg	980611-26A1	129	239	*ep*	s	30.50	31.18	5.52	1.69	0.01	0.21	28.25	0.04	0.00	0.00	97.40	c
cg	980611-26A1	130	240	*au*	s	52.88	0.30	2.62	4.72	0.14	17.29	21.05	0.15	0.00	0.52	99.66	c

Appendix II. EPMA-analysed mineral compositions.

unit	Sample No.	SITE	point	*min*	occ	SiO_2	TiO_2	Al_2O_3	FeO*	MnO	MgO	CaO	Na_2O	K_2O	Cr_2O_3	Total	remarks
cg	980611-26A1	131	241	*chl*	s	31.05	0.00	17.26	12.99	0.29	25.46	0.10	0.06	0.00	0.14	87.35	c
cg	980611-26A1	131	242	*pm*	s	35.07	0.67	9.68	16.18	0.24	10.96	18.58	0.00	0.00	0.55	91.94	c
cg	980611-26A1	132	243	*au*	s	47.39	1.66	4.87	13.70	0.39	11.50	18.18	0.45	0.00	0.04	98.17	c
cg	980611-26A1	133	244	*chl*	s	30.65	0.00	17.58	15.68	0.33	22.78	0.50	0.01	0.00	0.02	87.56	c
cg	980611-26A1	133	247	*au*	s	52.19	0.39	2.32	6.40	0.18	16.27	20.69	0.25	0.00	0.12	98.81	c
cg	980611-26A1	134	248	*au*	s	53.91	0.35	2.01	6.41	0.14	17.58	19.82	0.23	0.00	0.17	100.62	c
cg	980611-26A1	136	250	*npx*	s	54.92	0.07	2.68	18.14	0.18	5.60	10.05	8.86	0.00	0.03	100.54	c
cg	980611-26A1	137	251	*ep*	s	35.65	1.06	8.41	15.69	0.33	2.64	30.13	0.04	0.00	0.72	94.67	c
cg	980611-26A1	140	256	*au*	s	54.28	0.16	1.81	5.57	0.16	17.12	19.17	0.16	0.00	0.22	98.66	c
cg	980611-26A1	144	261	*au*	s	53.80	0.38	2.76	6.47	0.18	15.51	19.98	0.25	0.00	0.23	99.56	c
cg	980611-26A1	145	262	*pm*	s	38.52	0.03	21.64	7.92	0.15	2.65	21.31	0.02	0.00	0.01	92.28	c
cg	980611-26A1	146	263	*Npx*	s	56.61	0.02	2.34	14.45	0.20	7.62	12.04	7.18	0.00	0.05	100.50	c
cg	980611-26A1	149	265	*au*	gp	51.23	0.48	4.02	5.50	0.13	15.22	21.25	0.26	0.00	0.46	98.54	c
cg	980611-26A1	150	267	*au*	gp	52.05	1.03	4.02	3.93	0.13	15.92	21.52	0.41	0.00	1.26	100.29	c
cg	980611-26A1	151	268	*au*	gp	53.14	0.43	3.26	6.88	0.13	15.60	21.52	0.31	0.00	0.09	101.36	c
cg	980611-26A1	152	270	*au*	s	51.26	0.65	4.39	8.78	0.19	13.13	19.64	0.58	0.00	0.38	99.00	c
鳥	980707-23	157	273	*au*	R	53.82	0.42	3.41	5.37	0.14	16.11	21.17	0.22	0.00	0.78	101.44	c
鳥	980707-23	157	274	*au*	R	51.65	0.65	3.83	7.63	0.19	15.02	19.20	0.25	0.00	0.05	98.47	r
鳥	980707-23	158	275	*au*	R	52.93	0.43	3.68	6.04	0.10	15.47	20.56	0.25	0.00	0.63	100.09	c
鳥	980707-23	158	276	*au*	R	54.23	0.36	2.92	5.82	0.19	16.52	20.34	0.19	0.00	0.50	101.08	r
鳥	980707-23	159	277	*au*	R	51.68	0.60	4.23	6.31	0.16	15.53	20.18	0.26	0.00	0.63	99.59	c
鳥	980707-23	159	278	*au*	R	53.06	0.35	2.68	5.70	0.16	15.71	20.19	0.21	0.00	0.37	98.42	r
鳥	980707-23	161	281	*au*	R	53.67	0.48	3.68	6.13	0.08	16.26	20.46	0.26	0.00	0.68	101.69	c
鳥	980707-23	161	282	*au*	R	52.42	0.45	3.70	6.45	0.20	16.11	18.88	0.25	0.00	0.59	99.06	r
鳥	980603-7	163	286	*au*	R	53.84	0.40	3.48	5.24	0.15	16.11	21.01	0.26	0.00	1.01	101.49	r
鳥	980603-7	164	287	*au*	R	54.18	0.34	2.75	5.56	0.15	16.43	20.65	0.23	0.00	0.40	100.67	c
鳥	980603-7	165	289	*au*	R	53.07	0.61	3.13	8.13	0.25	15.28	19.37	0.21	0.00	0.02	100.06	c
鳥	980603-7	165	290	*au*	R	52.36	0.75	3.04	10.05	0.25	14.58	18.94	0.26	0.00	0.00	100.23	r
鳥	980612-3	167	294	*au*	R	54.11	0.49	1.98	8.82	0.22	15.95	19.38	0.19	0.00	0.00	101.14	c
鳥	980612-3	167	295	*au*	R	52.38	0.75	2.54	11.72	0.34	13.97	18.39	0.30	0.00	0.02	100.41	r
鳥	980612-3	168	296	*au*	R	53.16	0.43	2.67	6.31	0.10	15.93	20.04	0.25	0.00	0.11	98.99	c
鳥	980612-3	168	297	*au*	R	54.15	0.45	2.50	6.30	0.18	16.16	20.55	0.19	0.00	0.11	100.58	r
鳥	980612-3	169	299	*au*	R	53.84	0.32	2.05	5.85	0.20	16.27	19.95	0.20	0.00	0.32	99.00	r
鳥	980612-3	170	302	*au*	R	53.84	0.41	2.72	6.22	0.12	16.45	20.75	0.24	0.00	0.18	100.93	r
鳥	980612-3	170	303	*prh*	vein	44.03	0.00	24.12	0.04	0.04	0.04	25.04	0.11	0.01	0.00	93.42	c
鳥	980612-3	171	306	*au*	R	54.47	0.36	1.99	5.90	0.14	16.32	20.44	0.24	0.00	0.15	100.00	r
Hb	971113-17	54	307	*act*		54.21	0.05	1.36	14.49	0.31	14.51	12.59	0.32	0.00	0.06	97.89	
Hb	971113-17	53	312	*act*		53.22	0.02	3.21	16.03	0.39	14.72	10.13	0.17	0.00	0.00	97.90	
Hb	971113-17	53	313	*ab*		72.02	0.01	19.50	0.11	0.03	0.00	0.59	8.07	0.10	0.00	100.43	
Hb	971113-17	52	315	*ab*		70.27	0.00	16.89	1.95	0.03	1.79	2.01	8.35	0.09	0.00	101.38	
Hb	971113-17	52	316	*au*		51.96	1.07	3.62	7.61	0.19	16.75	19.39	0.28	0.00	0.29	101.15	
Hb	971113-17	50	319	*act*		54.36	0.00	1.85	15.25	0.39	14.12	12.27	0.30	0.00	0.00	98.54	
Hb	971113-17	50	320	*au*		51.86	1.26	2.82	9.29	0.24	15.73	19.66	0.24	0.00	0.03	101.12	
Hb	971113-17	50	323	*au*		51.49	0.91	3.54	8.16	0.26	16.57	19.25	0.30	0.00	0.21	100.69	
Hb	971113-17	49	326	*au*		51.88	1.00	3.16	9.45	0.25	16.01	18.66	0.32	0.00	0.12	100.84	
Hb	971113-17	49	327	*act*		54.63	0.07	1.83	14.72	0.35	14.59	11.96	0.32	0.19	0.00	98.66	
Hb	SCH-RT3	46	332	*act*		53.69	0.02	2.39	14.90	1.66	13.65	11.88	0.37	0.00	0.06	98.60	
Hb	SCH-RT3	45	336	*hb*		51.29	0.03	3.74	16.04	1.92	13.78	11.06	0.28	0.00	0.09	98.22	
Hb	SCH-RT3	44	339	*act*		52.18	0.00	3.13	15.96	1.67	12.95	11.80	0.61	0.04	0.04	98.37	
Hb	SCH-RT3	43	344	*ab*		66.75	0.06	21.88	1.44	0.03	0.43	1.38	6.49	1.79	0.00	100.25	
Hb	SSM-RT4	42	345	*act*		54.61	0.04	1.83	13.45	0.39	15.36	12.81	0.22	0.00	0.00	98.71	
Hb	SSM-RT4	42	346	*au*		52.33	0.82	3.19	8.23	0.20	17.61	18.56	0.26	0.00	0.05	101.23	
Hb	SSM-RT4	42	347	*ab*		71.74	0.00	19.46	1.13	0.02	0.99	0.32	7.84	0.36	0.00	101.87	
Hb	SSM-RT4	42	348	*au*		51.12	1.08	2.27	15.50	0.46	13.25	16.41	0.28	0.00	0.00	100.36	
Hb	SSM-RT4	39	350	*au*	gm	51.24	0.97	2.81	11.51	0.24	15.23	17.97	0.30	0.00	0.01	100.27	c
Hb	SSM-RT4	39	351	*au*	gm	50.42	1.36	2.51	15.52	0.35	12.33	17.75	0.36	0.00	0.02	100.60	r
Hb	SSM-RT4	39	352	*au*	gm	52.25	0.90	3.35	6.70	0.21	17.28	18.89	0.25	0.00	0.18	100.01	c
Hb	SSM-RT4	39	353	*ab*		66.46	0.03	20.31	3.22	0.09	2.49	1.05	7.23	0.18	0.03	101.09	
Hb	SCH RT-3?	173	356	*act*		58.50	0.03	4.33	14.50	0.30	9.44	9.22	0.14	0.25	0.01	96.70	
Hb	SCH RT-3?	174	360	*hb*		45.54	0.96	9.50	16.16	0.37	11.55	11.55	1.97	0.66	0.04	98.30	
Hb	SCH RT-3?	175	362	*hb*		50.60	0.22	4.31	15.07	0.63	14.50	11.20	0.65	0.06	0.05	97.29	
Hb	SCH RT-3?	175	365	*ab*		71.41	0.01	20.11	0.24	0.00	0.00	1.07	8.81	0.07	0.01	101.73	
Hb	SCH RT-3?	177	370	*hb*		46.99	1.01	8.05	15.96	0.73	12.82	9.85	1.40	0.17	0.01	96.99	
Hb	SCH RT-3?	178	371	*hb*		45.70	1.30	10.74	12.26	0.34	14.29	11.14	2.10	0.19	0.00	98.07	
Hb	SCH RT-3?	178	372	*hb*		43.53	1.79	12.09	12.33	0.26	14.13	11.79	2.18	0.44	0.00	98.55	
Hb	SCH RT-3?	190	374	*ep*		38.84	0.01	24.67	10.89	0.12	0.02	23.38	0.02	0.00	0.01	97.95	
Hb	SCH RT-3?	191	376	*hb*		51.14	0.45	3.99	17.20	1.07	13.34	11.21	0.58	0.00	0.00	98.98	
Hb	SCH RT-3?	191	378	*ep*		37.99	0.03	19.60	16.06	0.31	0.02	22.37	0.01	0.00	0.00	96.37	
cg	980611-26転	199	386	*Npx*	g	52.29	0.31	3.17	20.93	0.33	2.99	5.48	11.03	0.00	0.02	96.55	r
cg	980611-26転	199	387	*act*	g	55.67	0.06	0.19	6.41	0.16	19.70	12.01	0.29	0.00	0.06	94.53	c
cg	980611-26転	200	390	*ep*	s	35.09	0.07	19.77	11.72	0.13	0.02	19.53	0.00	0.00	0.03	86.34	c
cg	980611-26転	202	391	*prh*	g	43.36	0.03	22.56	0.99	0.04	0.03	24.34	0.11	0.00	0.00	91.47	c
cg	980611-26転	202	392	*prh*	g	41.94	0.00	22.34	1.28	0.04	0.00	24.49	0.11	0.00	0.04	90.24	c
cg	980611-26転	202	393	*anc*	g	59.79	0.00	22.24	0.04	0.04	0.00	0.01	8.91	0.04	0.00	91.07	c
cg	980611-26転	202	394	*prh*	g	42.12	0.02	22.46	0.68	0.02	0.00	24.74	0.13	0.00	0.02	90.18	c
cg	980611-26転	202	395	*anc*	g	61.68	0.00	22.22	0.17	0.02	0.03	0.00	8.31	0.10	0.00	92.52	c

Appendix II. EPMA-analysed mineral compositions.

unit	Sample No.	SITE	point	*min*	occ	SiO_2	TiO_2	Al_2O_3	FeO*	MnO	MgO	CaO	Na_2O	K_2O	Cr_2O_3	Total	remarks
cg	980611-26転	202	396	*anc*	g	63.24	0.00	21.57	0.11	0.00	0.00	0.03	8.48	0.12	0.01	93.56	c
cg	980611-26転	203	397	*prh*	g	43.63	0.00	21.28	2.86	0.00	0.01	25.20	0.10	0.00	0.04	93.12	c
cg	980611-26転	203	398	*anc*	g	59.62	0.00	21.95	0.14	0.00	0.00	0.82	7.67	0.17	0.00	90.37	c
cg	980611-26転	204	400	*prh*	g	43.58	0.00	22.98	1.18	0.00	0.02	26.27	0.00	0.00	0.05	94.07	c
cg	980611-26転	204	401	*prh*	g	43.64	0.00	23.21	0.86	0.00	0.00	25.13	0.00	0.00	0.00	92.84	c
cg	980611-26転	204	402	*anc*	g	64.09	0.00	22.28	0.06	0.00	0.00	0.01	8.53	0.14	0.04	95.14	c
cg	980611-26転	206	403	*au*	gp	49.17	0.86	5.72	6.88	0.11	15.12	21.09	0.20	0.00	0.45	99.58	c
cg	980611-26転	206	404	*gar*	g	32.63	1.17	1.26	23.76	0.12	0.31	32.50	0.00	0.00	0.29	92.02	c
cg	980611-26転	206	405	*au*	gp	52.20	0.40	2.36	6.77	0.18	17.48	19.03	0.18	0.00	0.34	98.94	c
cg	980611-26転	207	406	*pm*	s	37.66	0.01	23.69	5.45	0.14	2.79	21.78	0.09	0.00	0.00	91.61	c
cg	980611-26転	208	407	*au*	s	50.78	1.00	4.02	6.01	0.12	15.71	21.10	0.40	0.00	0.97	100.11	c
cg	980611-26転	209	408	*au*	s	52.40	0.29	1.88	4.93	0.15	17.91	20.08	0.18	0.00	0.28	98.10	c
cg	980611-26転	210	409	*au*	g-mp	52.73	0.35	3.20	5.53	0.13	17.70	20.42	0.16	0.00	0.60	100.82	c
cg	980611-26転	212	410	*au*	gp	50.21	0.55	5.02	5.52	0.13	16.28	19.76	0.23	0.00	1.11	98.80	c
cg	980611-26転	213	411	*au*	s	51.61	0.55	2.57	8.29	0.23	15.00	20.53	0.29	0.00	0.01	99.07	c
cg	980611-26転	214	412	*au*	s	51.08	0.55	2.59	8.30	0.21	14.93	20.37	0.32	0.00	0.00	98.33	c
cg	980611-26転	215	413	*au*	g-mp	53.04	0.33	2.38	6.22	0.18	17.71	19.90	0.17	0.00	0.34	100.28	c
cg	980611-26転	216	414	*anc*	g	66.03	0.00	21.23	0.06	0.00	0.00	0.03	7.49	0.16	0.00	94.98	c
cg	980611-26転	216	415	*anc*	g	63.11	0.00	22.07	0.00	0.02	0.00	0.04	8.84	0.16	0.00	94.23	c
cg	980611-26転	216	416	*anc*	g	60.47	0.00	23.58	0.03	0.02	0.00	0.02	9.47	0.10	0.01	93.71	c
cg	980611-26転	218	417	*au*	gp	48.23	1.08	6.34	7.15	0.17	13.60	21.82	0.26	0.00	0.24	98.90	c
cg	980611-26転	218	418	*au*	gp	45.81	2.13	7.27	9.56	0.21	11.84	21.30	0.64	0.00	0.00	98.77	c
cg	980611-26	221	419	*au*	s	51.07	0.50	4.53	5.20	0.14	15.77	21.42	0.27	0.00	1.08	99.99	c
cg	980611-26	222	420	*au*	gp	52.50	0.41	2.89	6.59	0.15	16.90	19.85	0.23	0.00	0.36	99.87	c
cg	980611-26	223	421	*au*	gp	52.22	0.50	3.23	7.29	0.19	17.44	18.62	0.25	0.00	0.27	100.00	c
Sz	990923-8	228	422	*au*	dol	45.03	3.97	8.22	7.02	0.14	12.32	22.82	0.47	0.00	0.04	100.02	c
Sz	990923-8	228	423	*au*	dol	43.29	4.38	9.15	7.41	0.13	11.61	22.33	0.52	0.00	0.01	98.83	r
Sz	990923-8	228	424	*pm*	agg	36.94	0.10	22.02	7.85	0.09	2.45	20.98	0.20	0.00	0.05	90.67	
Sz	990923-8	228	425	*pm*	agg	36.90	0.10	21.88	8.77	0.10	2.24	21.33	0.27	0.00	0.01	91.59	
Sz	990923-8	229	426	*Na-amp*	kaer	53.92	0.49	2.26	25.36	0.17	6.81	1.10	6.84	0.00	0.01	96.95	
Sz	990923-8	229	427	*Na-amp*	kaer	53.75	0.58	1.70	27.44	0.32	5.62	0.86	6.88	0.00	0.02	97.15	
Sz	990923-8	229	428	*au*	dol	48.89	1.98	4.94	6.12	0.09	14.12	22.43	0.47	0.00	0.00	99.02	c
Sz	990923-8	229	429	*au*	dol	49.62	1.75	3.98	6.58	0.16	14.50	22.53	0.44	0.00	0.00	99.55	r
Sz	990923-8	229	430	*aeg*	dol	52.16	4.90	1.11	24.70	0.16	0.10	0.64	13.50	0.00	0.05	97.30	r
Sz	990923-8	229	431	*chl*	agg	30.84	0.00	17.03	18.57	0.27	21.74	0.14	0.01	0.00	0.00	88.59	
Sz	990923-7	230	432	*lws*	agg	39.16	0.25	29.73	2.44	0.18	0.04	15.85	0.00	0.00	0.02	87.68	
Sz	990923-7	230	433	*lws*	agg	39.58	0.46	30.26	2.02	0.15	0.03	15.76	0.00	0.00	0.01	88.27	
Sz	990923-7	230	434	*lws*	agg	38.60	0.16	29.72	2.26	0.18	0.09	15.76	0.00	0.00	0.00	86.77	
Sz	990923-7	231	435	*lws*	agg	37.94	0.24	29.91	2.29	0.13	0.03	15.94	0.00	0.00	0.00	86.49	
Sz	990923-7	231	436	*lws*	agg	38.71	0.25	29.34	2.53	0.13	0.11	15.16	0.00	0.00	0.00	86.22	
Sz	971102-5	232	437	*ab*	vein	69.95	0.00	19.61	0.20	0.00	0.02	0.03	11.86	0.02	0.00	101.69	
Sz	971102-5	232	438	*Npx*	vein	53.23	0.18	2.99	17.36	2.04	5.10	10.53	7.68	0.00	0.00	99.11	ab
Sz	971102-5	232	440	*Npx*	vein	52.63	0.50	3.02	17.18	1.72	5.43	11.16	7.26	0.00	0.00	98.91	ab
Sz	971102-5	232	441	*Npx*	vein	53.88	0.17	1.63	18.44	2.89	6.70	9.66	5.69	0.00	0.02	99.08	ab
Sz	971102-5	233	444	*au*	ph	49.61	1.56	4.34	7.57	0.18	15.65	19.85	0.58	0.00	0.34	99.69	c
Sz	971102-5	233	445	*au*	ph	51.05	1.58	3.36	8.28	0.19	13.66	19.85	1.32	0.00	0.24	99.52	r
Sz	971102-5	233	446	*au*	ph	50.63	1.68	3.78	6.59	0.12	15.49	21.55	0.30	0.00	0.46	100.61	c
Sz	990923-7	234	448	*lws*	agg	39.54	0.17	29.62	2.55	0.14	0.14	15.58	0.00	0.03	0.00	87.78	
Sz	990923-7	234	449	*lws*	agg	39.13	0.31	29.64	2.40	0.24	0.10	15.55	0.01	0.00	0.02	87.40	
Sz	990923-7	234	450	*lws*	agg	39.13	0.32	30.00	2.25	0.14	0.04	15.99	0.05	0.00	0.02	87.94	
Sz	990923-7	234	451	*lws*	agg	39.33	0.27	29.59	2.48	0.20	0.04	15.93	0.01	0.00	0.00	87.87	
Sz	971102-5	235	452	*pm*	vein	37.97	0.05	24.22	4.97	0.64	3.07	21.21	0.18	0.00	0.00	92.32	
Sz	971102-5	235	453	*pm*	vein	38.13	0.00	24.33	4.76	0.77	2.70	20.71	0.25	0.00	0.00	91.65	
Sz	971102-5	235	456	*Npx*	vein	53.46	0.12	3.78	17.22	1.10	5.05	9.76	8.26	0.00	0.00	98.76	ab
Sz	971102-5	235	458	*Npx*	vein	54.45	0.09	5.07	15.80	0.94	4.82	8.56	8.26	0.00	0.01	98.00	ab
Sz	971102-5	235	460	*Npx*	vein	52.84	0.18	2.77	18.03	1.46	4.98	10.57	7.83	0.00	0.01	98.67	ab
Sz	971102-5	236	461	*pm*	vein	35.89	0.02	14.34	17.43	0.46	2.35	20.78	0.08	0.00	0.00	91.33	
Sz	971102-5	236	462	*qz*	vein	99.21	0.01	0.21	0.12	0.02	0.11	0.03	0.00	0.02	0.00	99.73	TEST
Sz	971102-5	236	463	*pm*	vein	35.29	0.02	14.47	16.95	0.27	4.53	18.26	0.05	0.00	0.03	89.86	
Sz	971102-5	236	464	*pm*	vein	35.45	0.03	14.20	17.50	0.37	2.45	21.42	0.09	0.00	0.01	91.50	
Sz	971102-5	236	465	*pm*	vein	35.78	0.04	15.48	16.21	0.50	2.53	20.41	0.08	0.00	0.00	91.02	
Sz	971102-5	236	466	*pm*	vein	35.99	0.09	15.31	16.49	0.19	1.93	21.26	0.08	0.00	0.00	91.34	
Sz	971102-5	236	467	*Npx*	vein	53.06	0.05	1.82	20.69	1.44	3.97	9.82	8.53	0.00	0.03	99.41	ab
Sz	971102-5	236	468	*pm*	vein	37.50	0.09	16.06	14.36	0.22	2.99	19.76	0.64	0.00	0.00	91.62	
Sz	971102-5	236	469	*Npx*	vein	53.37	0.12	4.17	17.15	0.70	5.09	8.37	9.28	0.00	0.01	98.27	ab
Sz	971102-5	237	470	*ab*	vein	71.61	0.04	19.63	0.94	0.06	0.21	1.63	7.81	0.05	0.00	101.99	
Sz	971102-5	237	472	*Npx*	vein	53.10	0.30	2.41	17.69	2.26	4.93	11.09	7.79	0.00	0.02	99.59	ab
Sz	971102-5	237	473	*Npx*	vein	49.96	0.41	3.93	17.20	1.61	7.69	9.19	6.68	0.00	0.00	96.67	ab
Sz	971102-5	237	474	*Npx*	vein	48.80	2.67	4.20	16.71	1.22	6.69	9.98	6.97	0.00	0.02	97.25	ab
Sz	971102-5	237	475	*pm*	(ol)	35.89	0.70	15.14	15.73	0.31	1.70	21.18	0.09	0.00	0.07	90.80	
Sz	971102-5	237	476	*pm*	(ol)	34.84	0.09	11.05	21.22	0.25	1.75	20.80	0.06	0.00	0.07	90.13	
Sz	971102-5	237	477	*pm*	(ol)	35.96	0.19	15.81	15.46	0.23	1.93	20.54	0.02	0.00	0.03	90.16	
Sz	971102-5	237	478	*pm*	(ol)	35.89	0.21	15.19	14.31	0.43	2.27	20.84	0.09	0.00	0.10	89.33	
Sz	971101-22	238	480	*Na-amp*	matrix	51.44	0.04	3.72	23.28	0.73	9.53	0.37	8.92	0.27	0.01	98.31	
Sz	971101-22	238	481	*Npx*	vein	53.90	0.28	7.13	19.06	0.06	2.65	3.95	11.99	0.00	0.02	99.03	ab
Sz	971101-22	238	482	*Npx*	vein	52.53	0.20	6.85	19.46	0.10	3.17	4.04	11.34	0.00	0.02	97.70	ab
Sz	971101-22	239	484	*Npx*	vein	52.25	1.33	1.97	24.12	0.18	1.54	5.03	11.10	0.00	0.00	97.52	ab

Appendix II. EPMA-analysed mineral compositions.

unit	Sample No.	SITE	point	*min*	occ	SiO_2	TiO_2	Al_2O_3	FeO*	MnO	MgO	CaO	Na_2O	K_2O	Cr_2O_3	Total	remarks
Sz	971101-22	239	485	*Npx*	vein	53.50	0.27	4.68	20.98	0.10	2.40	4.77	11.53	0.00	0.00	98.23	ab
Sz	971101-22	239	486	*Npx*	vein	52.51	0.61	2.95	23.27	0.16	1.76	5.00	12.03	0.00	0.00	98.27	ab
Sz	971101-22	239	487	*ab*	vein	72.17	0.00	19.63	0.07	0.02	0.01	0.05	9.83	0.03	0.00	101.81	
Sz	971101-22	240	488	*pm*		37.25	0.10	23.65	5.33	0.04	2.55	20.71	0.31	0.00	0.02	89.94	
Sz	971101-22	240	489	*pm*		37.60	0.03	23.70	5.37	0.11	2.66	21.03	0.24	0.00	0.04	90.78	
Sz	971101-22	240	490	*pm*		37.36	0.00	23.89	5.43	0.06	2.95	20.67	0.31	0.00	0.00	90.66	
Sz	971101-22	241	491	*Npx*	vein	53.76	0.73	5.36	20.20	0.14	1.94	4.08	12.20	0.00	0.00	98.40	ab
Sz	971101-22	241	492	*Npx*	vein	53.06	0.87	4.56	22.11	0.13	1.78	4.53	11.77	0.00	0.03	98.85	ab
Sz	971101-22	241	493	*Npx*	vein	53.72	0.23	6.55	19.20	0.16	2.85	4.74	11.22	0.00	0.01	98.69	ab
Sz	971101-22	241	494	*Npx*	vein	53.57	0.21	6.39	19.18	0.14	2.98	5.05	11.15	0.00	0.00	98.66	ab
Sz	971101-22	241	495	*Npx*	vein	53.94	0.28	6.79	19.21	0.11	2.84	4.24	11.48	0.00	0.00	98.88	ab
Sz	971101-22	241	496	*Npx*	vein	51.01	0.28	6.18	21.01	0.16	3.19	4.28	10.52	0.00	0.01	96.63	ab
Sz	971101-22	241	499	*Npx*	vein	51.55	0.08	10.55	18.53	0.18	6.52	2.07	8.94	0.00	0.00	98.40	ab
Sz	971101-22	241	500	*pm*		35.45	0.09	13.39	23.66	0.24	14.11	0.91	2.44	0.00	0.00	90.27	
Sz	971101-22	242	501	*pm*		36.41	0.08	21.41	9.51	0.14	8.38	15.62	0.26	0.00	0.05	91.85	
Sz	971101-22	242	502	*pm*		41.01	0.04	21.88	6.67	0.08	2.66	18.56	0.87	0.00	0.01	91.79	
Sz	990923-8	243	505	*Na-amp*	kaer	54.03	0.53	1.69	27.46	0.23	5.81	0.98	6.71	0.00	0.00	97.44	
Sz	990923-8	243	506	*kaer*		41.14	4.68	11.46	14.16	0.24	11.24	11.38	2.87	1.03	0.00	98.19	
Sz	990923-8	243	507	*Na-amp*	kaer	53.11	0.73	2.99	24.43	0.21	7.29	1.85	6.33	0.00	0.02	96.98	
Sz	990923-8	244	511	*chl*		31.18	0.03	15.60	22.24	0.38	17.54	0.58	0.31	0.00	0.04	87.90	
Sz	990923-8	244	512	*chl*		32.42	0.04	16.11	15.75	0.20	22.22	0.45	0.02	0.00	0.00	87.20	
Ft	990806-7	245	513	*pm*		36.65	0.34	18.77	9.29	0.51	2.54	20.54	0.06	0.00	0.00	88.69	
Ft	990806-7	245	514	*pm*		35.92	1.15	14.15	14.20	0.49	2.92	20.22	0.20	0.00	0.02	89.28	
Ft	990806-7	245	515	*lws*		39.31	0.29	30.24	1.23	0.04	0.16	16.07	0.02	0.00	0.03	87.39	
Ft	990806-7	246	517	*pm*		37.43	0.12	22.97	5.03	0.52	2.74	20.40	0.11	0.00	0.04	89.35	
Ft	990806-7	246	518	*pm*		36.47	0.19	19.98	7.54	0.46	3.10	20.20	0.06	0.00	0.03	88.04	
Ft	990806-7	246	519	*pm*		40.16	0.12	22.26	6.12	0.31	3.28	18.08	0.13	0.85	0.01	91.31	
Ft	990806-7	246	520	*lws*		38.51	0.35	30.12	1.45	0.07	0.33	15.52	0.00	0.00	0.00	86.36	
Ft	990806-7	246	522	*lws*		38.87	0.25	30.31	1.23	0.03	0.05	15.82	0.00	0.00	0.03	86.60	
Ft	990806-7	247	523	*pm*		35.80	1.03	13.11	15.78	0.40	2.87	20.69	0.15	0.00	0.04	89.86	
Ft	990806-7	247	524	*pm*		37.19	0.32	22.03	6.51	0.39	2.82	20.65	0.07	0.00	0.03	90.00	
Ft	990806-7	247	526	*lws*		39.16	0.39	30.36	1.23	0.03	0.02	16.09	0.00	0.00	0.00	87.30	
Ft	990806-7	247	527	*lws*		39.58	0.28	30.63	1.33	0.00	0.02	16.37	0.02	0.00	0.01	88.25	
Ft	990806-7	248	529	*lws*		38.83	0.27	29.78	1.57	0.01	0.13	16.15	0.01	0.01	0.01	86.77	
Ft	990806-7	248	530	*lws*		38.65	0.34	29.71	1.57	0.00	0.06	15.86	0.00	0.00	0.00	86.20	
Ft	990806-7	248	531	*pm*		36.86	0.16	18.97	9.53	0.43	3.00	20.47	0.10	0.00	0.01	89.53	
Ft	990806-7	248	532	*pm*		37.19	0.05	22.95	4.76	0.54	2.71	20.44	0.15	0.00	0.03	88.80	
Ft	990806-7	248	533	*pm*		36.63	0.16	20.31	7.61	0.43	2.75	20.45	0.12	0.00	0.00	88.46	
Ft	990806-7	248	534	*pm*		36.91	0.15	20.43	7.28	0.51	2.85	20.54	0.13	0.00	0.01	88.80	
Ft	990810-8	249	536	*Npx*	vein	54.24	0.35	9.05	18.18	0.16	2.24	2.79	12.21	0.00	0.03	99.23	ab
Ft	990810-8	249	537	*Npx*	vein	54.24	0.57	7.00	20.33	0.23	1.24	2.63	12.68	0.00	0.00	98.92	ab
Ft	990810-8	249	538	*Npx*	vein	54.16	0.41	5.89	20.34	0.22	2.09	4.00	11.93	0.00	0.01	99.05	ab
Ft	990810-8	250	539	*pm*		36.37	0.05	19.03	11.81	0.59	1.84	20.96	0.09	0.00	0.00	90.73	
Ft	990810-8	250	540	*pm*		36.81	0.04	20.61	10.30	0.62	2.16	20.33	0.14	0.00	0.00	91.02	
Ft	990810-8	251	542	*Npx*	vein	53.80	0.36	5.11	21.45	0.28	2.00	4.20	11.75	0.00	0.01	98.94	ab
Ft	990810-8	251	543	*Npx*	vein	53.92	0.62	6.05	20.72	0.14	1.48	2.80	12.39	0.00	0.03	98.15	ab
Ft	990810-8	252	548	*Npx*	vein	52.93	0.66	4.92	21.98	0.41	1.73	3.95	11.09	0.00	0.05	97.70	ab+qz
Ft	990810-8	252	549	*npx*		50.66	0.33	7.22	21.58	0.30	4.65	3.28	9.95	0.00	0.01	97.97	
Ft	990810-8	253	553	*Na-amp*		53.00	0.28	5.64	23.91	0.52	6.39	1.00	5.94	0.00	0.03	96.71	
Ft	990810-8	253	554	*Na-amp*		56.21	0.19	6.14	22.51	0.39	5.24	0.78	6.00	0.00	0.03	97.49	
Ft	990809-2	254	556	*pm*		45.37	0.14	22.17	5.04	0.23	3.81	12.33	0.10	3.31	0.00	92.50	
Ft	990809-2	255	558	*pm*		36.37	0.24	22.31	6.02	0.37	2.88	20.82	0.19	0.00	0.04	89.23	
Ft	990809-2	256	561	*lws*		39.18	0.36	30.21	1.70	0.07	0.35	16.45	0.00	0.05	0.06	88.43	
Ft	990809-2	257	563	*lws*		39.96	0.08	30.31	2.07	0.04	0.05	16.10	0.13	0.00	0.00	88.75	
Ft	990926-20	260	567	*lws*		39.22	0.19	29.96	1.05	0.02	0.17	15.80	0.04	0.08	0.00	86.55	
Ft	990926-20	260	568	*pm*		38.31	0.07	24.17	5.50	0.15	2.17	21.50	0.08	0.00	0.00	91.93	
Ft	990926-20	261	569	*pm*		38.81	0.11	23.48	6.18	0.11	2.23	21.35	0.43	0.00	0.02	92.73	
Ft	990926-20	262	572	*Npx*	vein	54.20	0.32	7.50	17.29	0.18	3.91	4.26	10.59	0.00	0.02	98.27	qz
Ft	990926-20	262	573	*au*		51.63	1.19	3.36	6.32	0.12	14.78	21.21	1.01	0.00	0.24	99.86	
Ft	990926-20	262	574	*au*		48.24	2.05	5.66	8.28	0.16	13.20	21.65	0.68	0.00	0.00	99.92	
Ft	990926-20	262	575	*au*		49.39	1.69	4.65	7.75	0.09	13.50	21.22	0.96	0.00	0.03	99.28	
Ft	990926-20	262	576	*Npx*	vein	52.87	3.26	3.58	21.96	0.11	1.65	2.67	12.60	0.00	0.03	98.72	qz
Ft	990926-20	263	582	*Npx*	vein	53.94	0.34	7.84	18.76	0.42	1.83	4.48	10.97	0.00	0.00	98.57	qz+ab
Ft	990926-20	263	584	*chl*		32.01	0.09	15.59	27.98	0.44	11.14	0.61	1.47	0.00	0.00	89.32	
Ft	990926-20	263	585	*chl*		31.54	0.08	14.79	23.35	0.39	15.02	0.50	1.76	0.00	0.02	87.44	
Ft	990926-20	263	586	*chl*		27.86	0.05	16.93	28.31	0.47	12.73	0.25	0.45	0.00	0.01	87.06	
Ft	990926-20	263	587	*chl*		27.05	0.09	17.97	28.20	0.46	13.52	0.07	0.05	0.00	0.00	87.41	
Ft	990926-20	264	591	*chl*		30.67	0.07	15.04	17.66	0.36	22.99	0.21	0.02	0.00	0.00	87.02	
Ft	990926-20	264	592	*Npx*	vein	53.49	1.68	5.23	20.38	0.13	1.85	2.89	13.56	0.00	0.02	99.23	qz+ab
Ft	990926-20	263	600	*Npx*	vein	55.02	0.31	8.22	18.43	0.52	1.37	4.71	11.39	0.00	0.00	99.96	qz+ab
Ft	990926-20	263	601	*Npx*	vein	54.88	0.30	8.28	18.38	0.31	1.40	4.18	12.37	0.00	0.03	100.12	qz+ab
Ft	990926-20	263	602	*Npx*	vein	55.20	0.30	8.63	18.25	0.27	1.48	3.75	12.40	0.00	0.00	100.28	qz+ab
Ft	990926-20	263	603	*Npx*	vein	54.46	0.31	7.79	19.02	0.53	1.14	4.86	11.65	0.00	0.00	99.76	qz+ab
Ft	990926-20	263	604	*Npx*	vein	53.78	0.27	7.86	18.15	0.40	2.12	4.18	11.08	0.00	0.03	97.85	qz+ab
Ft	990926-20	263	605	*Npx*	vein	54.41	0.28	8.29	18.75	0.32	2.01	4.07	11.51	0.00	0.03	99.66	qz+ab
Ft	990926-20	263	606	*Npx*	vein	54.28	0.31	7.65	19.13	0.44	1.27	4.46	11.54	0.00	0.04	99.11	qz+ab
Ft	990926-20	263	609	*Npx*	vein	55.37	0.35	9.13	17.71	0.11	1.65	2.61	12.56	0.00	0.00	99.48	qz+ab
Ft	990926-20	263	611	*Npx*	vein	48.53	0.31	10.71	17.96	0.21	7.28	1.83	9.43	0.00	0.01	96.26	qz+ab

Appendix II. EPMA-analysed mineral compositions.

unit	Sample No.	SITE	point	*min*	occ	SiO_2	TiO_2	Al_2O_3	FeO*	MnO	MgO	CaO	Na_2O	K_2O	Cr_2O_3	Total	remarks
Ft	980810-8	252	612	*Npx*	vein	53.67	0.35	4.52	21.42	0.36	2.29	4.64	11.25	0.00	0.00	98.50	qz+ab
Ft	980810-8	252	613	*Npx*	vein	54.30	0.54	6.56	19.03	0.20	1.79	3.86	12.00	0.00	0.02	98.30	qz+ab
Ft	980810-8	252	614	*Npx*	vein	54.27	0.53	5.42	20.82	0.18	1.78	4.02	11.76	0.00	0.00	98.78	qz+ab
Ft	980810-8	252	615	*Npx*	vein	53.81	0.30	4.79	21.48	0.34	2.63	4.54	11.07	0.00	0.00	98.95	qz+ab
Ft	990926-20	264	617	*lws*		38.14	0.04	30.33	1.32	0.01	0.03	16.75	0.00	0.00	0.02	86.64	
Ft	990926-20	264	618	*lws*		39.52	0.05	31.01	0.85	0.00	0.01	16.47	0.03	0.00	0.00	87.94	
Ft	990926-20	264	619	*lws*		39.68	0.24	29.43	2.68	0.01	0.04	16.53	0.00	0.00	0.00	88.61	
Pr1	980714-8	265	620	*Npx*	vein	56.81	0.30	6.81	19.45	0.02	0.72	1.15	12.00	0.00	0.00	97.26	qz
Pr1	980714-8	266	623	*Npx*	vein	54.48	0.30	4.83	22.01	0.06	1.89	1.23	12.02	0.00	0.04	96.87	qz
Pr1	980714-8	266	624	*Npx*	vein	54.91	0.08	5.15	22.02	0.07	0.96	1.66	12.90	0.00	0.00	97.74	qz
Pr1	980714-8	268	635	*Npx*	vein	53.68	0.31	3.04	25.65	0.04	0.77	1.16	13.29	0.00	0.00	97.94	qz+ab
Pr1	980714-8	268	636	*Npx*	vein	55.81	0.46	3.83	23.22	0.06	1.71	1.22	12.51	0.00	0.00	98.82	qz+ab
Pr1	980714-8	268	637	*ab*		70.56	0.04	18.46	1.53	0.00	0.37	0.07	7.54	0.45	0.02	99.03	
Pr1	980714-11A	270	645	*Na-amp*		51.71	1.12	1.55	23.94	0.57	7.40	3.68	6.07	0.40	0.00	96.43	
Pr1	980714-11A	270	646	*Na-amp*		54.10	0.17	3.05	27.48	0.29	4.87	0.44	7.14	0.00	0.00	97.53	
Pr1	980714-11A	271	648	*Npx*	pool	55.54	0.05	7.32	20.58	0.15	1.04	1.50	13.31	0.00	0.01	99.50	ab
Pr1	980714-11A	271	649	*chl*		27.41	0.00	16.27	33.11	0.70	10.37	0.04	0.00	0.00	0.00	87.90	
Pr1	980714-11A	271	650	*chl*		27.21	0.00	16.36	33.02	0.91	10.89	0.03	0.01	0.00	0.00	88.43	
Pr1	980714-11A	271	652	*chl*		27.53	0.00	16.17	33.26	0.86	10.47	0.06	0.02	0.00	0.00	88.36	
Pr1	980714-11A	271	653	*Npx*	pool	53.26	0.00	3.35	27.22	0.08	0.71	0.96	13.70	0.00	0.01	99.29	ab
Pr1	980714-11A	272	654	*Npx*	au?	54.03	0.13	5.54	21.93	0.41	1.28	3.25	12.21	0.00	0.00	98.79	ab
Pr1	980714-11A	272	656	*Npx*	au?	54.06	0.16	5.73	21.64	0.26	2.13	3.23	11.85	0.00	0.00	99.07	ab
Pr1	990810-19	273	658	*Na-amp*		54.98	0.09	1.80	27.53	0.38	5.56	0.12	7.10	0.00	0.00	97.55	
Pr1	990810-19	273	659	*Npx*	au	54.85	0.10	6.12	23.19	0.09	0.45	0.96	14.14	0.00	0.01	99.92	ab
Pr1	990810-19	273	660	*Npx*	au	53.97	0.18	3.96	24.18	0.23	1.22	3.15	12.58	0.00	0.00	99.47	ab
Pr1	990810-19	273	661	*Npx*	au	53.76	0.09	5.31	20.81	0.40	1.84	4.76	11.31	0.00	0.00	98.27	ab
Pr1	990810-19	273	662	*Npx*	au	54.85	0.06	5.99	22.81	0.06	0.45	1.14	13.77	0.00	0.00	99.14	ab
Pr1	990810-19	273	663	*chl*		27.70	0.06	18.01	29.01	0.75	12.66	0.16	0.24	0.00	0.01	88.60	
Pr1	990810-19	274	664	*Npx*	vein	54.56	0.00	6.44	22.79	0.02	0.34	1.12	13.88	0.00	0.02	99.17	qz+ab
Pr1	990810-19	274	665	*Npx*	vein	55.34	0.00	8.00	19.91	0.03	0.32	1.05	13.68	0.00	0.00	98.33	qz+ab
Pr1	990810-19	274	666	*Npx*	vein	55.32	0.00	7.00	21.45	0.08	0.35	0.92	14.09	0.00	0.00	99.21	qz+ab
Pr1	990810-19	274	668	*Npx*	vein	53.76	0.00	2.46	27.37	0.04	0.22	0.60	14.26	0.00	0.03	98.75	qz+ab
Pr1	990810-19	274	669	*Npx*	vein	54.19	0.00	3.94	25.04	0.00	0.27	0.65	14.04	0.00	0.02	98.14	qz+ab
Pr1	990810-19	274	670	*Npx*	vein	54.34	0.02	4.00	25.66	0.02	0.13	0.73	14.25	0.00	0.00	99.13	qz+ab
Pr1	990810-19	275	675	*Npx*	vein	55.45	0.00	7.96	19.68	0.06	1.15	1.45	12.79	0.00	0.00	98.53	qz+ab
Pr1	990810-19	275	676	*Npx*	vein	54.60	0.16	4.87	22.03	0.32	1.56	3.78	12.46	0.00	0.00	99.78	qz+ab
Pr1	990810-19	276	678	*Npx*	vein	53.69	0.18	5.27	21.00	0.39	1.80	4.24	12.20	0.00	0.00	98.76	ab
Pr1	990810-19	276	679	*Npx*	vein	55.91	0.00	9.78	18.49	0.07	0.35	0.63	14.12	0.00	0.00	99.34	ab
Pr1	990810-19	276	680	*Npx*	vein	53.15	0.02	2.63	26.73	0.03	0.27	0.55	13.53	0.00	0.00	96.90	ab
Pr1	990810-19	276	682	*Npx*	vein	54.64	0.00	4.55	24.65	0.03	0.20	0.57	14.31	0.00	0.02	98.95	ab
Pr1	990810-19	277	684	*ep*		37.37	0.01	22.10	13.20	0.36	0.04	22.21	0.00	0.00	0.01	95.30	c
Pr1	990810-19	277	685	*ep*		36.91	0.04	22.28	11.60	0.38	0.03	21.54	0.00	0.00	0.00	92.77	m
Pr1	990810-19	277	686	*ep*		36.02	0.14	19.20	14.52	0.42	0.09	20.18	0.05	0.00	0.00	90.62	r
Pr1	990810-19	278	688	*Npx*	au	53.23	0.05	8.14	21.79	0.12	1.42	0.82	12.76	0.00	0.00	98.31	ab
Pr1	990810-19	278	689	*Npx*	au	54.64	0.23	6.46	21.56	0.07	0.75	1.95	13.32	0.00	0.01	98.98	ab
Pr1	990809-25	279	691	*ep*		37.26	0.24	20.02	15.25	0.11	0.03	22.12	0.00	0.00	0.00	95.03	
Pr1	990809-25	279	692	*ep*		37.62	0.06	20.49	14.51	0.07	0.00	22.43	0.00	0.00	0.01	95.19	
Pr1	990809-25	279	693	*pm*		37.34	0.06	21.96	7.66	0.15	2.51	21.71	0.04	0.00	0.00	91.43	
Pr1	990809-25	279	694	*pm*		37.36	0.04	22.58	6.31	0.17	3.06	21.81	0.09	0.00	0.03	91.45	
Pr1	990809-25	279	695	*ep*		37.39	0.03	22.54	12.57	1.11	0.05	21.30	0.01	0.00	0.04	95.03	
Pr1	990809-25	279	696	*ep*		37.80	0.09	22.71	12.64	1.16	0.04	21.19	0.00	0.00	0.07	95.70	
Pr1	990809-25	279	697	*ep*		37.78	0.03	22.53	12.50	0.47	0.01	22.21	0.00	0.00	0.00	95.52	
Pr1	990809-25	280	698	*Npx*	au	52.49	0.20	2.41	18.97	0.07	4.76	7.38	9.75	0.00	0.49	96.51	ab
Pr1	990809-25	280	699	*Npx*	au	52.59	0.72	3.53	15.91	0.17	6.66	10.83	7.51	0.00	0.42	98.33	ab
Pr1	990809-25	280	700	*Npx*	au	54.31	0.45	3.77	18.96	0.11	4.18	6.04	10.26	0.00	0.55	98.62	ab
Pr1	990809-25	280	701	*pm*		37.01	0.08	20.15	9.71	0.32	2.11	21.19	0.05	0.00	0.02	90.64	
Pr1	990809-25	280	703	*pm*		37.11	0.09	21.70	7.48	0.28	2.32	21.41	0.11	0.00	0.02	90.52	
Pr1	990809-25	280	704	*pm*		37.00	0.07	21.02	8.28	0.26	2.53	21.79	0.09	0.00	0.03	91.05	
Pr1	990809-25	280	705	*pm*		37.19	0.10	21.26	8.21	0.29	*2.54*	21.21	0.07	0.00	0.06	90.92	
Pr1	990809-25	280	706	*pm*		37.53	0.10	21.76	7.40	0.27	2.41	21.56	0.08	0.00	0.08	91.18	
Pr1	990809-25	280	707	*pm*		37.18	0.07	21.94	7.20	0.32	2.35	21.75	0.05	0.00	0.00	90.88	
Pr1	980714-11A	282	708	*Npx*	pool	55.60	0.04	7.87	20.99	0.08	0.86	0.99	13.59	0.00	0.02	100.04	ab
Pr1	980714-11A	282	709	*Npx*	pool	55.10	0.03	6.44	21.47	0.11	1.16	2.22	13.29	0.00	0.02	99.84	ab
Pr1	980714-11A	282	712	*Npx*	pool	54.52	0.00	5.35	23.10	0.10	1.01	1.54	13.23	0.00	0.00	98.85	ab
Pr1	980714-11A	283	714	*Npx*	pool	54.54	0.04	5.36	23.71	0.06	0.64	1.05	14.15	0.00	0.00	99.57	ab
Pr1	980714-11A	283	715	*Npx*	pool	54.79	0.03	4.87	23.59	0.06	1.08	1.75	13.34	0.00	0.00	99.51	ab
Pr1	980714-11A	283	717	*Npx*	pool	54.81	0.15	8.35	20.52	0.08	1.05	1.04	13.41	0.00	0.00	99.41	ab
Pr2	990629-1	284	720	*Npx*	vein	54.73	0.07	4.01	24.90	0.05	0.32	0.87	13.82	0.00	0.00	98.77	ab
Pr2	990629-1	284	721	*Npx*	vein	55.49	0.26	7.79	20.25	0.00	0.74	1.15	13.71	0.00	0.00	99.40	ab
Pr2	990629-1	284	722	*Npx*	vein	55.25	0.34	7.89	19.79	0.01	0.67	1.15	13.54	0.00	0.02	98.67	ab
Pr2	990629-1	284	724	*Npx*	vein	55.14	0.20	6.12	21.40	0.00	0.64	1.47	13.27	0.00	0.04	98.28	ab
Pr2	990629-1	284	726	*Npx*	vein	54.44	0.03	4.92	23.76	0.06	0.56	1.34	14.08	0.00	0.03	99.20	ab
Pr2	990629-1	285	728	*lws*		38.68	0.12	29.39	2.72	0.02	0.00	16.38	0.00	0.00	0.02	87.32	
Pr2	990629-1	285	729	*lws*		38.89	0.02	29.47	2.94	0.02	0.02	16.31	0.00	0.00	0.02	87.68	
Pr2	990629-1	285	730	*lws*		39.37	0.03	30.17	2.29	0.03	0.04	16.20	0.00	0.00	0.00	88.12	
Pr2	990629-1	285	731	*lws*		39.57	0.11	30.23	2.16	0.00	0.03	16.71	0.03	0.00	0.00	88.83	
Pr2	990629-1	285	732	*lws*		39.78	0.09	30.72	1.87	0.04	0.01	16.44	0.00	0.00	0.01	88.96	
Pr2	990629-1	285	733	*lws*		39.72	0.04	30.95	1.74	0.01	0.00	16.45	0.00	0.00	0.00	88.91	

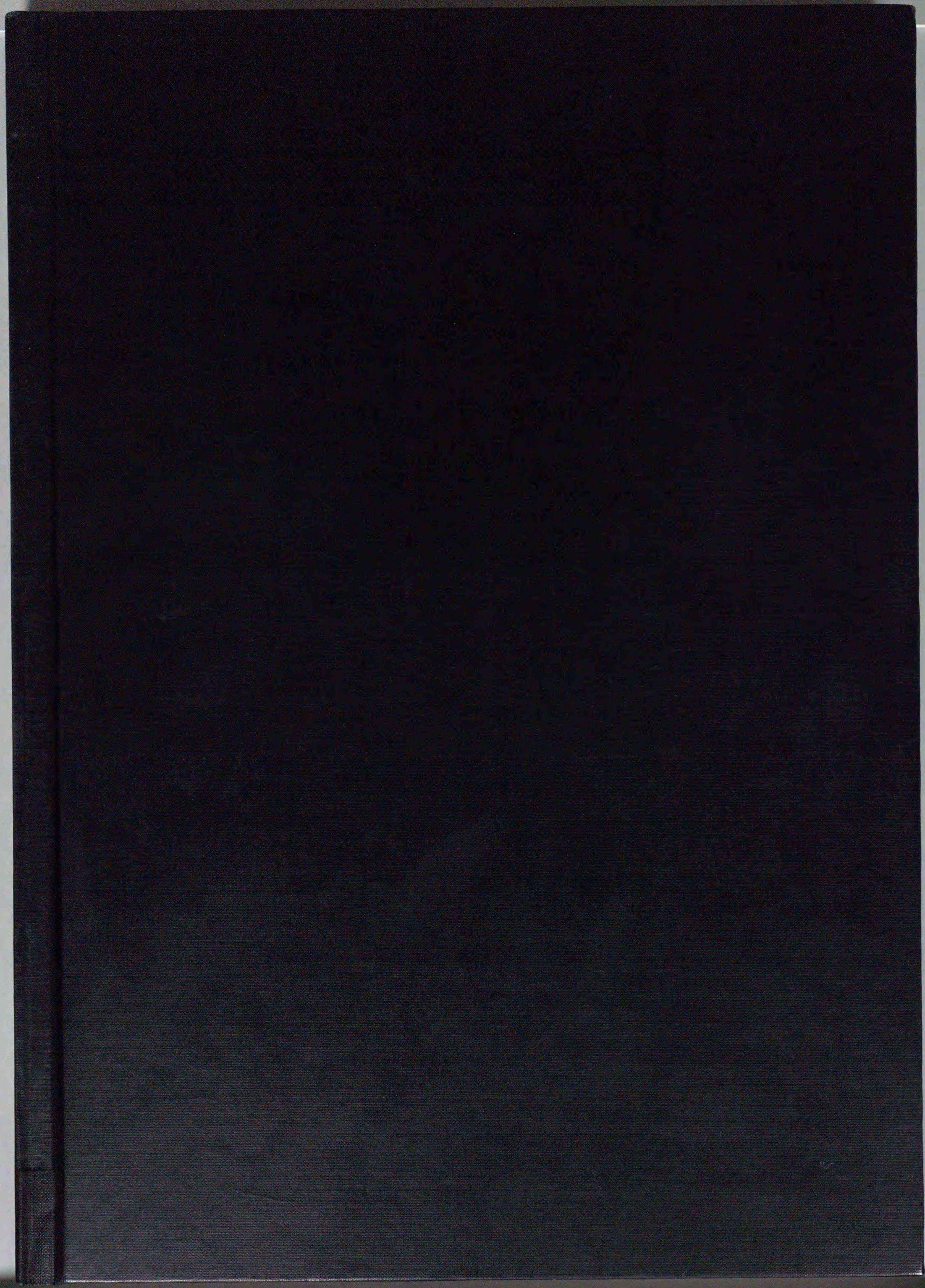
Appendix II. EPMA-analysed mineral compositions.

unit	Sample No.	SITE	point	*min*	occ	SiO_2	TiO_2	Al_2O_3	FeO*	MnO	MgO	CaO	Na_2O	K_2O	Cr_2O_3	Total	remarks
Pr2	990629-1	285	734	*lws*		39.25	0.43	29.45	2.50	0.04	0.05	16.55	0.00	0.00	0.00	88.26	
Pr2	990629-1	286	735	*Npx*	vein	54.06	0.02	2.38	26.90	0.05	0.64	1.35	13.68	0.00	0.00	99.07	qz+ab
Pr2	990629-1	286	737	*Npx*	vein	54.97	0.24	6.39	21.11	0.12	0.64	1.36	13.22	0.00	0.01	98.06	qz+ab
Pr2	990629-1	287	740	*Npx*	vein	55.07	0.04	5.93	22.85	0.02	0.64	0.87	13.68	0.00	0.00	99.11	qz+ab
Pr2	990629-1	287	741	*Npx*	vein	55.57	0.10	8.18	20.51	0.06	0.39	0.68	14.21	0.00	0.01	99.69	qz+ab
Pr2	990629-1	287	742	*Npx*	vein	54.90	0.05	6.28	22.08	0.03	0.42	0.83	13.68	0.00	0.00	98.27	qz+ab
Pr2	990629-1	287	743	*Npx*	vein	54.11	0.23	7.39	19.69	0.05	1.06	2.92	12.76	0.00	0.00	98.20	qz+ab
Pr2	990629-1	287	744	*Npx*	vein	54.81	0.32	6.04	21.23	0.05	0.96	1.79	13.18	0.00	0.01	98.41	qz+ab
Pr2	990629-1	287	745	*Npx*	vein	54.68	0.09	5.16	23.88	0.04	0.40	0.89	14.02	0.00	0.01	99.16	qz+ab
Pr2	990629-1	287	746	*Npx*	vein	54.34	0.07	3.44	25.73	0.02	0.50	1.13	13.85	0.00	0.04	99.11	qz+ab
Pr2	990629-1	287	747	*Npx*	vein	54.37	0.00	4.95	24.22	0.00	0.43	0.78	14.08	0.00	0.01	98.84	qz+ab
Pr2	990802-5	292	752	*Npx*	vein	53.90	0.27	5.64	21.09	0.01	1.04	2.71	12.84	0.00	0.00	97.51	qz
Pr2	990802-5	292	754	*au*	qz	48.65	1.97	4.12	12.96	0.25	11.73	20.57	0.43	0.00	0.02	100.68	
Pr2	990802-5	292	755	*Npx*	vein	55.04	0.13	6.35	21.16	0.00	1.25	1.29	13.29	0.00	0.01	98.54	qz
PrM	980608-4	304	758	*chl*		39.45	0.06	12.18	21.17	0.24	14.03	1.74	2.16	0.00	0.00	91.05	
PrM	980608-4	304	759	*act*		50.93	0.66	4.15	19.43	0.19	10.77	7.73	3.37	0.00	0.02	97.24	
PrM	980608-4	305	761	*hb*		50.27	0.40	3.69	20.80	0.29	11.66	9.84	0.96	0.00	0.00	97.92	
PrM	980608-4	308	762	*Npx*	au	52.51	0.39	3.19	16.53	0.27	7.13	11.79	6.68	0.00	0.01	98.50	ab
PrM	980608-4	308	763	*Npx*	au	51.65	0.52	2.54	17.35	0.29	7.58	12.55	5.79	0.00	0.01	98.27	ab
PrM	980608-4	309	765	*win*		56.11	0.14	4.92	17.33	0.14	9.44	5.60	5.23	0.00	0.00	98.91	
PrM	980608-4	309	766	*hb*		48.95	0.50	5.05	20.21	0.24	10.75	11.04	1.02	0.00	0.00	97.76	
PrM	980608-4	309	767	*hb*		47.70	1.06	5.84	20.74	0.20	10.48	10.69	1.39	0.08	0.01	98.17	
PrM	980608-4	310	768	*act*		51.04	0.55	3.52	20.11	0.39	11.97	10.43	0.73	0.00	0.00	98.73	
PrM	980608-4	310	769	*hb*		52.74	0.34	2.68	19.82	0.25	11.51	8.18	2.83	0.00	0.00	98.35	
PrM	981014-1A	311	771	*Npx*	vein	53.34	0.00	1.64	21.67	0.43	4.27	9.69	9.01	0.00	0.02	100.07	ab
PrM	981014-1A	311	772	*Npx*	vein	53.21	0.22	2.86	21.53	0.20	3.43	7.72	10.04	0.00	0.01	99.22	ab
PrM	981014-1A	311	773	*Npx*	vein	52.95	0.22	2.52	21.97	0.22	3.23	8.03	10.01	0.00	0.03	99.17	ab
PrM	981014-1A	311	774	*Npx*	vein	53.26	0.12	4.32	19.42	0.12	3.72	7.40	10.35	0.00	0.00	98.71	ab
PrM	981014-1A	313	776	*Npx*	vein	52.06	0.05	0.38	18.43	1.23	6.19	16.25	4.65	0.00	0.00	99.23	ab
PrM	981014-1A	313	777	*Npx*	vein	53.33	0.03	1.97	20.58	0.13	4.33	8.67	9.34	0.00	0.01	98.39	ab
PrM	981014-1A	313	778	*Npx*	vein	53.19	0.14	2.20	20.84	0.09	4.07	7.97	9.71	0.00	0.00	98.19	ab
PrM	981014-1A	313	779	*Npx*	vein	53.25	0.01	1.91	22.01	0.11	3.61	7.54	10.14	0.00	0.00	98.57	ab
PrM	981014-1A	313	780	*Npx*	vein	52.10	0.02	0.18	18.90	1.38	5.78	16.23	4.73	0.00	0.04	99.36	ab
PrM	981014-1A	313	781	*Npx*	vein	53.04	0.04	1.66	21.50	0.12	4.28	8.40	9.62	0.00	0.00	98.65	ab
PrM	981014-1A	314	782	*ep*		37.46	0.07	21.83	13.82	0.11	0.00	23.17	0.02	0.00	0.02	96.49	
PrM	981014-1A	314	783	*ep*		37.34	0.14	21.69	14.04	0.11	0.05	23.37	0.01	0.00	0.00	96.75	
PrM	981014-1A	314	784	*ep*		37.53	0.01	21.96	13.91	0.22	0.02	23.30	0.04	0.00	0.00	96.99	
PrM	981014-1A	314	785	*chl*		27.80	0.01	18.71	19.91	0.45	20.58	0.04	0.02	0.00	0.00	87.51	
PrM	981014-4	315	786	*Npx*	glass	53.79	0.08	1.78	7.16	0.16	12.58	20.58	2.60	0.00	0.33	99.04	chl
PrM	981014-4	315	787	*Npx*	glass	53.87	0.00	1.61	8.27	0.16	12.67	20.47	2.74	0.00	0.34	100.13	chl
PrM	981014-4	315	788	*Npx*	glass	53.70	0.01	1.12	7.72	0.19	13.33	21.70	2.20	0.00	0.33	100.29	chl
PrM	981014-4	315	789	*Npx*	glass	53.75	0.03	1.11	7.36	0.16	13.32	21.69	2.10	0.00	0.31	99.81	chl
PrM	981014-4	315	790	*Npx*	glass	50.33	0.05	2.98	8.52	0.19	14.11	18.44	2.15	0.00	0.36	97.12	chl
PrM	981014-4	315	791	*Npx*	glass	53.93	0.07	1.69	8.58	0.13	13.13	20.41	2.74	0.00	0.36	101.05	chl
PrM	981014-4	315	792	*Npx*	glass	54.19	0.08	2.13	8.56	0.14	12.15	19.87	3.22	0.00	0.35	100.69	chl
PrM	981014-4	317	796	*ep*		37.72	0.06	22.35	12.61	0.10	0.04	22.85	0.04	0.00	0.38	96.13	
PrM	981014-4	317	797	*ep*		37.38	0.01	22.18	12.87	0.03	0.04	22.13	0.00	0.00	0.35	94.98	
PrM	981014-4	317	798	*ep*		37.55	0.04	22.08	13.01	0.12	0.11	22.18	0.00	0.00	0.41	95.49	
PrM	981014-4	318	799	*Npx*	glass	52.76	0.14	1.81	8.43	0.18	12.16	21.41	2.41	0.00	0.39	99.68	chl
PrM	981014-4	318	800			53.64	0.10	1.64	8.54	0.15	12.19	20.30	2.99	0.00	0.30	99.85	
PrM	981014-4	318	801			53.75	0.02	1.42	8.53	0.14	11.93	19.44	3.11	0.00	0.25	98.59	
PrM	981014-4	318	802			53.62	0.04	1.62	8.35	0.15	12.31	20.82	3.08	0.00	0.31	100.30	
PrM	981014-4	319	804	*Npx*		54.16	0.10	2.01	8.08	0.15	12.20	20.32	3.12	0.00	0.38	100.51	
PrM	981014-4	319	805	*Npx*		52.01	0.03	2.39	8.52	0.13	13.10	19.37	2.62	0.00	0.37	98.54	
PrM	981014-4	321	806	*Npx*	glass	54.04	0.00	1.15	7.89	0.16	13.25	21.82	2.09	0.00	0.15	100.53	chl
PrM	981014-4	321	807			54.71	0.00	1.35	7.09	0.18	15.62	19.20	1.59	0.00	0.09	99.84	
PrM	981014-4	321	808			49.84	0.22	2.22	9.27	0.21	12.50	22.91	1.38	0.00	0.23	98.77	
PrM	981014-4	321	809			53.82	0.08	1.10	7.83	0.10	13.41	21.24	2.34	0.00	0.15	100.06	
PrM	981014-4	321	810			54.16	0.00	1.27	7.75	0.22	12.91	21.18	2.37	0.00	0.14	99.99	
PrM	981014-4	321	811		pm?	54.43	0.02	2.20	5.86	0.39	14.75	20.73	1.47	0.00	0.09	99.93	
PrM	981014-3	324	816	*Npx*	glass	53.85	0.16	1.12	7.04	0.13	14.05	21.43	1.84	0.00	0.27	99.89	chl
PrM	981014-3	324	817	*Npx*	glass	53.78	0.28	0.97	7.14	0.15	13.75	21.99	2.05	0.00	0.30	100.40	chl
PrM	981014-3	324	818	*Npx*	glass	54.49	0.05	1.03	7.55	0.14	13.59	21.80	2.23	0.00	0.25	101.13	chl
PrM	981014-3	324	819	*Npx*	glass	54.35	0.03	1.05	7.85	0.16	13.36	21.86	2.39	0.00	0.24	101.28	chl
PrM	981014-3	325	820	*Npx*	glass	53.77	0.11	0.92	7.53	0.13	13.73	21.41	2.06	0.00	0.25	99.90	chl
Pr2	980510-8	326	821	*Npx*	ves	58.63	0.00	24.48	0.31	0.05	0.11	0.40	15.16	0.00	0.00	99.13	ab
Pr2	980510-8	326	824	*Npx*	ves	57.58	0.02	23.95	1.13	0.12	0.50	0.69	13.29	1.49	0.00	98.76	ab
Pr2	980510-8	327	830	*Npx*	ves	58.13	0.02	24.24	0.68	0.06	0.17	0.57	14.49	0.75	0.00	99.11	ab
Pr2	980510-8	327	831	*Npx*	ves	58.91	0.00	24.24	0.73	0.08	0.29	0.44	14.94	0.09	0.00	99.72	ab
Pr2	980510-8	327	832	*Npx*	ves	57.91	0.00	24.14	0.29	0.04	0.12	0.99	14.90	0.16	0.00	98.54	ab
Pr2	980510-8	327	833	*Npx*	ves	57.27	0.01	24.04	1.48	0.09	0.80	0.37	13.74	0.92	0.00	98.71	ab
Pr2	980510-8	329	835	*Npx*	ves	59.25	0.00	24.62	0.46	0.08	0.14	0.29	15.10	0.13	0.00	100.08	ab
PrM	980501-10	331	845	*Npx*	vein	53.30	0.12	2.24	7.48	0.64	12.05	21.43	2.08	0.00	0.02	99.35	ab
PrM	980501-10	331	846	*Npx*	vein	53.79	0.12	2.40	7.78	0.60	12.14	20.96	2.42	0.00	0.03	100.23	ab
PrM	980501-10	331	847	*Npx*	vein	54.03	0.18	3.62	6.82	0.26	11.78	19.45	3.35	0.00	0.01	99.51	ab
PrM	980501-10	331	849	*ep*	vein	38.13	0.06	24.79	8.90	0.11	0.21	23.88	0.04	0.00	0.00	96.12	
Pr2	980510-7	332	850	*Na-amp*	kaer	55.34	0.25	4.63	20.97	0.10	8.14	0.49	7.13	0.00	0.05	97.10	
Pr2	980510-7	332	851	*Na-amp*	kaer	55.38	0.56	4.27	21.40	0.10	7.86	0.21	7.43	0.00	0.03	97.24	

Appendix II. EPMA-analysed mineral compositions.

unit	Sample No.	SITE	point	*min*	occ	SiO_2	TiO_2	Al_2O_3	FeO*	MnO	MgO	CaO	Na_2O	K_2O	Cr_2O_3	Total	remarks
Pr2	980510-7	332	852	*Na-amp*	kaer	55.02	0.17	4.13	21.08	0.06	8.32	1.17	7.15	0.00	0.03	97.12	
Pr2	980510-7	334	855	*Na-amp*	kaer	55.23	0.09	3.55	21.87	0.10	8.33	0.51	7.35	0.00	0.00	97.04	
Pr2	980510-7	334	856	*Na-amp*	kaer	55.18	0.04	4.63	20.73	0.19	8.56	0.42	7.39	0.00	0.03	97.17	
Pr1	980611-12	338	860	*Na-amp*	glass	53.57	0.34	2.44	22.18	0.10	9.36	1.43	6.85	0.00	0.04	96.30	S1
Pr1	980611-12	338	865	*Na-amp*	glass	45.71	12.26	1.74	15.71	0.11	5.80	10.80	4.58	0.00	0.02	96.74	S2
Pr1	980611-12	340	871	*chl*	glass	35.29	0.13	13.65	17.84	0.16	14.96	3.77	1.36	1.25	0.03	88.44	S1
Pr1	980611-12	340	874	*chl*	glass	36.84	0.01	13.11	20.62	0.22	16.93	0.24	1.85	0.19	0.02	90.04	S2
Pr1	980611-12	340	875	*Na-amp*	glass	53.77	0.19	2.98	22.07	0.14	9.42	0.73	6.79	0.12	0.04	96.25	S2
Mk	981102-13	341	879	*pm*		36.29	0.08	22.94	7.50	0.17	1.52	22.49	0.14	0.00	0.01	91.14	
Mk	981102-13	341	880	*pm*		35.88	0.03	22.55	7.61	0.17	1.13	22.47	0.10	0.00	0.00	89.93	
Mk	981102-13	341	884	*pm*		35.54	0.08	22.87	8.46	0.26	2.37	21.08	0.16	0.00	0.01	90.82	
Mk	981102-13	341	885	*pm*		36.05	0.12	23.46	7.59	0.42	1.23	22.30	0.14	0.00	0.00	91.32	
Mk	981102-13	344	886	*lws*		42.46	0.34	25.27	3.48	0.06	0.02	15.10	0.03	0.00	0.00	86.74	
Mk	981102-10	346	888	*pm*		36.41	0.03	22.35	7.85	0.30	2.03	22.38	0.10	0.00	0.00	91.44	
Mk	981102-10	346	889	*pm*		36.46	0.02	21.87	8.75	0.34	1.98	22.11	0.09	0.00	0.02	91.64	
Mk	981102-10	346	890	*pm*		36.40	0.00	22.59	7.83	0.24	2.09	22.54	0.13	0.00	0.03	91.85	
Mk	981102-10	346	891	*pm*		36.38	0.02	23.12	7.05	0.21	1.85	22.24	0.11	0.00	0.06	91.03	
Mk	981102-10	346	892	*pm*		36.37	0.00	22.86	7.82	0.20	2.13	22.04	0.15	0.00	0.01	91.57	
Mk	981102-10	347	894	*Npx*	vein	52.41	0.21	2.90	23.41	0.15	2.39	5.83	10.81	0.00	0.01	98.12	qz
Mk	981102-10	347	896	*Npx*	vein	52.31	0.13	2.53	24.23	0.20	2.37	6.24	10.64	0.00	0.00	98.64	qz
Mk	981102-10	347	898	*Npx*	vein	52.70	0.01	3.01	22.23	0.14	2.66	6.52	10.32	0.00	0.00	97.57	qz
Mk	981102-10	347	900	*Npx*	vein	52.34	0.10	2.96	22.90	0.14	2.81	6.69	10.43	0.00	0.09	98.46	qz
Mk	981014-8	352	902	*Npx*	vein	54.53	0.25	7.89	19.37	0.12	1.48	2.80	12.67	0.00	0.00	99.11	ab
Mk	981014-8	352	907	*Npx*	vein	52.73	0.51	3.15	24.67	0.19	1.46	4.64	11.64	0.00	0.01	98.97	ab
Mk	981014-8	352	908	*Npx*	vein	52.86	0.52	3.08	24.49	0.28	1.42	4.79	11.54	0.00	0.01	99.00	ab
Mk	981014-8	352	909	*Npx*	vein	54.72	0.17	8.11	19.02	0.09	1.32	2.68	12.86	0.00	0.00	98.99	ab
Mk	981014-8	352	910	*Npx*	vein	54.07	0.40	5.95	21.47	0.16	1.24	3.10	12.92	0.00	0.02	99.31	ab
Mk	981014-8	352	911	*Npx*	vein	53.27	0.18	7.04	19.51	0.08	1.71	2.98	12.27	0.00	0.00	97.03	ab

Appendix II. EPMA-analysed mineral compositions.



inches 1 2 3 4 5 6 7 8

cm 1 2 3 4 5 6 7 8 9 10 11 12 13 14 15 16 17 18 19

Kodak Color Control Patches

© Kodak, 2007 TM: Kodak

Blue Cyan Green Yellow Red Magenta White 3/Color Black

C Y M

Kodak Gray Scale

© Kodak, 2007 TM: Kodak

A 1 2 3 4 5 6 **M** 8 9 10 11 12 13 14 15 **B** 17 18 19